

==== California =====
Cooperative Oceanic
Fisheries Investigations
==== Reports =====

VOLUME 59

DECEMBER 2018

**CALIFORNIA
COOPERATIVE
OCEANIC
FISHERIES
INVESTIGATIONS**

Reports

VOLUME 59
JANUARY 1 TO DECEMBER 31, 2018

Cooperating Agencies:

CALIFORNIA DEPARTMENT OF FISH AND WILDLIFE
UNIVERSITY OF CALIFORNIA, SCRIPPS INSTITUTION OF OCEANOGRAPHY
NATIONAL OCEANIC AND ATMOSPHERIC ADMINISTRATION, NATIONAL MARINE FISHERIES SERVICE

CALCOFI COORDINATOR John N. Heine
EDITOR John N. Heine

This report is not copyrighted, except where otherwise indicated, and may be reproduced in other publications provided credit is given to California Cooperative Oceanic Fisheries Investigations and to the author(s). Inquiries concerning this report should be addressed to CalCOFI Coordinator, Scripps Institution of Oceanography, La Jolla, CA 92038-0218.

EDITORIAL BOARD

John N. Heine
Brice Semmens

Printed and distributed December 2018, La Jolla, California
ISSN 0575-3317

CONTENTS

Scientific Contributions

State of the California Current 2017–18: Still Not Quite Normal in the North and Getting Interesting in the South. <i>Andrew R. Thompson, Isaac D. Schroeder, Steven J. Bograd, Elliott L. Hazen, Michael G. Jacox, Andrew Leising, Brian K. Wells, John Largier, Jennifer Fisher, Eric Bjorkstedt, Roxanne R. Robertson, Francisco P. Chavez, Mati Kahru, Ralf Goericke, Sam McClatchie, Clare E. Peabody, Tim Baumgartner, Bertha E. Lavaniegos, Jose Gomez-Valdes, Richard D. Brodeur, Elizabeth A. Daly, Cheryl A. Morgan, Toby D. Auth, Brian J. Burke, John Field, Keith Sakuma, Edward D. Weber, William Watson, Julia Coates, Ryan Schoenbaum, Laura Rogers-Bennett, Robert M. Suryan, Jane Dolliver, Stephanie Loreda, Jennifer Zamon, Stephanie R. Schneider, Richard T. Golightly, Pete Warzybok, Jaime Jahncke, Jarrod A. Santora, Sarah Ann Thompson, William Sydeman, and Sharon R. Melin</i>	1
Evaluation of the Influence of Age and Length on Pacific Sardine (<i>Sardinops sagax</i>) Maturation and Characterization of Its Temporal Variability. <i>Kevin Piner, Jenny Mcdaniel, Hui-Hua Lee, Kevin Hill, and Beverly Macewicz</i>	67
Spring Spawning Distribution of Pacific Sardine in US and Mexican Waters. <i>J. A. Valencia-Gasti, E. D. Weber, T. Baumgartner, R. Durazo, S. McClatchie, and C. E. Lennert-Cody</i>	79
Population Dynamics of the Bigeye Croaker <i>Micropogonias megalops</i> in the Northern Gulf of California. <i>Edgar Arnaldo Arzola-Sotelo, Juana López-Martínez, Carlos Hiram Rábago-Quíroz, Jesús Guadalupe Padilla-Serrato, and Enrique Morales-Bojórquez</i>	86
Reproductive Tactics of California Halibut (<i>Paralichthys californicus</i>): Combining Spawning Season, Interspawning Interval, and Batch Fecundity to Estimate Annual Reproductive Output for a Multiple-Batch Spawning Fish. <i>Cheryl L. Barnes and Richard M. Starr</i>	102
Instructions to Authors	115
CalCOFI Basic Station Plan	inside back cover

SCIENTIFIC CONTRIBUTIONS

STATE OF THE CALIFORNIA CURRENT 2017–18: STILL NOT QUITE NORMAL IN THE NORTH AND GETTING INTERESTING IN THE SOUTH

ANDREW R. THOMPSON*

National Marine Fisheries Service
Southwest Fisheries Science Center
8901 La Jolla Shores Drive
La Jolla, CA 92037-1509
andrew.thompson@noaa.gov

ISAAC D. SCHROEDER^{1,2},

STEVEN J. BOGRAD¹, ELLIOTT L. HAZEN¹,
MICHAEL G. JACO^{1,3}, ANDREW LEISING¹,
AND BRIAN K. WELLS⁴

¹Southwest Fisheries Science Center
National Marine Fisheries Service
99 Pacific Street, Suite 255A
Monterey, CA 93940-7200

²Institute of Marine Sciences
University of California, Santa Cruz, CA
and Southwest Fisheries Science Center
NOAA

Monterey, CA

³Earth System Research Laboratory
NOAA

Boulder, CO 80305

⁴Southwest Fisheries Science Center
National Marine Fisheries Service
NOAA
Santa Cruz, CA 95064

JOHN L. LARGIER

Bodega Marine Laboratory
University of California Davis,
Bodega Bay, CA 94923

JENNIFER L. FISHER¹, KYM JACOBSON²,
SAMANTHA ZEMAN¹

¹Cooperative Institute for
Marine Resources Studies
Oregon State University
Hatfield Marine Science Center
Newport, OR 97365

²Northwest Fisheries Science Center
Hatfield Marine Science Center
Newport, OR 97365

ERIC P. BJORKSTEDT¹ AND
ROXANNE R. ROBERTSON²

¹Southwest Fisheries Science Center
National Marine Fisheries Service
NOAA
Santa Cruz, CA 95064

²CIMEC, Humboldt State University

FRANCISCO P. CHAVEZ

Monterey Bay Aquarium Research Institute
Moss Landing, CA 95039

MATI KAHRU AND RALF GOERICKE

Scripps Institution of Oceanography
University of California, San Diego
La Jolla, CA 92093

SAM MCCLATCHIE

38 Upland Rd, Huia
Auckland 0604, New Zealand

CLARE E. PEABODY

National Marine Fisheries Service
Southwest Fisheries Science Center
8901 La Jolla Shores Drive
La Jolla, CA 92037-1509

TIMOTHY R. BAUMGARTNER,
BERTHA E. LAVANIEGOS, AND
JOSE GOMEZ-VALDES

Oceanology Division
Centro de Investigación Científica y
Educación Superior de Ensenada
Carretera Ensenada-Tijuana No. 3918
Zona Playitas C.P. 22860
Ensenada, Baja California, Mexico

RICHARD D. BRODEUR¹,

ELIZABETH A. DALY²,

CHERYL A. MORGAN², TOBY D. AUTH²
AND BRIAN J. BURKE³

¹NOAA-Fisheries
Northwest Fisheries Science Center
Hatfield Marine Science Center
Newport, OR 97365

²Cooperative Institute for
Marine Resources Studies
Oregon State University
Hatfield Marine Science Center
Newport, OR 97365

³Fish Ecology Division
Northwest Fisheries Science Center
National Marine Fisheries Service
National Oceanic and
Atmospheric Administration
2725 Montlake Boulevard E
Seattle, WA 98112

JOHN FIELD AND KEITH SAKUMA

Southwest Fisheries Science Center
National Marine Fisheries Service
NOAA
Santa Cruz, CA 95064

EDWARD D. WEBER AND
WILLIAM WATSON

National Marine Fisheries Service
Southwest Fisheries Science Center
8901 La Jolla Shores Drive
La Jolla, CA 92037-1509

JULIA COATES¹, RYAN SCHOENBAUM¹,
AND LAURA ROGERS-BENNETT²

¹California Department of Fish and Wildlife
1933 Cliff Drive, Suite 9
Santa Barbara, CA 93109

²California Department of Fish and Wildlife
Bodega Marine Laboratory
University of California, Davis
2099 Westshore Road
Bodega Bay, CA 94923

ROBERT M. SURYAN¹,
JANE DOLLIVER², AND
STEPHANIE LOREDO²

¹NOAA Alaska Fisheries Science Center
Auke Bay Laboratories/
Ted Stevens Marine Research Institute
17109 Pt. Lena Loop Road
Juneau, AK 99801

²Department of Fisheries and Wildlife
Oregon State University
Hatfield Marine Science Center
Newport, OR 97365

JEANNETTE E. ZAMON

Northwest Fisheries Science Center
Point Adams Research Station
520 Heceta Place
Hammond OR 97121

STEPHANIE R. SCHNEIDER¹ AND
RICHARD T. GOLIGHTLY²

¹Moss Landing Marine Labs
8272 Moss Landing Road
Moss Landing, CA 95039

²Department of Wildlife
Humboldt State University
1 Harpst Street
Arcata, CA 95521

PETE WARZYBOK AND JAIME JAHNCKE

Point Blue Conservation Science
3820 Cypress Drive, Suite 11
Petaluma, CA 94954

JARROD A. SANTORA¹,
SARAH ANN THOMPSON², AND
WILLIAM SYDEMAN²

¹Department of Applied Mathematics
and Statistics
Center for Stock Assessment Research
University of California, Santa Cruz
Santa Cruz, CA 95060

²Farallon Institute for
Advanced Ecosystem Research
Petaluma, CA 94952

SHARON R. MELIN

National Marine Fisheries Service
Alaska Fisheries Science Center
Marine Mammal Laboratory
NOAA

7600 Sand Point Way N. E.
Seattle, WA 98115

ABSTRACT

Following the marine heat wave of 2014–16, the California Current System (CCS) trended towards more typical conditions north of Point Conception, California, from mid-2017 to mid-2018, but became highly abnormal in the south by mid-2018. Two basin-scale indices (Pacific Decadal Oscillation and Oceanic Niño Index) were close to neutral, but the North Pacific Gyre Oscillation was extremely low at the end of 2017 and beginning of 2018. Regional analyses demonstrated that upwelling was close to normal throughout most of the CCS with the exception of high upwelling from northern California to Washington in summer and fall of 2017. Sea surface temperature was close to normal throughout most of the CCS but warmed to record levels in summer 2018 in southern California and northern Baja California. In spring 2018, surface chlorophyll *a* was negatively anomalous throughout most of the US West Coast with localized hot spots around the Columbia River, in the Gulf of Farallones, and Monterey Bay. Lipid-rich copepod densities and sizes returned to normal levels in the northern CCS, and euphausiid abundances were above average in central California but below average in southern California in spring 2018. Abundances of 7 zooplankton taxa were slightly to well above average off of northern Baja California in late 2017. Pyrosomes, which are associated with warm water, were found throughout the CCS.

The fish assemblage off Oregon and Washington was comprised of both northern and southern/offshore species. In the central region (near Monterey Bay) most fishes were close to long-term mean abundances; however, adult northern anchovy (*Engraulis mordax*) abundance was the highest on record. The ichthyoplankton assemblage off southern California had a tropical signal similar to 2014–15 as warm-water associated mesopelagic abundances were close to record highs and cold water mesopelagics abundances were very low. Anchovy larvae abundances in southern California were the highest since the 1960s.

Indicators that can affect salmon survival were mixed in 2018. On the one hand, several indices forecast high salmon return (moderate-high salmon yearling abundance, high larval fish (salmon prey) abundance, normal lipid-rich copepod abundances). On the other hand, low survival was predicted by high fall PDO, high abundances of offshore larval fishes, and above average abundance of lipid-poor copepods. This unusual mix of indicators makes it difficult to forecast salmon returns in upcoming years.

Common murre (*Uria aalge*) reproduction was historically low in the northern CCS in 2017 as colonies experienced complete reproductive failure both

at Yaquina Head, Oregon, and Castle Rock, California. In both cases, forage was scarce, birds conducted long foraging excursions which left eggs unattended for extended periods, and many eggs were consumed by avian predators. Brandt's (*Phalacrocorax peniscillatus*) and pelagic (*P. pelagicus*) cormorants had above average reproductive success in 2017 at Yaquina Head, but Brandt's cormorant also had total reproductive failure in 2017 at Castle Rock. At Southeast Farallon Island murre, Brandt's cormorant, and pelagic cormorant productivity was close to average in 2017, and Brandt's cormorant and murre were slightly above average in 2018. Preliminary 2018 results from Yaquina Head also indicated that murre successfully produced chicks for the first time since 2014. At-sea bird surveys in the north demonstrated that sooty shearwater and common murre abundances were historically low in 2017, but increased to some of the highest values on record in 2018. By contrast, the at-sea surveys off central California found that murre densities were anomalously high in 2017 but fell to an average level in 2018.

Improving California sea lion (*Zalophus californianus*) pup condition continued from 2016 into 2017 as live pup counts, pup weight, and rate of growth were above average. Augmented pup conditions in 2016–17 was likely driven by increased availability of anchovy, as anchovy remains were found in nearly 100% of sea lion scat. There were record high encounters with Humpback whales (*Megaptera novaeangliae*) off central California in 2018.

Overall, much of the CCS was in more of a normal state through mid-2018 relative to the past 5 years. However, remnants of the 2014–16 marine heat wave were still resonating in the north, and another highly anomalously warm water event affected the southern part of the CCS in summer 2018. Thus, while the CCS was returning to typical conditions in the north, it was anything but normal in the south in 2018.

INTRODUCTION

The California Current System (CCS; fig. 1) is nothing if not dynamic with physical and biological conditions often changing greatly between years. Analyses of data from the earliest days of the California Cooperative Oceanic Fisheries Investigations (CalCOFI) program in the 1950s demonstrated that oceanographic conditions can be highly variable from year to year, leading to substantial changes in the distributions and abundances of marine organisms (Moser et al. 1987; Hsieh et al. 2005). Changes can either be confined to particular regions within the larger system (Brodeur et al. 2006; Goericke et al. 2007) or permeate the entire area, affecting biological assemblages from Baja California, Mexico to Washington, USA (Black et al. 2018).

TABLE 1

Overview of conditions throughout the California Current. For basin indices and physical conditions, blue font suggests that conditions are cool, pink font that conditions are moderately warmer than average and red that conditions are much warmer than normal. For biological indices, green indicates that conditions are conducive for high production, pink moderately below average production, and red well below average.

Indicator	Basin	Oregon/ Washington	Central/Northern California	Southern California	Northern Baja California
ONI	Slightly below average				
PDO	average				
NPGO	very, very low				
NPH	Below average				
Upwelling (spring 2018)		average	slightly above average	slightly above average	
Cumulative upwelling		average	average	slightly above average	
SST (spring 2018)		average	average	average (but far above average in summer 2018)	average (but far above average in summer 2018)
Chlorophyll <i>a</i>		Slightly below average	Slightly below average	Slightly below average	Slightly below average
Copepods/krill		southern species above average; northern species average	<i>Euphausia pacifica</i> larger than average at Trinidad Head Line. Euphausiid abundances above average in central CA.		Highest abundance of copepods since records began in 1998. Euphausiids average.
Forage fish and squid		post-larval biomass very low in spring 2018; larval fish abundance high in winter 2018 but dominated by southern taxa	anchovy, squid, and sanddabs high; hake and sardine low	anchovy very high; subtropical mesopelagics very high	
Salmon survival		yearling Chinook abundance high and yearling coho average. Salmon forage assemblage suggests poor salmon survival and adult return			
Seabird productivity (summer 2017)		complete reproductive failure for murre, average reproduction for Brandt's cormorant and high reproduction for Pelagic cormorant	complete reproductive failure for murre in no. CA. Average murre reproduction in central CA.		
Seabird at-sea abundance (summer 2018)		common murre average, sooty shearwater high	black-footed albatross, Cassian's auklet, murre, pink-footed shearwater low, rhinoceros auklet average, sooty shearwater high	black-footed albatross, Cook's petrel low; pink-footed shearwater, sooty shearwater average; elegant turn, Sabine's gull high	
Sea lions				pup number, weight and growth high	
Whales			record high encounters of humpback		

The entire CCS was affected by anomalously warm conditions from 2014–16. The heating began in late 2013 in the Gulf of Alaska and by mid-2014 elevated sea surface temperature (SST) was observed all the way to southern Baja California (Bond et al. 2015; Leising et al. 2015). The 2014 warming event was primarily confined to near-surface waters (Leising et al. 2015), but it was widespread and persistent, and was augmented in 2015–16 by one of the strongest El Niños on record (Di Lorenzo and Mantua 2016; McClatchie et al. 2016b; Rudnick et al. 2017). Warming ultimately penetrated deeper waters, to at

least several hundred meters, and persisted for several years. This long temporal stretch of warm water, termed a marine heat wave, was unprecedented as 2014–16 was the warmest 3-year stretch on record (Jacox et al. 2018a).

From 2016 to 2017 oceanographic conditions backed off from the extremes of the previous 3 years (Wells et al. 2017). In the central and southern regions of the CCS, SST, chlorophyll *a*, and many biological conditions (e.g., forage fish assemblages) approached long-term averages. In the northern part of the CCS, however, above-normal SST and low chlorophyll *a* persisted into 2016–17,

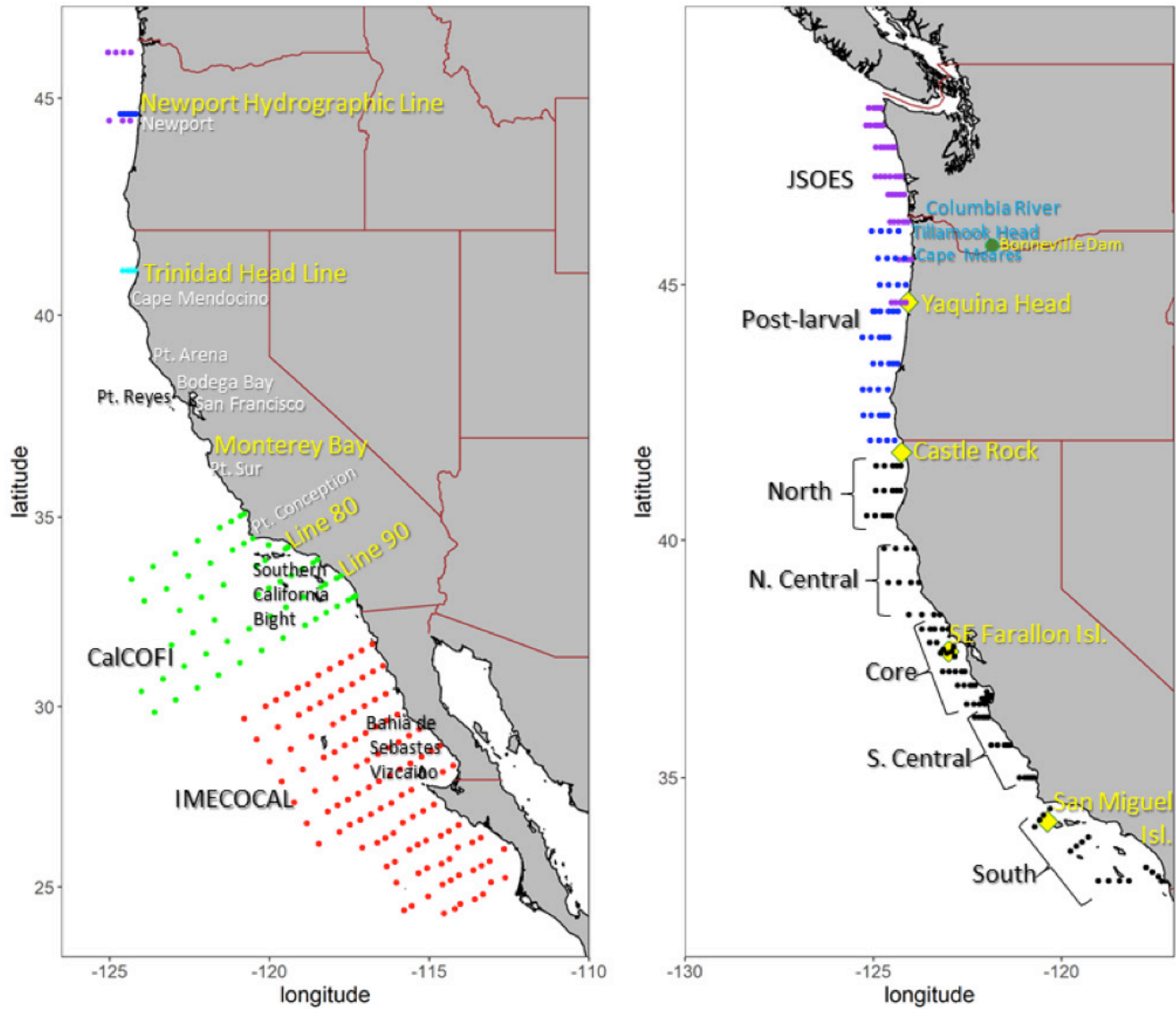


Figure 1. Left: Map where bongo tows were conducted. From north: purple = pre-larval surveys taken in summer; blue = pre-larval survey from winter; cyan = Trinidad Head taken year-round; green = core CalCOFI stations sampled quarterly; red = IMECOCAL stations sampled roughly quarterly. Right: Map where rope trawls and fixed observations for birds or marine mammals were taken. From north: purple = juvenile salmon and Ocean Ecosystem Survey (JJOES) in the upper 20 m; blue = post-larval midwater trawl; black = Rockfish Recruitment and Ecosystem Assessment Survey (RREAS), brackets define the five regions of the RREAS. Yellow diamonds define locations of bird (Yaquina Head, Castle Rock, Southeast Farallon Islands) and sea lion (San Miguel Island) surveys. The Bonneville Dam, (where salmon returns to the Columbia River are tracked) is depicted by the green circle.

and in some places anomalous warming had yet to dissipate through spring 2018 (Jackson et al. 2018). The goal of the current report is to track conditions through 2018 to determine if the return to average conditions persisted past mid-2017 or if recent conditions continued to deviate from average.

BASIN-SCALE CONDITIONS

North Pacific Climate Indices

Temperatures tended to cool throughout the CCS from mid-2016 to mid-2017 (Wells et al. 2017), following the large marine heat wave that brought record-high

temperatures to the CCS from 2014 to 2016 (Bond et al. 2015; Jacox et al. 2018a). Temperatures in 2017 were near the long-term mean; however, there were regional differences with higher temperature anomalies in the northern CCS (Wells et al. 2017). From mid-2017 to mid-2018 temperatures throughout much of the CCS were similar to those observed the previous year. However, in the Southern California Bight and northern Baja California, temperatures rapidly increased though July and August 2018, and record high SSTs were recorded near the coast in La Jolla, California.¹

¹<https://scripps.ucsd.edu/news/highest-ever-seawater-temperature-recorded-scripps-pier>

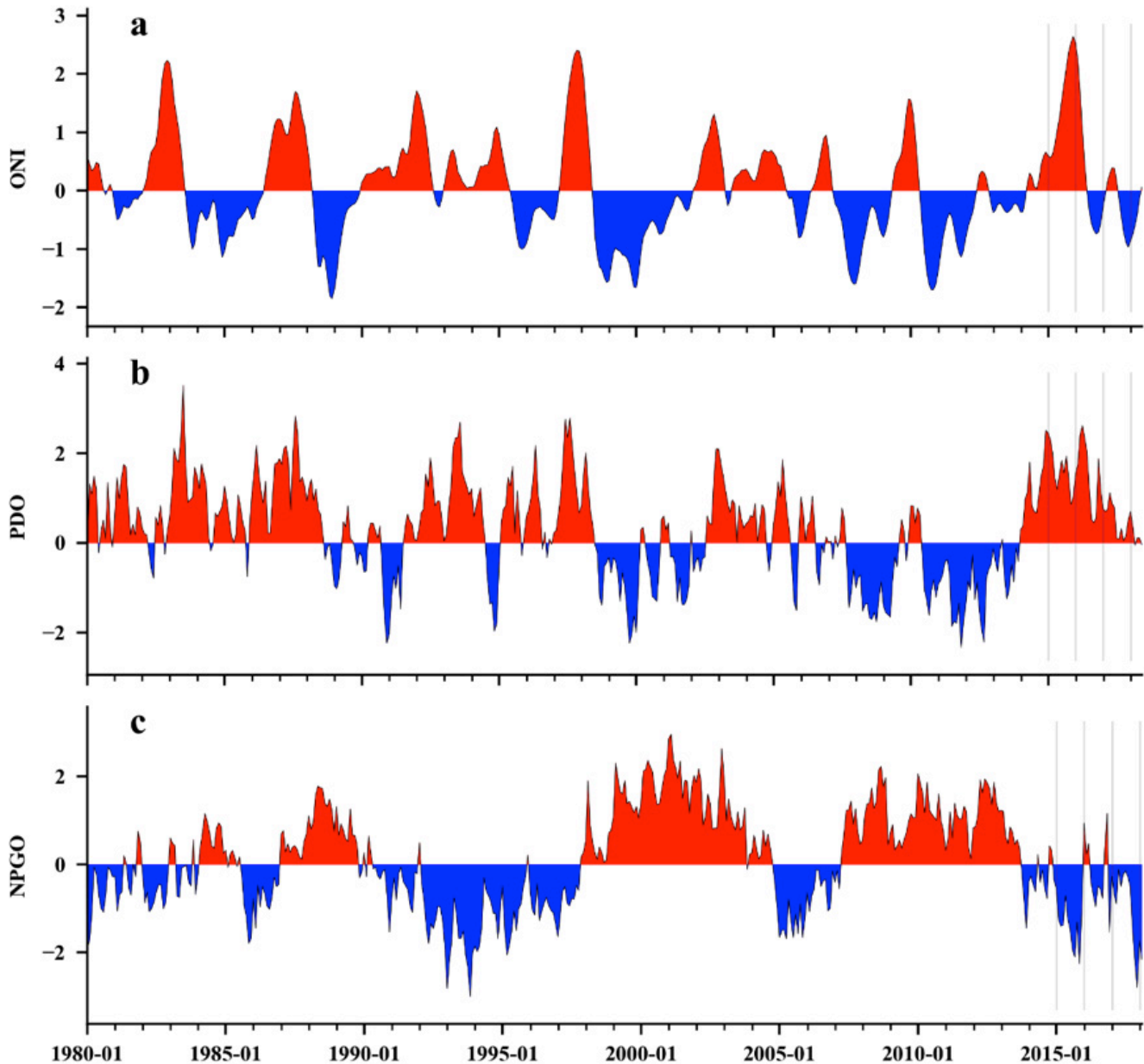


Figure 2. Time series of monthly values for three ocean climate indices especially relevant to the California Current: a) Oceanic Niño Index (ONI; January 1980 to June 2018), b) Pacific Decadal Oscillation (PDO; January 1980 to June 2018), and c) North Pacific Gyre Oscillation (NPGO; January 1980 to February 2018). Vertical lines mark January 2015, 2016, 2017, and 2018. Monthly data obtained from <http://upwell.pfeg.noaa.gov/erddap/>.

The Oceanic Niño Index² (ONI), a three-month running mean of SST anomalies averaged over 5°S–5°N and 120°W–170°W (NINO3.4 region), transitioned from peak El Niño conditions at the start of 2016 to weak La Niña conditions by the end of 2016 (fig. 2A). While the 2015–16 ONI values rivaled those of the record 1997–98 El Niño event, its impact along the US West Coast was less pronounced (Jacox et al. 2016). In 2017 ONI values briefly switched to positive during the spring and summer, but were lower than the 0.5°C threshold that signifies an El Niño event. Negative ONI

values lower than –0.5°C (the threshold for a La Niña event) occurred during October 2017 and lasted until March 2018 (fig. 2A). The ONI then increased in the subsequent 3 months and was at 0.1 in July 2018. As of 24 September 2018 NOAA’s Climate Prediction Center³ forecast a 55% chance for a tropical El Niño to develop in fall 2018 and a 70% chance by winter 2018–19.

The Pacific Decadal Oscillation⁴ (PDO) index describes the temporal evolution of dominant spatial patterns of SST anomalies over the North Pacific

²<http://www.cpc.ncep.noaa.gov/data/indices/>

³http://www.cpc.ncep.noaa.gov/products/analysis_monitoring/lanina/

⁴<http://research.jisao.washington.edu/pdo/PDO.latest.txt>

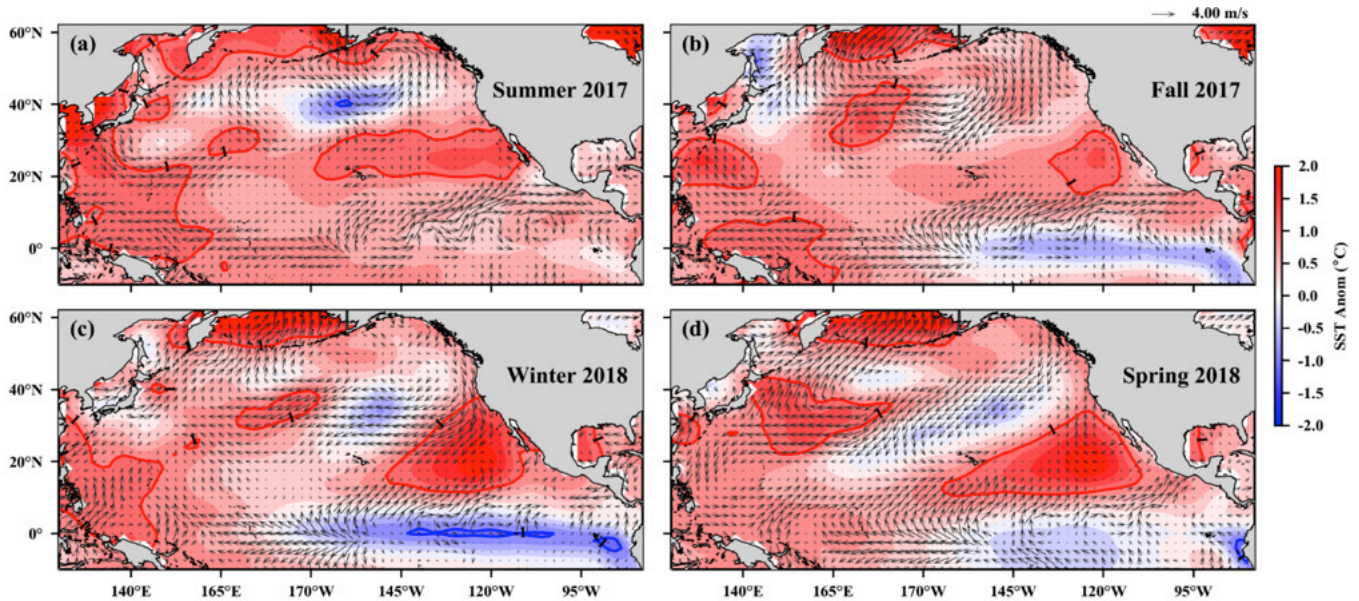


Figure 3. Anomalies of surface wind velocity and sea surface temperature (SST) in the North Pacific Ocean for summer (a: June–August) 2017, fall (b: September–November) 2017, winter (c: December–February) 2018, and spring (d: March–May) 2018. Arrows denote magnitude and direction of wind anomaly (scale arrow at top right). Contours denote SST anomaly. Shading interval is 0.25°C and contour intervals at $\pm 1^{\circ}\text{C}$ are shown. Wind climatology period is 1968–96. SST climatology period is 1950–79. Wind NCEP/NCAR Reanalysis data and NOAA Extended Reconstructed SST V5 data were obtained from <http://www.esrl.noaa.gov>.

(Mantua et al. 1997). Positive PDO values are associated with a shallower upwelling cell in the northern CCS (Di Lorenzo et al. 2008). The PDO was positive for all of 2016 with peak values in the spring and lowest values in the summer (fig. 2B). The April 2016 value of 2.62 was the largest value during the large marine heat wave and El Niño event of 2014–16. Positive PDO values persisted for all of 2017 but were relatively low, particularly during the summer. As of March 2018 the PDO recorded the first negative value since December 2013 (-0.05) and remained close to zero (-0.04) through June 2018.

The North Pacific Gyre Oscillation⁵ (NPGO) is a low-frequency signal of sea surface height variations across the North Pacific, indicating variations in the circulation of the North Pacific Subtropical Gyre and Alaskan Gyre (Di Lorenzo et al. 2008). Positive values of the NPGO are linked with increased equatorward flow in the California Current, along with increased surface salinities, nutrients, and chlorophyll *a* values in the southern–central CCS (Di Lorenzo et al. 2009). Negative NPGO values are associated with decreases in these variables, inferring less subarctic source waters, fewer nutrients, reduced upwelling, and generally lower production in the CCS. The NPGO had short-duration positive values in the winter of 2016–17 and fall of 2016, which were some of the few positive values observed since 2013 (fig. 2C). The 2017 NPGO values were negative throughout the year, with the largest

negative values in the fall. In fact, the negative values from October 2017 to February 2018 were some of the lowest NPGO values documented in records dating back to 1950.

North Pacific Climate Patterns

A basin-scale examination of seasonal SST and surface wind anomalies allows for the interpretation of the spatial evolution of climate patterns and wind forcing over the North Pacific (figs. 2, 4). During summer 2017, positive SST anomalies extended across the central and eastern Equatorial Pacific (fig. 3), which was reflected in the positive ONI values (fig. 2). Tropical La Niña conditions emerged during fall 2017 and were fully actualized by winter 2018, with temperature anomalies between -0.5 to -1°C in the NINO3.4 region⁶ (fig. 3). However, the spring 2018 temperature anomalies increased and only a small region along the South American coast had temperature anomalies less than -1°C . Warm temperature anomalies persisted from fall 2017 through spring 2018 in the Bering Sea and the Gulf of Alaska, with the Bering Sea having temperature anomalies higher than 1°C . In the eastern Pacific a general pattern of negative anomalies centered along 40°N and positive anomalies centered along 20°N appeared in all seasons, though the negative anomalies were very small in spatial extent during fall 2017. The negative anomalies were mostly less than -1°C and were a continuation of spatial patterns observed since the summer of 2016 (Wells et al.

⁵<http://www.o3d.org/npgo/roms.html>

⁶The NINO3.4 region is bound by 90°W – 150°W and 5°S – 5°N

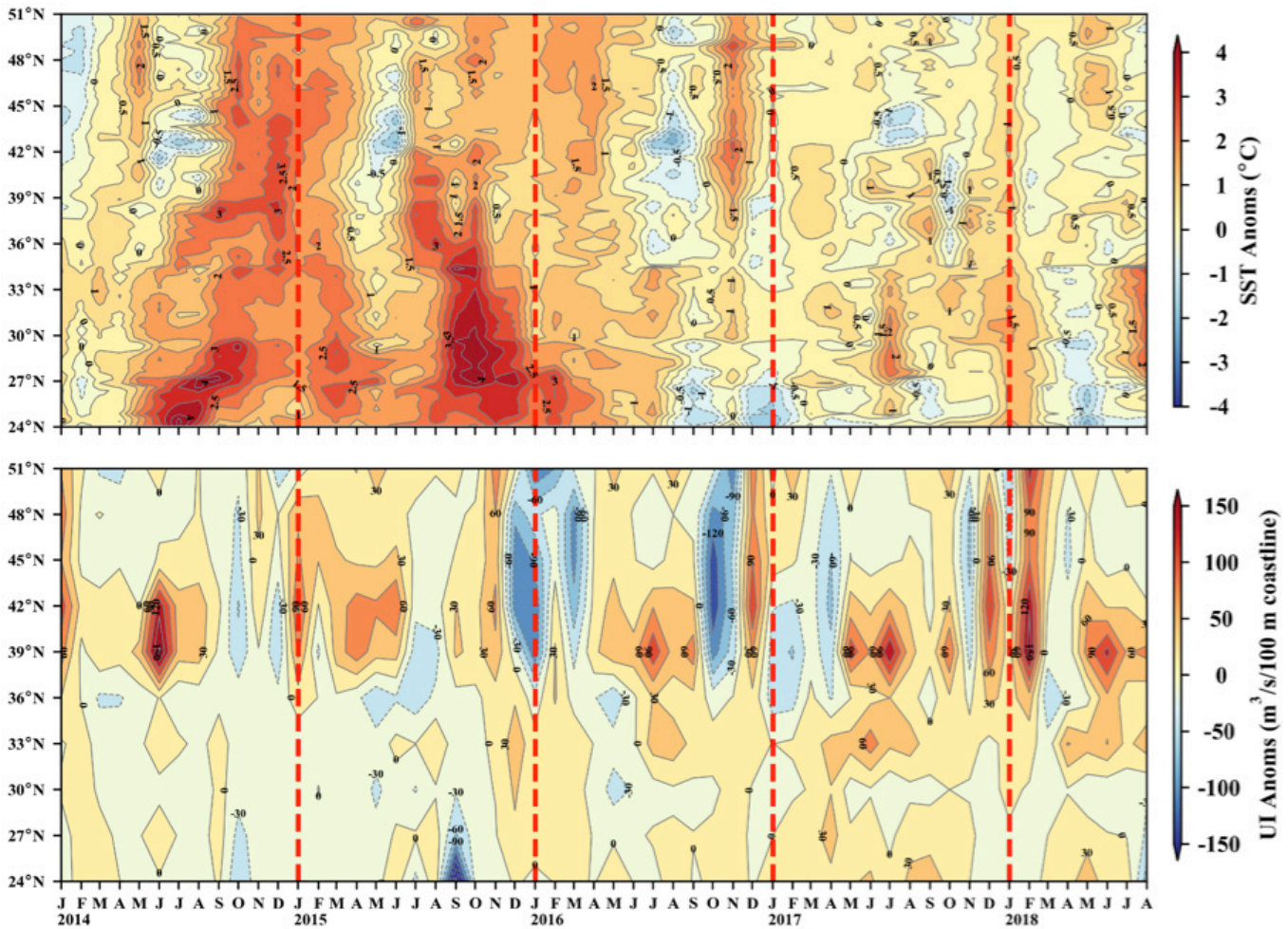


Figure 4. (A) Monthly sea surface temperature (SST) anomalies (top) and upwelling index (UI) anomalies (bottom) for January 2014–August 2018. The SST anomalies are averaged from the coast to 75 km offshore. Positive and negative upwelling anomalies denote greater than average upwelling or downwelling (usually during the winter), respectively. Anomalies are relative to 1982–2018 monthly means. Daily optimum interpolation AVHRR SST data obtained from <http://coastwatch.pfeg.noaa.gov/erddap/griddap/ncdcOisst2Agg>. Six-hourly upwelling index data obtained from <http://oceanview.pfeg.noaa.gov/erddap/tabledap/>.

2017). The positive anomalies were above 1°C, with the largest onshore values extending from San Francisco Bay, California, to southern Baja California, Mexico, during winter 2017–18 and spring 2018.

The trade winds over the western Equatorial Pacific were stronger than normal in all four seasons from summer 2017 to spring 2018 as indicated by the anomalous easterly winds between 165°E–180° (fig. 3). Lower than average sea-level pressure during summer 2017 produced cyclonic wind anomalies in the Gulf of Alaska. By fall 2017 and winter 2018 the low pressure was replaced by anomalously high pressure and anticyclonic wind patterns in the Bering Sea and Gulf of Alaska. Within the CCS winds along the coast were near the long-term average during summer and fall 2018. Large northerly wind anomalies occurred during winter 2017–18 indicating stronger upwelling-favorable winds in the central CCS region and a relaxation of downwelling winds along the coast of Washington and Oregon. The

upwelling-producing winds that usually start during the spring were considerably weaker than the long-term average as indicated by the southerly wind anomalies.

COAST-WIDE CONDITIONS

Upwelling in the California Current

Monthly anomalies of SST (averaged from the coast to 100 km offshore) and upwelling are used to examine anomalous coastal upwelling conditions within the CCS from January 2016 to May 2018 (fig. 4). Upwelling estimates come from two sources: the Bakun upwelling index (UI; fig. 4A) (Bakun 1973; Schwing et al. 1996), and the Coastal Upwelling Transport Index (CUTI), which is derived from a data-assimilative regional ocean model (fig. 4B) (Jacox et al. 2014; Jacox et al. 2018b). We present both upwelling indices because the UI has long been used in many past studies of the California Current, but in some places, particularly south of 39°N,

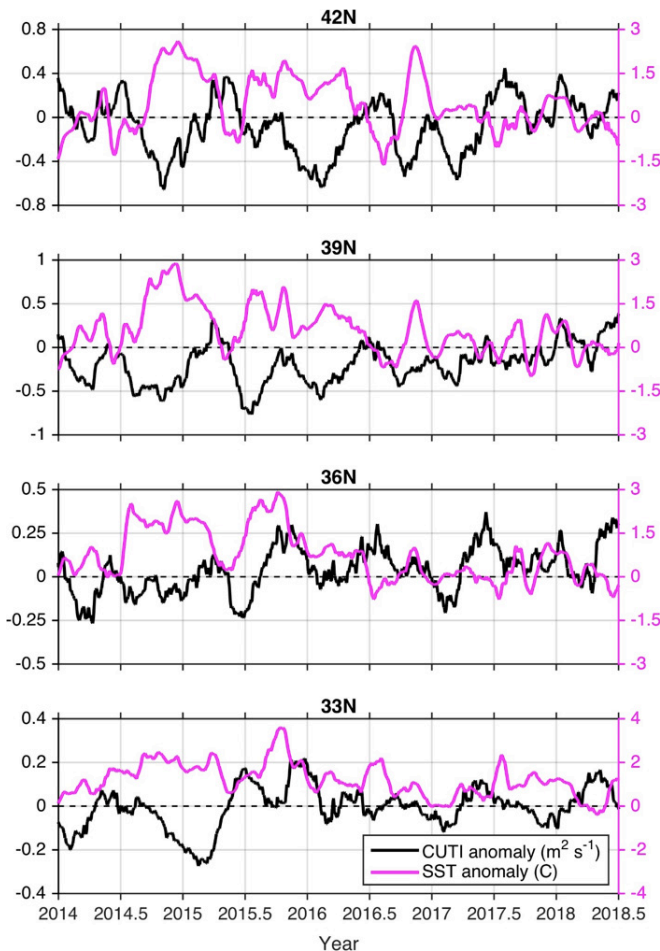


Figure 4. (B) The Coastal Upwelling Transport Index (CUTI; black) and SST anomalies (magenta) relative to the 1980–2010 climatology, derived from a data assimilative ocean reanalysis of the California Current System (Jacox et al. 2018), are shown at four latitudes off the US West Coast. Values are averaged from the coast to 75 km offshore. SST is smoothed with a 30-day running mean; CUTI is smoothed with a 90-day running mean. Model output is obtained from oceanmodeling.ucsc.edu and CUTI is obtained from <https://oceanview.pfeg.noaa.gov/products/upwelling/>.

it is a less reliable indicator of upwelling due to relatively poor estimation of the wind stress and modulation of upwelling by the cross-shore geostrophic flow (Bakun 1973; Jacox et al. 2014; Jacox et al. 2018b).

High SST anomalies due to the 2014–16 marine heat wave were evident until spring 2016 (fig. 4). Positive SST anomalies ($>1^{\circ}\text{C}$) persisted through much of the region during winter 2015–16 and spring 2016, especially for locations north of 42°N and south of 30°N . From January to May 2017, SST anomalies north of 42°N were near the long-term average, with the exception of a few localized periods of $\sim +0.5^{\circ}\text{C}$ anomalies. Positive SST anomalies were higher for latitudes south of 42°N and a few locations experienced anomalies greater than 1°C during summer/fall 2017. January 2018 SST anomalies were 0.5 to 1°C warmer than average for all latitudes. A slight drop in temperature anomalies, to near climato-

logical values, occurred in February to March. Starting in June 2018, large positive anomalies appeared in the southern California Bight between latitudes 27° – 33°N , culminating with anomalies exceeding 2°C by August.

In the winter of 2015–16, upwelling anomalies were negative north of 33°N (fig. 4), which reflects conditions during the previous El Niño winters. However, these upwelling anomalies were positive at 33°N and farther south, an atypical pattern that contributed to a relatively muted impact of the 2015–16 El Niño off California (Jacox et al. 2016; Frischknecht et al. 2017). The most upwelling-favorable anomalies during 2016 occurred from July to September for latitudes between 36° – 42°N , followed by strong downwelling anomalies in October and November 2016 north of 36°N . The largest negative upwelling anomalies during early 2017 were for latitudes 36° – 45°N . Upwelling during May to October 2017 was generally average to above average for the whole coast, with the largest positive anomalies in late spring/early summer. Strong positive upwelling anomalies occurred between 39° – 42°N at the end of 2017 and beginning of 2018. Upwelling anomalies were positive again in late spring 2018 after a period of average to slightly below average upwelling in the preceding months. SST and upwelling anomalies along the coast are highly negatively correlated throughout the CCS, with the strongest correlations at more northern latitudes due to a strong coupling between local winds and SST (fig. 4B) (Frischknecht et al. 2015).

The cumulative upwelling index (CUI) is the cumulative sum of the daily UI values starting January 1 and ending on December 31, and it provides an estimate of the net influence of upwelling on ecosystem structure and productivity over the course of the year (Bograd et al. 2009). In general, upwelling was slightly stronger in 2018 than the previous two years (fig. 5). During winter 2015–16, upwelling north of 39°N was low due to the El Niño and strong upwelling only began in the summer. South of 39°N , upwelling anomalies were neutral to positive in early 2016, counter to what would be expected from a strong El Niño (Jacox et al. 2015). Upwelling during 2017 was near the long-term average for the whole coast except between 36° – 42°N . For these latitudes, the CUI curves during winter 2017–18 were below the climatological curve, and upwelling began in early May. Strong upwelling during February 2018 pushed the CUI curves to above the long-term average; however, downwelling starting in April dropped the CUI curves towards the long-term average for latitudes 36°N and 45° – 48°N . Summer 2018 upwelling was strong at 39°N , with the CUI curve at one of its highest yearly values at the end of August.

Periods of upwelling, or farther north reduced downwelling, during the winter can limit stratification

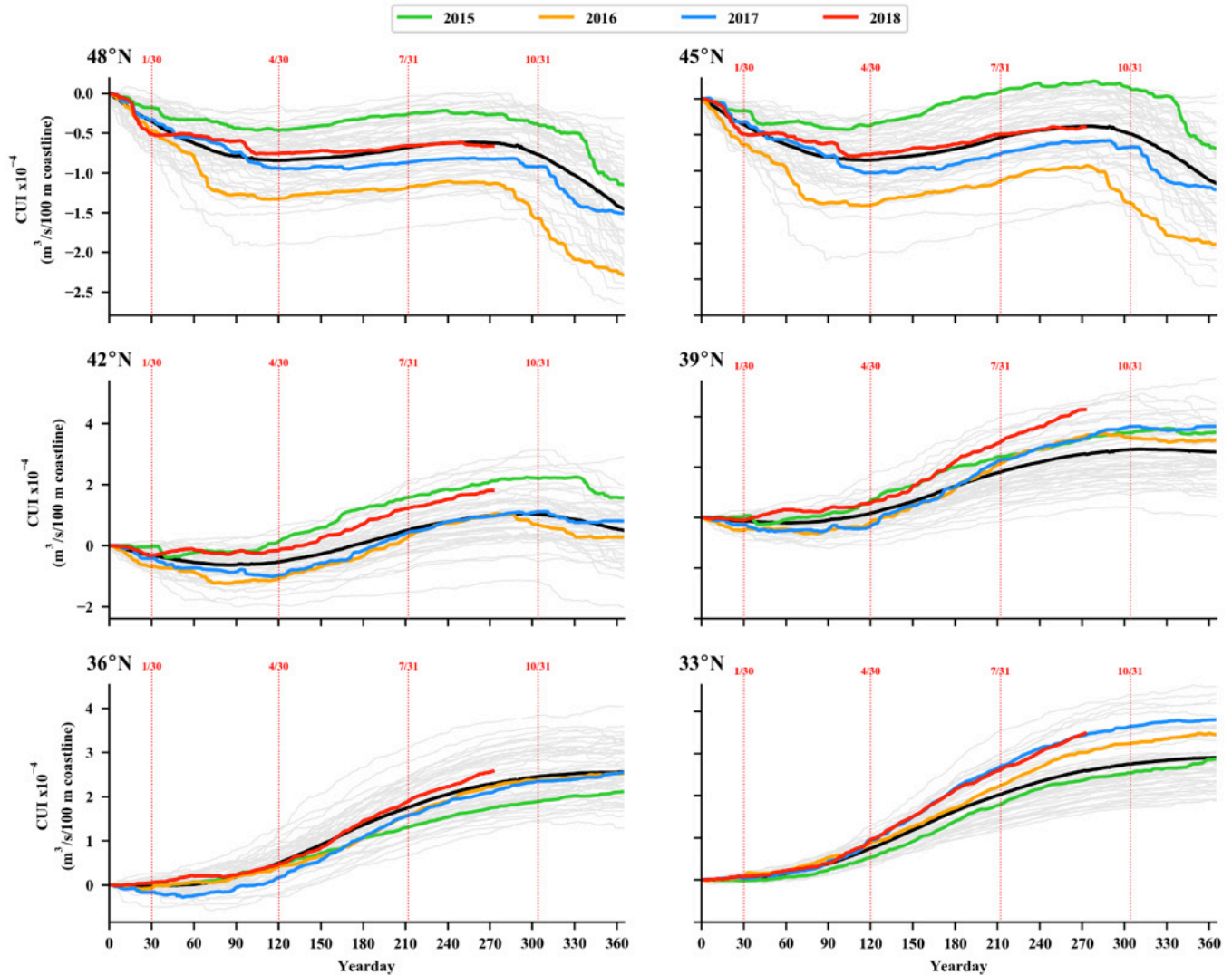


Figure 5. Cumulative upwelling index (CUI) starting on January 1 calculated from the daily upwelling index at three locations along the West Coast of North America. Grey lines are all yearly CUI for 1967–2014, colored CUI curves are for the years 2015–18. The climatological mean CUI is the black line. The red dashed vertical lines mark the end of January, April, July, and October. Daily upwelling index data obtained from <http://upwell.pfeg.noaa.gov/erddap/>.

and facilitate introduction of nutrients to the surface, acting to precondition the ecosystem for increased production in the spring (Schroeder et al. 2009; Black et al. 2010). The area of the surface atmospheric pressures associated with the North Pacific High (NPH) can be used as an index of this winter preconditioning (Schroeder et al. 2013). Since 2014 there has been a continual weak NPH during the winter (January–February; fig. 6). The NPH area increased in 2018 relative to the past four years but was still much smaller than the exceptionally large area in 2013.

Coastal Sea Surface and Subsurface Temperatures

SSTs measured by National Data Buoy Center buoys along the West Coast were generally above the long-

term mean for all buoys from 2015–18 (fig. 7). There were periods of reduced temperatures that were below the long-term mean, such as during August 2016 for buoys north of Bodega Bay and during October 2017 for buoys 46022 (northern California) and 46013 (Bodega Bay). During 2018 a shift towards cooler temperatures occurred in February for buoys north of Santa Monica. These shifts to cooler temperatures were associated with increased northerly, upwelling-favorable winds. In February 2018 winds were strongly upwelling-favorable but switched directions or diminished during March. Buoys along the southern California coast (46011 and 46025) experienced periods of very high temperatures during summer 2018, with buoy 46025 (Santa Monica) experiencing the longest duration of sustained positive anomalies.

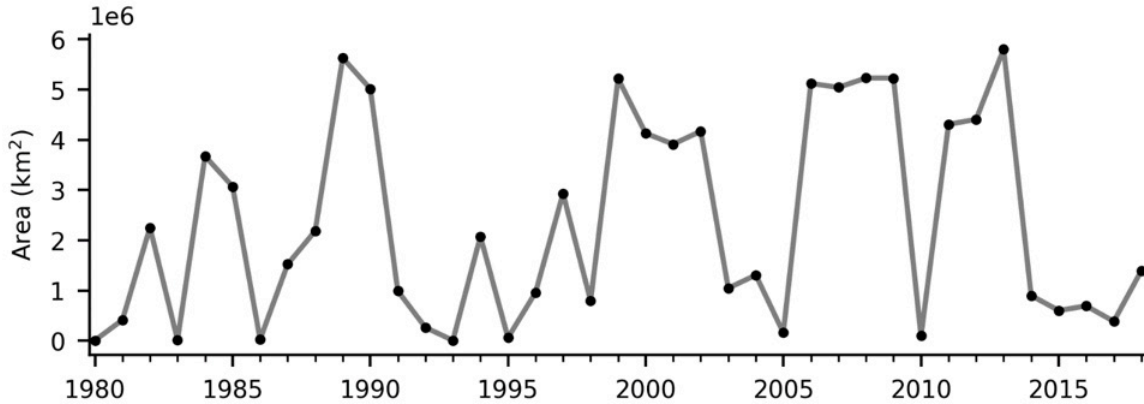


Figure 6. The area of high atmospheric pressure of the North Pacific High averaged over January and February each year, 1980-2018. The area is the areal extent of the 1020 hPa isobar located in the eastern North Pacific.

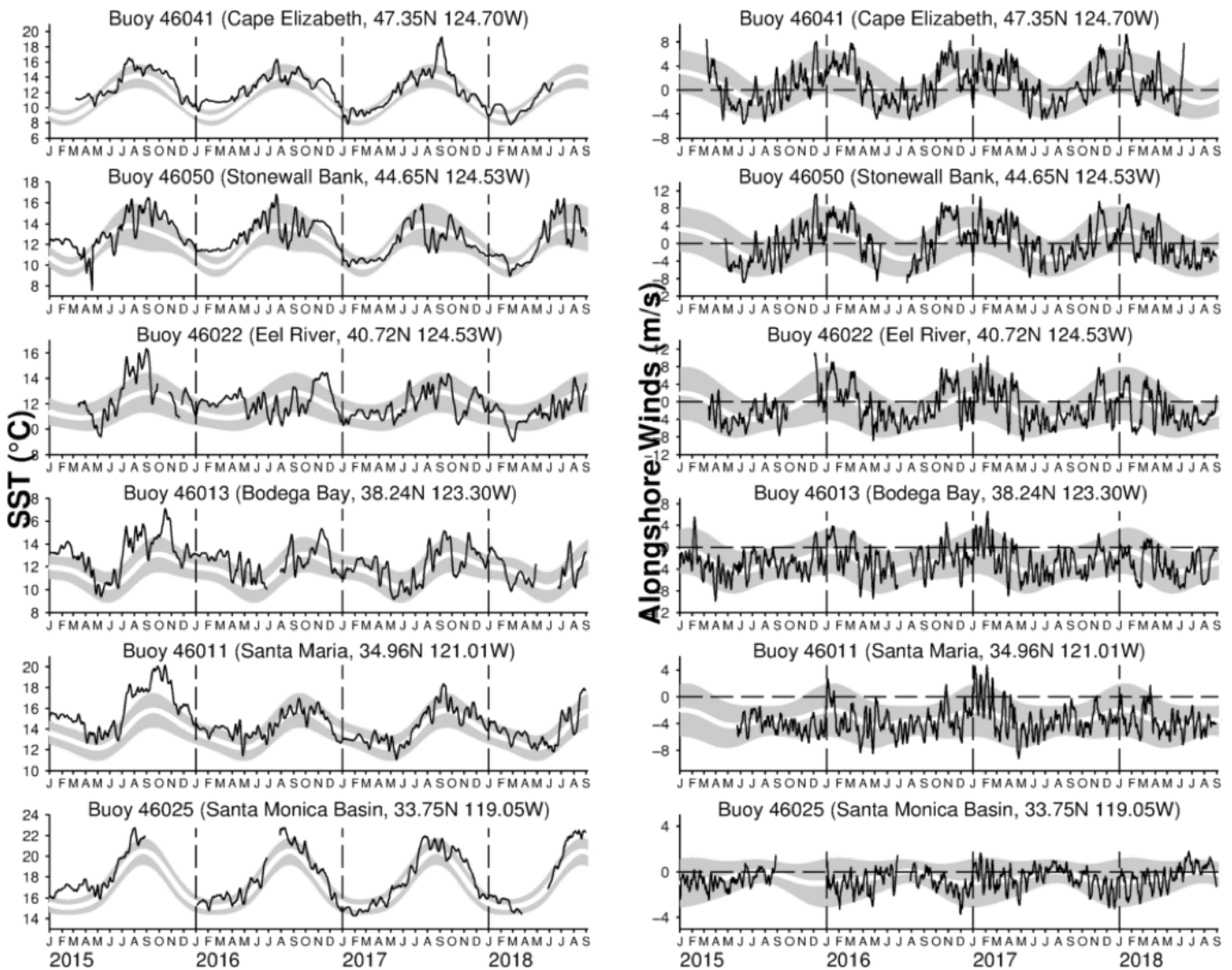


Figure 7. Time series of daily sea surface temperatures (left) and alongshore winds (right) from various National Data Buoy Center (NDBC) coastal buoys along the CCS for January 2016 to August 2018. The wide white line is the biharmonic annual climatological cycle at each buoy. Shaded areas are the standard errors for each Julian day. Series have been smoothed with a 7-day running mean. Data provided by NOAA NDBC. Additional buoy information can be found at <http://www.ndbc.noaa.gov/>.

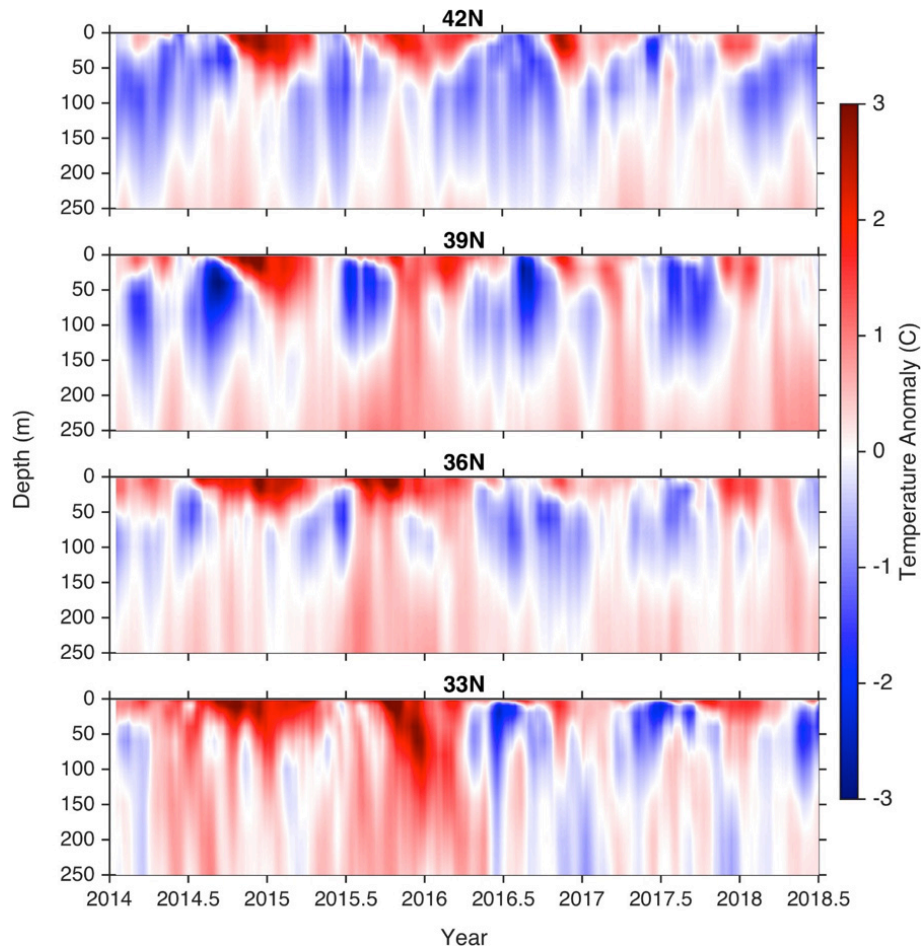


Figure 8. Temperature anomalies relative to the 1999–2011 climatology, derived from a data assimilative ocean reanalysis of the California Current System (<http://oceanmodeling.ucsc.edu/ccsrt/>), are shown at four latitudes off the US West Coast. Temperatures are averaged from the coast to 100 km offshore and smoothed with a 30-day running mean.

The signature of the northeast Pacific marine heat wave was evident at all latitudes beginning in late 2014 and extending through mid-2016, with penetration deeper in the water column at more southern latitudes (fig. 8), based on upper ocean temperature anomalies from ROMS averaged from the coast to 100 km offshore at latitudes of 33°, 36°, 39° and 42°N. Since mid-2016, subsurface temperatures cooled throughout much of the CCS (fig. 8), though surface temperatures remain elevated particularly in winter, which may indicate reemergence of preexisting temperature anomalies when the mixed layer deepens (Alexander et al. 1999).

Primary Production in the California Current System

Spring 2018 chlorophyll *a* anomalies had similar spatial patterns to those in 2017, with negative anomalies along the majority of the coast (fig. 9, top panels).⁷

⁷https://www.nwfsc.noaa.gov/research/divisions/efs/microbes/hab/habs_toxins/hab_species/pn/index.cfm

Positive anomalies in 2018 were localized around the Columbia River, San Francisco Bay, and along the coast south of Monterey Bay. Predicted domoic acid concentrations were higher and more widespread between Monterey Bay and the southern US border in 2018 than in the previous two years (fig. 9, bottom panels). Furthermore, predicted domoic acid concentrations did not appear to be concentrated in areas of positive chlorophyll anomalies, unlike in previous years (Wells et al. 2017).

Despite widespread predictions of high domoic acid concentrations in 2017–18, harmful algal blooms along the California coast returned to “normal” conditions, with toxin events localized to many previously identified hot spots, including southern California, Santa Barbara Channel, Monterey Bay, and off the coast of Humboldt County, California. While there were no region-wide blooms or closures, domoic acid levels in southern California and the Santa Barbara Channel equaled or exceeded the 2015

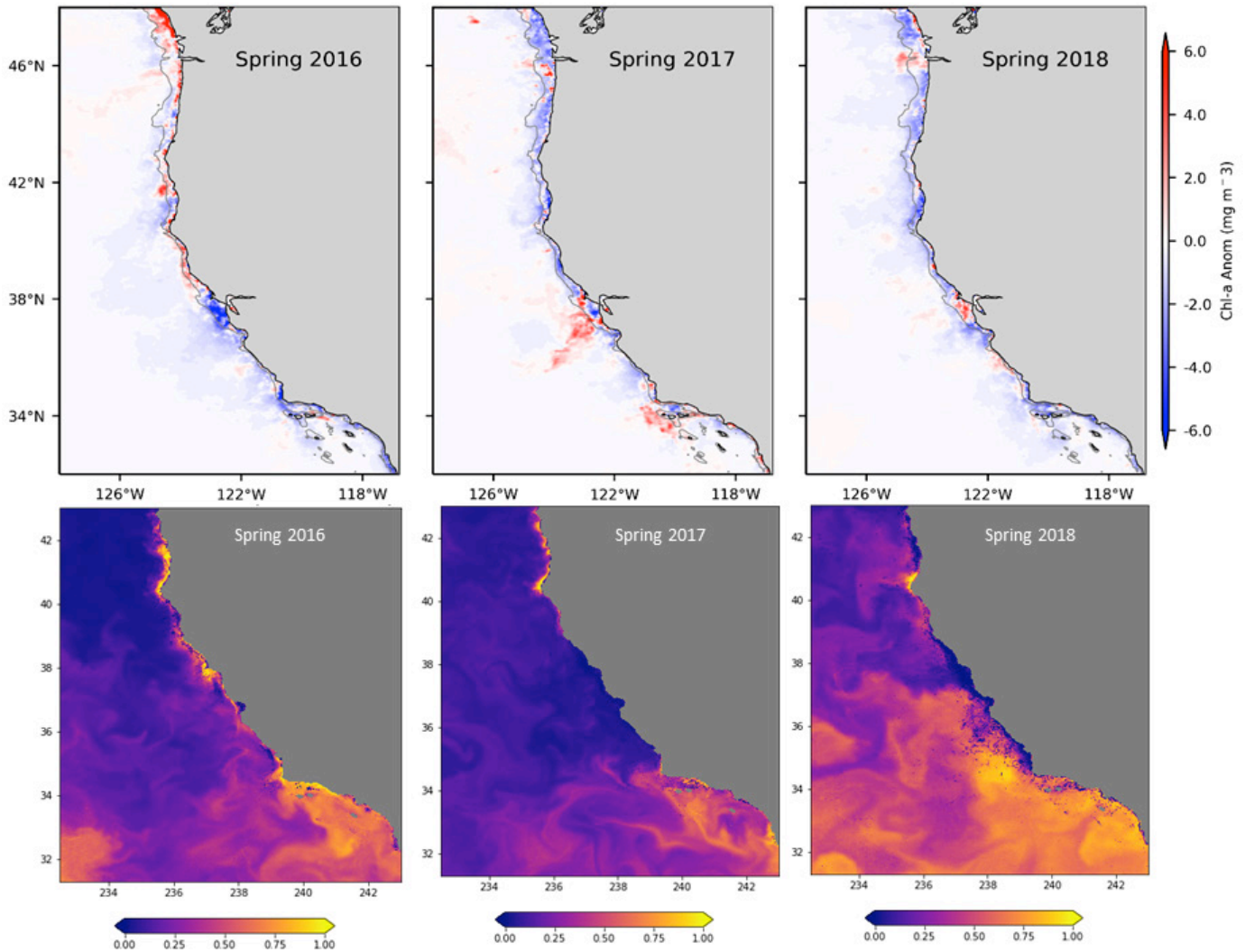


Figure 9. Top) Chlorophyll a anomalies from Aqua MODIS for: spring (March–May) of 2016–18. Monthly anomalies were averaged onto a $0.1^\circ \times 0.1^\circ$ grid and the climatology was based on the time period from 2003–17. The data were obtained from <http://coastwatch.pfel.noaa.gov/>. Bottom) Predicted probability of domoic acid > 500 nanograms/L from spring 2016–18 from <http://www.cencoos.org/data/models/habs/previous>.

bloom event and resulted in a suspected bird die-off and elevated marine mammal strandings in that region during spring 2017.

Currents

During spring 2017 surface currents⁸ were predominantly southward from the Columbia River (46°N) south to Point Conception (34°N) and continued to be southward south of Point Conception in the far-western portion of the Southern California Bight (fig. 10). Although the southward tendency continued through summer, surface currents were marked by

a noted offshore orientation throughout the region. In the fall, alongshore flow switched northward for the region north of Cape Mendocino (40°N), while it remained southward and offshore-directed south of Cape Mendocino. Offshore anticyclonic mesoscale eddies, centered around 39°N and 36°N , interacted with shelf jets off Point Arena, Point Reyes, and Point Sur. Coherent westward flow out of the Santa Barbara Channel continued from summer through fall and into winter. Over the shelf in winter, northward transport was observed from Point Conception (34°N) north to the Columbia River (46°N) and broad coherent northward flows were observed north of Cape Mendocino, whereas farther south, offshore-directed flow persisted and the influence of offshore mesoscale features were observed around 35°N .

⁸These data on surface currents were obtained from High-Frequency (HF) Radar, with vectors calculated hourly at 6-km resolution using optimal interpolation. Real-time displays can be viewed at www.sccoos.org/data/hfrnet/ and www.cencoos.org/sections/conditions/Google_currents/ as well as at websites maintained by the institutions that contributed the data reported here.

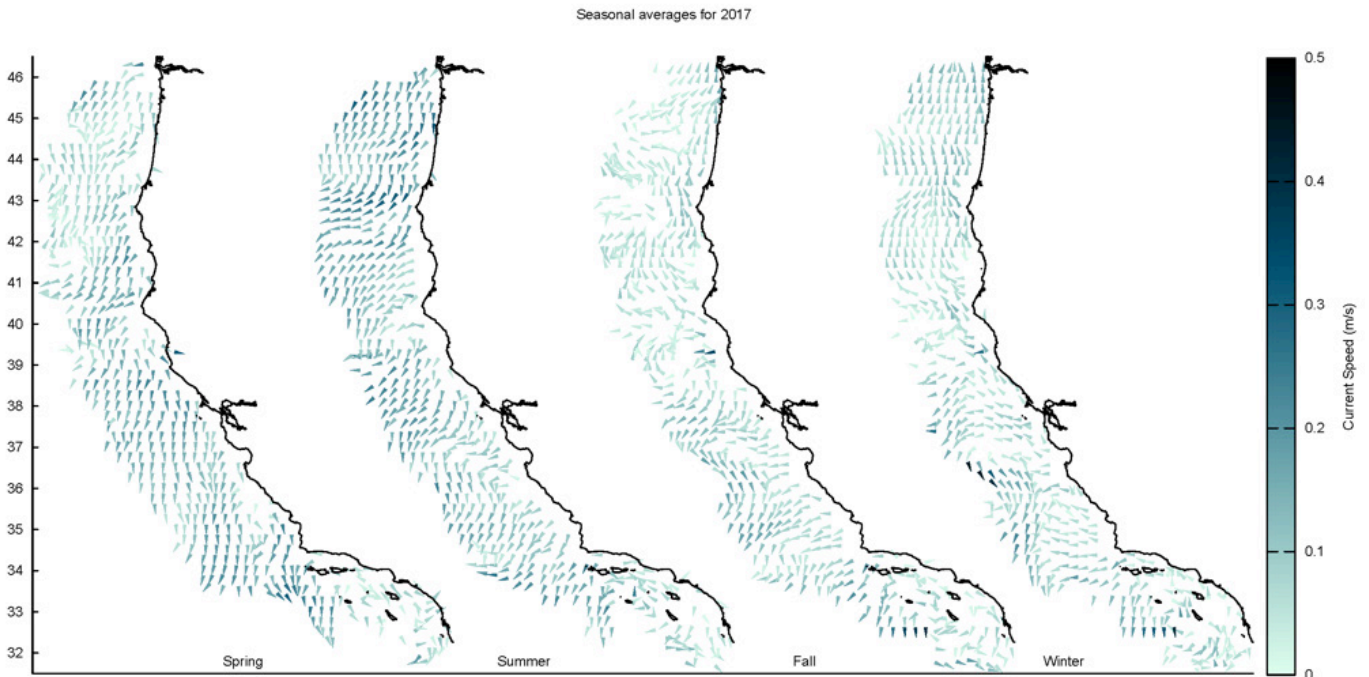


Figure 10. Maps of seasonal mean surface currents observed in the CCS with HF radar. From left to right, the panels present data for spring (March–May 2017), summer (June–August 2017), fall (September–November 2017), and winter (December–February 2018). Current speed is indicated by depth of shading and direction given by orientation of arrow extending from observation location. Currents are displayed with a spatial resolution of 0.25° which means that nearshore flows are not well represented here.

REGIONAL OBSERVATIONS OF ENVIRONMENT AND LOWER TROPHIC LEVELS

Northern California Current: Oregon (Newport Hydrographic Line)

The temperature anomaly at 50 m from station NH-5 off Newport, Oregon, was positive for almost the entire duration between 2014 and 2018, although the magnitude of the anomaly decreased in 2017 and 2018 (fig. 11). At 150 m at station NH-25 off Newport, the temperature anomaly was also strongly positive from the spring of 2014 until summer 2017. In late 2017 the temperature anomaly at 150 m was quite high, but it fell to a negative anomaly in early 2018, then rose again and became positively anomalous in mid-2018. Warm ocean conditions in this region are associated with a lipid-poor copepod community and a gelatinous-dominated zooplankton community that has persisted from September of 2014 (Peterson et al. 2017) into 2018. However, the strength of the anomalies has lessened since fall 2017, signaling that the pelagic ecosystem may be in a state of flux.

In 2017, the upwelling season (physical spring transition) began on April 26, eleven days later than the 40-year climatological average, and ended on 15 October (figs. 4, 5). The resulting upwelling season was average in length, with overall cumulative upwelling being slightly higher than the long-term mean (figs. 4, 5). Upwelling was weak in May and June 2017 with some

strong periods of downwelling which resulted in positive SST anomalies and strongly positive 150 m temperature anomalies on the shelf (fig. 7, buoy 46050). Upwelling was persistent from mid-June until mid-September. During this period SST anomalies were negative and temperature at 150 m on the shelf was neutral. Hypoxic oxygen concentrations below 1.4 ml/L were observed⁹ on the shelf, with an oxygen value of 0.29 ml/L recorded in September of 2017 that was the lowest measurement observed in the 12-year time series (data not shown). Following the upwelling season in 2017, strong winter storms mixed the deep water on the slope off Oregon and negative temperature anomalies persisted for two months during the winter of 2017–18; however, the shelf waters remained warmer than average throughout the winter and into the summer of 2018 (fig. 11). With the exception of two months during the 2015 and 2017 upwelling season, nitrogen concentrations on the shelf remained below average since the fall of 2015 and continue to be low into 2018 (fig. 11).

The zooplankton community¹⁰ was largely comprised of lipid-poor southern species from September 2014 until the summer of 2017 when the copepod

⁹https://www.nwfsc.noaa.gov/news/blogs/display_blogentry.cfm?blogid=1&month=9&year=2017

¹⁰Copepod data were based on samples collected with a 0.5 m diameter ring net of 202- μ m mesh, hauled from near the bottom to the sea surface. A TSK flowmeter was used to estimate volume of water sampled.

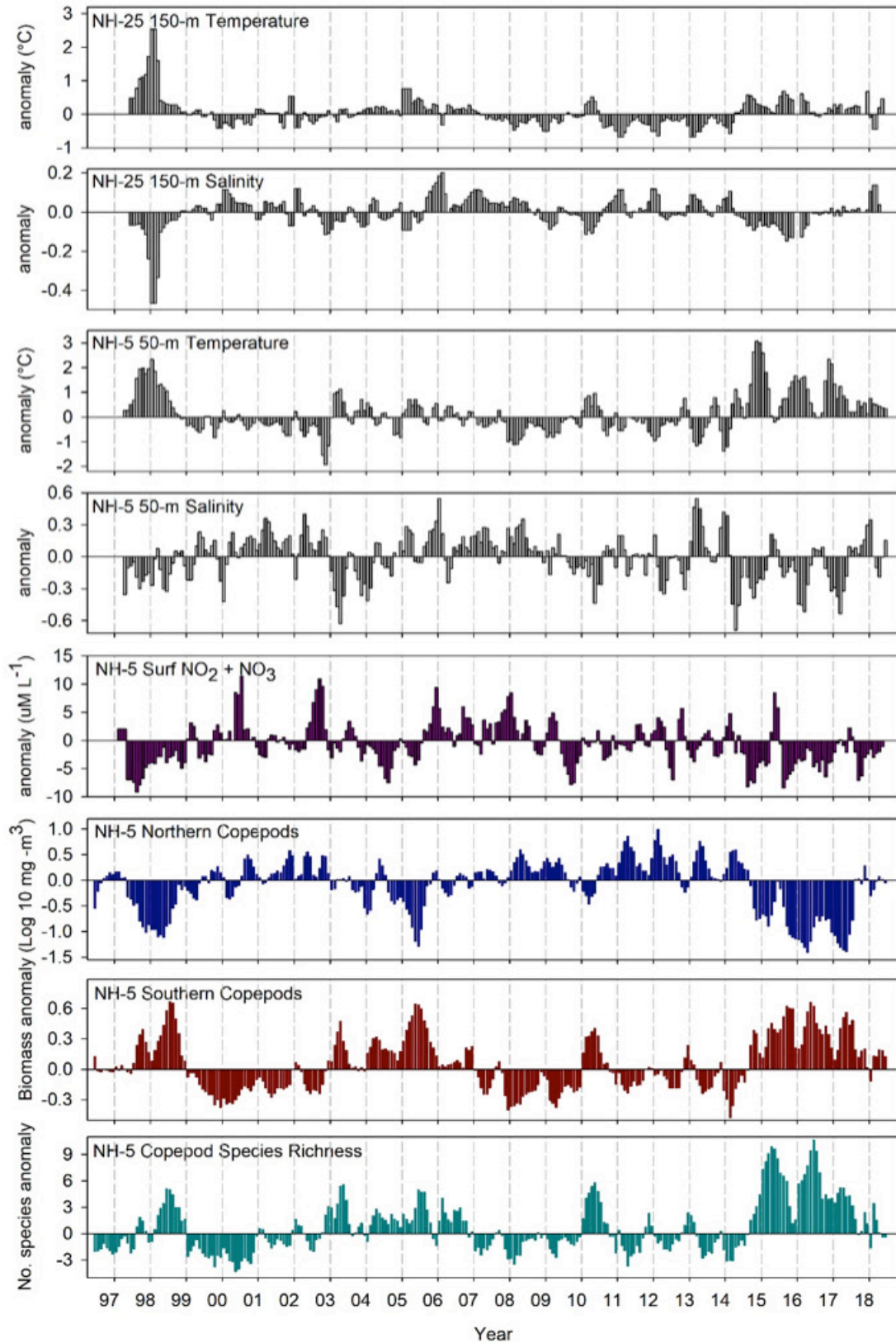


Figure 11. Time series plots of local physical and biological anomalies (monthly climatology removed) from 1996–present at NH-25 (Latitude: 44.6517 N Longitude: 124.65 W; top two panels) NH-5 (Latitude: 44.6517 N Longitude: 124.1770 W; lower six panels) along the Newport Hydrographic Line. Temperature and salinity are from 150 m and 50 m at NH-25 and NH-5, respectively, NO₂ + NO₃ from the surface, and copepod biomass and species richness anomalies are integrated over the upper 60 m. All data were smoothed with a 3-month running mean to remove high frequency variability.

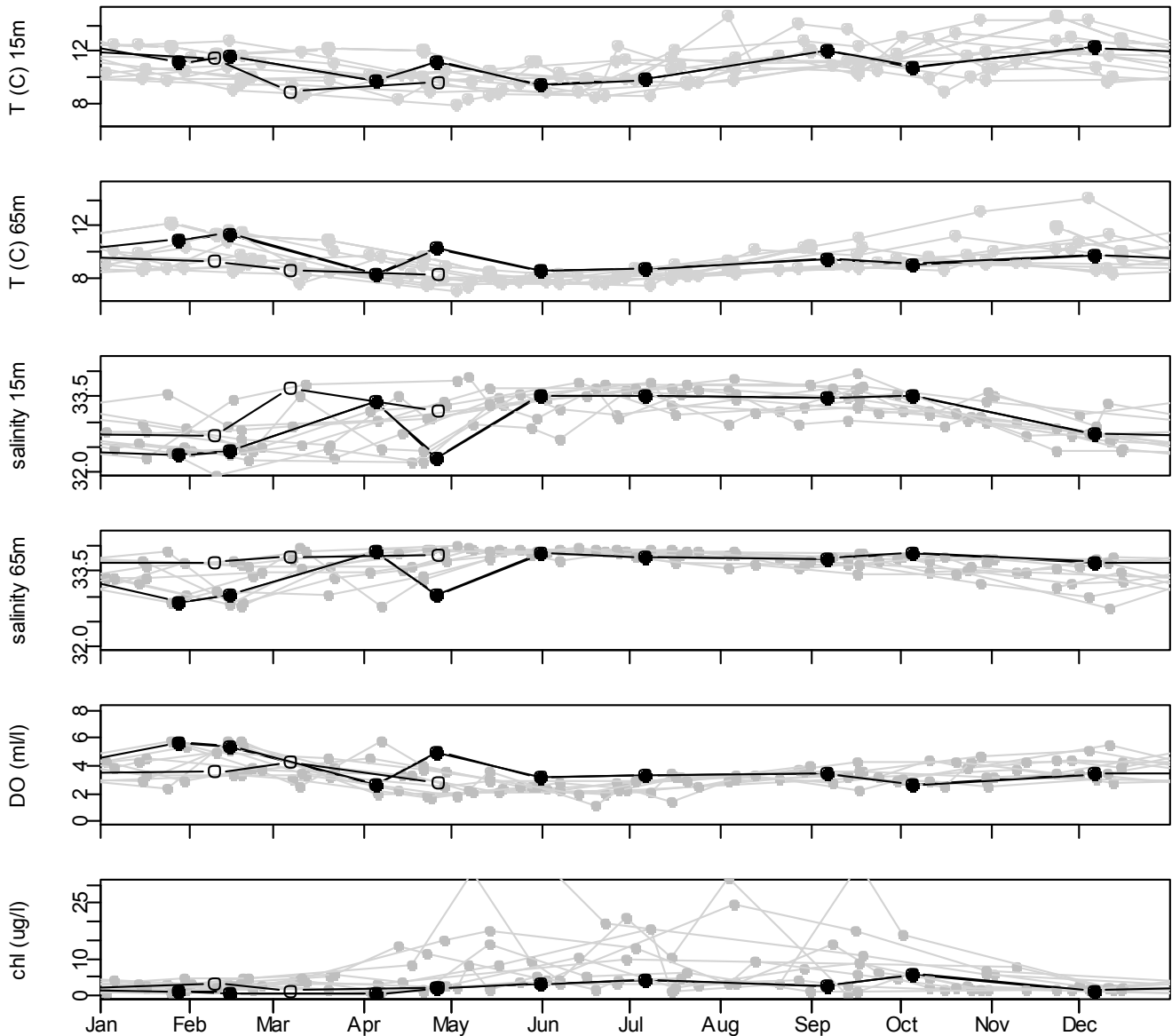


Figure 12. Hydrographic observations along the Trinidad Head Line (THL) at station TH02. Panels from top to bottom show temperature (T) at 15 m, temperature at 65 m (near the sea floor), salinity at 15 m, salinity at 65 m, dissolved oxygen (DO) at 65 m, and mean (uncalibrated) chlorophyll a (chl) concentration from 2–30 m. Closed black circles are 2017, open circles are 2018, and grey are previous years of the time series.

community transitioned to a more neutral state (fig. 11). When strongly positive temperature anomalies occurred from fall 2014 until summer 2017, strongly positive anomalies of copepod species richness and southern copepod biomass were observed on the Oregon shelf, coupled with strongly negative anomalies of northern copepod biomass. During the persistent upwelling season in 2017 (June–September), the positive temperature anomalies on the shelf and slope weakened as did the strongly positive southern copepod biomass and species richness anomalies, while the northern copepod biomass became neutral. In winter of 2017–18, species richness anomalies and the biomass anomalies of the northern copepods oscillated

from weakly positive to weakly negative, while positive anomalies of the southern copepods persisted.

In 2015 and 2016, the copepod community did not transition from a warm-water winter copepod community to a cold-water summer community (data not shown). This ecologically important biological transition to a lipid-rich, cold-water community also did not occur in 1998, when warm ocean conditions occurred in the NCC. However, this transition did occur in late June 2017, 52 days later than the 21-year average climatology. In 2018 this biological transition occurred in late May, 22 days later than the climatology (data not shown). During the spring and summer of 2018, the shelf and slope water were still warmer than average off

Oregon and abundances of southern copepods on the shelf were higher than normal. However, the biomass of the northern copepods was more neutral, signaling that the pelagic ecosystem was in a state of flux between a warm and a cold upwelling copepod community.

Another indication that the pelagic ecosystem did not fully return to a cold water, lipid-rich state in 2018 is the presence in high densities of the subtropical colonial tunicate (*Pyrosoma atlanticum*; pyrosomes). These organisms are common in subtropical open ocean environments, and they bloomed in large numbers throughout the coastal waters from Oregon to the Gulf of Alaska during the winter of 2016 (Brodeur et al. 2018). These organisms were collected in large numbers throughout 2017 when they increased in density and individual size compared to 2016 (data not shown). After the onset of upwelling in 2017, these organisms were rarely collected on the shelf off Newport Oregon, but following the fall transition, they again started washing up on Oregon beaches in high densities. Pyrosomes were collected again during our surveys in the winter and spring of 2018 when they were observed in the highest densities compared to our previous surveys, indicating that the pelagic ecosystem has still not returned to a neutral state.

Northern California Current: Northern California (Trinidad Head Line: THL)

Coastal waters off northern California (THL, station TH02), were relatively warm and fresh during early 2017, but cooled in response to moderate upwelling during summer, and remained near typical (seasonal) temperatures throughout the rest of the year (fig. 12).¹¹ Limited relaxation from upwelling and minimal storm activity during winter 2018 maintained relatively cool, salty waters over the shelf, and near-bottom waters continued to cool as spring upwelling commenced. Surface waters warmed in late spring, but were still cool relative to 2017. Chlorophyll *a* concentrations remained low throughout 2017 and spring 2018. No hypoxic events were observed.

Zooplankton community and population data in 2017 and 2018 indicated a shift toward assemblages and size structure more typical of conditions prior to the marine heat wave. Warm water krill *Euphausia recurva* and *Nyctiphanes simplex* were observed during the first half of 2017 but have since been absent along the THL. In contrast, observations of *Thysanoessa spinifera* adults, a cool-water species which had been largely absent during the marine heat wave, increased in frequency in 2017. By early 2018 *T. spinifera* was observed in relatively high abundance compared to the previous three years (data not shown). Mean length of *Euphausia pacifica* increased throughout the 2017 upwelling season and for most of the year average size was near or slightly above the time series mean, but did not achieve sizes typical of the seasonal summer maxima observed prior to the marine heat wave (fig. 13). The decline in mean length observed during 2017–18 winter was typical of pre-heat wave conditions, with wintertime mean lengths remaining greater than those observed during much of the previous three years. Early 2018 data indicated a relatively strong response to seasonal upwelling: by late April average length was comparable to lengths measured prior to the arrival of the marine heat wave in late 2014. Large pyrosomes were frequently encountered in early 2017 but had mostly disappeared by summer. Small pyrosomes persisted through fall. Large pyrosomes were again observed in early 2018, but less frequently and at lower densities relative to 2016 and 2017. Small ctenophores were abundant for a brief time during spring 2018.

¹¹Hydrographic data and plankton samples have been collected along the Trinidad Head Line since late 2007 as a source of information on ecosystem state and response to climate forcing. Hydrographic data are collected with a Sea Bird Electronics (SBE) model 19 plus V2 CTD (19 plus until September 2014) cast to a maximum depth of 500 m (150 m until August 2014) or to within a few meters of the seafloor. Zooplankton are sampled with a 0.7 m diameter Bongo net fitted with dark mesh (505 µm) and General Oceanics flowmeters deployed rapidly to a maximum depth of 100 m (or within a few meters of the sea floor) and retrieved along an oblique profile by maintaining a steady wire retrieval rate (20 m min⁻¹) and adjusting ship speed through the water to maintain a wire angle (45° ± 5°) throughout the tow.

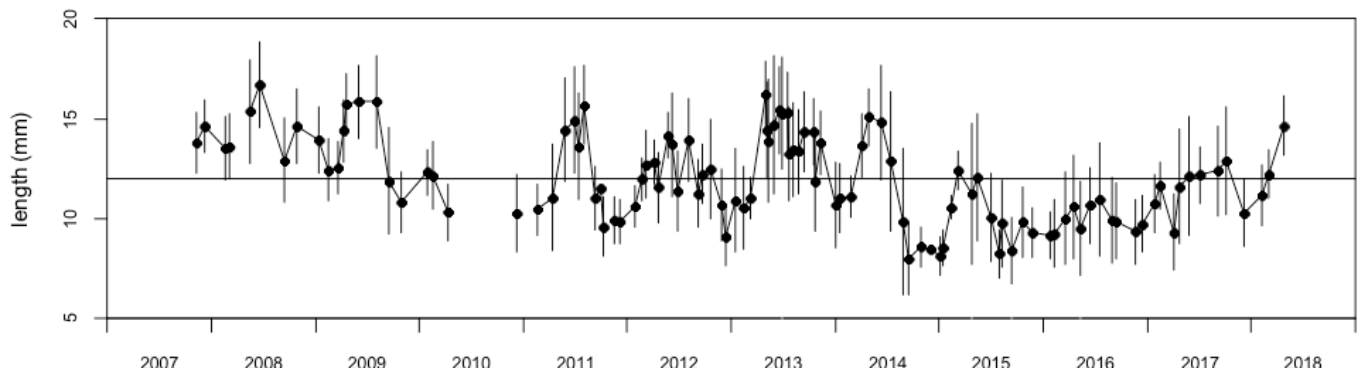


Figure 13. Density-weighted mean (points) and standard deviation (whiskers) of rostral-dorsal length of adult *Euphausia pacifica* collected along the Trinidad Head Line (aggregated over stations TH01 to TH05). Horizontal line indicates mean length taken over entire time series. Samples are collected by fishing bongo nets (505 µm mesh) obliquely from a maximum depth of 100 m (or within a few meters of the sea floor in shallower areas) to the surface.

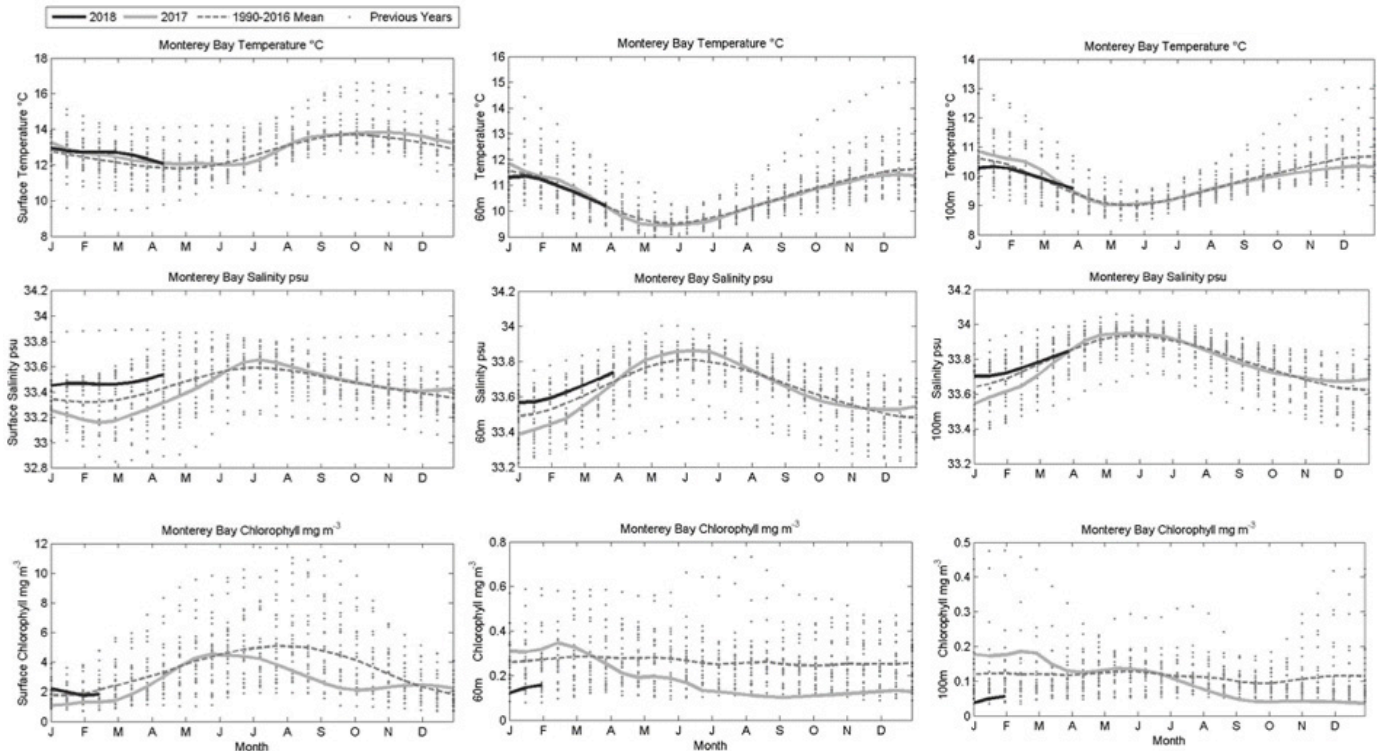


Figure 14. Temperature (top panels), salinity (middle panels), and chlorophyll *a* concentration (bottom panels) at the surface (left panels), 60 m (center panels), and 100 m (right panels) observed at the M1 mooring in Monterey Bay, CA.

Central California Current: Monterey Bay

Temperatures at the surface, 60 m and 100 m, were very close to average through 2017 and the first four months in 2018 (fig. 14). Salinity was also close to average at all depths throughout all months in 2017, was slightly elevated near the surface from January–April in 2018, but was closer to average in 2018 at 60 m and 100 m. In contrast with temperature and salinity, chlorophyll *a* patterns changed greatly with depth. At the surface, chlorophyll *a* was average from January–June, fell well below average from August–October, then returned to average in November 2017 and remained at average values through mid-February 2018. At 60 m chlorophyll *a* was slightly above average in the beginning of 2017, fell below average in April, and was well below average from June 2017–February 2018. At 100 m chlorophyll *a* was above average at the onset of 2017, became average from April–July 2017, then fell to well below average from August 2017 to February 2018.

Central and Southern California: Remotely Sensed SST and Chlorophyll *a*

Remotely-sensed¹² SST and chlorophyll *a* data were averaged throughout inshore (fig. 15A, area 3) and transitional (fig. 15A, area 2) regions in central California and inshore (fig. 15A, area 6) and transitional areas (fig. 15A, area 5) in southern California. Analyses

showed that conditions in 2017 and the first half of 2018 were close to typical in all four regions; this was a marked change from extreme anomalies of 2014–16 that in many areas resulted in all-time highest measurements of SST and all-time lowest chlorophyll *a* (Kahru et al. 2018) and minima in the frequency of surface fronts. During 2017 SST remained slightly above the long-term average (by nearly 1°C), but by mid-2018 the SST values were close to the long-term means (fig. 15B). In July–August 2018, however, SST in southern California waters rose rapidly and had a positive anomaly >2°C in July 2018. Elevated SST was restricted to the inshore southern California region in July 2018 (fig. 15B, area 6) as offshore SST values were close to average (fig. 15B, area 5). Chlorophyll *a* values were close to normal in 2017 and in the first half of 2018 (fig. 15C, area 6). In 2017–18 chlorophyll *a* was slightly below the long-term means in the transitional areas (fig. 15C, areas 2 and 5) and very close to normal in the coastal areas (fig. 15C, areas 3 and 6). Despite high SST in southern California, chlorophyll *a* was at an average level in July 2018.

¹²SST data were derived from the version 2.0 daily datasets of optimally interpolated global blended AVHRR temperatures (https://podaac.jpl.nasa.gov/dataset/AVHRR_OI-NCEI-L4-GLOB-v2.0?ids=Platform&values=NOAA-18). Chla data were derived from the merged multisensor regionally optimized Anomalies were calculated relative to the long-term (1981–2018 for SST, 1996–2018 for Chla) mean monthly values. For SST these were difference anomalies; for Chla the anomalies are reported as ratio anomalies expressed as %.

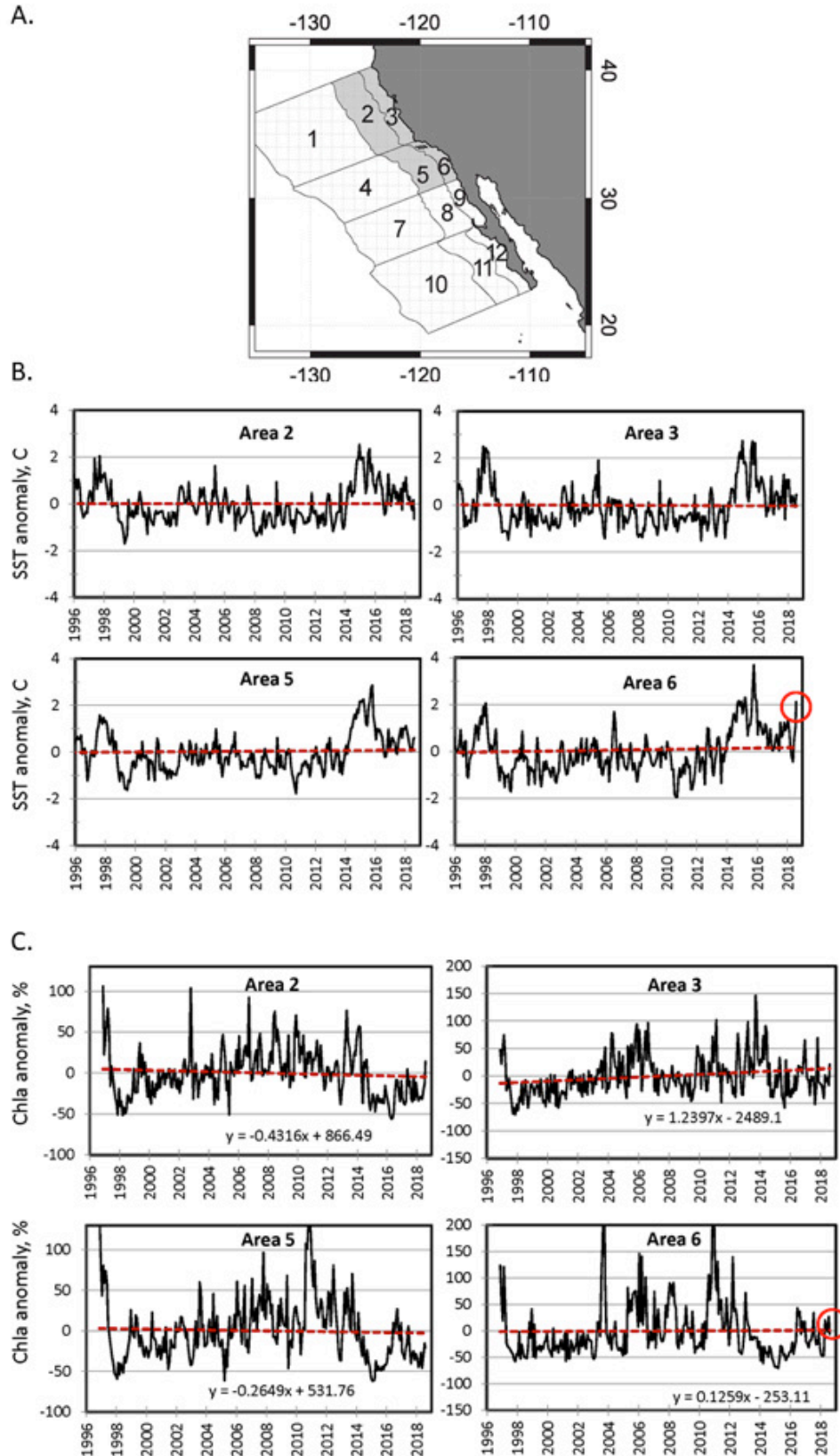


Figure 15. A) Map of the selected coastal (0–100 km from coast, areas 3, 6) and transition (100–300 km from coast, areas 2, 5) areas off central and southern California; B) SST anomalies relative to monthly means of Sept. 1981–June 2018; and C) chlorophyll a anomalies relative to monthly means of Nov. 1996–June 2018 in each area. The red dashed lines show the mean linear trends. Red circles in Area 6 highlight June 2018 when SST rose dramatically but chlorophyll a remained close to the long-term mean.

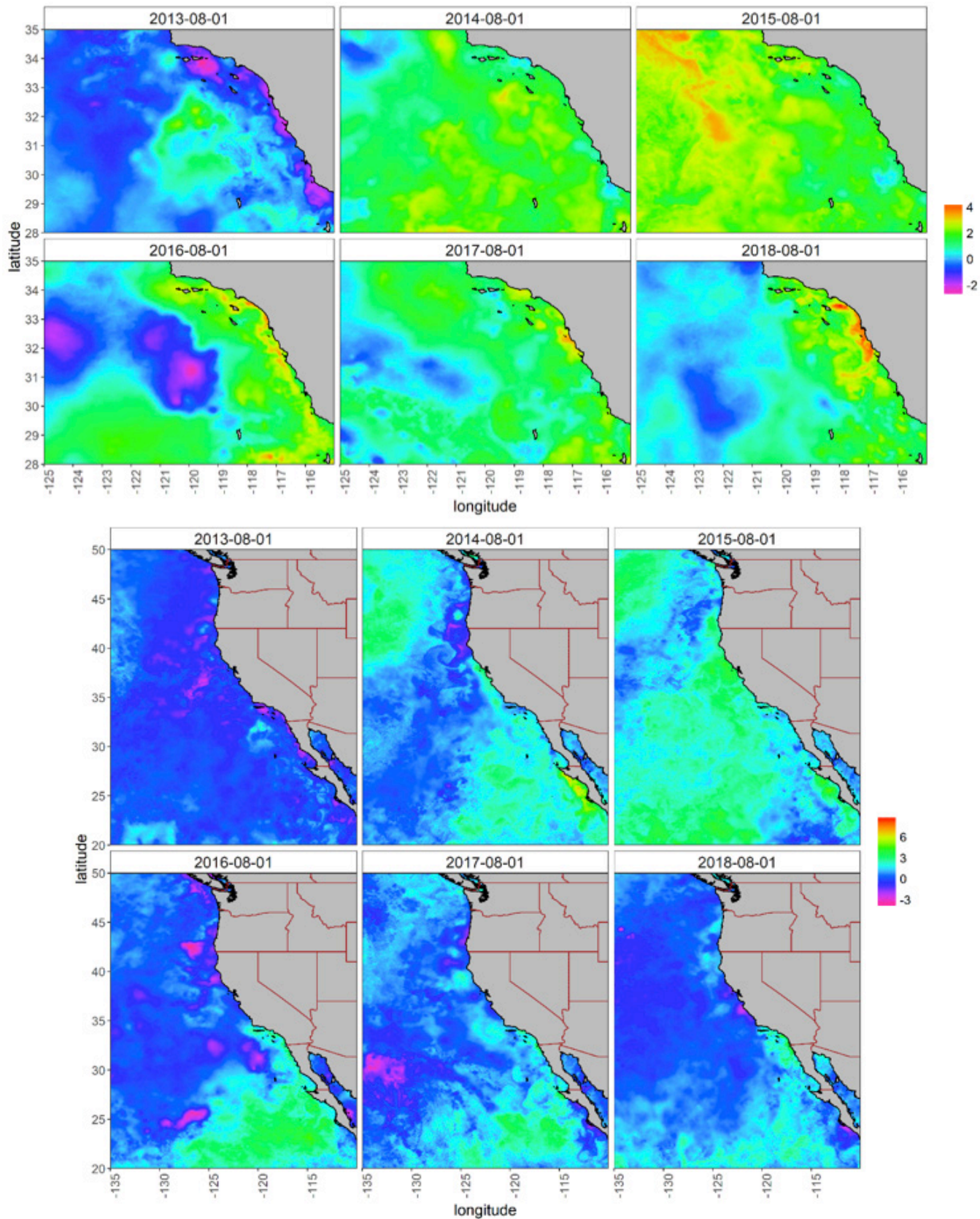


Figure 16. Remotely sensed SST anomalies on August 1, 2013-18. Top panels are centered on the southern California Bight. Bottom panels expand the focus to also envision the central and northern CCS.

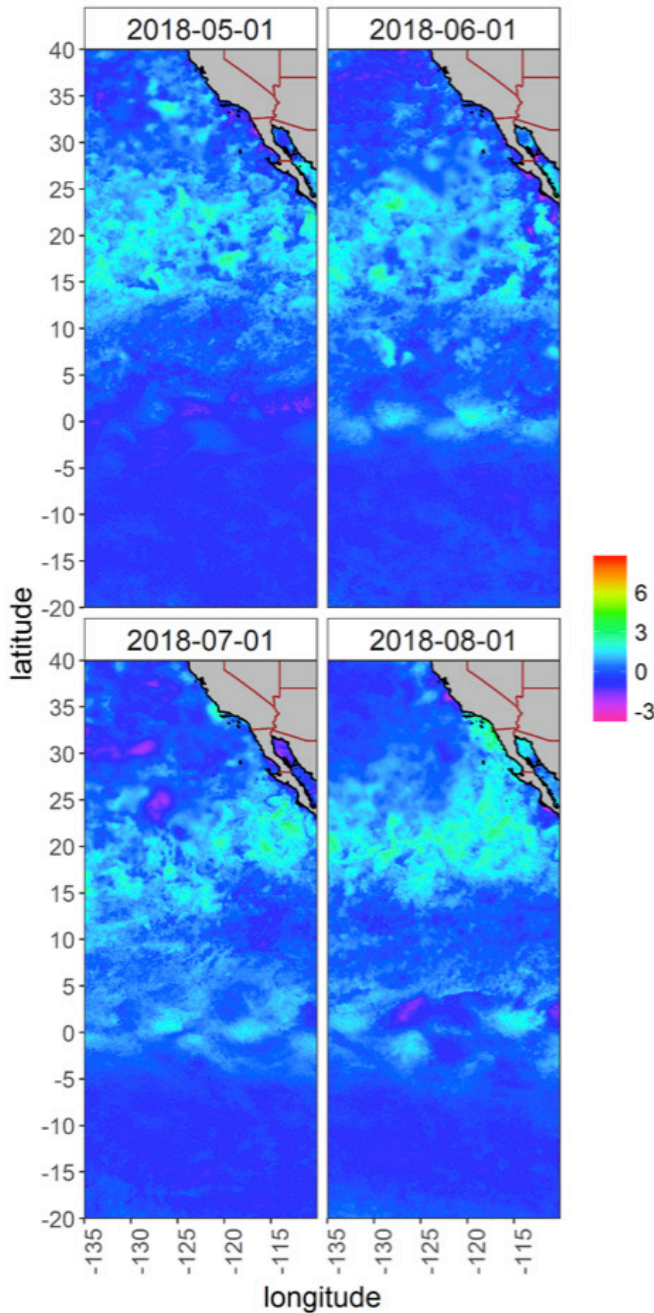


Figure 17. Remotely sensed SST anomalies on the first day of May–August 2018 in the central and equatorial Pacific with the SCB in the upper right corner of each panel.

Satellite SST¹³ imagery in August from 2013–18 demonstrated that subsequent to 2013 temperatures were consistently anomalously high in southern California (fig. 16 top panels). While elevated summer SST extended north of Point Conception and permeated most of the CCS in 2014–15, warm SST in the CCS

¹³SST measured by Multi-scale Ultra-high Resolution (MUR) SST Analysis Anomaly fv04.1, Global, 0.01°, Daily. <https://podaac.jpl.nasa.gov/dataset/MUR-JPL-L4-GLOB-v4.1>

was primarily between Point Conception and Bahia de Sebastes Vizcaino, Baja California, in August 2016–18 (fig. 16 bottom panels). Evaluation of SST anomalies at a broader scale shows the evolution of the warm water off southern California and northern Baja California in summer 2018 (fig. 17). While SST was consistently above normal in the central Pacific between May and August 2018, SST was actually below normal on May 1 between southern California and Bahia de Sebastes Vizcaino. By June 1 and through July 1 SST from southern California to Bahia de Sebastes Vizcaino was slightly above normal. By August 1, however, SST was close to 4°C above normal in many areas in this region. In fact, the daily maximal temperature of 25.9°C recorded August 1 off the Scripps Pier in La Jolla, California, was the highest in the 102-year record (fig. 18). Further, SST increased in the central and eastern Pacific between approximately 20° and 30°N such that a swath of warm water linked the central Pacific with southern California and northern Baja California (fig. 17).

Southern California Current: CalCOFI Survey in Southern California¹⁴

From mid-2017 to spring 2018, mixed layer (ML) temperature anomalies were slightly, but significantly, above the long-term average (fig. 19A) in spite of mild La Niña conditions at the equator (according to the ONI index; fig. 2B). Higher than normal ML temperatures were observed in all regions of the CalCOFI study area except the upwelling region¹⁵ through spring. During June 2018, however, very high temperature anomalies were observed in the northern part of the Southern California Bight (fig. 20A). ML salinity increased significantly from the summer of 2017 through early 2018 (fig. 19B, C). This increase was particularly strong in the far offshore and the California Current region, less so in the coastal upwelling regions, and undetectable in the Southern California Bight (data not shown). In the California Current region, the anomalies reached depths of 125 m, but only 75 m in the offshore region. The association of the anomalies with the offshore and the California Current is evident during the early summer of 2018 (fig. 20B) when positive salinity anomalies were particularly strong in the California Current region. These patterns make it likely that these anomalies are linked

¹⁴Methods used to collect and analyze samples from CalCOFI cruises are described in detail at CalCOFI.org/methods. Results are presented as time series of properties averaged over all 66 standard CalCOFI stations covered during a cruise or as anomalies of such values with respect to the 1984–2012 period.

¹⁵When appropriate, averages from selected regions are used based on a subset of the 66 standard CalCOFI stations. These regions (and corresponding CalCOFI stations) are the offshore (Line77Station100, L80St100, L83St100, L87St100–110, L90St90–120, L93St80–120), the southern California Current (L77St70–90, L80St70–90, L83St70–90, L87St70–90, L90St60–80), upwelling areas (L77St49–60; L80St51–60; St82.46, L83St51–60, L87St45–55) and the Southern California Bight (L83St41–42, L87St33–40, L90St28–45, L93St27–45).

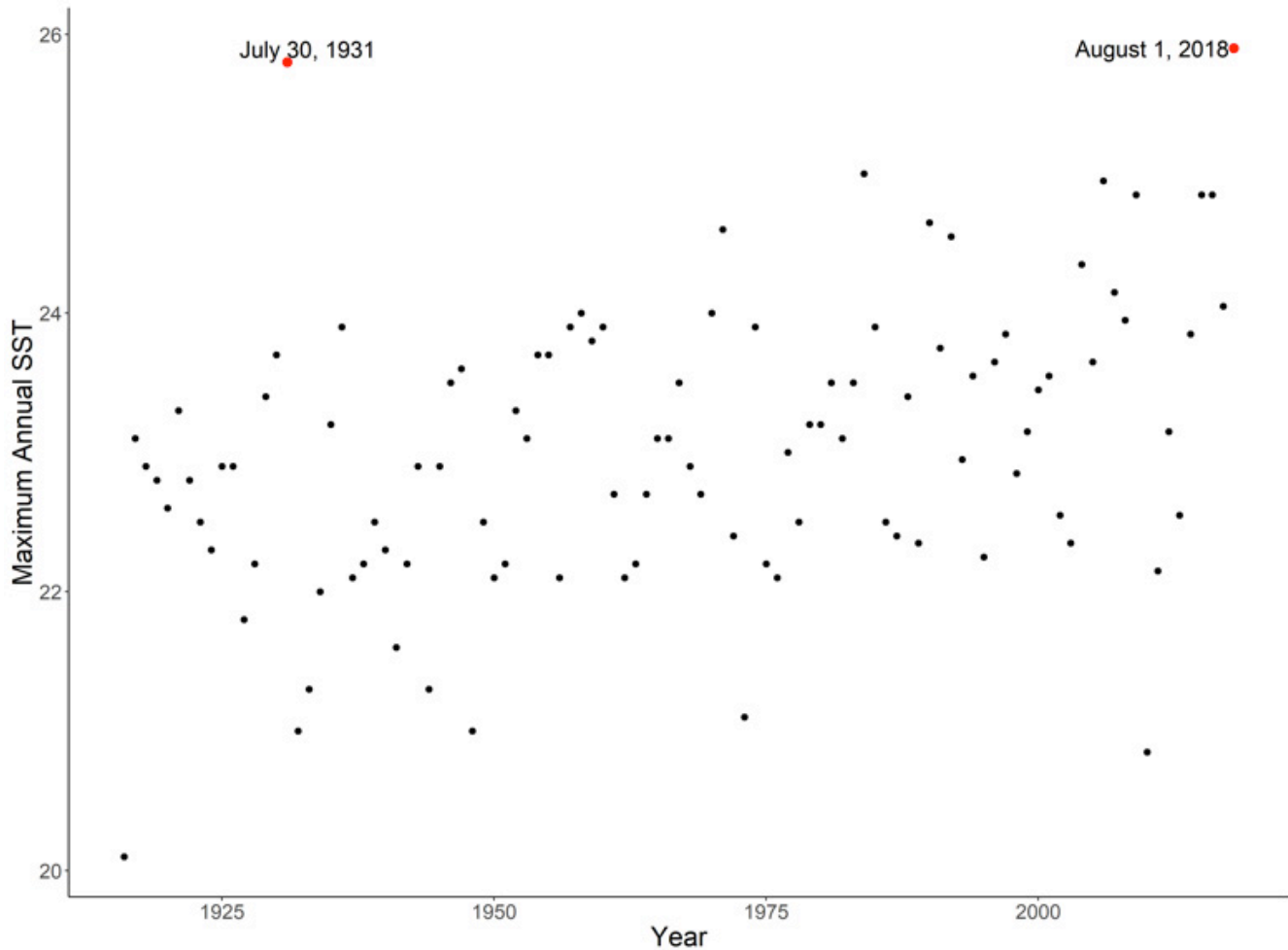


Figure 18. Maximum daily SST in a year from the Scripps Pier in La Jolla, California. The two highest days, July 30, 1931 and August 1, 2018 are highlighted in red.

to changes in the surface waters of the eastern North Pacific. Indeed, the remote-sensing based salinity time series of Xie et al. (2014)¹⁶ shows a large salinity anomaly in the eastern North Pacific during 2016, moving towards the North American continent during 2016–17 and impinging on the CalCOFI sample frame in spring and summer 2018.

Strong variations of ML salinity (fig. 19C) in the past have been linked to changes in the NPGO index, which is also thought to control concentrations of nutrients and phytoplankton biomass in the California Current System (Di Lorenzo et al. 2008). However, recent trends in salinity in southern California and NPGO do not align. To further investigate this pattern, CalCOFI domain salinities (fig. 19B, n=137) were regressed against values of the NPGO at coupled sampling times. The regression was highly significant, but the r^2 was very low (0.12). Further, the residuals were significantly temporally autocorrelated (Durbin-

Watson test $p < 0.0001$). A partial autocorrelation analysis suggested that the salinity time series needed to be modeled as an autoregressive (AR1) process. Thus, an ARX(1,0) model was fit to the salinity time series with the NPGO time series as a predictor. The autoregressive part of the regression was large ($a = 0.59$) and highly significant ($p < 0.001$), but the effect of the NPGO on salinity was no longer significant ($p > 0.4$). These results suggest that CalCOFI domain salinity variability over the last few decades is no longer “explained” by the NPGO. This result adds to the growing body of evidence that cautions against using ocean climate indices such as the PDO, and by inference the NPGO, to predict ocean state (Newman et al. 2016).

To investigate the salinity maximum further, properties on the σ_t 25.8 isopycnal averaged over the California Current were studied. Since the beginning of 2017, the depth of the isopycnal, on average 117 m (range of 95–149 m), was close to its long-term average (fig. 21A). Spiciness on the isopycnal over the last year increased (fig. 21B), mirroring the increase in ML

¹⁶updated at <ftp://ftp.cpc.ncep.noaa.gov/precip/BASS/>

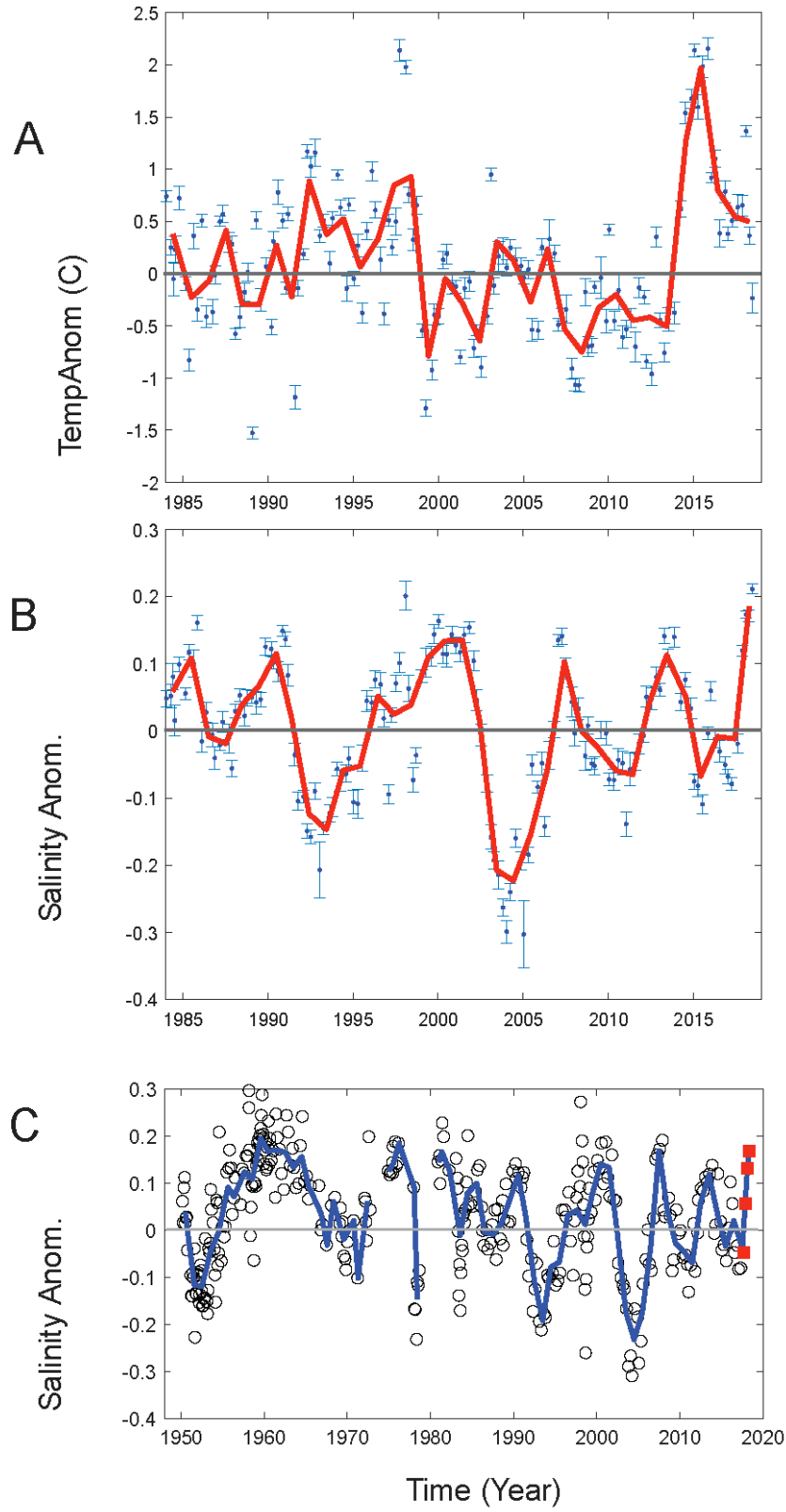


Figure 19. Cruise averages of mixed layer (ML) temperature anomalies (A) and ML salinity anomalies (B) for the 66 standard CalCOFI stations (fig. 1) for 1984 to the summer (June) of 2018, and C) ML salinity anomalies along CalCOFI Line 90 (St 30-90) are shown for 1950 to the present. Whiskers indicate the 95% confidence intervals for the means. Red solid lines represent annual averages, grey horizontal lines the climatological mean, which is zero in the case of anomalies. Anomalies are based on the 1984 to 2012 period.

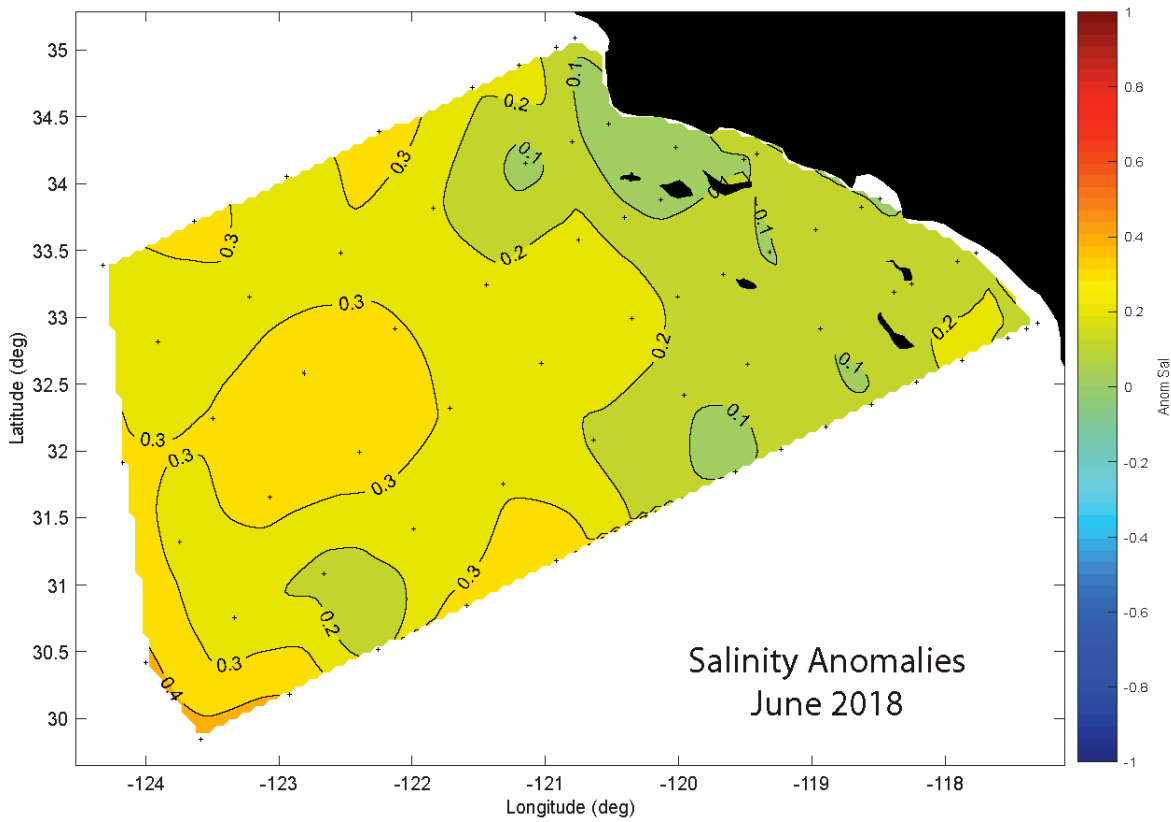
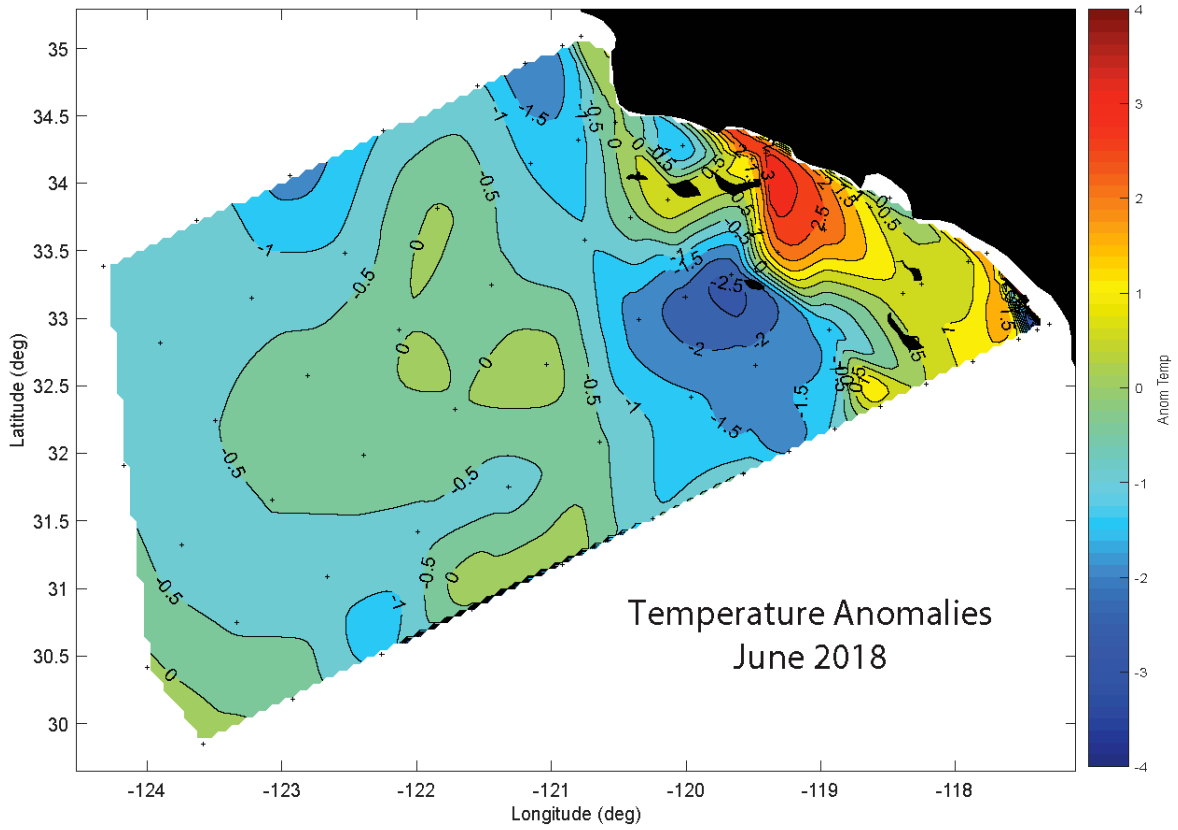


Figure 20. A) Temperature and B) salinity anomalies at 10 m for the summer 2018 CalCOFI cruise.

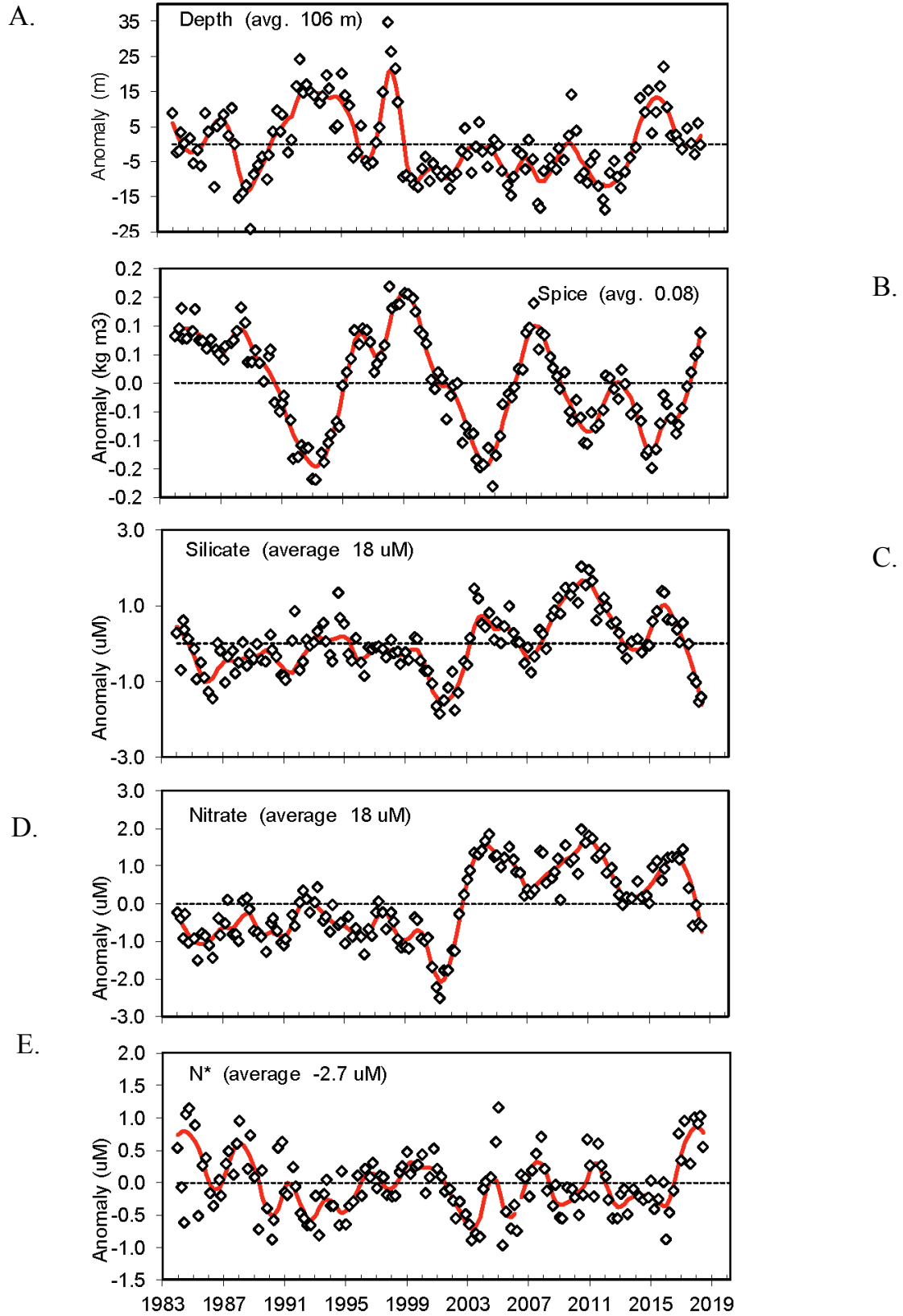


Figure 21. Anomalies of hydrographic properties at the 25.8 isopycnal (open diamonds) averaged over the 66 standard CalCOFI stations. Shown are anomalies of A) isopycnal depth, B) spiciness, and concentrations of C) silicate D) nitrate, and E) phosphate (N*). The solid red line represents a loess fit to the data; average values for the properties are listed.

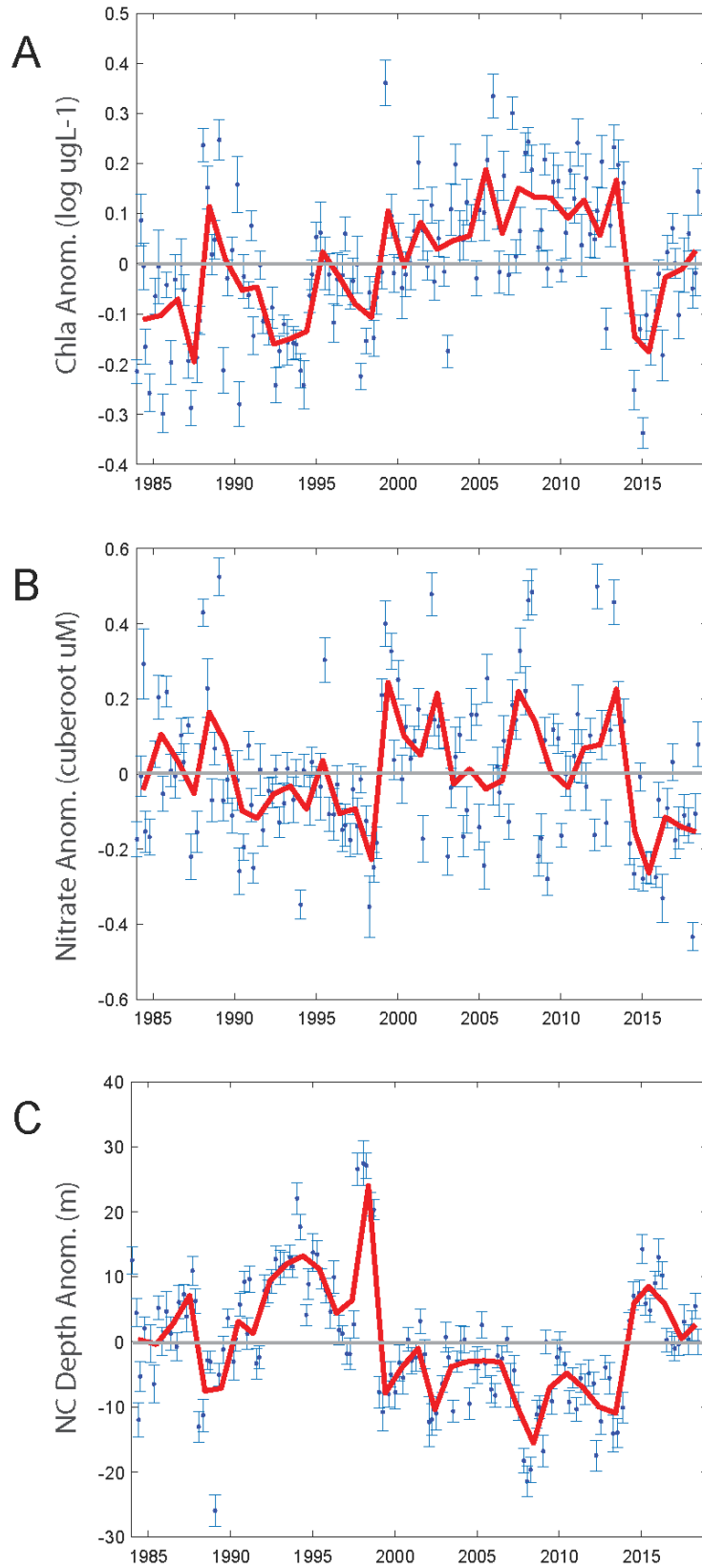


Figure 22. Cruise averages of properties at 10 m depth for the CalCOFI standard 66-station grid. A) The log10 of chlorophyll a. B) the cube root of nitrate. C) nitracline depth. Data are derived and plotted as described for Figure 19.

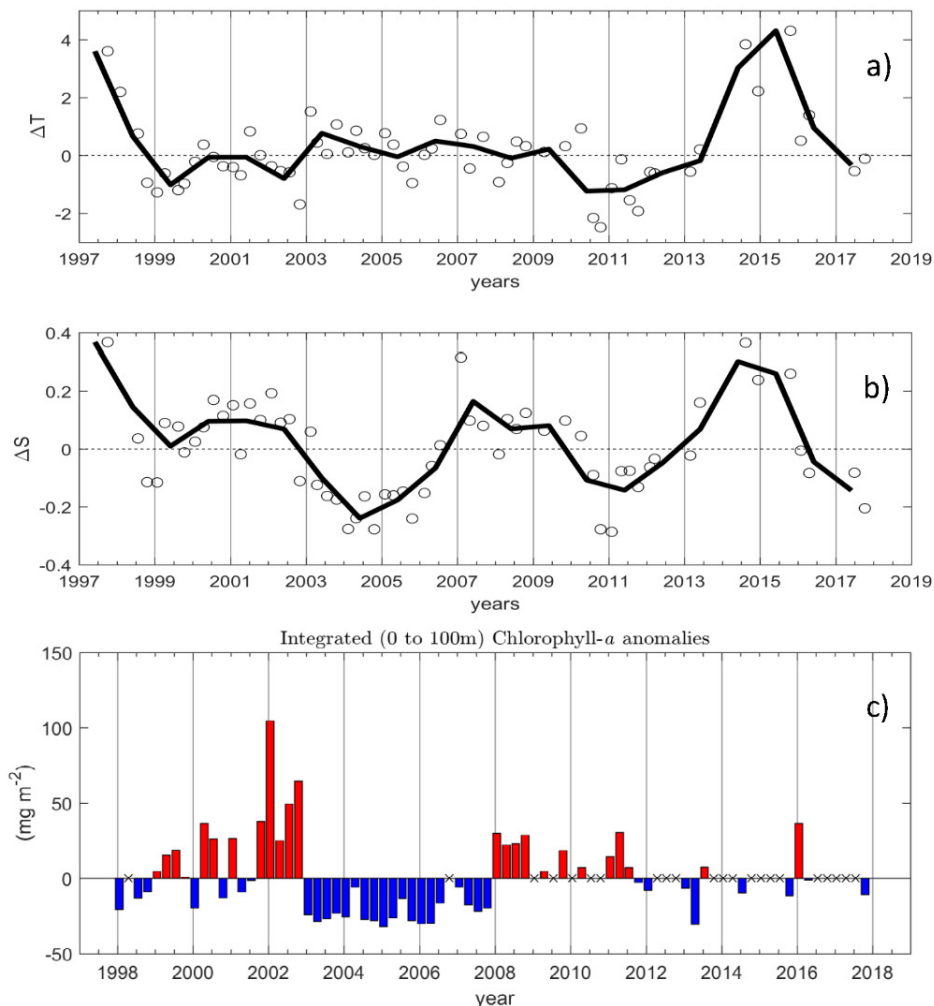


Figure 23. Interannual variability of a) mixed layer temperature (°C); b) mixed layer salinity (PSU) anomalies in the IMECOCAL survey area from October, 1997 through October, 2017 (white circles) and the mean of each year (heavy line); c) depth integrated (0–100 m) chlorophyll *a* anomalies (mg m⁻²) over the IMECOCAL survey area indicated by red and blue bars. The anomalies were obtained by removing the seasonal means from the chlorophyll *a* data (1998–2017). Missing data points from the series of chlorophyll *a* anomalies are indicated by “x.”

salinity. Concurrent with the increase of spiciness, concentrations of nutrients on the isopycnal decreased dramatically (fig. 21C–E). These results are similar to those of McClatchie et al. (2018) and are consistent with an increasing impact of warm saline and low nutrient subtropical waters in the CalCOFI region, suggesting a change in the balance of its source waters.

During the 2014 marine heat wave and the 2015–16 El Niño ML chlorophyll *a* was extremely low, but over the last two years it increased to values similar to the long-term average (fig. 22A). Depth distributions of chlorophyll *a* in different regions paint a similar picture; in the offshore and the Southern California Bight it was similar to long-term averages with the exception of the California Current region where chlorophyll *a* was below average (data not shown). It is possible that this difference is driven by a decrease of nutrients in the California Current (fig. 21). ML nitrate concentrations

(fig. 22B) have covaried with ML chlorophyll *a* since 2014 suggesting that the latter was controlled by the former. Variations of nitracline depth¹⁷ suggest that the supply of nitrate from depth limits ML nitrate concentrations (fig. 22C).

Southern California Current: Baja California (IMECOCAL)¹⁸

Temperature anomalies within the ML from October, 1997 through October 2017 over the northern IMECOCAL region (fig. 23A) demonstrated that the anomalous warming in 2014–15 began to diminish

¹⁷The nitracline depth is defined as the depth where concentrations of nitrate reach values of 1 μM, calculated from measurements at discrete depths using linear interpolation

¹⁸The IMECOCAL program has conducted quarterly cruises of the Baja California peninsula beginning in October 1997. However after 2012 has been more sporadic and during 2016 and 2017 coverage was limited to the northern region off Baja California (28–32°N).

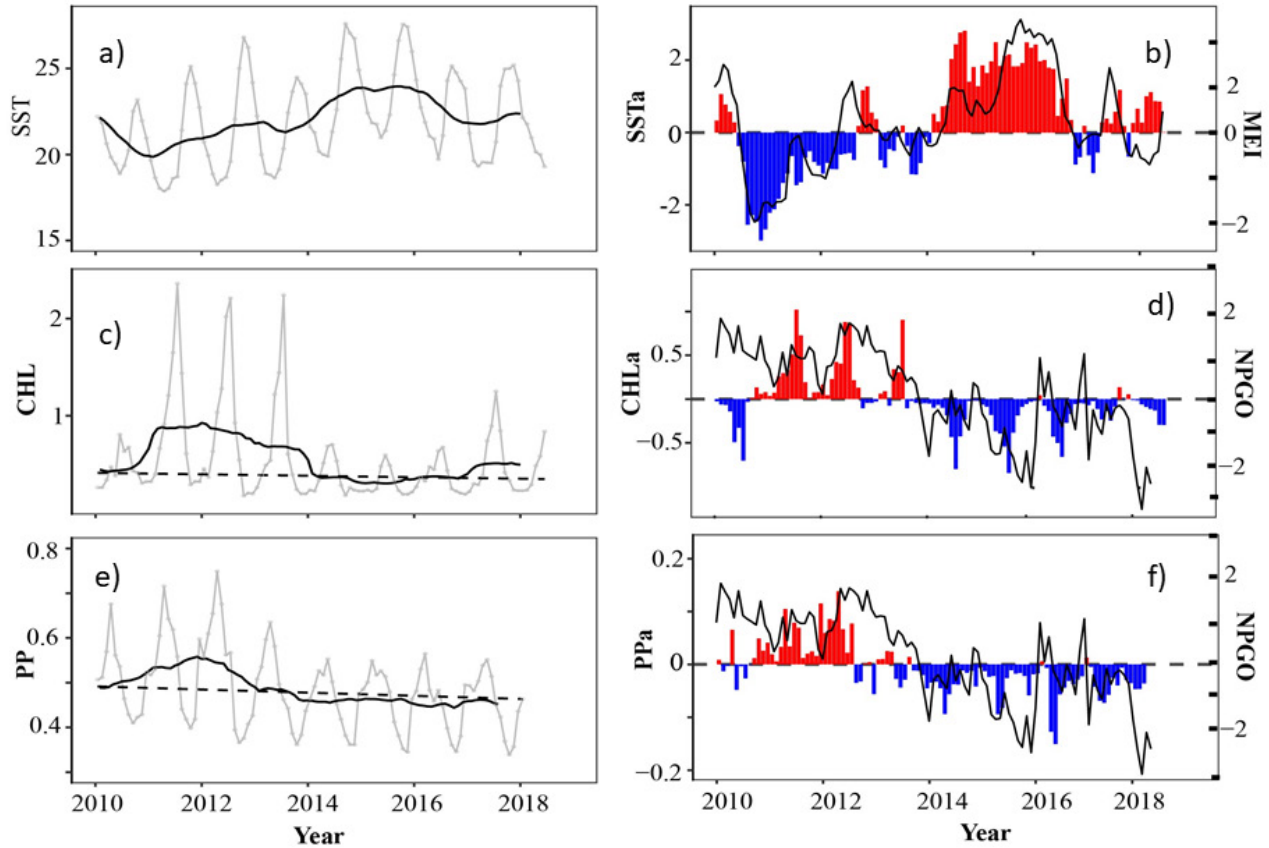


Figure 24. Satellite-derived time series (left panels) and anomalies (right panels) from 2010 through 2018 in the northern region of the IMECOCAL survey domain (28°–32°N) for a) sea surface temperature (SST: C°) and b) anomalies (SSTa: C°); c) chlorophyll *a* (CHL: mg m⁻³) and d) anomalies (CHLa: mg m⁻³); and e) primary production (PP: gCm⁻² d⁻¹) and f) anomalies (PPa: gCm⁻² d⁻¹). The SST anomalies (SSTa) are shown together with the Multivariate ENSO Index (MEI); the chlorophyll anomalies (CHLa) and the primary production anomalies (PPa) are shown along with the NPGO index. The light grey lines are the annual cycles composed of monthly averages in the SST, CHL, and PP plots; the heavy black lines are 12 month running means. The long-term means of CHL and PP are shown by heavy dashed lines.

in early 2016, and ML temperature anomalies in 2017 were slightly negative. Similarly, ML salinity anomalies decreased to negative levels in 2016 and 2017 (fig. 23B).¹⁹ Chlorophyll *a* anomalies averaged from the surface to 100 m were slightly negative in October 2017 (fig. 23C).

Evaluation of interannual variability of depth-integrated chlorophyll *a* anomalies²⁰ from 1998 through October 2017 in the IMECOCAL region indicates that there is significant decadal-scale as well as inter-annual variability (fig. 23C). It should be noted that there are important differences in this chlorophyll *a*

anomaly series from the IMECOCAL region compared to that presented in Figure 18 in Wells et al. (2017) due to a necessary correction in the calibration of the chlorophyll *a* data. The series now appears to better agree with the chlorophyll *a* anomalies in areas 5 and 6 of the CalCOFI region (fig. 4 in McClatchie et al. 2016b).

Monthly satellite-derived measurement of SST²¹ over the IMECOCAL region showed that it was cooler than normal in early 2017 but became warmer than normal in late 2017 and was approximately 1°C above normal by mid-2018 (figs. 24A, B). Satellite measurements of chlorophyll *a* and primary production were mostly negatively anomalous from mid-2017 to early 2018 (figs. 24C–F). In fact, these variables have been below average nearly all the time within the IMECOCAL region from late 2013 to early 2018 (figs. 24C–F). Notably, trends in SST, chlorophyll *a*, and primary production seemed to correspond with basin scale indices as SST correlated positively with the Multivariate

¹⁹The hydrographic data were Seabird sensors factory calibrated prior to each cruise. CTD data were processed with Seasoft based on EOS-80; thermodynamic variables were then computed using MATLAB functions from SEA-MAT. The mixed layer depth was estimated following methodology in Jeronimo and Gomes-Valdes (2010) for the IMECOCAL grid. Harmonics were computed for mixed layer properties for all stations for which sufficient data exists. The long-term variability follows the approach used by (Bograd and Lynn 2003).

²⁰Phytoplankton chlorophyll *a* data were taken from water collected at discrete depths in the upper 100 m, filtering through Whatman GF/F filters following the fluorometric method (<https://www.nodc.noaa.gov/archive/arc0001/9900162/2.2/data/0-data/jgofscd/Files/protocols/chap14.html>). Depth integrated chlorophyll *a* (0–100m) anomalies were estimated by removing seasonal means.

²¹Monthly composites of satellite sea surface temperature and chlorophyll at 4 x 4 km resolution derived from the MODIS-Aqua sensor were downloaded from <http://coastwatch.pfeg.noaa.gov>.

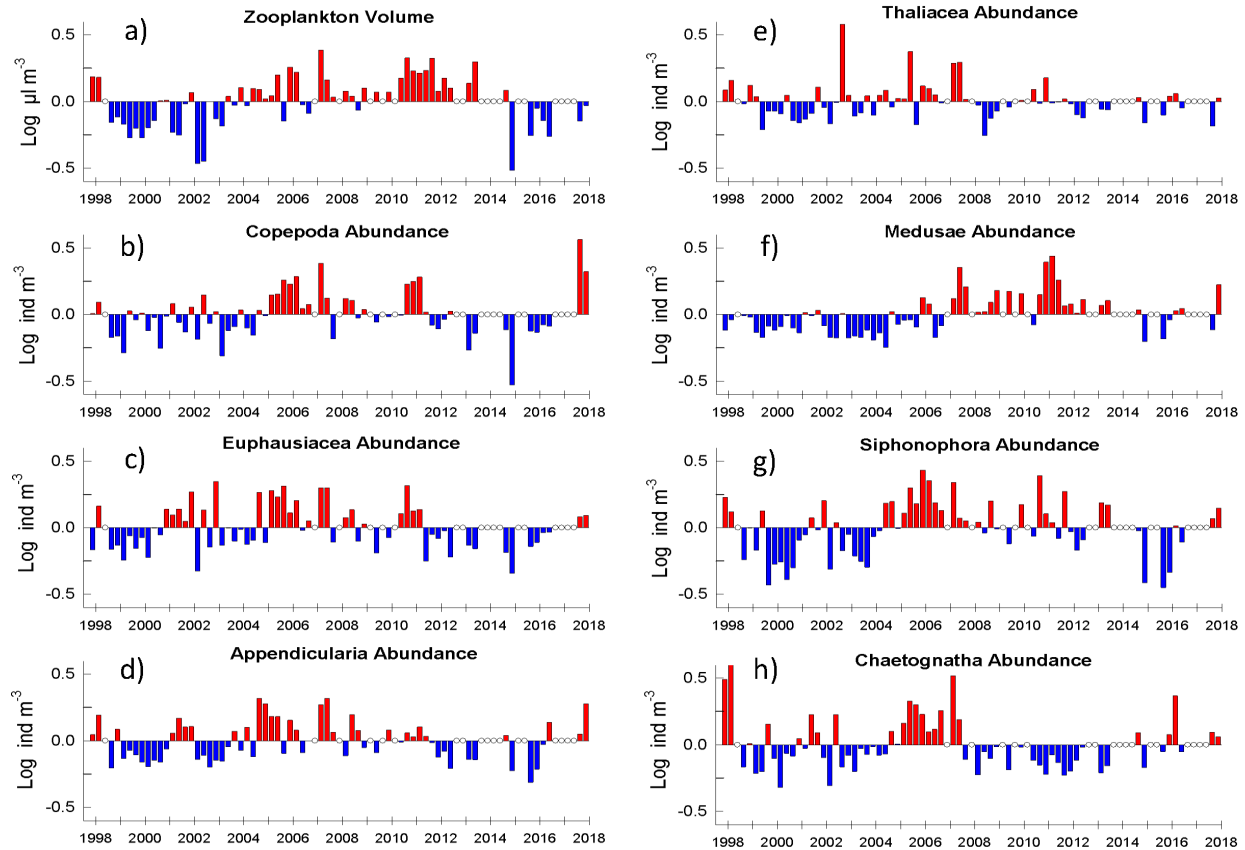


Figure 25. Zooplankton anomalies from bongo tows between Bahia Sebastian Vizcaino and Ensenada. The upper left panel shows zooplankton volume anomalies (a) and the rest show zooplankton abundance anomalies for the main functional groups: Copepoda (b), Euphausiacea (c), Appendicularia (d), Thaliacea (e), Medusae (f), Siphonophora (g), and Chaetognatha (h). Each bar represents a single cruise and open circles represent cruises that did not take place or were omitted due to limited sampling. Data were converted to logarithms prior to estimation of anomalies. The anomalies were season-specific.

ENSO Index²² (fig. 24B), and both chlorophyll *a* and primary production correlated positively with the NPGO (fig. 2, figs. 24D, F).

In June 2017 the zooplankton²³ volume anomaly was slightly negative and much closer to average than the extremely low values from 2014–16 (fig. 25A). The rise in zooplankton volume in 2017 was largely driven by a large increase in copepod abundance (fig. 25B). Euphausiid abundance also rose in 2017 relative to 2014–16 but not as much as copepod abundance (fig. 25C). Among gelatinous herbivores, Appendicularia increased greatly (fig. 24D) and Thaliacea slightly (fig. 25E) in October 2017. In June 2017, however, the Thaliacea abundance anomaly was negative (fig. 25D) mainly due to low numbers of salps and doliolids. Because salps can constitute a large proportion of the overall zooplankton volume (Lavaniegos and Ohman 2007), the negative zooplankton volume anomaly in late 2017 was likely driven by low salp abundances (fig. 25A). Gelatinous

carnivores, Medusae (fig. 25F) and Siphonophora (fig. 25G) displayed moderately positive anomalies in October 2017. Chaetognath abundance anomaly was very close to zero in October 2017 (fig. 25H).

REGIONAL EPIPELAGIC MICRONEKTON AND SALMON OBSERVATIONS

Northern California Current: Washington and Oregon

*Newport Hydrographic Line and Pre-Recruit Survey*²⁴

The ichthyoplankton assemblage along the central-

²²<https://www.esrl.noaa.gov/psd/enso/mei/>

²³Zooplankton were sampled with oblique tows of a bongo net (500-µm mesh) from 210 m to the surface. Displacement volume was measured for all samples; zooplankton taxa were only counted for nighttime samples.

²⁴Ichthyoplankton samples were collected from 3–4 stations representing coastal (<100 m in depth), shelf (100–1000 m), and offshore (>1000 m) regions along both the Newport Hydrographic (NH; 44.65°N, 124.35–125.12°W) and Columbia River (CR; 46.16°N, 124.22–125.18°W) lines off the coast of Oregon during May–July in 2007–18 (For complete sampling methods, see Auth [2011]). Post-larval (i.e., juvenile and adult) fish were collected using a modified-Cobb midwater trawl (MWT) with a 26-m headrope and a 9.5-mm codend liner fished for 15 min at a headrope depth of 30 m and ship speed of ~2 kt. MWT collections were made at 3–6 evenly-spaced, cross-shelf stations representing coastal, shelf, and offshore regions along nine half-degree latitudinal transects between 42.0 and 46.0°N latitude in the northern California Current region during May–July in 2011–18 (although no sampling was conducted in 2012). Sampled volume was assumed to be uniform for all hauls. All fish collected were counted and identified to the lowest taxonomic level possible onboard, although pre-recruit rockfish were frozen and taken back to the lab for identification using precise meristic and pigmentation metrics.

Larval fish

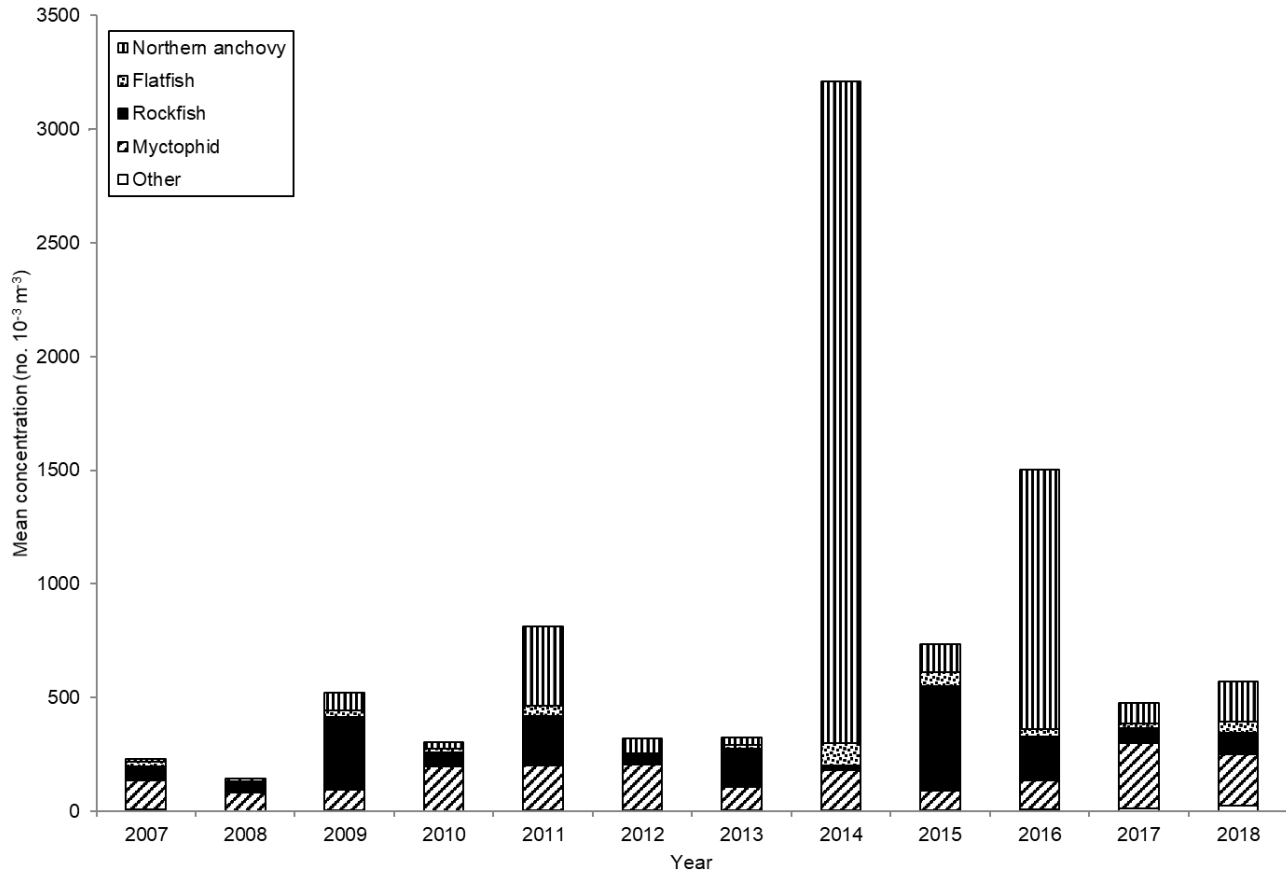


Figure 26. Mean concentrations (no. 10⁻³ m⁻³) of the dominant larval fish taxa collected during May–July in 2007–18 along the Newport Hydrographic (NH; 44.65°N, 124.35–125.12°W) and Columbia River (CR; 46.16°N, 124.22–125.18°W) lines off the coast of Oregon.

northern coast of Oregon in May 2018 was largely unremarkable in terms of composition and relative concentrations of the dominant taxa (fig. 26). Total mean larval concentration was the fifth highest in the 12-year time series. Larval flatfish in 2018 were found in the third highest concentration of the time series, myctophids in the second highest, and “other” taxa in the highest concentration, although this last group accounted for only 4% of the total mean larval concentration.

The post-larval fish community in the northern California Current in May 2018 had the second lowest abundance of the seven-year time series, continuing its decline since 2016 (fig. 27). The abundance of “other” taxa was the lowest in the time series, primarily due to the complete absence of Pacific hake (*Merluccius productus*; hake) in the 2018 samples, which had comprised 83% of the mean abundance of “other” taxa and ~60% of the total mean abundance of all post-larval fish in 2017. Rockfish (*Sebastes*) abundance in 2018 was average for the time series, with the dominant species consisting of shortbelly (*Sebastes jordani*; 64% of total rockfish), darkblotched (*S. crameri*; 20%), chilipepper (*S. goodei*;

5%), blue²⁵ (*S. mystinus*; 3%), and canary (*S. pinniger*; 2%). In addition, pyrosomes continued to be found in extraordinarily high numbers throughout the sampling area (data not shown).

Columbia River Plume Region: Juvenile Salmon and Ocean Ecosystem Survey (JSOES)

The fish and invertebrate assemblage collected from trawls in the upper 20 m²⁶ in June in the northern California Current was very distinct between 2015 and 2017 (fig. 28). During that time, it was dominated by taxa

²⁵It is possible that some of the rockfish identified as Blue were the recently-described Deacon rockfish, *S. diaconus* (Frable et al. 2015)

²⁶This survey has been conducted by the Northwest Fisheries Science Center (NWFS) in late June every year between 1998 and 2018. Sampling occurred along 11 east–west transect lines off Washington and Oregon (fig. 1), ranging from approximately 45° to 48°N. Trawls were conducted at 6 to 8 stations on each transect from the shallowest bottom depth possible (~30 m) out to ~50 km from shore, often extending beyond the continental shelf (Brodeur et al. 2005, Barcelo et al. 2018). Sampling was conducted during daytime in the upper 20 m of the water column at every station using a pelagic rope trawl with the head rope at about 1 m, that had a 336 m² mouth opening with variable mesh sizes (162.6 cm at mouth to 8.9 cm at cod end). To retain catches of small nekton, a 6.1-m long, 0.8-cm mesh knodless liner was sewn into the cod end. The rope trawl was towed for 30 minutes at a speed over ground of approximately 6 km hr⁻¹.

Post-larval fish

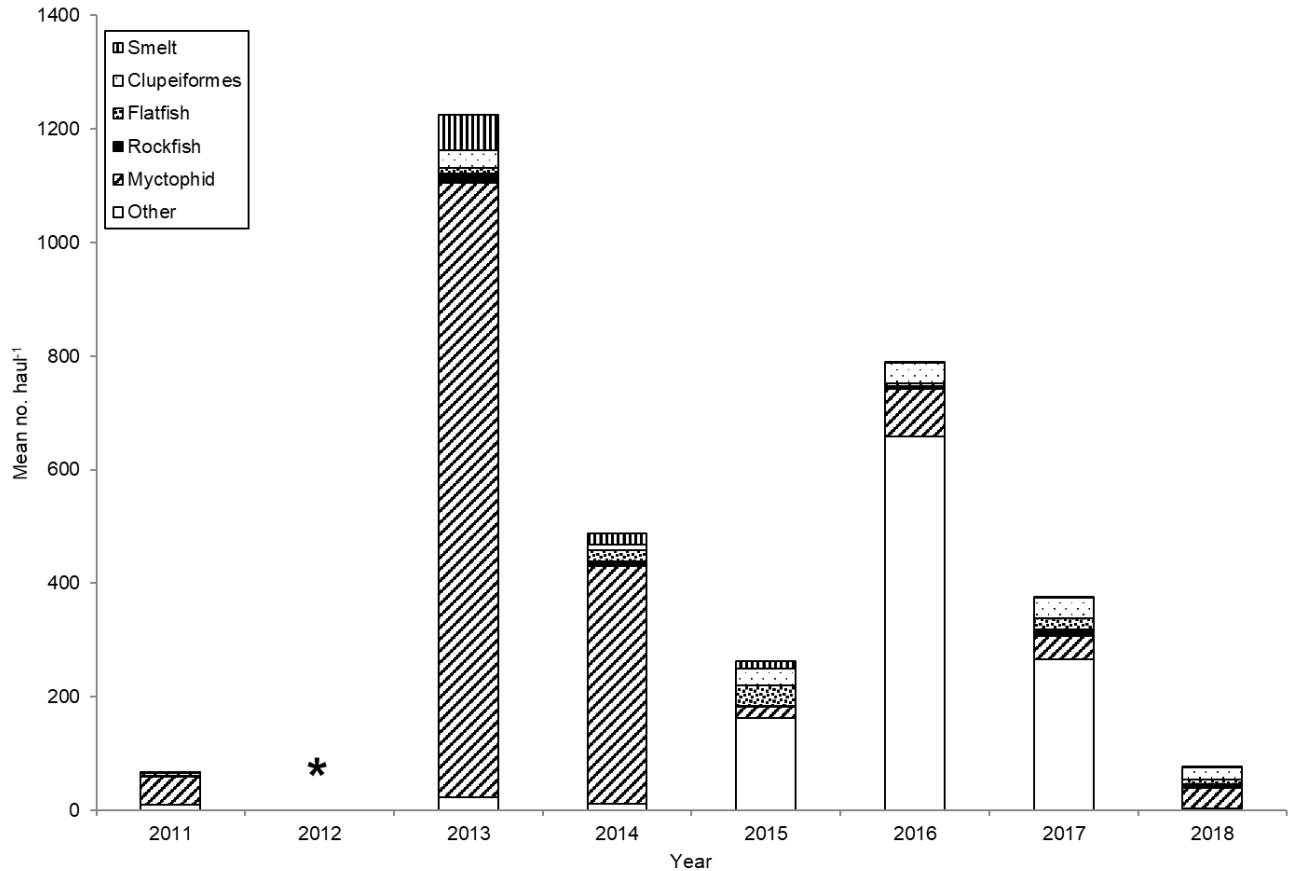


Figure 27. Mean catches (no. haul⁻¹) of the dominant post-larval fish taxa collected during May–July in 2011–18 along nine half-degree latitudinal transects between 42.0° and 46.0°N latitude in the northern California Current region. * = no samples were collected in 2012.

such as pyrosomes, Pacific mackerel (*Scomber pacificus*), and Jack mackerel (*Trachurus symmetricus*) that normally occur in warmer ocean waters to the south of the study area. An NMS ordination clearly showed that the 2015–17 assemblages were outliers, distinct not only from the 1999 La Niña assemblages, but also from the assemblage sampled during the 2005 warm event (Brodeur et al. 2006) in the northern California Current (fig. 28).

The fish and invertebrate community was less anomalous in 2018 than during the preceding three years (fig. 28). However, some taxa (e.g., market squid [*Doryteuthis opalescens*], Pacific Pompano [*Peprilus simillimus*], Jack mackerel) were present that had previously been absent or very low in our catches prior to 2015. Other common taxa in 2018 included gelatinous species, yearling Chinook (*Oncorhynchus tshawytscha*), coho (*O. kisutch*), juvenile chum (*O. keta*) salmon, and Pacific herring (*Clupea pallasii*). Pyrosomes, that were first captured by this survey in 2017 were still present, although in lower abundances than the in the previous year.

Since 2015, the jellyfish community off Washington and Oregon has been quite different than previous years. Usually, the large, cool-water scyphozoan species, sea nettle (*Chrysaora fuscescens*) is numerically dominant. However, during the warm ocean years of 2015–16, the normally more offshore water jellyfishes (*Aequorea* spp.) were much more abundant while densities of *Chrysaora* were low (fig. 29). In 2017, both *Chrysaora* and *Aequorea* were caught in average densities. However in 2018, while *Chrysaora* numbers remained about average, *Aequorea* increased to 3rd most abundant in the 20 years of sampling jellyfish (jellyfish were not quantified prior to 1998).

Catches of yearling salmon off Washington and Oregon in June are thought to be accurate indicators of early ocean survival of yearling Chinook and coho salmon. The abundance of yearling Chinook salmon during June surveys has a significant, positive relationship to returning spring Chinook jack and adult counts at the Bonnaville Dam (with 1 and 2 year lags, respectively; see fig. 1 for dam location), as does the abundance of yearling

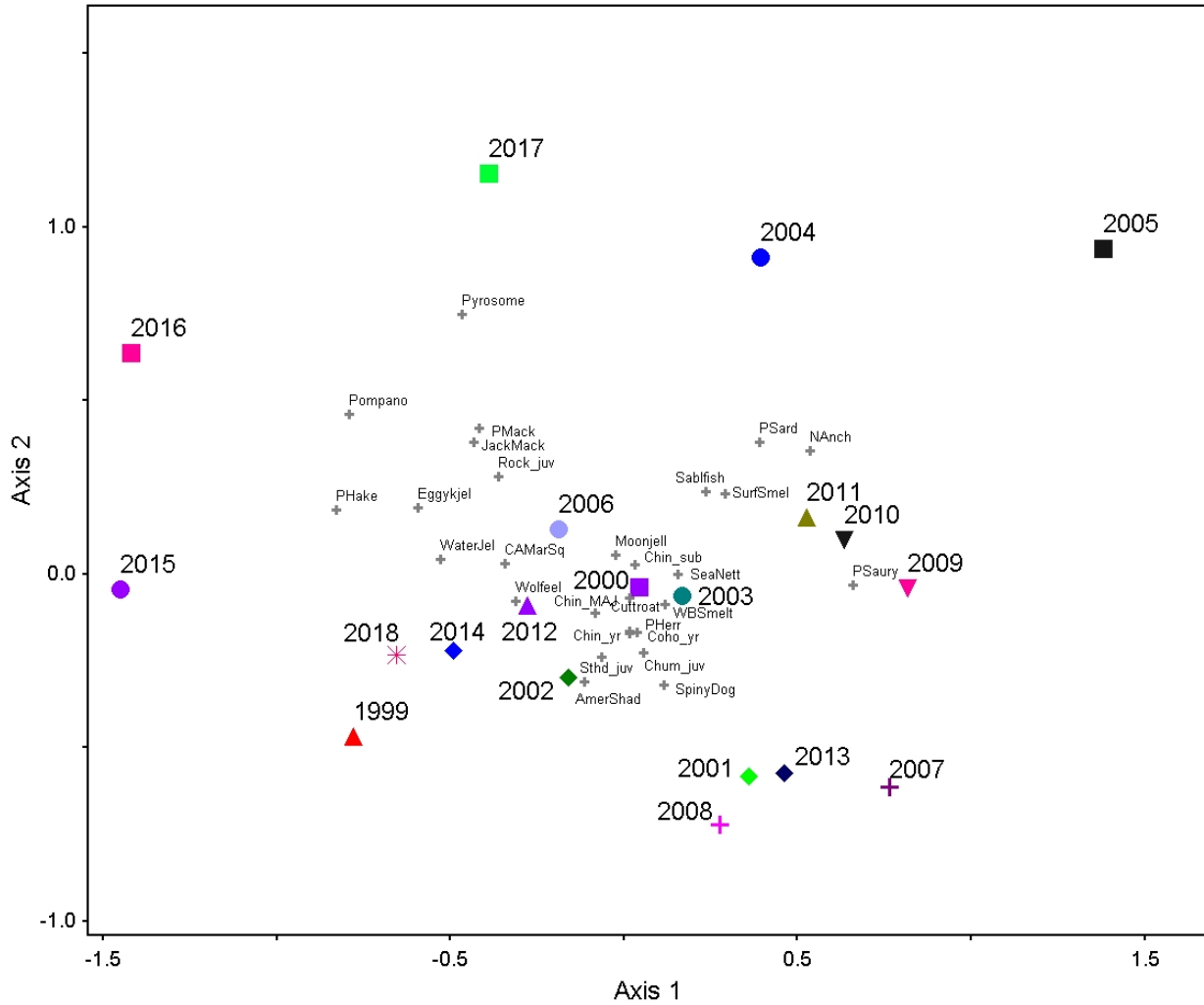


Figure 28. NMS ordination of northern California Current pelagic assemblages. The NMS ordination explained 78.9% of the total variability in the first two dimensions.

coho salmon to subsequent coho smolt to adult survival (Morgan et al. 2018). Catch per unit effort (CPUE, number per km trawled) of both yearling Chinook and coho salmon during the June 2017 survey was the lowest of the 20-year time series from 1998 to 2017 (fig. 30). In June of 2018, yearling Chinook salmon catches were close to average, but yearling coho salmon catches were the 2nd highest in the 21-year time series (fig. 30). Based on correlations observed in previous years, this suggests that adult returns of spring Chinook in 2020 will be close to average and coho salmon returns in 2019 will be higher than average.

Taken as a whole, the nekton community in summer of 2018 off Washington and Oregon indicate that the ecosystem was in a mixed state. On the one hand, the 2014 surface warming and the 2015–16 El Niño still had a noticeable impact on the nekton in this region, as taxa such as water jellyfish, pyrosomes, and Pacific pompano were abundant. On the other hand, higher catches of sea

nettles and juvenile salmonids suggest that the ecosystem may be returning to a more “normal” state.

Salmon and salmon forage indicators in northern California Current

Fish larvae in winter (January–March) derived from the Newport Hydrographic²⁷ line provides an index of juvenile salmon prey when they enter the ocean in spring and summer (Daly et al. 2017). When prey biomass was high, as in 2000 or 2008, smolt to adult returns or salmon adult returns tend to be high in the corresponding return years. When prey biomass was low, such as in 1998 or 2003–04, food conditions were poor and salmon returns were low. For the fourth year in a row,

²⁷Ichthyoplankton samples were collected from 5 stations spaced ~9 km apart along the NH line. Sampling was conducted approximately every 2 wk between January and March. Only samples from January–March were used, assuming that larvae collected during these months would have had sufficient time to grow to the average size of prey eaten by juvenile salmon in late spring and early summer.

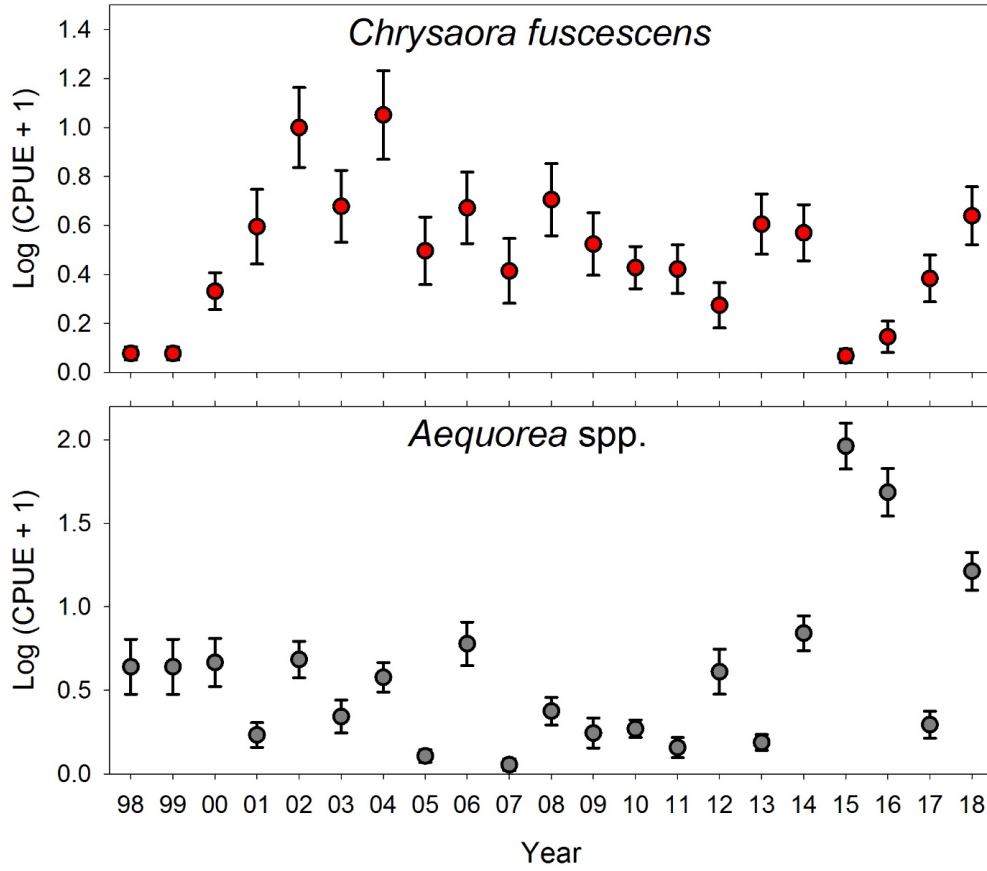


Figure 29. Catches of the dominant jellyfish taxa in pelagic surveys off the coast of Washington and Oregon in June from 1999 to 2018. Data are the means and standard error of the $\log_{10}(\text{catch per km}^2 + 1)$ of *Chrysaora fuscescens* (upper) and *Aequorea* spp. (lower) in the survey area.

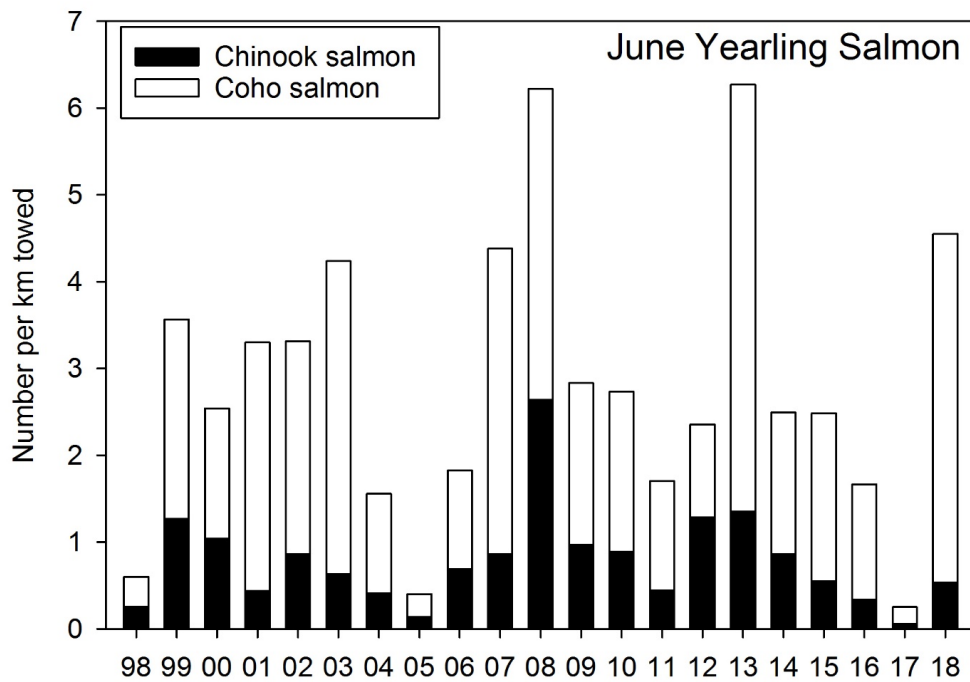


Figure 30. Catches (number per km towed) of juvenile coho (black bars) and Chinook (white bars) salmon off the coast of Oregon and Washington in June from 1998-2018.

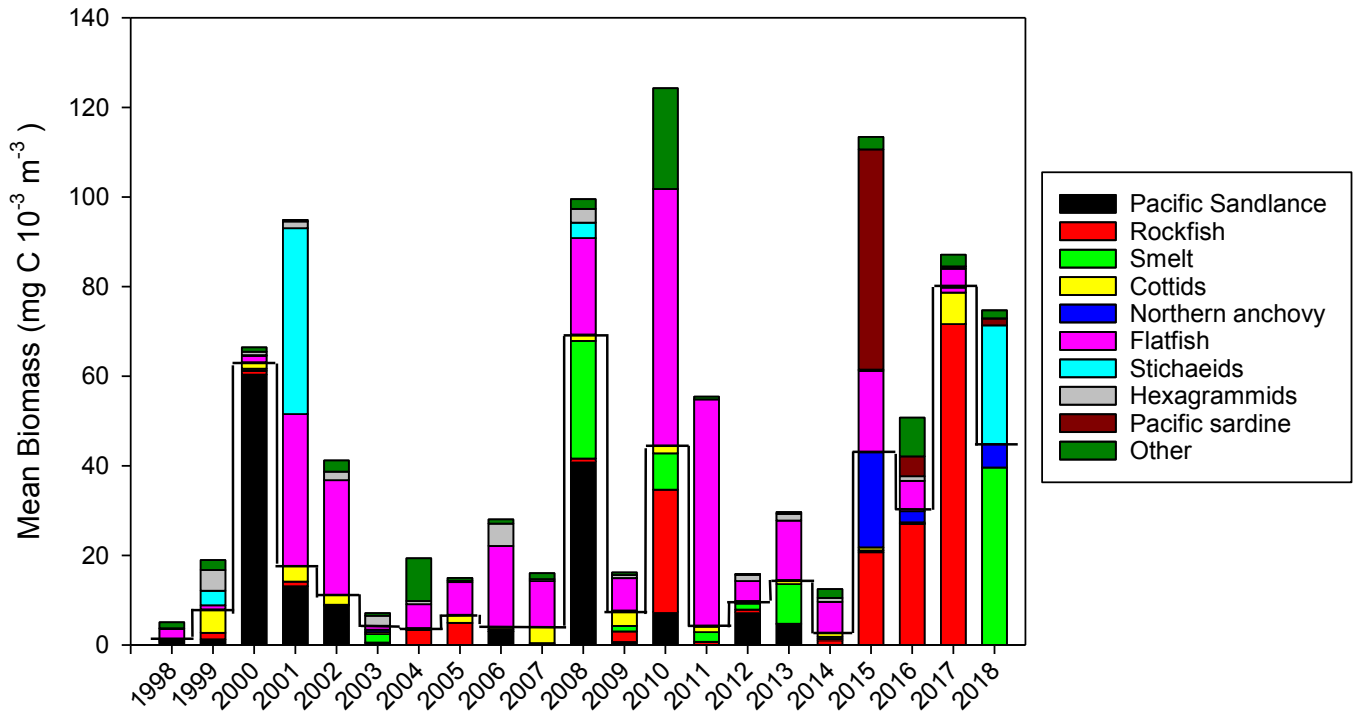


Figure 31. Annual mean biomass (mg C 10³ m³) of the five important salmon prey taxa (below solid line) and five other dominant larval fish taxa (above solid line) collected during winter (January–March) in 1998–2018 along the Newport Hydrographic (NH) line off the coast of Oregon (44.65°N, 24.18–124.65°W). Figure updated from one presented in Daly et al. (2013).

the biomass of fish larvae in winter was high but generally comprised of offshore taxa indicative of warm ocean conditions (e.g., rockfishes; Auth et al. 2018). The 2018 winter biomass of fish larvae that salmon prey upon was the 4th highest in the 21-year time series and biomass in 2015–18 were all within the highest 7 biomass years (fig. 31).

Recent work (Daly et al. 2017) demonstrated that in addition to overall prey biomass the taxonomic composition of fish prey (fig. 31) available for salmon to consume can influence salmon survival. Salmon returns tend to be low when the prey assemblage is comprised of offshore taxa that are advected inshore. In 2018, the winter prey assemblage was comprised largely of species associated with relatively warm, offshore water such as rockfishes (fig. 31), which forecasts low returns of spring Chinook salmon in 2020 and coho salmon in 2019.

The PDO is another index that has been used to predict salmon survival. When the PDO in October–December of the prior year is high, salmon survival tends to be low. In fall 2017 the PDO was the 7th most positive (fig. 2A) of the time series

Based on axis 1 values (59.6% variance explained; fig. 32) from the PCO of the prey composition of winter ichthyoplankton, the index of the 2018 prey composition suggests poor food conditions for 2018 out-migrating juvenile salmon. The relationship between the PCO1 axis values (prey composition)

with spring Chinook salmon adult returns to Bonneville Dam, Oregon (fig. 1) two years later is: $R^2 = 0.44$; $p\text{-value} = 0.004$; (1998–2015; 1999 outlier year excluded). The correlation between overall biomass of ichthyoplankton in winter and returns of spring Chinook salmon to Bonneville Dam, Oregon, estimates around 161,000 adults returning in 2020, whereas the prey composition suggests one of the poorest returns of the time series at ~89,000 (see Daly et al. 2017 for detailed methodology).

From 1998–2014 winter ichthyoplankton biomass was high when the ocean was cool and vice versa, and salmon survival was low in warm years, possibly due to reduced food resources in spring and summer. Since 2014, however, conditions have been warm, but with high ichthyoplankton biomass. Since 2015, the biomass of offshore warm ocean taxa that have been increasingly observed in the diets of juvenile salmon (Daly et al. 2017), may have led to lower return rates of adults. For example, when juvenile salmon consumed nearshore taxa such as Pacific sand lance (*Ammodytes hexapterus*), sculpins (Cottidae), and smelts (Osmeridae), adult returns were high in subsequent years. By contrast, when yearling Chinook salmon or steelhead (*Oncorhynchus mykiss*) consumed higher amounts of offshore rockfish in May or June, adult returns were typically lower (Daly et al. 2017). Similarly, Dale et al. (2017) found that subyearling Chinook salmon

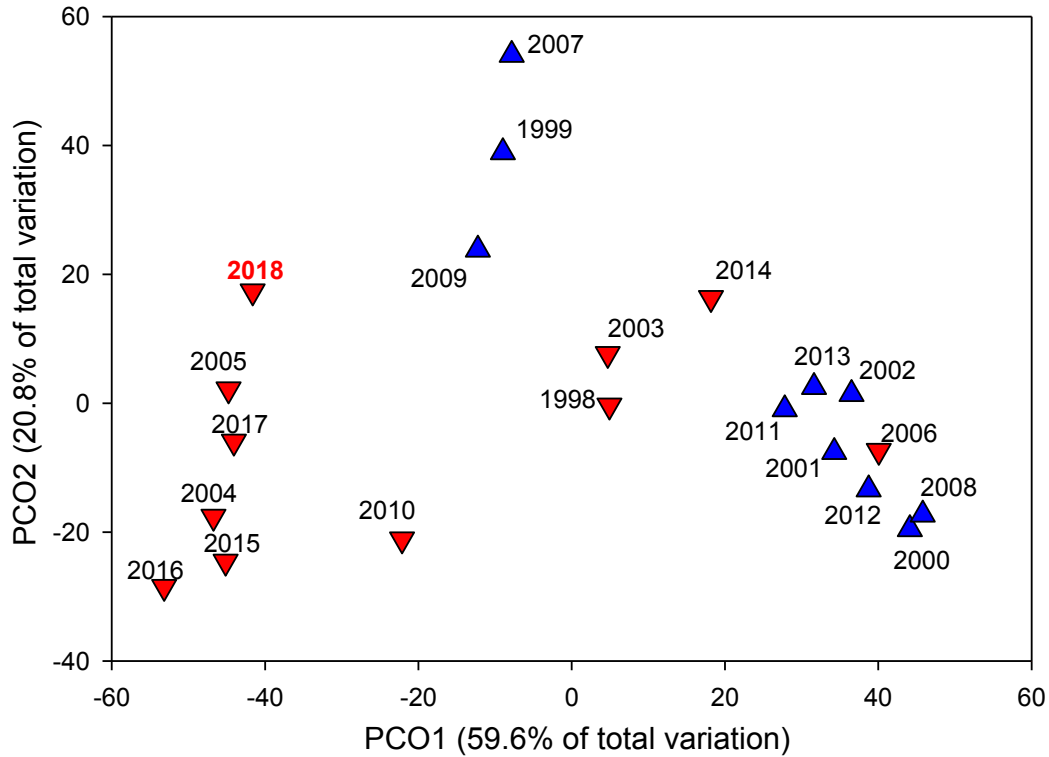


Figure 32. Principal Coordinate Analysis of the prey composition of winter ichthyoplankton that are important prey for out-migrating juvenile salmon (Pacific sand lance, smelts, cottids, northern anchovy, and rockfishes). Red symbols indicate positive winter PDO (warm ocean temperatures) and blue indicate negative winter PDO (cold ocean temperatures). The larvae were collected during winter (January–March) in 1998–2018 along the Newport Hydrographic (NH) line off the coast of Oregon (44.65°N, 124.18–124.65°W). Figure updated from one presented in Daly et al. (2017).

returns were low when feeding upon northern anchovy (*Engraulis mordax*; anchovy) which spawn under warm water conditions off Oregon.

Central California

Catches of juvenile groundfish and epipelagic micronekton from the Rockfish Recruitment and Ecosystem Assessment Survey (RREAS)²⁸ (Sakuma et al. 2016) in late spring of 2018 indicated declines from the high abundance levels during 2015–17 for pelagic young-of-the-year (YOY) rockfishes and sanddabs (*Citharichthys* spp.) throughout most regions off California (fig. 33). The exception was the fairly high YOY rockfish abundance sampled within the southern California Bight. There was a significant increase in the abundance of adult northern anchovy in the core and south central regions (fig. 32), and their abundance exceeded the previous highs in 2005–06. A small number of adult Pacific sardine (*Sardinops sagax*; sardine) were encountered, more than in roughly the last ten years,

but still very low relative to high abundance levels in the late 1990s and early 2000s. YOY anchovy and sardine (not shown) were also at relatively high levels in the survey, particularly in the southern survey region. Market squid and krill (Euphausiids) were at fairly high abundance levels in most regions, particularly the core and Southern California Bight (not shown). Pelagic red crabs (*Pleuroncodes planipes*) were also abundant in the Southern California Bight during the late spring of 2018, a phenomenon sustained since 2015 (not shown).

Shifts in the abundance of various gelatinous organisms reversed in 2018. Catches of *Thetys* salps and other salps were at higher levels in 2018, while catches of pyrosomes dropped considerably from the very high levels seen in 2017 in most regions, particularly in southern and core regions (fig. 34). Pyrosomes continued to be quite abundant in the northern regions, consistent with the high pyrosome catches observed off Oregon and Washington in northern surveys. There was a sharp reversal of the previously low catches of scyphozoan jellyfish (primarily *Aurelia* spp. and *Chrysaora fuscescens*) from previous years, as both of those species were encountered at their greatest relative abundances since the survey commenced in 1990 (fig. 34).

The nMDS analysis based on mean log catch of the fish and cephalopod community from the core RREAS

²⁸Epipelagic micronekton samples were collected during May and June by the Southwest Fisheries Science Center Rockfish Recruitment and Ecosystem Assessment Survey and the Northwest Fisheries Science Center Pre-recruit Groundfish Survey, covering a geographic range from the US/Mexico border (32.5°N) to southern Washington (46.5°N). A modified midwater Cobb trawl (10–30 m headrope depth) was used to sample pelagic species along the CCE in the mixed layer where juvenile salmon are typically found. Methods were standardized between regions beginning in 2011 (Sakuma et al. 2016).

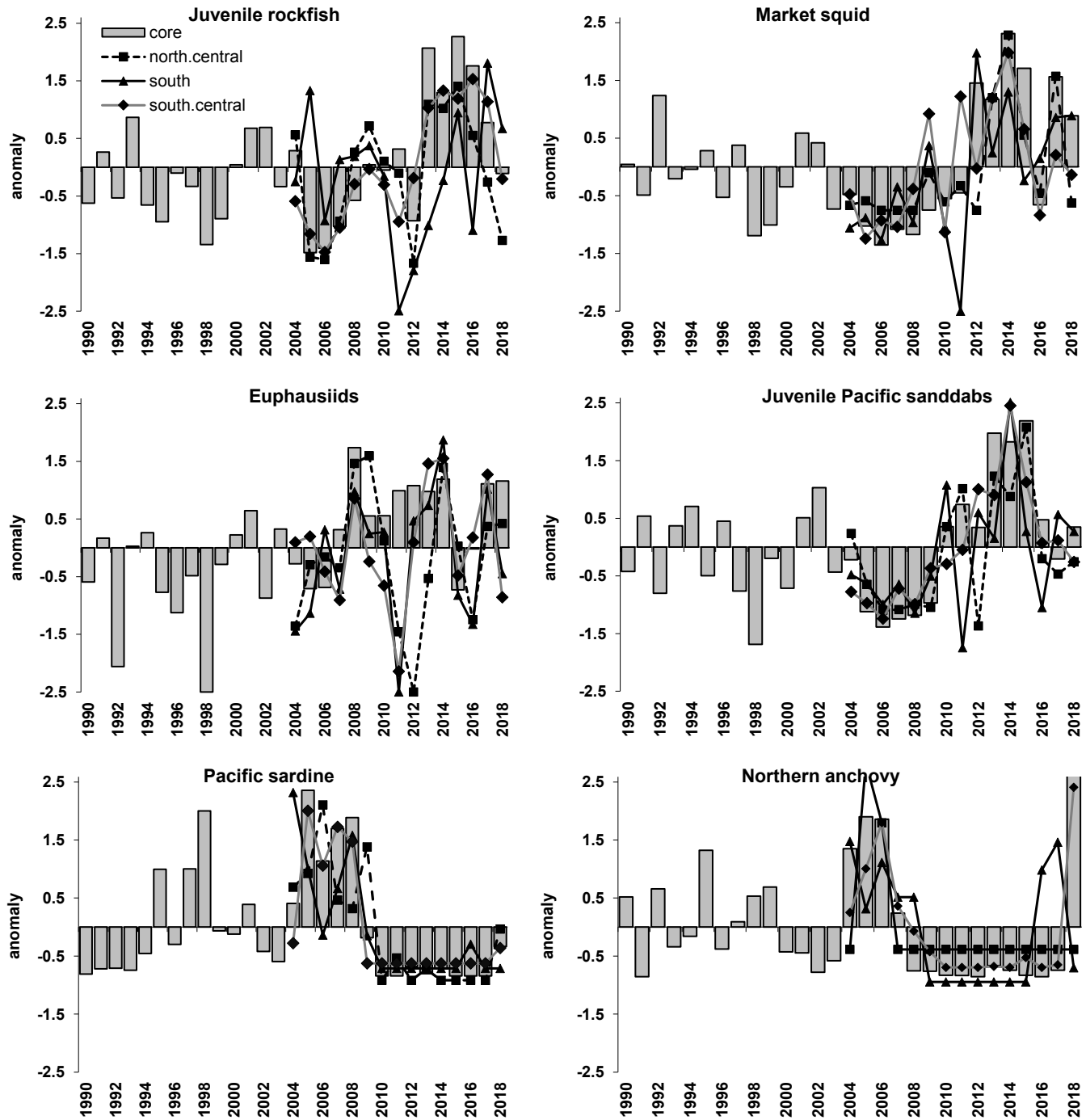


Figure 33. Standardized anomalies (of average $\ln(\text{catch}+1)$) catches for key forage taxa sampled by the Rockfish Recruitment and Ecosystem Assessment Survey.

region between 1990 and 2018 showed that 2018 clustered close to 2013–15 and was most similar to 2017 (fig. 35 top). The top five most abundant taxa between 1990 and 2017 were, in order, sanddabs, rockfish, young of the year hake, squid and myctophids, and all of these taxa were the top six most abundant in 2018. Adult anchovy, however, were the one exception in 2018 as it was the 3rd most abundant taxon (fig. 35 bottom; red

dot represents anchovy while blue dots are other taxa). The influence of anchovy was reflected by a high value of nMDS axis 2 in 2018 (fig. 35 top). The 2018 sampling year was somewhat uncommon as it featured high abundances of both anchovy and sanddabs (there is negative correlation between these species throughout the time-series; sanddab abundance = $-0.75 \times$ anchovy abundance + 2.57, $r = 0.45$). In 2018 adult sardine

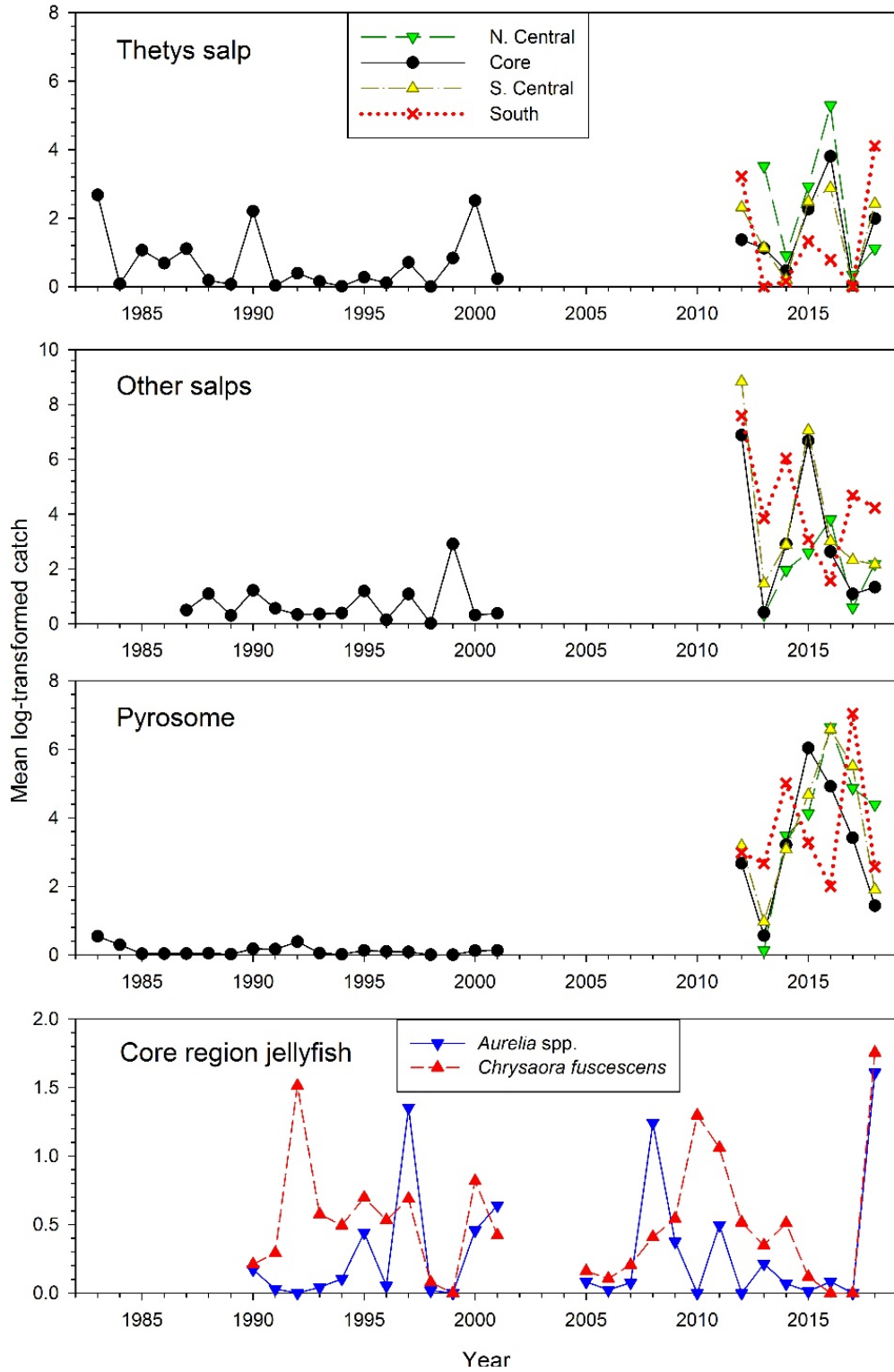


Figure 34. Standardized catches of and pelagic tunicates (*Thetys* salps, other salps, and pyrosomes) and jellyfish (*Aurelia* spp. and *Chrysaora fuscescens*) in the core and expanded survey regions.

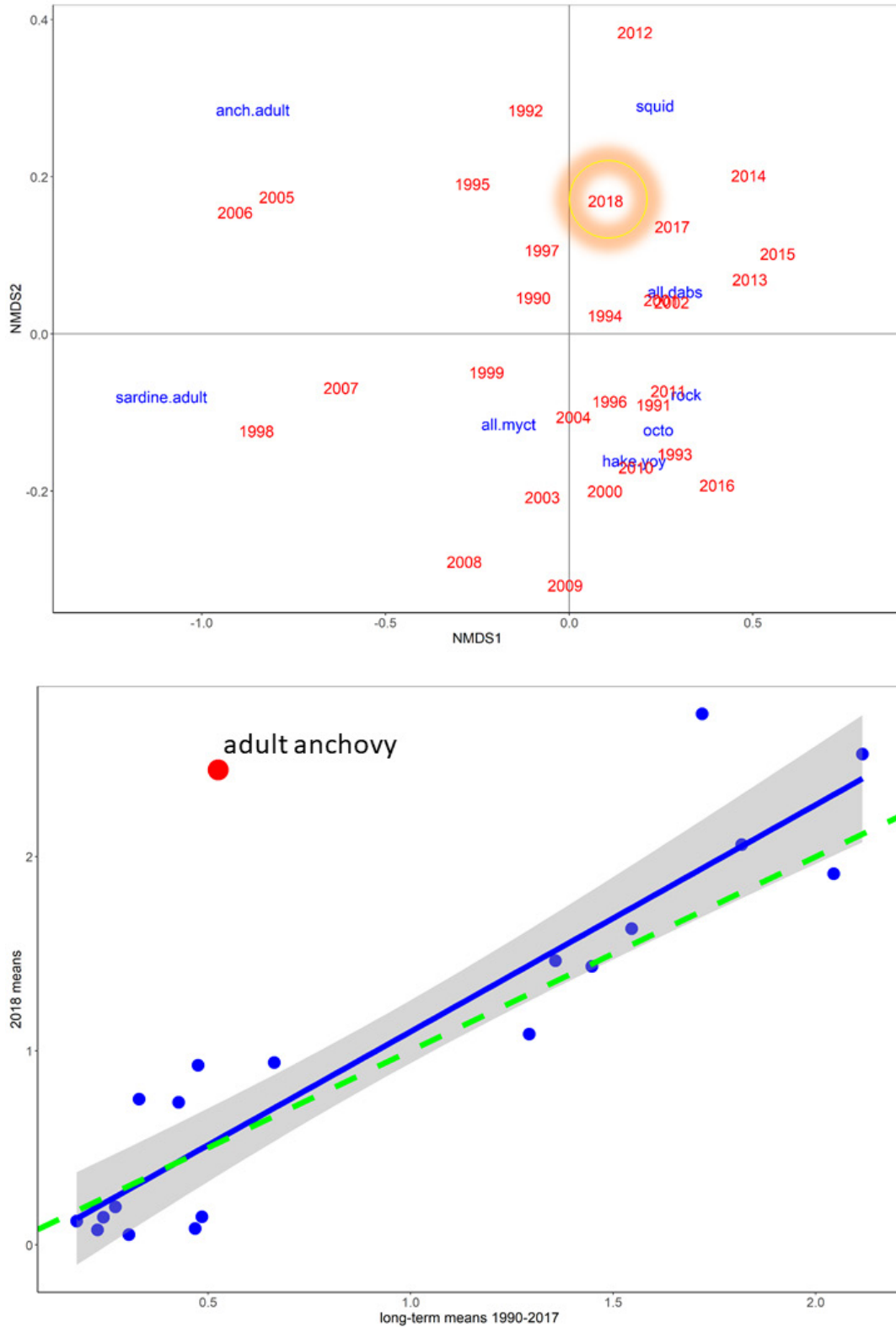


Figure 35. Top) NMDS analysis for eight key taxonomic groups of forage species sampled in the central California core region from 1990–2018. The following species are included: all.dabs = combined speckled and Pacific sanddab; all.myct = myctophids; anch.adult = northern anchovy; hake.yoy = young of the year hake; octo = octopus; rock = juvenile rockfish; squid = market squid. 2018 is circled. Bottom) Mean (average $\ln(\text{catch}+1)$) in 2018 (y axis) vs. sum of mean (average $\ln(\text{catch}+1)$) from 1990–2017 for the 20 most common taxa collected in the core region. Each dot represents a unique taxon. The main outlier, anchovy, is in red. The blue line is the best fit line for all species except anchovy ($R^2 = 0.86$, $p < 0.0001$). The green line is the line of unity (intercept = 0, slope = 1). A species' abundance would be exactly average if fell directly on the green line; values below the green line are lower than normal and vice-versa.

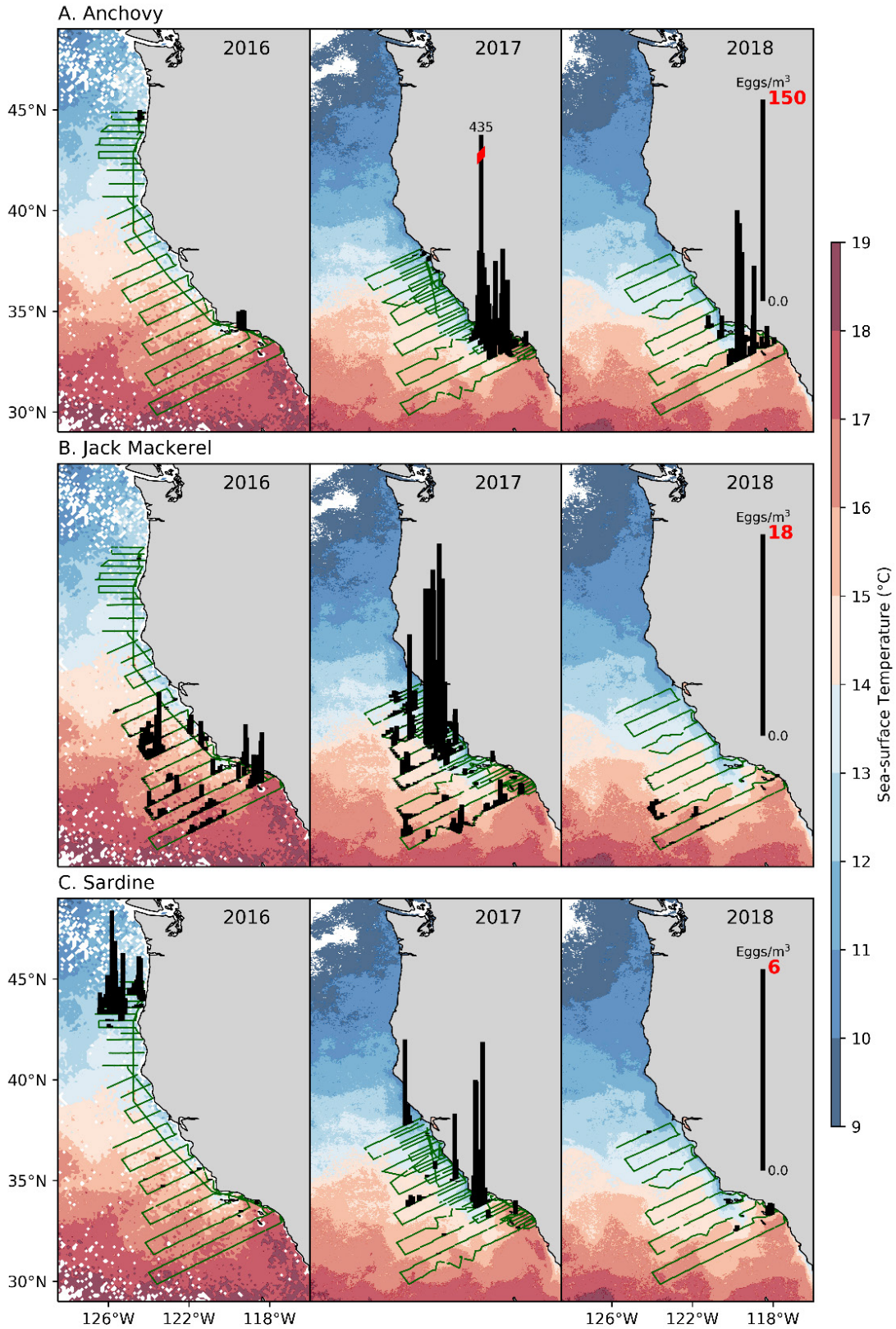


Figure 36. Density of eggs of northern anchovy A), Jack mackerel B), and sardine C) collected with the continuous underway fish-egg sampler (CUFES) during the spring 2016-18 CalCOFI cruise. Data are overlaid on satellite-derived sea surface temperatures (AVHRR 1.4-km resolution; C). Note that scales differ among species.

abundance was very low and 2018 loaded far in multivariate space from years when this species was relatively abundant. Plotting 2018 means for each taxa versus long-term means further emphasized that the assemblage in the core region of the RREAS reflected long-term means for most taxa with the glaring exception of anchovy (fig. 35 bottom).

Southern California

Anchovy eggs collected with a continuous under-way fish egg sampler²⁹ (CUFES) in spring 2018 were somewhat less abundant than in 2017 (fig. 36) but much more abundant than any other year since the mid-1990s (CUFES sampling began in 1996). Most anchovy eggs were collected in the Southern California Bight along CalCOFI line 90, with smaller abundances occurring near Point Conception and the Channel Islands (fig. 36). No anchovy eggs were collected north of Point Conception in 2018. We note that sampling of eggs occurred as part of the spring CalCOFI cruise (5–27 April 2018). Anchovy spawning peaks during March in most years (Moser et al. 2001). Thus, the spawning pattern may not be representative of the full anchovy spawning season.

CUFES sampling also showed that Jack mackerel and sardine egg abundances were extremely low in spring of 2018 (fig. 36); this is consistent with a declining trend since the mid-2000s. Where Jack mackerel eggs did occur in 2018, they were far offshore in the southwest portion of the CalCOFI core sampling area (fig. 36). The only year in the available time series in which Jack mackerel egg abundances were comparably low was during the severe El Niño of 1998. Sardine eggs generally were restricted to the inshore area of the Southern California Bight (fig. 36). Sardine eggs have been rare since 2014 but were the least abundant during 2018 of any year in the available time series.

Whereas fish assemblages were trending towards average conditions in the first half of 2018 throughout most of the CCS, this was not the case in southern California. Rather, the 2018 ichthyoplankton assemblage collected from the spring CalCOFI cruise from lines 80 and 90³⁰ was more similar to 2014–16 than it was to 2017. In spring 2018 several mesopelagic taxa that are associated with warm water and have biogeographic centers of distribution south of southern California were highly abundant. Specifically, Panama lightfish (*Vincigurria luetia*) had the 7th highest abundance on record, Mexican lampfish (*Triphoturus mexicanus*) the 2nd highest (behind

only 2015), dogtooth lampfish (*Ceratoscopelus townsendi*) 15th highest, and species in the family Gonostomatidae (bristlemouths, comprised largely of species in the genera *Cyclothone* 3rd highest (fig. 37). By contrast, northern lampfish (*Stenobranchius leucopsarus*) and blue lanternfish (*Tarletonbeania crenularis*), the most common mesopelagic species with centers of distribution north of southern California, had some of the lowest abundances since 1951 in spring 2018 (fig. 37).

Similar to CUFES results (fig. 36), abundances of sardine, Jack mackerel, and Pacific mackerel larvae remained at historically low levels in southern California in spring 2018 (fig. 38). However, while CUFES suggested a decrease in anchovy eggs between 2017–18 (fig. 36), anchovy larvae in CalCOFI samples were much higher in 2018 than 2017 (fig. 38). Indeed, spring anchovy abundance was the 3rd highest since 1951 and the highest since the mid-1960s (fig. 38).

Larval abundances of common groundfishes in southern California also were extreme in 2018 (fig. 39). Sanddabs (mostly Pacific sanddab, *Citharichthys sordidus*, and speckled sanddab, *C. stigmaeus*) have been very low since 2015 and were low again in 2018 (fig. 38). Slender sole (*Lyopsetta exilis*) and English sole (*Parophrys vetulus*) abundances, however, were very high in 2018, displaying the 5th and 2nd highest abundances, respectively, on record (fig. 39). Abundances of rockfishes were close to average in 2018 (25th highest out of 56 years; fig. 39).

From a multivariate (nMDS) perspective, 2018 aligned closely on nMDS1 with 1985–87 and 2014–16 (fig. 40 top). All of these years were characterized by having high abundances of the four southern mesopelagic species shown in Figure 37 (red font in figs. 40 top and 40 bottom). Larval abundances in 2018 were lower on the nMDS2 axis relative to 1985–87 and 2014–16, likely reflecting the influence of anchovy, which loaded negatively on nMDS2. Notably, the 2018 assemblage was quite different from 2017 as the 2017 assemblage was characterized by taxa with centers of distribution within or close to southern California (colored green in fig. 40 top). Plotting mean abundances of taxa in 2018 versus long-term means further emphasized how different from average the assemblage was in 2018 (fig. 40 bottom). Two species with northern biogeographic ranges (northern lampfish and hake) and one centered on southern California (Jack mackerel) were well below long-term means in 2018 (fig. 40 bottom), while the three species with southern ranges (Mexican lampfish, Panama lightfish, and bristlemouths) as well as the cosmopolitan English sole and California smoothtongue (*Leuroglossus stilbius*) were well above long-term means (fig. 40 bottom). Anchovy and sardine were not included in Figure 40

²⁹Water is continuously pumped from 3-m depth and particles are collected over sequential sampling intervals (e.g., 5–30 minutes) on a cod end.

³⁰Ichthyoplankton is collected with bongo nets equipped with a flowmeter, 0.71-m diameter rings and 505- μ m mesh. Nets are lowered to 210 m (or within 20 m of the bottom at shallow stations) and towed at a constant rate at a 45° angle to the surface. This analysis uses only samples from CalCOFI lines 80 and 90.

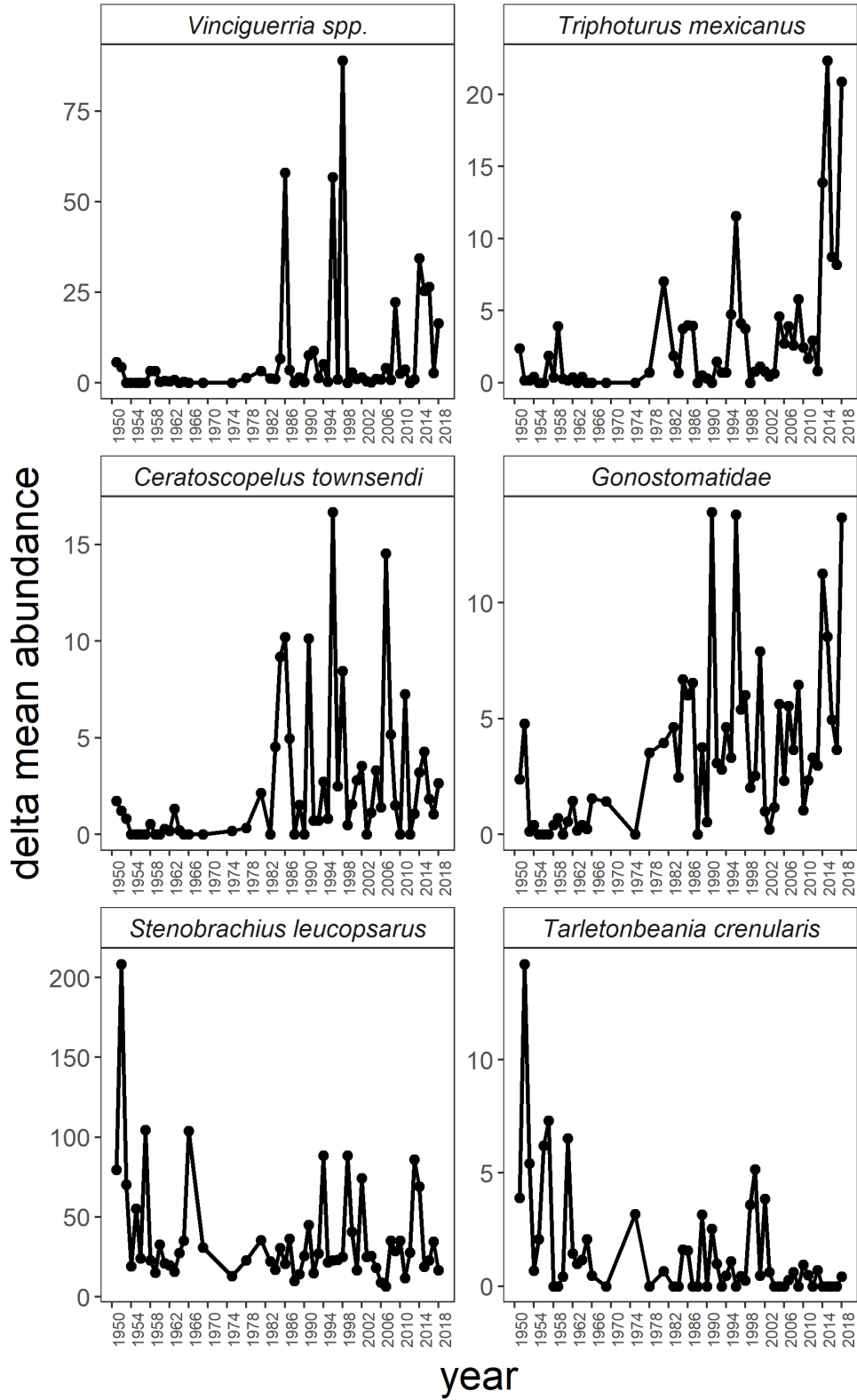


Figure 37. Mean abundances from CalCOFI lines 80 and 90 of larvae from four mesopelagic taxa with southern (*Vinciguerria lucetia*, *Triphoturus mexicanus*, *Ceratoscopelus townsendi*, and *Gonostomatidae*) and northern (*Stenobrachius leucopsarus* and *Tarletonbeania crenularis*) biogeographic distributions relative to southern California from 1951–2018.

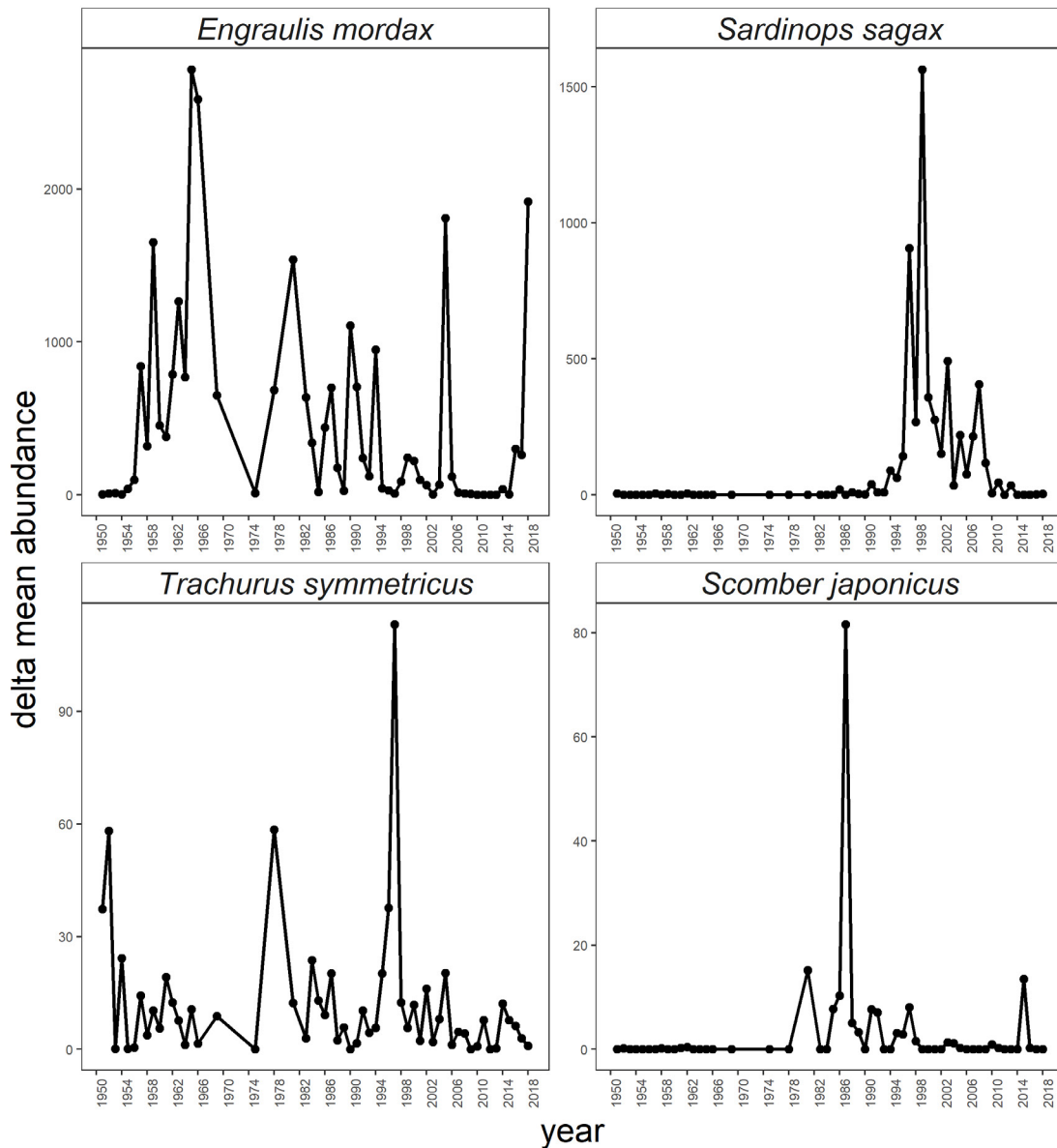


Figure 38. Mean abundances from CalCOFI lines 80 and 90 of larvae of four coastal pelagic species from 1951–2018.

bottom because the scale of their abundances are so much higher than the other taxa, but anchovy were much higher and sardine much lower than long-term means.

Management of the spiny lobster (*Panulirus interruptus*) fisheries in California currently relies exclusively on fisheries-dependent data streams. Thus, leveraging the value of lobster larval (phyllosoma) collections by CalCOFI to understand fishery productivity and

assess the influence of ocean conditions is an important goal for the California Department of Fish and Wildlife, who are charged with managing this fishery. A 57-year time series of the offshore abundance of early stage phyllosoma larvae from CalCOFI bongo net samples within the Southern California Bight was generated by Koslow et al. (2012) who concluded that phyllosoma tend to be higher when ocean conditions are warm (e.g., years with high SST, positive PDO

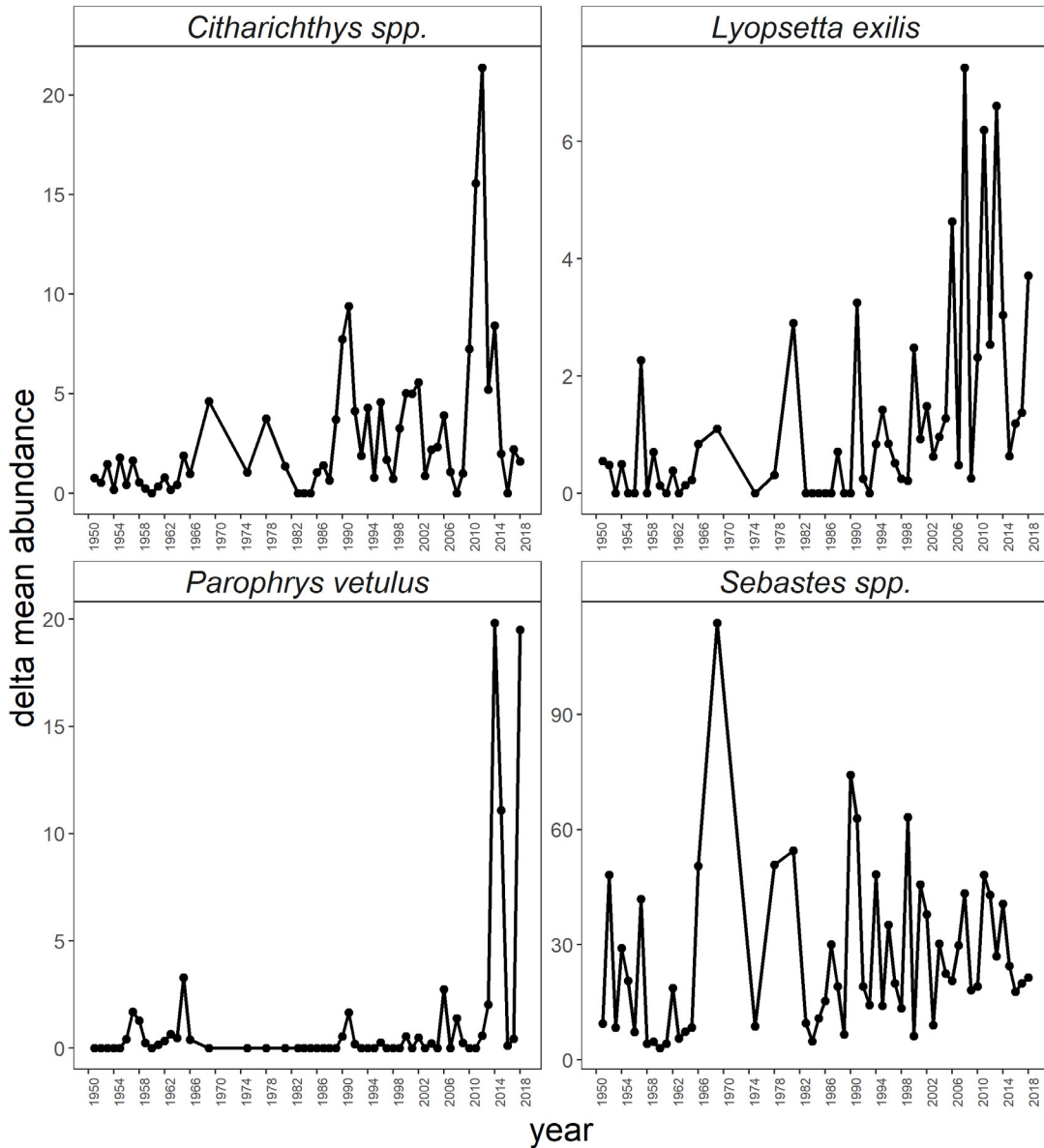


Figure 39. Mean abundances from CalCOFI lines 80 and 90 of larvae of four groundfish species from 1951–2018.

and MEI indices). In addition, phyllosoma abundance was significantly correlated with lobster landings seven years later.

CalCOFI phyllosoma data are now available through 2015, thus allowing us to examine the impact of the warm conditions of 2014–15 on lobster productivity and determine if the relationship between SST and phyllosoma abundance persists after adding years subsequent to 2008 (the last year analyzed by Koslow et al.

2012). Phyllosoma abundance was at a record high in 2014 and 14th highest in 2015 (fig. 41 top). The relationship between SST and phyllosoma abundance with data through 2015 was essentially the same ($r = 0.38$, $p = 0.006$) as reported by Koslow et al. (2012) ($r = 0.39$, $p < 0.001$; fig. 41 bottom). Based on this relationship, we expect that phyllosoma abundances remained elevated from 2016–18, and will test this prediction as data becomes available.

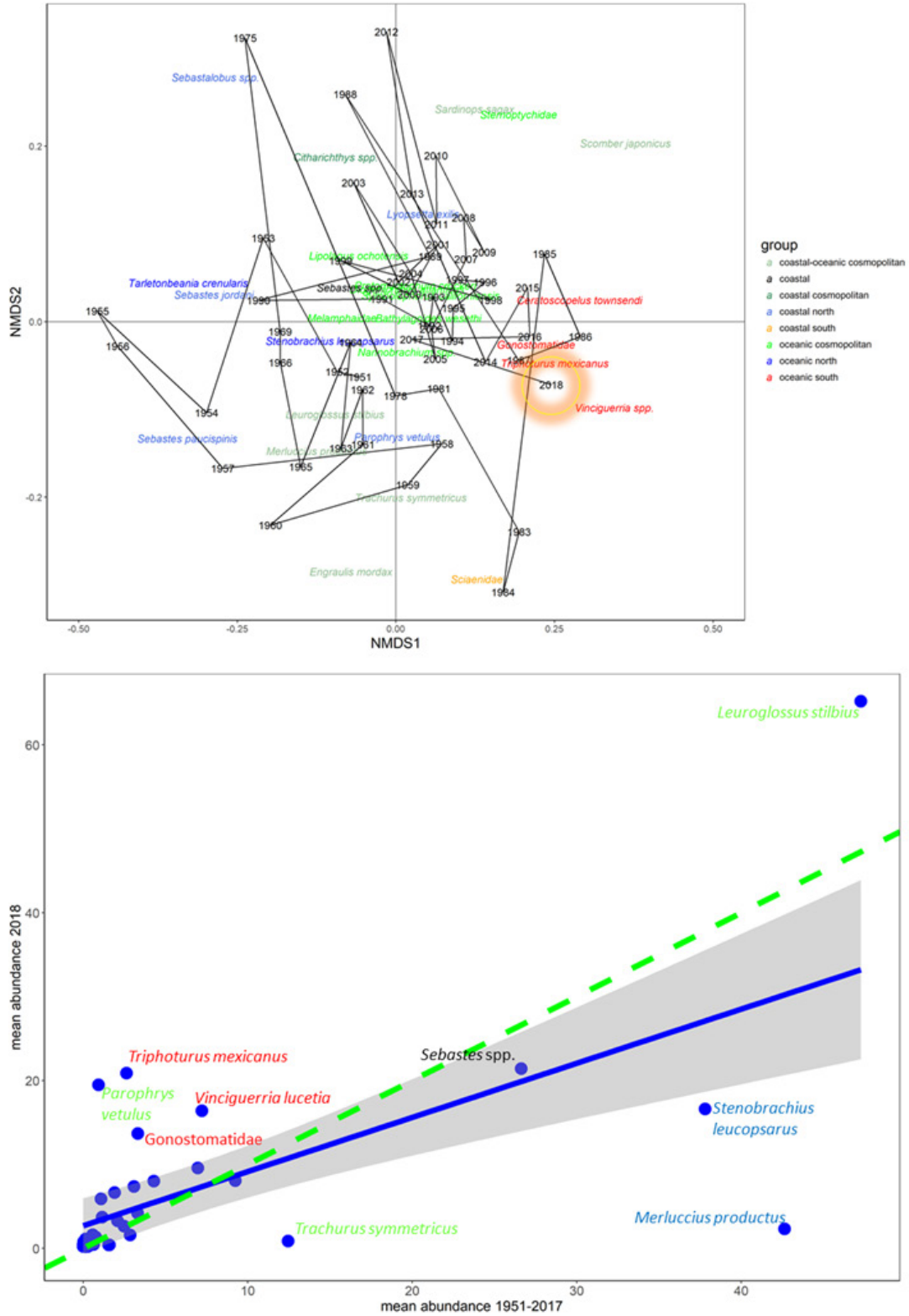


Figure 40. Top) NMDS analysis for taxa sampled from CalCOFI lines 80 and 90 from 1951–2018. Taxa names are colored based on habitat and biogeographic ranges. Bottom) Mean in 2018 (y axis) vs. long-term mean (1951–2018) of common taxa collected from CalCOFI lines 80 and 90. Each dot represents a unique taxon. The blue line is the best fit line for all species except anchovy and sardine ($R^2 = 0.42$, $p < 0.001$). The green line is the line of unity as in Figure 35. Species far above and below the line are demarcated with colors that correspond to habitat and biogeographic range as defined in panel A.

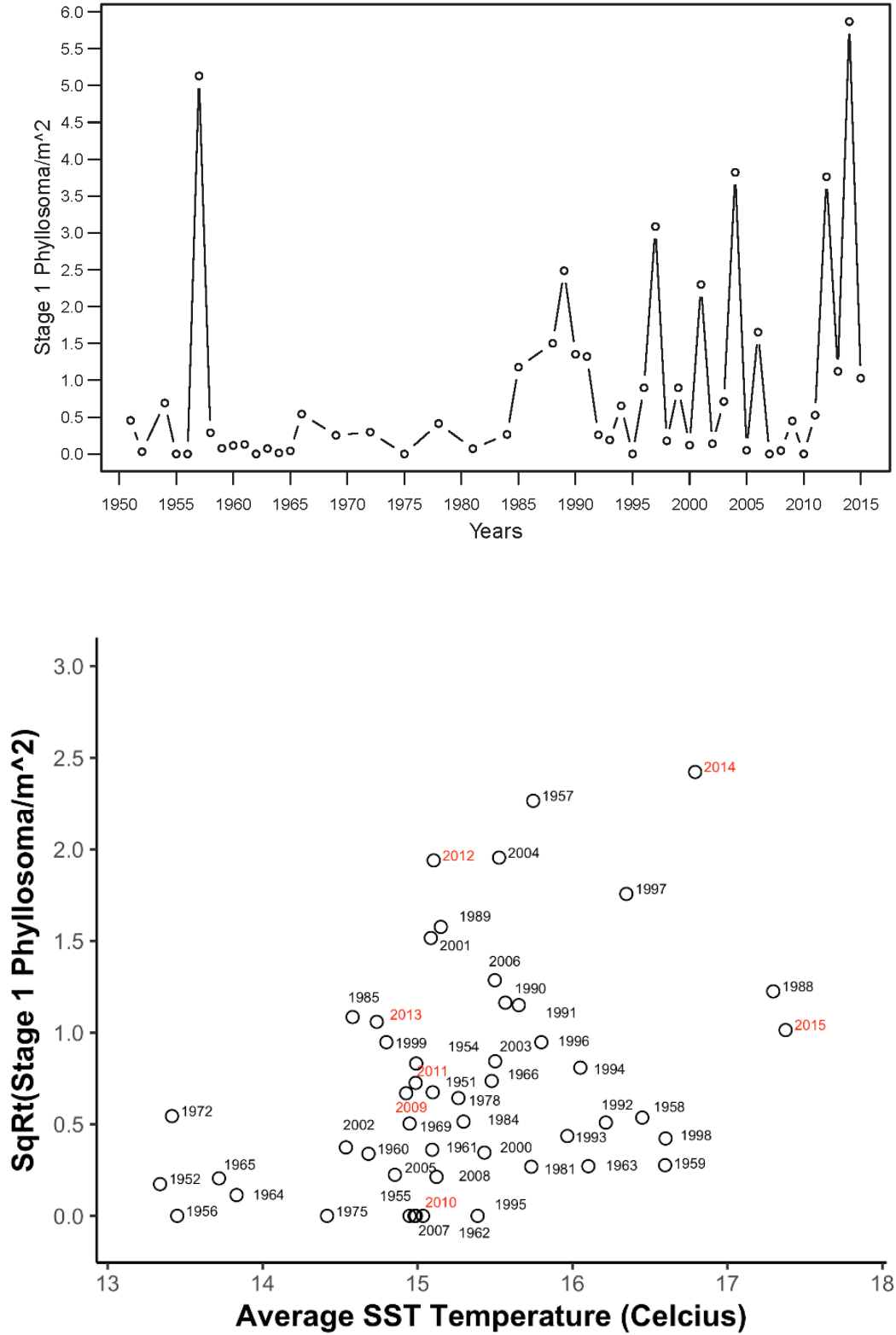


Figure 41. Top) Abundance of stage 1 lobster (*Panulirus interruptus*) phyllosoma larvae from 1951-2015. Bottom) Mean annual sea surface temperature (10 m) plotted against square-root transformed early-stage phyllosoma abundance. All sampling was from core CalCOFI stations over the continental shelf (\leq station 60). Years in black represent years that were previously analyzed in Koslow et al. (2012) while years in red represent the most recent years not previously analyzed.

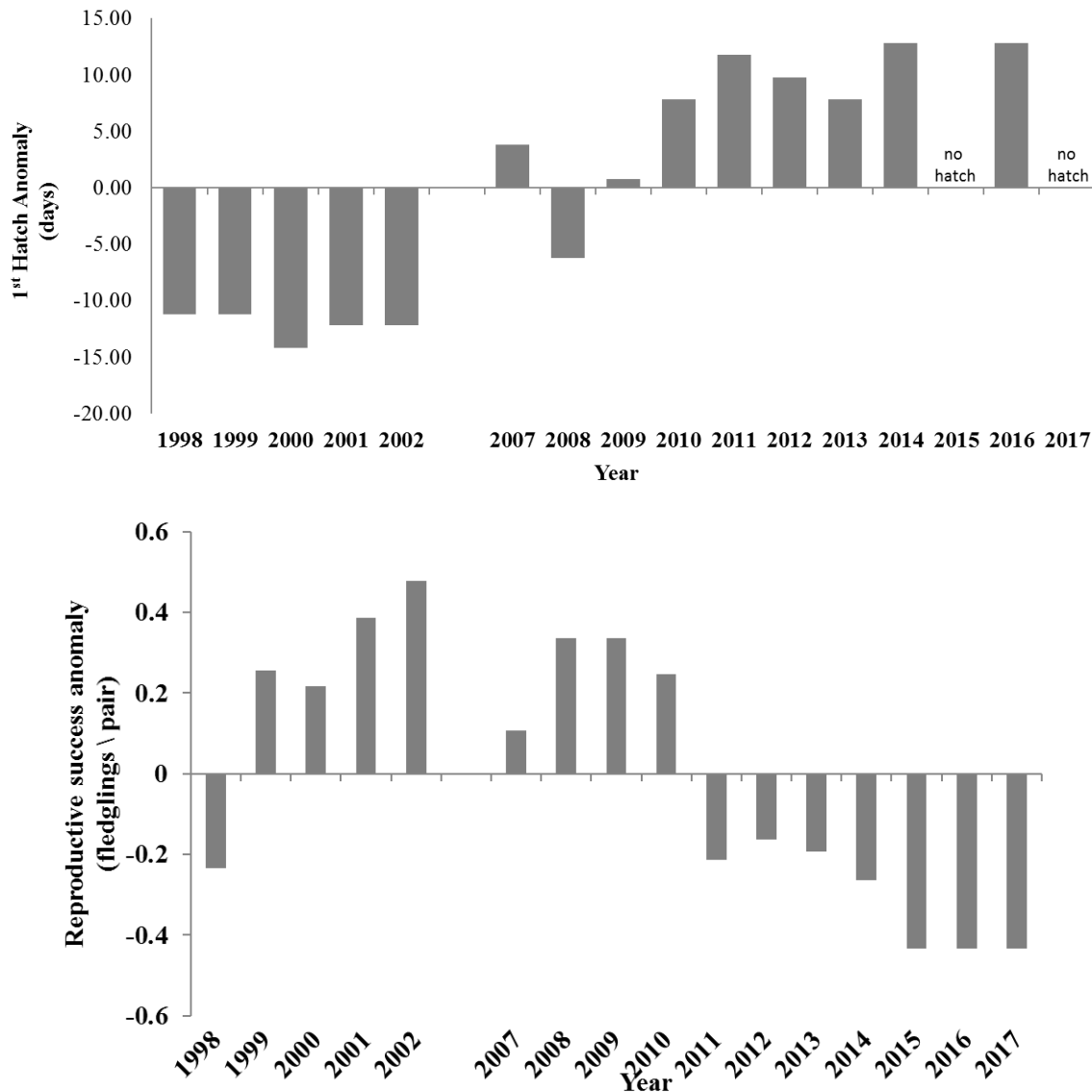


Figure 42. Anomalies of first chick hatch date (upper panel) and reproductive success (lower panel) for common murre nesting at Yaquina Head, Oregon, 1998–2017. 2017 was the third year that the colony failed to produce chicks from all but one small area where <10 chicks fledged each year.

REGIONAL PATTERNS IN BIRDS

Northern California Current: Yaquina Head, Oregon

Common murre (*Uria aalge*; murre) at Yaquina Head, Oregon, experienced complete reproductive failure throughout the entire colony in 2017. This was the first year in 16 years of data collection that no eggs were incubated long enough to hatch a chick at any location in the colony. This also was the third consecutive year that no murre chicks were produced throughout most of the colony, and breeding conditions in 2017 were the worst of the past three years (fig. 42). As in previous years the reproductive failure was caused by both top-

down predation and bottom-up food limitation. While the top-down signal is the most evident, the bottom-up signal was notable. For example, the only location where a few murre chicks fledged in 2015 and 2016 was a small rock near sea level that is generally not affected by avian predators. Even at this mostly predator-free site, no eggs survived for chicks to hatch in 2017. Murre reproductive success was 0 fledglings/pair, which is the lowest recorded for the colony since surveys began in 1998 and was even lower than during the 1998 El Niño (Gladics et al. 2015). Preliminary results from 2018 indicate that murre experienced improved reproductive success compared to the past three years of colony failure (data not shown).

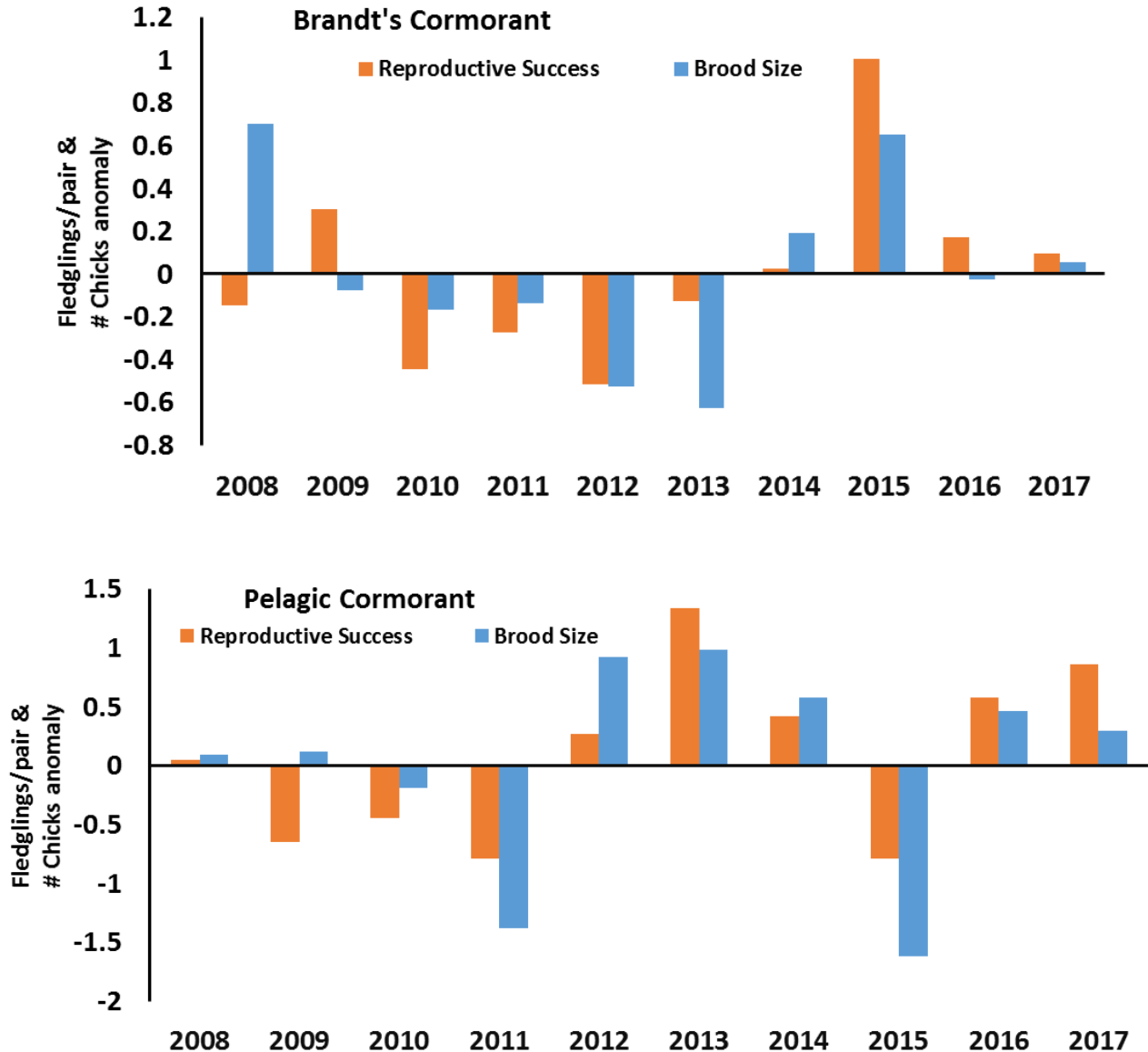


Figure 43. Anomalies of reproductive success and brood size for cormorants nesting at Yaquina Head, Oregon, 2008–17. Cormorants had average to above average reproductive success and brood size.

Since 2011 much of the reproductive loss for murre at Yaquina Head has been due to egg and chick predation (Horton 2014). Murre egg and adult losses in 2017 were less than in 2016, but still similar (2.38 eggs destroyed per hour of observation, n = 203 hours) to the post 2011–16 mean of high disturbance years. Lower egg depredation rates compared to 2016 is partly because fewer eggs were present to be consumed. In 2017, predation pressure was so intense, and murre were not committed to breeding (due to predation pressure and lack of sufficient prey resources), that average incubation time was less than 3 days before the egg was lost—well under the approximately 30 or more days needed to hatch a chick. As in most previous years,

disturbances were primarily (80%) caused by bald eagles (*Haliaeetus leucocephalus*).

In contrast to murre, Brandt’s (*Phalacrocorax peniscillatus*) and pelagic (*P. pelagicus*) cormorants both successfully reared young in 2017. Brandt’s cormorants’ reproductive success (0.79 fledglings/nest) was similar to 2014 and 2016, but less than 2015 (1.70 fledglings/nest) and overall slightly above the long-term mean (fig. 43). Median hatch date (July 6) was slightly earlier than average for Brandt’s cormorant (fig. 44), while average brood size (1.73 chicks) was close to the long-term mean (fig. 43).

Pelagic cormorants had their second highest reproductive success since 2008 (1.65 fledglings/nest), only surpassed by 2013 (2.13 fledglings/nest; fig. 43).

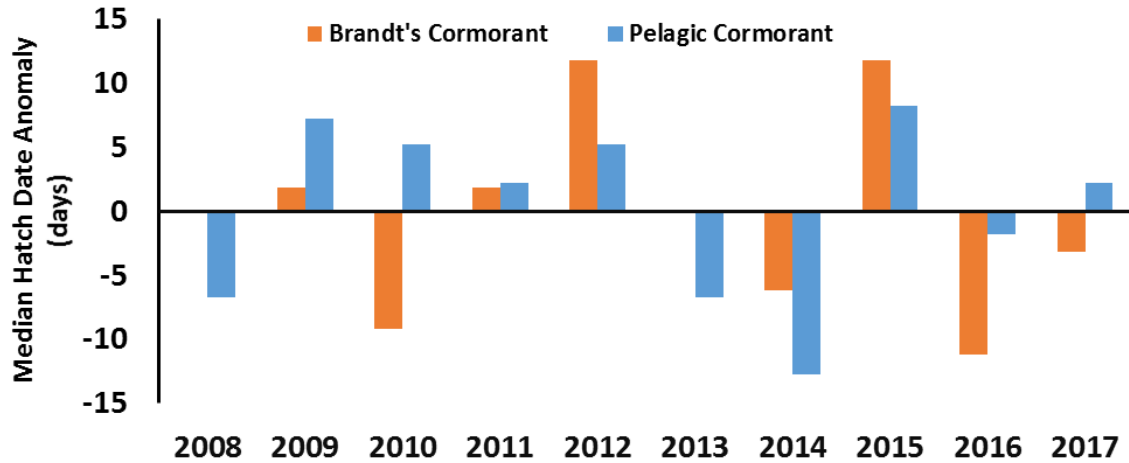


Figure 44. Anomalies of median hatch dates for Brandt's and pelagic cormorants at Yaquina Head, Oregon 2008-17. Brandt's hatch date was over a week earlier, while pelagic cormorant hatch date was near the long-term mean.

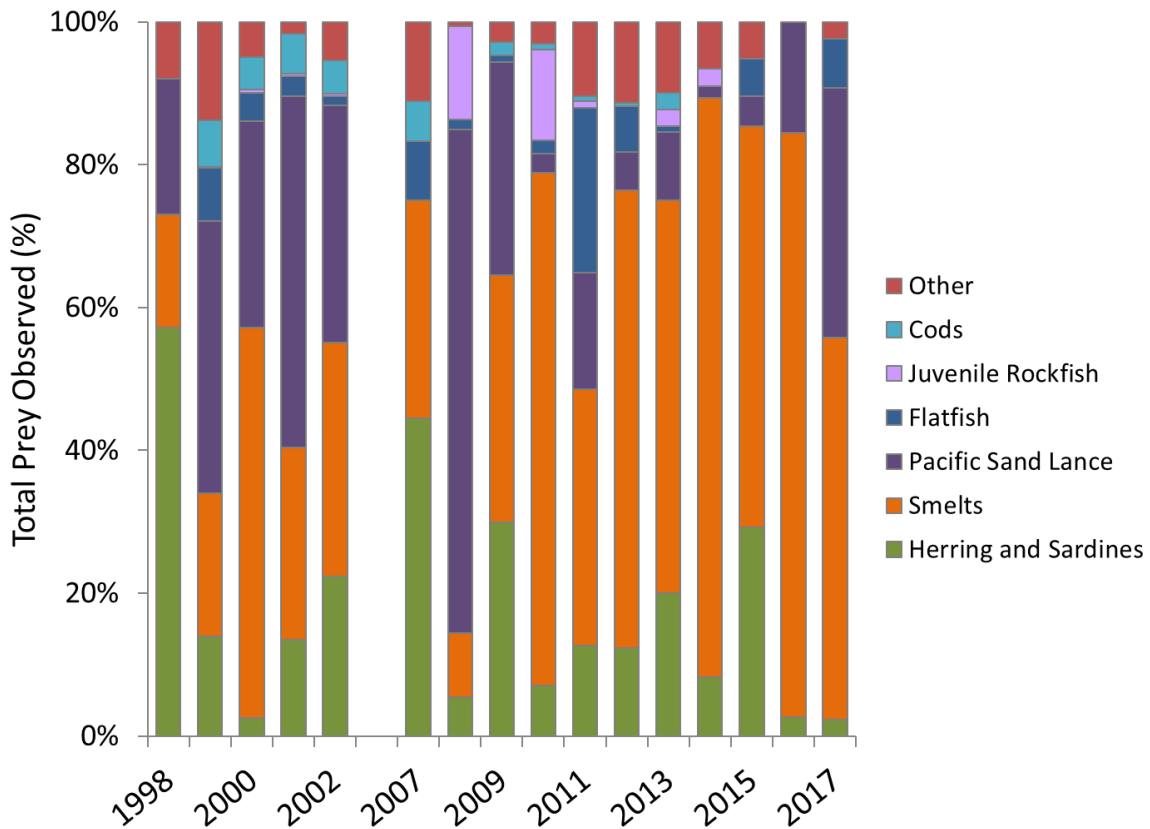


Figure 45. Prey fed to common murre chicks (% occurrence) at Yaquina Head, Oregon, 1998-2017.

There were 46 nests visible from observation platforms, second only to 2014 (34 nests) and a more than 400% increase from 2015 and 50% increase from 2016 (data not shown). Pelagic cormorant reproductive success has been highly variable during our time series (fig. 43). Median hatch date, which can track potential systemic changes to phenology, was July 18, which was a bit later than the long-term average (fig. 44).

During the duration of the time-series the four main forage fish species fed to murre chicks were smelt (*Osmeridae*), herring, sardine, and Pacific sand lance (fig. 45). The failure of most of the colony prior to chick rearing made it challenging to quantify diet composition in 2015-17. Although there were no instances when fish were actually fed to chicks in 2017, we were able to directly observe which fish were in the

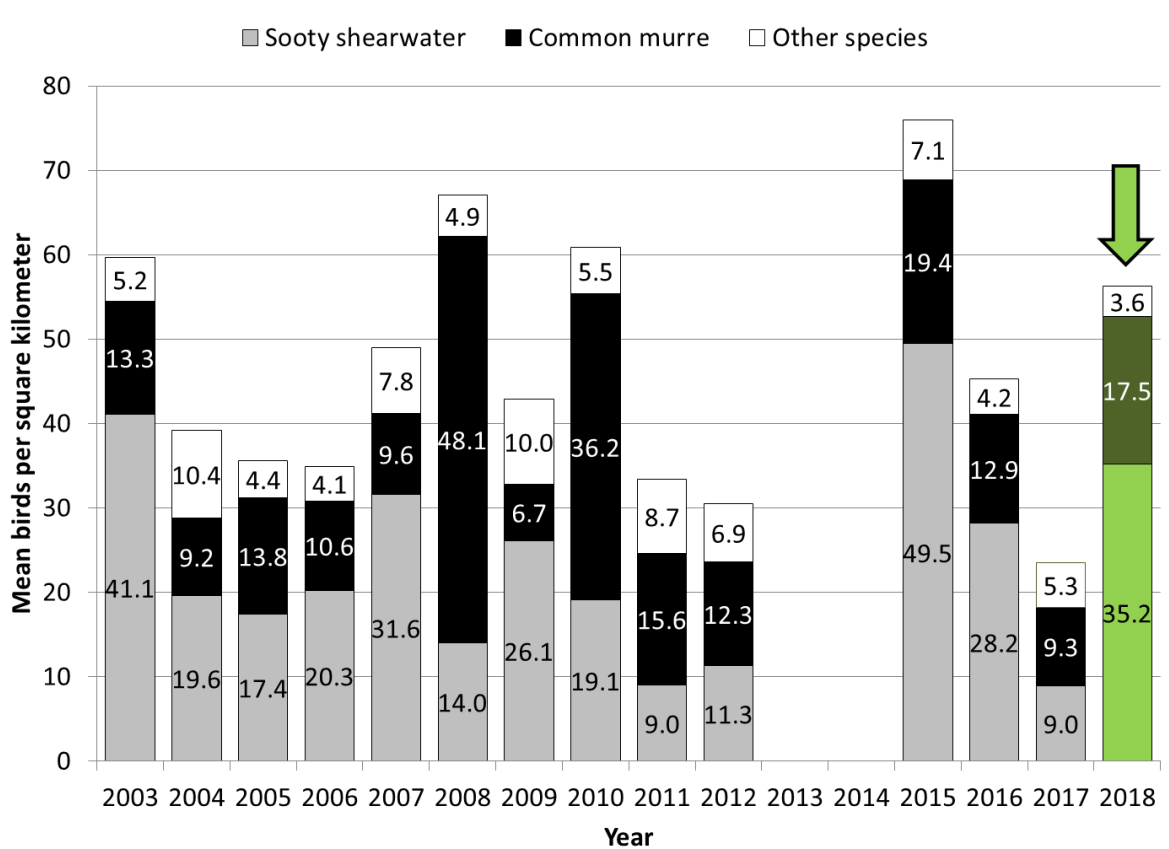


Figure 46. Mean seabird density observed on the continental shelf between Cape Flattery, WA (48.23°N) and Newport, OR (44.67°N) during annual JSOES surveys during late June. In 2018 sooty shearwater and common murre are depicted by light and dark green, respectively.

beaks of birds flying into the colony. Diets in 2017 were again dominated by smelt (53%), similar to 2015, but less so than 2014 (81%) and 2016 (82%), continuing a trend of smelt-dominated diets for six of the past eight years (since 2010; fig. 45). Murre diets in 2017 had an unexpectedly high percentage of sand lance (35%), which has been scarce in the diets since 2010 and is generally associated with cold water temperatures (Gladics et al. 2014, Gladics et al. 2015). Clupeids (primarily Pacific herring) are generally associated with warmer water off Oregon and positive PDO indices (Gladics et al. 2015; Daly et al. 2017), although their occurrence in recent warm and positive PDO years has been lower than during previous warm water events.

Northern California Current: Cape Flattery, Washington to Newport, Oregon

Information on seabird density patterns for the northern domain of the California Current during June is provided from the JSOES (this survey also provided data from Figures 28–30). Bird densities in 2018 were more typical compared to the extremely low densities in 2017 (fig. 46). Mean total bird densities for the 2018 survey were the 5th highest reported in the 14-year JSOES data set (56.2 birds per km² compared to a

median value of 44.1 birds per km²). The majority of birds observed during the survey (93.8% of all individuals counted) were sooty shearwaters (*Ardenna grisea*, 68.2%) and murre (25.6%). Sooty shearwater abundance was the 3rd highest on record for this survey (35.2 birds per km², compared to the time-series median of 19.9 birds per km²; fig. 46). Sooty shearwater were highly aggregated as 93.3% of all individuals observed during the survey were on the two transects closest to the mouth of the Columbia River (between the Columbia River at 46.16°N and Cape Meares, OR, at 45.48°N). Given that sooty shearwaters do not breed in the northern hemisphere, this aggregation pattern probably indicates that birds were aggregating on prey items such as forage fishes, squid, or krill abundant near the Columbia River mouth.

Similar to the pattern seen in sooty shearwaters, murre abundance in 2018 was the 4th highest on record (17.5 birds per km², compared to the time-series median of 13.1 birds per km²). Murre were also aggregated near the Columbia River mouth, with 72.9% of all individuals observed on the two transects closest to the Columbia River (Columbia River and Cape Meares, Oregon; fig. 1). While aggregations of murre are to be expected near Cape Meares regardless of prey abundance due to

the large murre breeding colonies located in this area (~200,000 birds), the Columbia River transect is ~80 km north of Cape Meares, and ~30 km from the nearest murre colony that is near Tillamook Head, Oregon (fig. 1). It is reasonable to infer the large numbers of murre seen near the Columbia River mouth—like the shearwaters in the same area—were attracted to abundant prey items.

The 2018 JSOES surface trawls during this same survey showed that market squid were present in fairly high abundance (fig. 28), although it is not known whether birds were consuming squid. Pacific herring and surf smelt (*Hypomesus pretiosus*) were also present in surface trawls (fig. 28), and these species are known to occur in both shearwater and murre diets. There is mounting evidence that the region near the Columbia River mouth is an important foraging habitat in the northern California Current for both sooty shearwater and common murre, and that there is a direct connection between river plume dynamics and seabird prey abundance in the marine environment (Adams et al. 2012; Zamon et al. 2014; Phillips et al. 2017; Phillips et al. 2018). Data from 2018 seabird distributions support the hypothesis that the Columbia River plume plays an important role in trophic interactions for seabirds in this domain of the California Current.

Northern California Current: Castle Rock National Wildlife Refuge

Murre are the most abundant surface nesting seabird at Castle Rock, California³¹, and their reproductive success, nesting phenology, and chick diet have been studied since 2007. The percent of nesting pairs that successfully fledged young in 2017 was based on 77 breeding pairs monitored every other day for the duration of nesting. As at Yaquina Head, Oregon, murre experienced complete reproductive failure at this island (0 fledglings per pair) in 2017 for the first time since monitoring began 11 years ago (fig. 47A). Many murre (83%) abandoned nests prior to hatching, presumably due to inability to maintain incubatory obligations while meeting their own energetic needs from prey available in waters within flight distance of Castle Rock. For the few nests producing chicks, 100% of the chicks died prior to fledging, with starvation being the primary cause of death. While the bottom-up food limitation was the primary cause of mortality, the food limitation caused murre to frequently leave chicks alone at the colony in search of

prey, and these unprotected chicks were sometimes consumed opportunistically by western gulls (*Larus occidentalis*) that also nest at the island. Reproductive failure of murre at Castle Rock is consequential for the overall population of murre nesting in the California Current as this island is one of the most populous colonies south of Alaska (Carter et al. 2001).

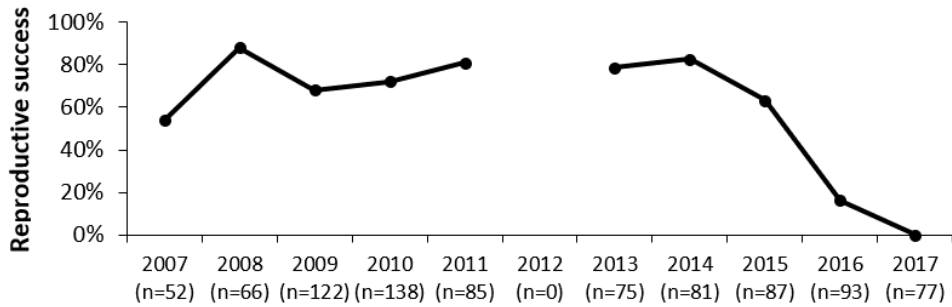
In 2017, the average nest initiation date for common murre was 23 May, which was 13 days later than the long-term average at this colony (fig. 47B). This delay in nesting is indicative of a delay in upwelling or other environmental conditions that limit the abundance of prey (Schroeder et al. 2009). Although the timing of nesting by murre is not a direct response to the onset of upwelling in the spring, the increased availability of food associated with upwelling improves the body condition of egg-laying females and thereby influences the timing of nesting (Reed et al. 2006).

Typically, diet surveys would be conducted 6 days per week during the chick-rearing period to determine composition of prey fed to common murre chicks. In 2017, however, very few prey were actually seen at Castle Rock despite extensive survey efforts. We assume that the lack of observations was due to the scarcity of prey and early starvation of chicks. Only four individual fish were observed: two anchovy, one Pacific sand lance, and one flatfish (fig. 47C). These observations provide further evidence that, as detected from fish surveys off Oregon (figs. 26–28, 31–32), the prey community in much of the northern California Current continued to be comprised of atypical species that are associated with relatively warm water (similar to 2016), and that the 2016–17 forage community differed greatly from those found between 2007–15 (fig. 47C). Although it is not possible to draw conclusions about the composition of prey based on 4 observations, we can state with confidence that prey was scarce around Castle Rock in 2017.

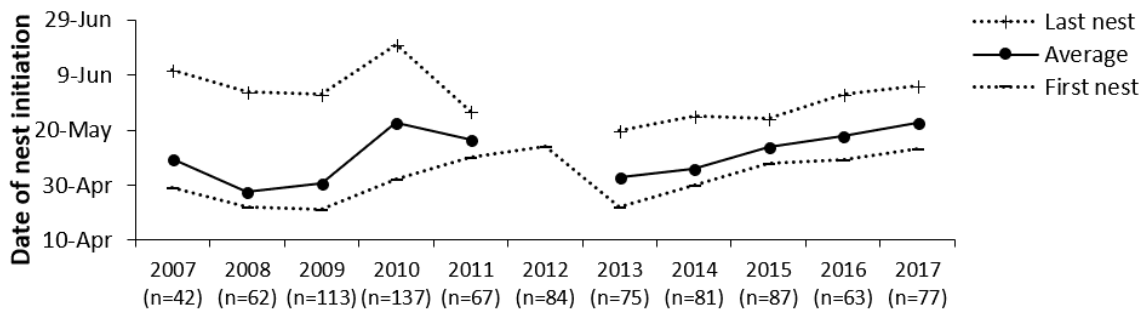
Brandt's cormorant is the second-most abundant surface-nesting seabird at Castle Rock, and their reproductive success has been studied since 2011. In 2017, we observed 31 breeding pairs at Castle Rock. These pairs typically initiated nesting but, of the 31, only 58% (n=18) produced eggs in 2017. In addition to this reduced breeding effort, all nests that were initiated failed prior to hatching due to nest abandonment and no chicks were observed in 2017 (fig. 47D). Notably, this finding contrasts with Yaquina Head, Oregon, where Brandt's cormorant reproductive success was slightly above the long-term average (fig. 43). Similar to murre, this level of failure has never been documented at Castle Rock, and provides further evidence that prey was so scarce that adult cormorants were unable to meet their own energetic needs by foraging within flight distance of Castle Rock and had to abandon nests to avoid starvation.

³¹Castle Rock National Wildlife Refuge, an island off Crescent City, California has frequently been the most populous single-island seabird breeding colony in California (Carter et al. 2001). A remotely-controlled video monitoring system was installed at this island in 2006. For purposes of assessing the state of the California Current, the reproductive performance of common murre and Brandt's cormorants is provided. For common murre, nesting phenology and chick diet between 2007 and 2016 is also provided.

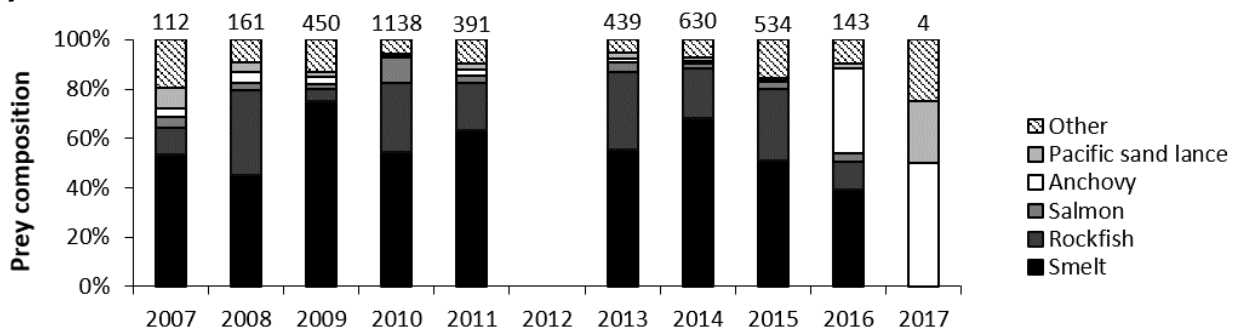
(A) Common Murre reproductive success



(B) Common Murre nesting phenology



(C) Common Murre chick diet



(D) Brandt's Cormorant reproductive success

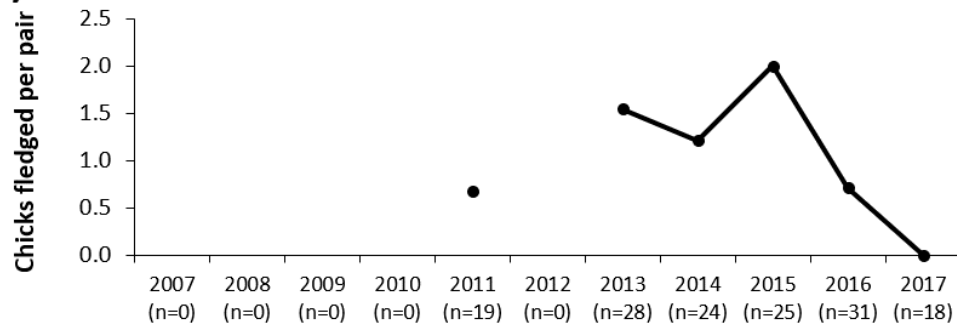


Figure 47. Reproductive data for seabirds nesting at Castle Rock National Wildlife Refuge, Del Norte County, CA between 2007 and 2017; (A) Percent of common murre nesting pairs that successfully fledged young. The sample size (n) represents the total number of nesting pairs observed per year, and this figure does not include the success of replacement clutches. (B) First, average, and last dates for nests initiated by common murre. The date of nest initiation was defined as the day that an egg was laid at a nest site. The sample size (n) represents the total number of nests observed each year where nest initiation dates were accurate to ± 3.5 days. (C) Composition of prey delivered to chicks by common murre. Numbers above each bar indicate the total number of prey identified each year. (D) Chicks fledged per nesting pair of Brandt's cormorant. The sample size (n) represents the total number of nesting pairs observed per year, and this figure does not include the success of replacement clutches. For each section, data from 2012 is lacking due to premature failure of the video monitoring system.

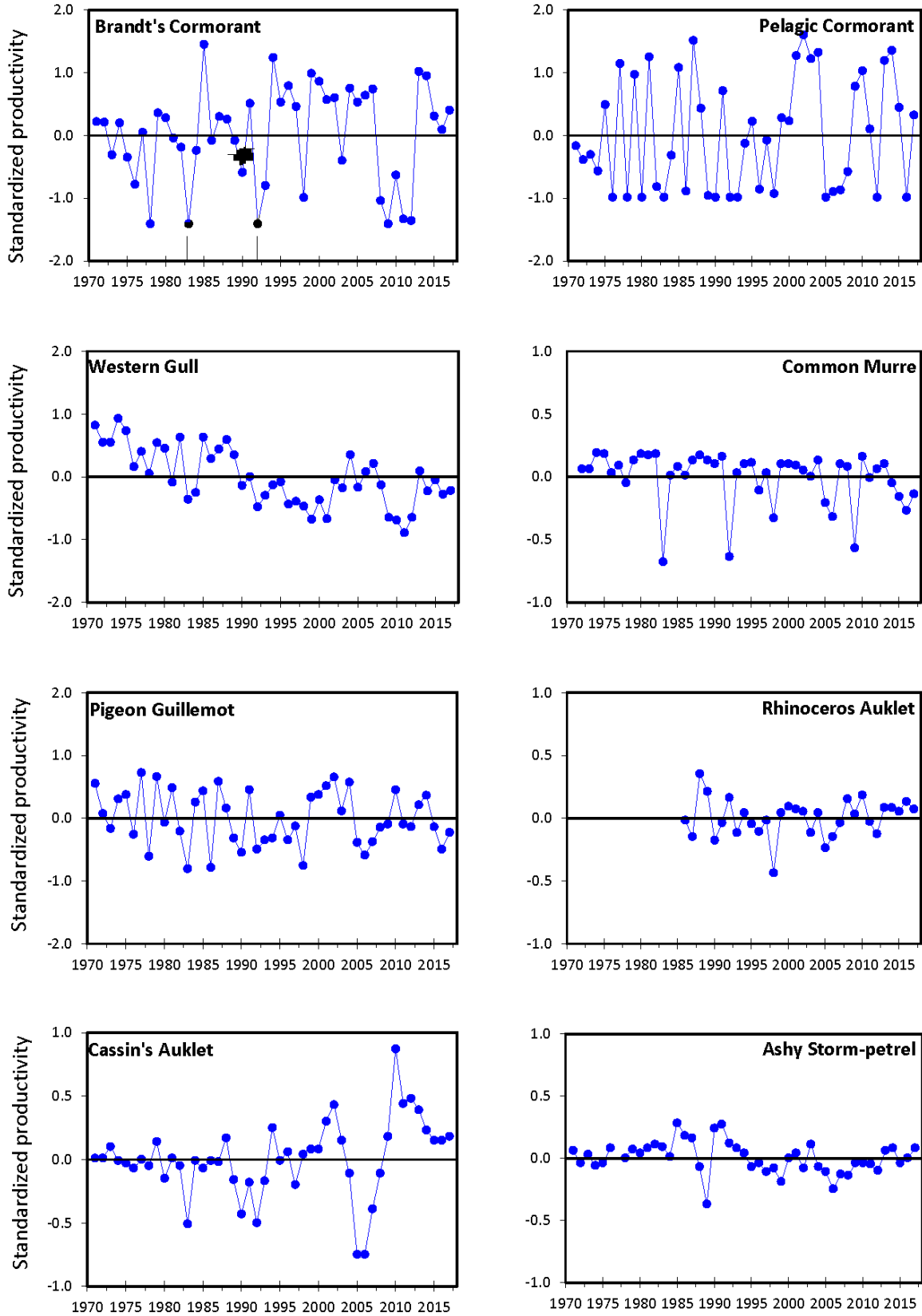


Figure 48. Standardized productivity anomalies through 2017 (annual productivity minus the 1971–2017 mean) for 8 species of seabirds on Southeast Farallon Island.

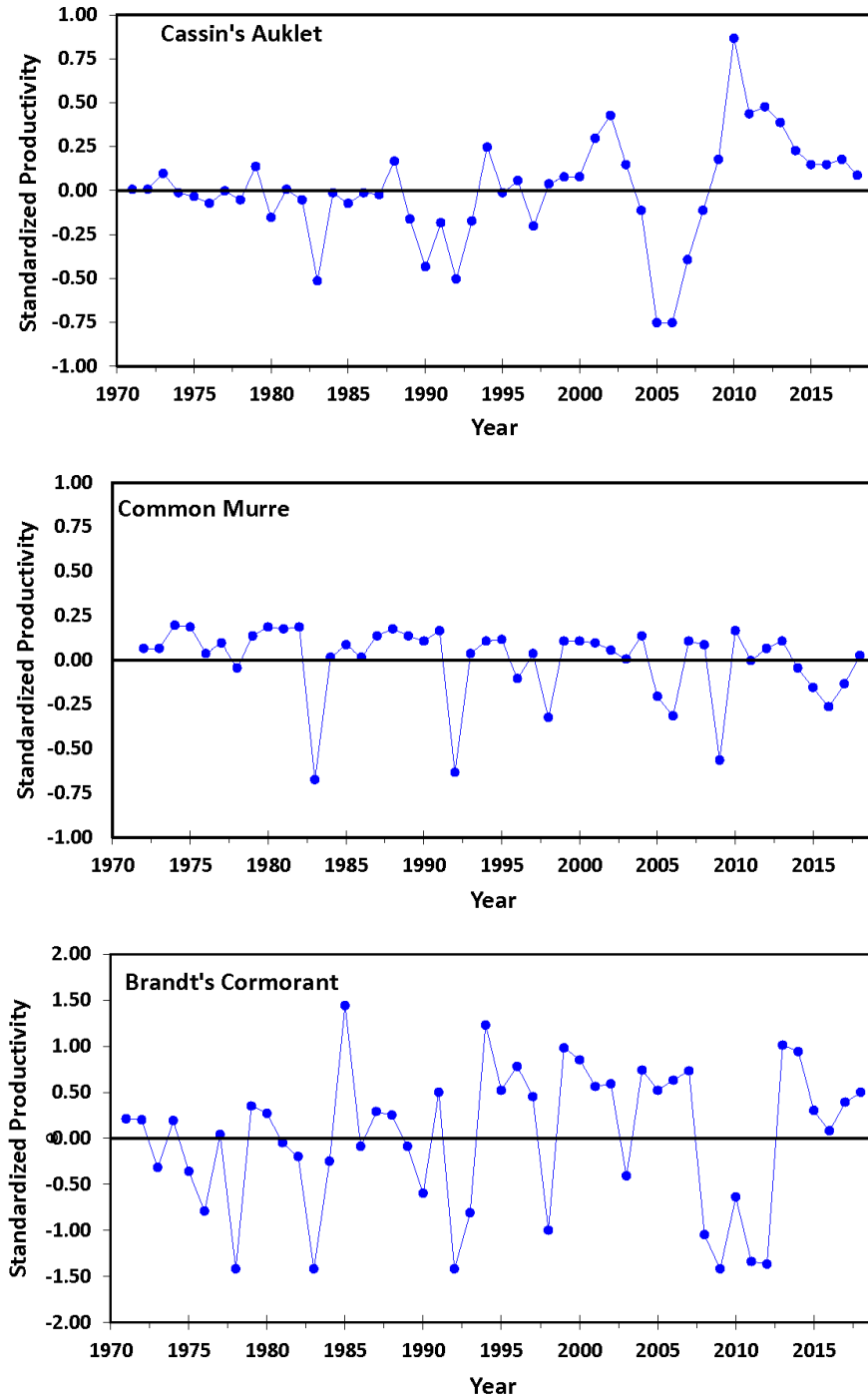


Figure 49. Standardized productivity anomalies through 2018 (annual productivity minus the 1971–2018 mean) for 3 species of seabirds on Southeast Farallon Island.

Central California: Southeast Farallon Island

Reproductive success was average or below average for most birds at Southeast Farallon Island in 2016, which is typical during El Niño conditions (Wells et al. 2017). Productivity increased for all birds but rhinoceros auklet in 2017. In 2017 Brandt’s cormorant, pelagic cormorant, Cassin’s auklet (*Ptychoramphus aleuticus*),

rhinoceros auklet (*Cerorhinca monocerata*), and ashy storm petrel (*Oceanodroma homochroa*) production was above average, while western gull, murre, and pigeon guillemot (*Cepphus columba*) were just below average (fig. 48). Productivity values were available for 3 species in 2018, and Brandt’s cormorant was well above average, Cassin’s auklet just above average, and murre average (fig. 49).

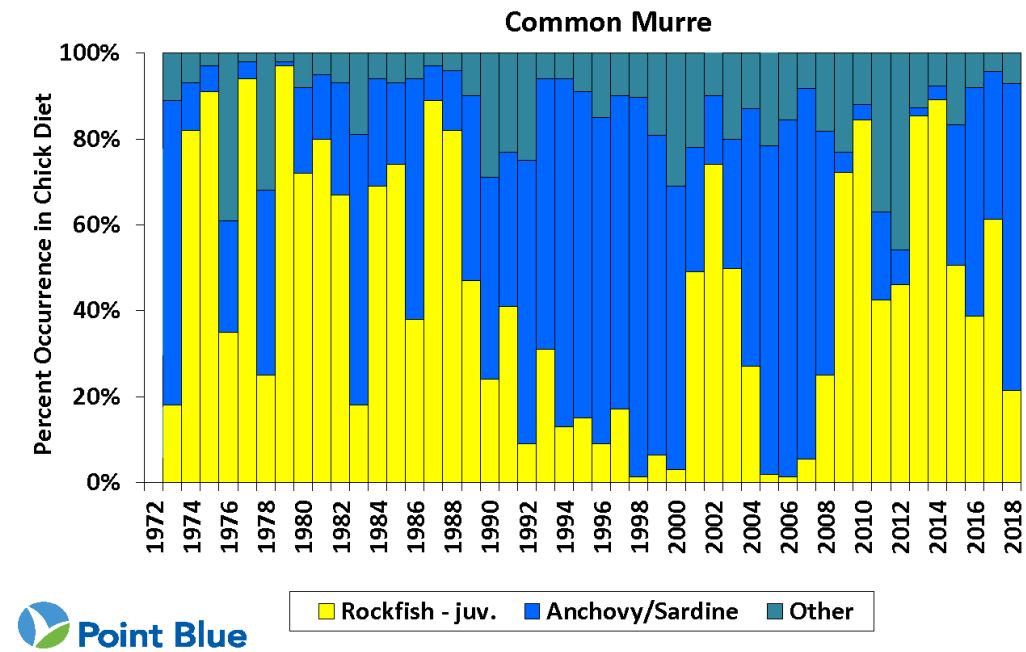
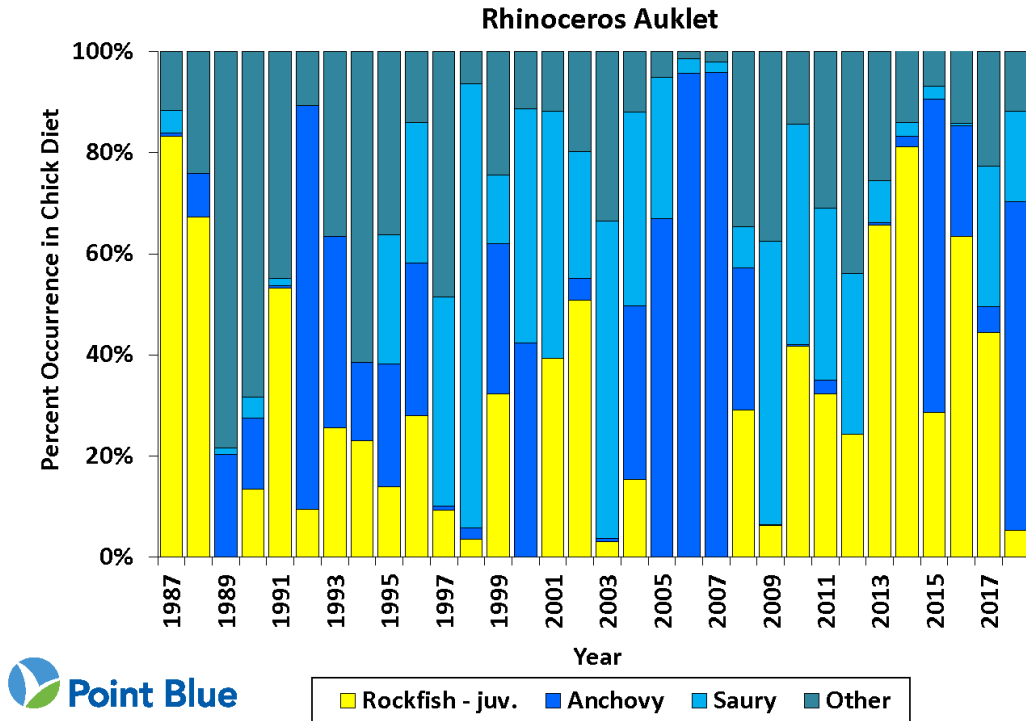


Figure 50. Diets of rhinoceros auklet and common murre returning to feed chicks on Southeast Farallon Island.

The recent increase in anchovy abundance off central California (fig. 33) was reflected in the fish that birds fed their chicks. Whereas juvenile rockfish was the most common component of rhinoceros auklet and common murre chick diets in 2017, over 50% of diet for both species was comprised of anchovy in 2018 (fig. 50).

Central and Southern California: RREAS and CalCOFI

Seabird distribution and abundance anomalies are presented from the RREAS core region (fig. 51). The RREAS typically encounters higher concentrations of resident breeding species within the Gulf of the

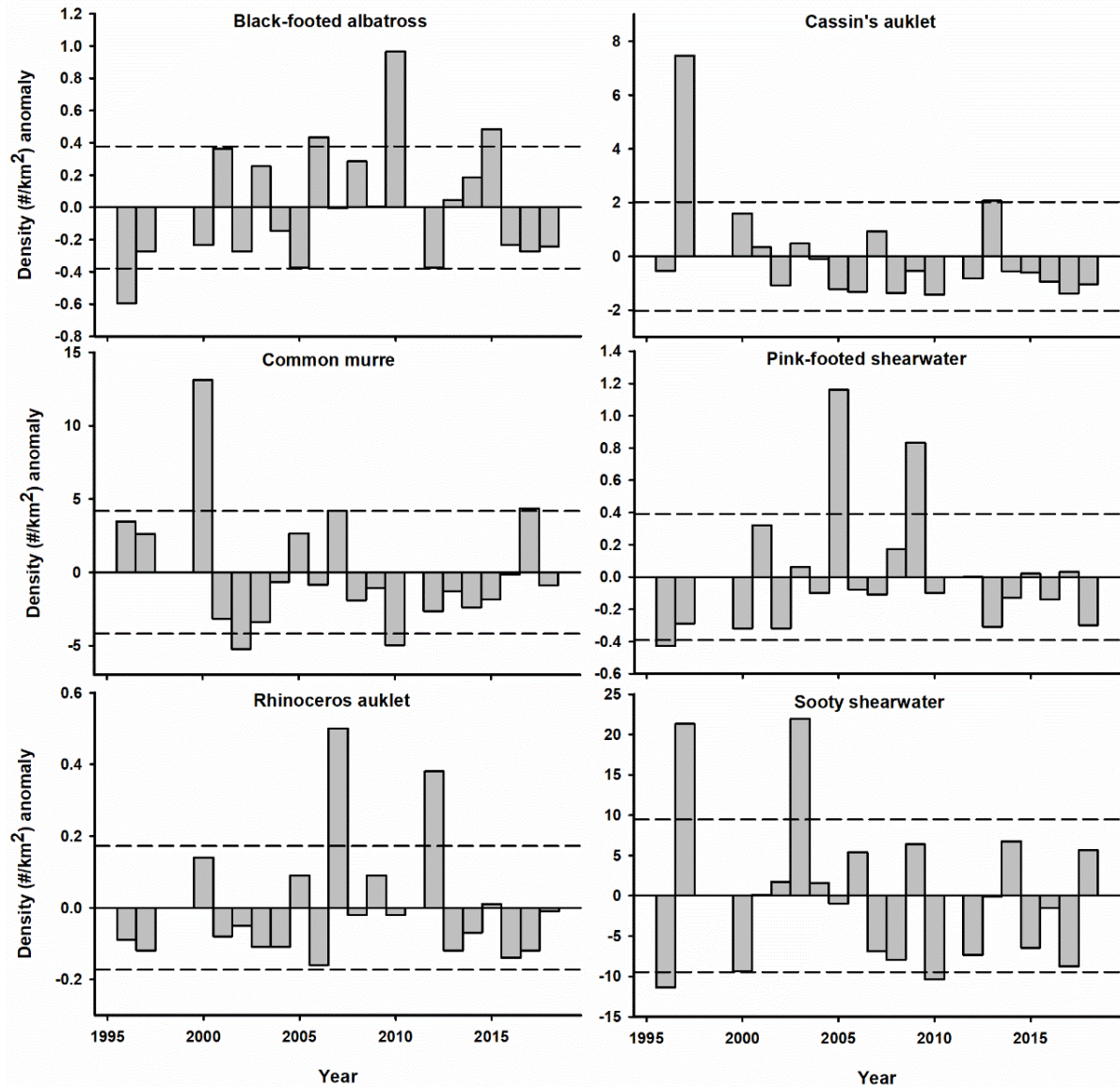


Figure 51. Density anomalies ($\#/km^2$) for seabirds on the core area (central California) of the Rockfish Recruitment and Ecosystem Assessment Survey (RREAS) survey 1996–2018. Surveys were not conducted in 1998, 1999, and 2011. The dashed lines indicate ± 1 standard deviation.

Farallones. Resident breeders such as murre, Cassin’s auklet, and rhinoceros auklet displayed negative density anomalies during the recent large marine heat wave (2014–16; fig. 51). However, the murre density anomaly in 2017 was strongly positive for the first time since 2005 and 2007, and may be related to increased concentrations of non-breeding individuals. By contrast, migrant black-footed albatross (*Phoebastria nigripes*) densities were anomalously low since 2015 and pink-footed shearwaters (*Puffinus creatopus*) continued to display negative anomalies subsequent to 2009. Interestingly, compared to the CalCOFI region (below), the sooty shearwater density anomaly was positive off central California during spring 2018 and may indicate that shearwater aggregations were concentrated in response

to good foraging conditions (e.g., increase adult anchovy; figs. 33, 35) in this region (fig. 51).

Anomalies of seabird density in spring within the CalCOFI region can be indicative of variation in species’ habitat affinities such as warm- (black-footed albatross, Cook’s petrel [*Pterodroma cookii*], and elegant tern [*Thalasseus elegans*]) and cold-water (pink-footed shearwater, Sabine’s gull [*Xema sabini*], and sooty shearwater) conditions (Hyrenbach and Veit 2003; Santora and Sydeman 2015). Spring seabird density anomalies may also be correlated with other factors such as prey availability (Sydeman et al. 2015) and population trends or range shifts in breeding or wintering distributions (Velarde et al. 2015). Within the CalCOFI region, anomalies of cold-water species

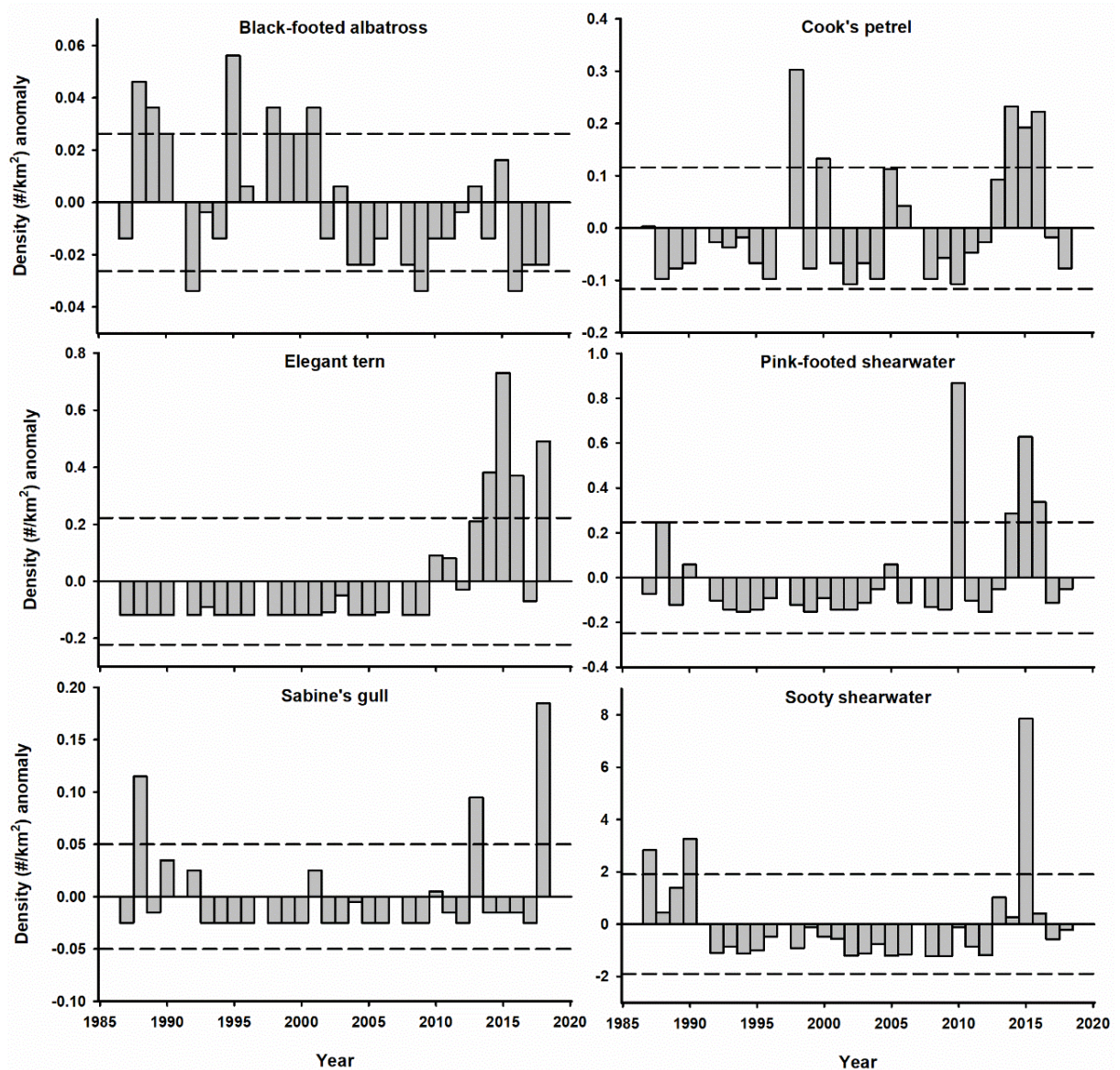


Figure 52. Density anomalies (#/km²) for seabirds from the spring CalCOFI surveys, 1987–2018. No survey was conducted in 1991, 1997, or 2007. The dashed lines indicate ± 1 standard deviation.

were generally neutral compared to the consecutive strong positive anomalies observed during the recent large marine heat wave (2014–16). For example, the trans-hemisphere migrants, sooty shearwater and pink-footed shearwater, displayed strong positive anomalies during the large marine heat wave and slight negative anomalies during spring 2017 and 2018 (fig. 52). The strong positive anomalies for shearwaters during the heat wave likely represent increased concentrations of these numerically dominant species within productive coastal waters of the Southern California Bight due to the lack of suitable foraging habitat within the northern CCS and Gulf of Alaska (Veit et al. 1996; Thompson et al. 2012). However, Sabine’s gull, another cold-water species, displayed the strongest positive density anomaly

on record in 2018, which may indicate this species’ migration was impacted by the return to relatively cool ocean conditions during spring. Species with warm-water affinity, such as Cook’s petrel, showed negative density anomalies during spring 2018 compared to their sustained strong positive anomalies during 2014–16 (fig. 52). Black-footed albatross density anomalies also continued to display a long-term decline which may be related to the overall decline of their populations in Hawaii and elsewhere in the North Pacific (fig. 52). By contrast, the second highest spring density anomaly of elegant tern was observed during 2018 (fig. 52), and the recent increasing trend suggests this pattern reflects the continuing northward range expansion of this species within the CCS (Velarde et al. 2015).

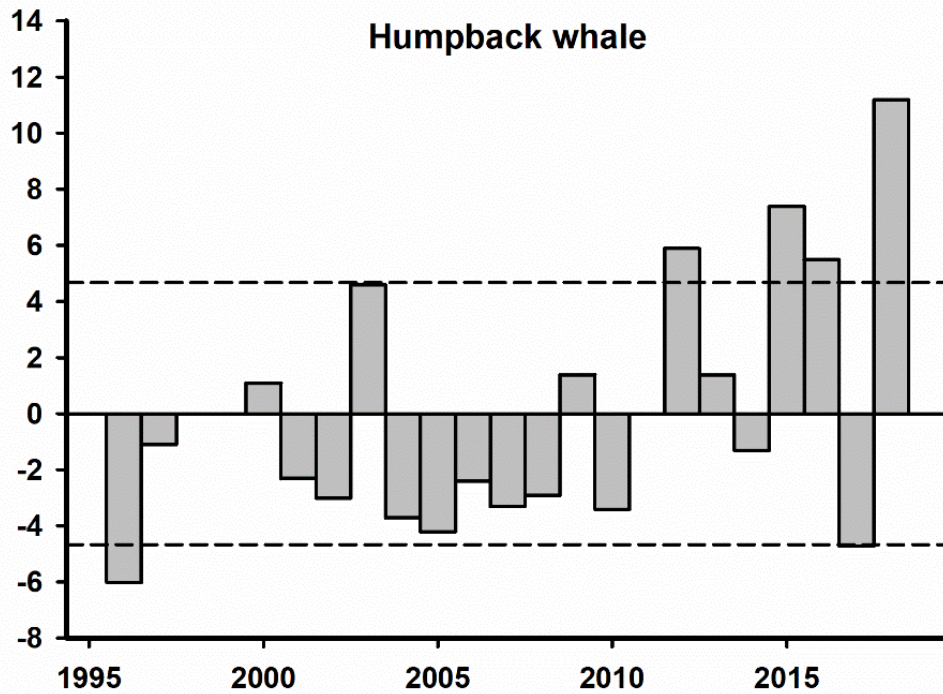


Figure 53. Encounter rate anomaly (#/100 km) for humpback whales from the core area of the RREAS survey 1996–2018. No survey was conducted in 1998, 1999, and 2011. The dashed lines indicate ± 1 standard deviation.

MARINE MAMMALS

Central CA: Humpback Whales

Whale surveys on the RREAS within central California documented that the humpback whale (*Megaptera novaeangliae*) encounter rate anomaly continued to increase over the past decade. In fact, encounter rates in spring 2018 were the highest ever observed (fig. 53). This may indicate either that humpback whale populations are increasing or that foraging conditions (e.g., availability of krill and anchovy aggregations) are favorable for concentrating whales during spring. Furthermore, compared to the recent marine heat wave (e.g., 2014–16), where humpback whales were concentrated closer to shore (Santora et al. unpublished data), during 2018, humpback whales were both frequently sighted along the outer shelf and within submarine canyons, coinciding with high concentrations of euphausiids, and inshore where increased adult anchovy were observed during the RREAS.

Southern CA: Sea Lions

California sea lions (*Zalophus californianus*) are permanent residents of the CCS, breeding in the California Channel Islands and feeding throughout the CCS in coastal and offshore habitats. They are also sensitive to changes in the CCS on different temporal and spatial scales and so provide a good indicator species for

the status of the CCS at the upper trophic level (Melin et al. 2012). Four indices are used to measure trends in the population: 1) live pup census, 2) pup condition at 4 months of age, 3) pup growth rates during the period of maternal nutritional dependence, and 4) nursing female diet during the maternal care period on San Miguel Island, California.³² The live pup census is a measure of successful births and is an indicator of prey availability to and nutritional status of nursing females from October to the following June.³³ Pup condition and growth rates during the period of nutritional dependence measure the transfer of energy from the mother to the pup through lactation between June and the following February, which is dependent on prey available to nursing females during that time. The frequency of occurrence of prey in the diet of nursing females provides a relative measure of the available for-

³²San Miguel Island, California (fig. 1, right panel) is one of the largest colonies of California sea lions, representing about 45% of the US breeding population. As such, it is a useful colony to measure trends and population responses to changes in the marine environment.

³³We used the number of pups alive at the time of the live pup census conducted in late July and the average weights of pups at 4 months and 7 months of age between 1997 and 2017 as indices of the population response to annual conditions in the CCS. The number of live pups in late July represents the number of pups that survived from birth to about 6 weeks of age. Live pups were counted after all pups were born (between 20–30 July) each year. A mean of the number of live pups was calculated from the total number of live pups counted by each observer. A long-term average live pup count based on counts between 1997 and 2017 was used to create annual anomaly percentages from the long-term average.

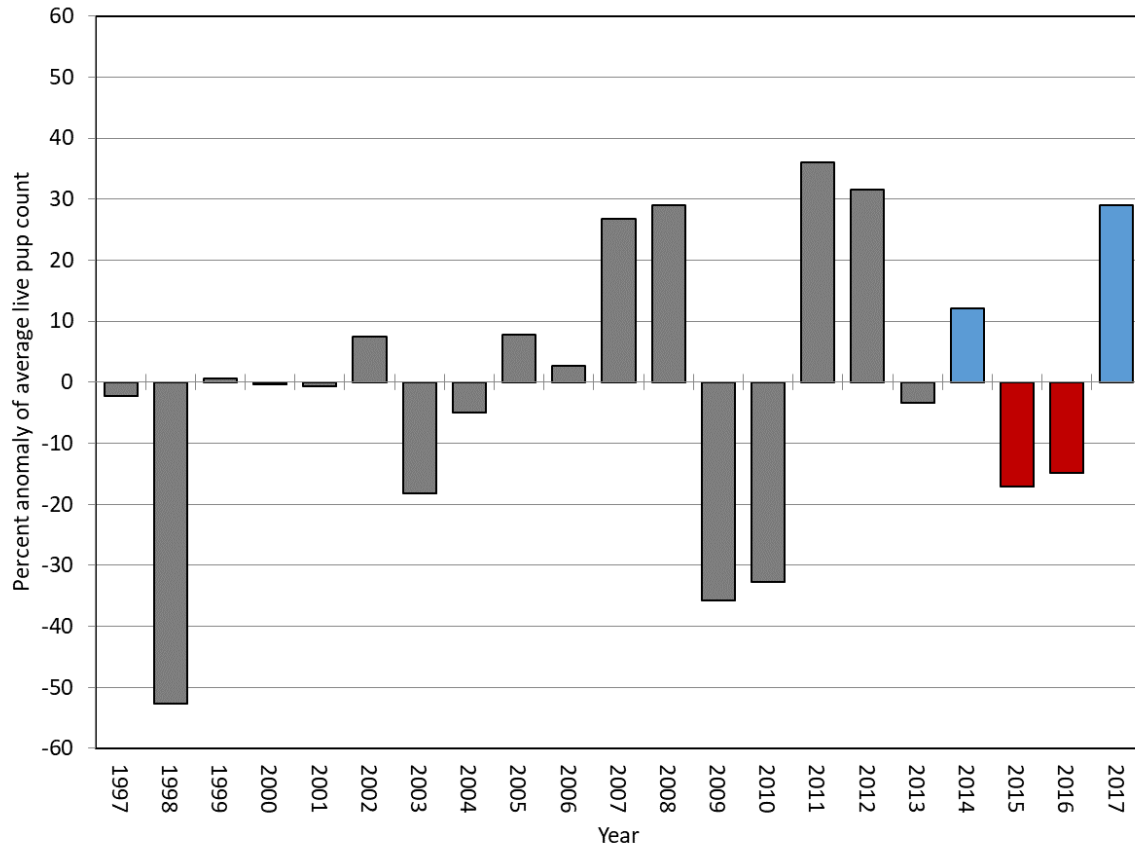


Figure 54. The percent anomaly of live California sea lion pup counts at San Miguel Island, California, based on a long-term average of live pup counts between 1997–2017 in late July when surviving pups were about 6 weeks old. Red (negative) bars represent shifts in index in relation to 2014–15 heat wave and 2015–16 El Niño; blue (positive) bars represent positive anomalies as conditions transitioned back to more typical conditions.

age community during the period of pup nutritional dependence.³⁴

The 2014–15 marine heat wave and 2015–16 El Niño conditions affected the number of births (fig. 54), pup condition (fig. 55) and pup growth (fig. 56) of three cohorts of California sea lions in 2014, 2015, and 2016. The effects varied for each cohort based on the timing of the events relative to pupping and rearing seasons. The onset of the marine heat wave in November 2014 followed a normal pupping season with the number of live pups similar to the long-term average (fig. 57). However, as the event intensified in the following winter and spring foraging conditions rapidly deteriorated for nursing females resulting in poor pup condition and lower growth rates for the 2014 cohort (figs. 55, 56). The 2015 cohort was born as the CCS transitioned from the marine heat wave to El Niño conditions in summer 2015. This led to a lower number of births in 2015 (fig.

54) and as El Niño conditions intensified, the 2015 pup cohort was in poor condition (fig. 55) and had the lowest growth rates (fig. 56) for pups in the time series. As El Niño conditions subsided in spring 2016, the number of births remained low (fig. 54) but pup condition (fig. 55) and growth rates (fig. 56) returned to normal. By 2017, when the south and central CCS returned to cooler oceanic patterns, all the indices returned to normal or exceeded the long-term averages (figs. 54–56).

Relative to the entire 1997–2017 time series, the annual number of live California sea lion pups³⁵ has been quite variable since 2007 (fig. 54) owing to several regional events that altered the availability of prey to pregnant and nursing females, the strongest of which were the 2009 upwelling relaxation event and 2010 El Niño conditions. However, the marine heat wave in 2014–15 resulted in a significant decline (26%) in the

³⁴Each year, between 200 and 500 pups were weighed when about 4 months old. Pups were sexed, weighed, tagged, branded, and released. Up to 60 pups were captured in February and weighed and measured at 7 months of age. Of the 60 pups captured in February, up to 30 pups were branded and provided a longitudinal dataset for estimating a daily growth rate between 4 months and 7 months old.

³⁵We used a linear mixed-effects model fit by REML in R to predict average weights on 1 October and 1 February in each year because the weighing dates were not the same among years. The model contained random effects with a sex and days interaction (days = the number of days between weighing and 1 October and 1 February) which allowed the growth rate to vary by sex and year, and a full interaction fixed effects of sex and days. The average weights between 1997 and 2017 were compared to the long-term average for the average pup weights between 1975 and 2017.

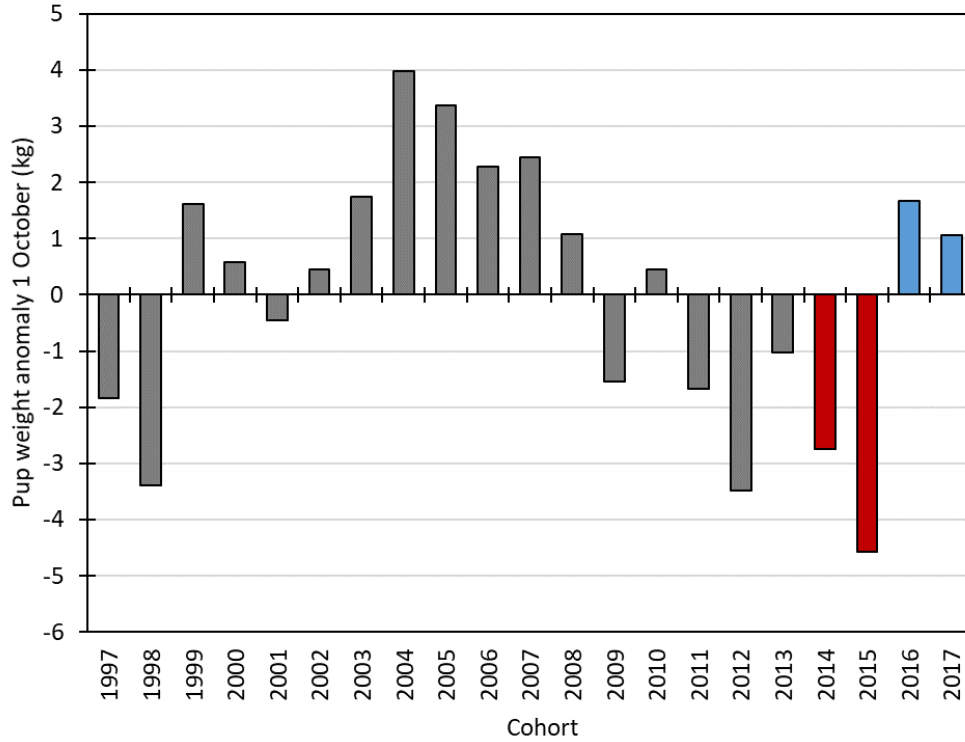


Figure 55. Average pup weight anomaly (kg) from predicted average weights of 4-month-old female California sea lion pups at San Miguel Island, California, from the long-term average between 1997 and 2017. Red (negative) bars represent shifts in index in relation to 2014–15 heat wave and 2015–16 El Niño; blue (positive) bars represent positive anomalies as conditions transitioned back to more typical conditions.

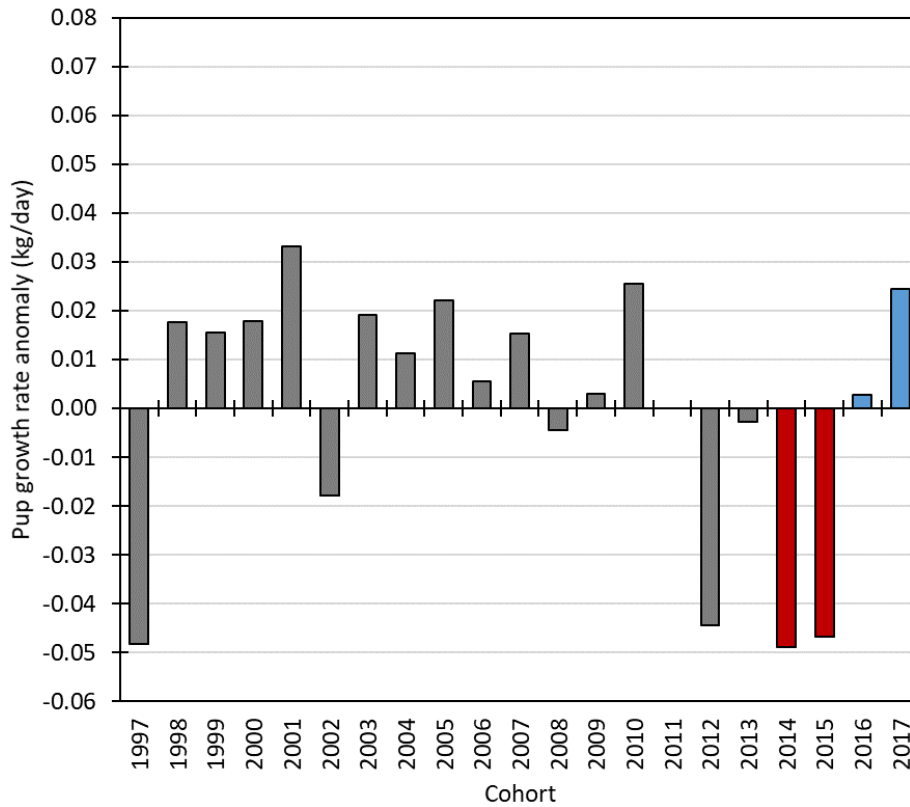


Figure 56. Average daily growth rate anomaly (kg/day) of California sea lion pups from 4 and 7 months old at San Miguel Island, California, from the long-term average between 1997 and 2017. Red (negative) bars represent shifts in index in relation to 2014–15 heat wave and 2015–16 El Niño; blue (positive) bars represent positive anomalies as conditions transitioned back to more typical conditions.

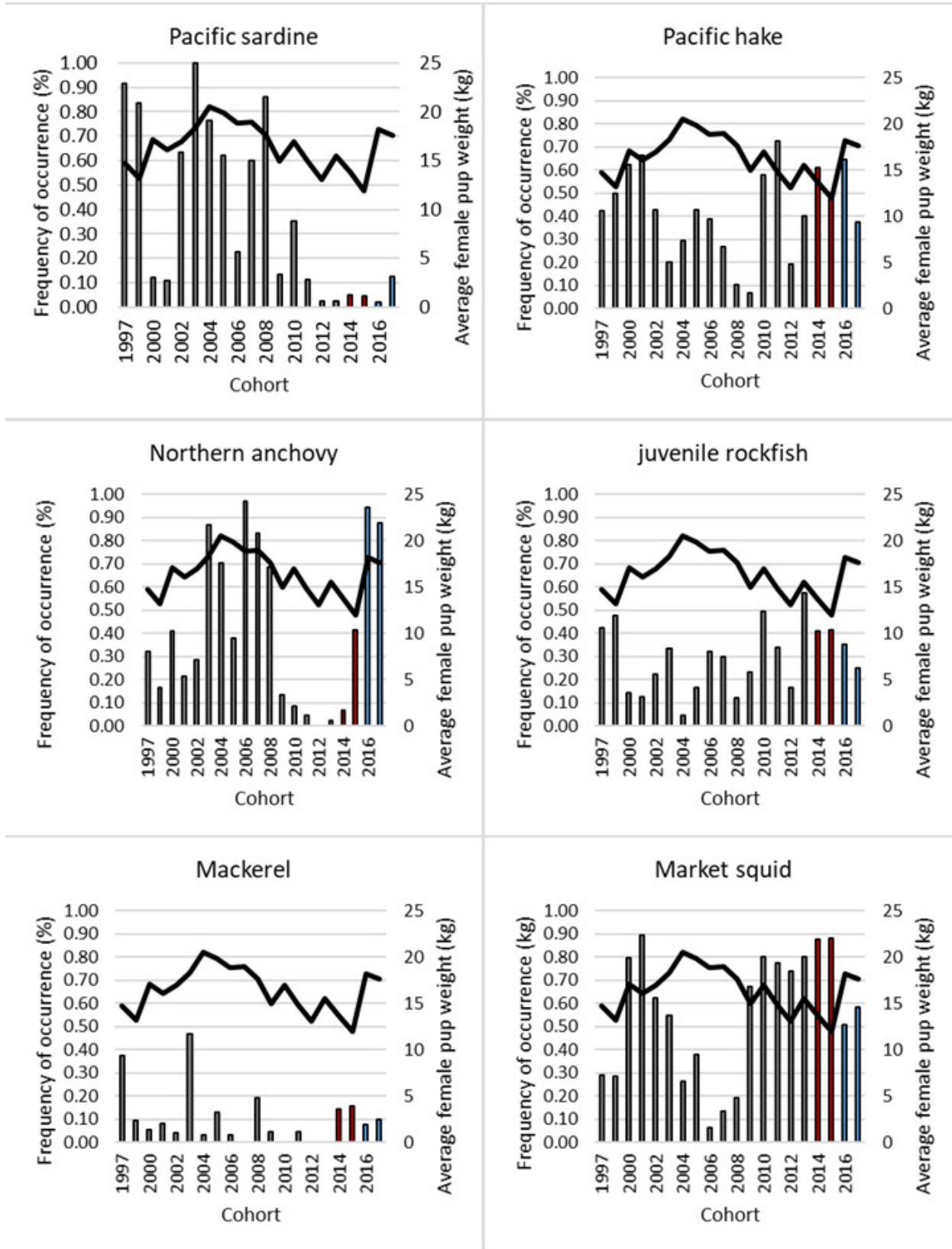


Figure 57. Frequency of occurrence of prey taxa (bars) identified from nursing female fecal samples collected at San Miguel Island during the first 4 months of lactation and average California sea lion pup weight at 4-months-old (line), 1997–2017. Red (negative) and blue (positive) bars represent shifts in index in relation to 2014–15 heat wave and 2015–16 El Niño.

number of live California sea lion pups between 2014 and 2015. The live pup census in 2016 showed some improvement with the number of pups increasing 3% from 2015 to 2016, however it was still 15% below the time series average (fig. 54). In 2017, the number of live pups increased 52% from 2016 and exceeded the long-term average by 29%. The return of births to the long-term average in 2017 indicates that the lower number of births in 2015 and 2016 were not simply the result of fewer reproductive females in the population, but that due to the poor foraging conditions during the gestation period, fewer reproductive females were able to energetically support pregnancies.

Between 1999 and 2008, pup condition at 4 months of age was above or near the long-term average. Since 2009, California sea lion pup condition has remained below the time series average with the 2015 cohort representing the poorest condition on record (fig. 55). Pup condition improved and returned to above normal in 2016 and 2017. The trend in pup growth rate was relatively stable over the time series with most years showing average or above average pup growth between October and February until 2012 (fig. 56), when growth rates declined significantly and marked the onset of the 2013–17 Unusual Mortality Event. Pup growth rates reached record lows for the 2014 and 2015 cohorts before returning to normal in 2016 and improving substantially in 2017, with the third highest growth rate since 1997.

The summer diet of nursing females between 1997 and 2017 showed a marked shift beginning in 2009 with a significant decline in the frequency of occurrence of sardine and anchovy from over 50% from 2003–08 to less than 5% from 2012–14 for both species (fig. 57). Sardine and anchovy were replaced in the diet by higher frequencies of hake and juvenile rockfish, but the dominant species was market squid, consistently occurring at frequencies greater than 60% from 2009–15. This diet persisted during the 2014–15 marine heat wave and the following 2015–16 El Niño conditions. The diet began to shift in 2015 when anchovy began to increase, rising to 94% occurrence in 2016 and remaining high in 2017. In addition, other taxa remained above 20% in 2016 and 2017, increasing the diversity of taxa in the diet. However, the occurrence of sardine in the diet remained at record lows.

The California sea lion population response to the unusually warm marine conditions in 2014–16 affected a greater number of pup cohorts than past El Niño events due to the persistence of the conditions over three reproductive cycles. In addition, these cohorts continued the trend of poor condition and growth that began in 2009, resulting in six of the last eight pup cohorts having below average condition and growth

rates. Poor condition at 4 months of age has been linked to lower survival rates of pups (DeLong et al. 2017) that contributed to a slowing of the population growth rate in recent years (Laake et al. 2018). The declining trend in pup condition at 4 months of age was associated with a shift in the species composition of the nursing female diet over the same period, most notably the almost complete disappearance of sardine and anchovy from the diet (fig. 57). Indeed, McClatchie et al. (2016a) documented a strong, positive correlation between the availability of anchovy and sardine and sea lion pup weight from 2004–14. An improvement in pup condition in 2016 and 2017 coincided with an increase in anchovy and greater taxa diversity in the nursing female diet. The quantity of high quality food consumed by nursing females affects the transfer of energy from the female to the pup during the period that the pup is nutritionally dependent on its mother, and therefore affects pup condition and growth rates. Based on the nursing female diet, the shifts in the prey community clearly began before the marine heat wave and El Niño and reflect a sustained period of abnormally warm marine conditions that altered the sea lion prey community. The resurgence of anchovy populations along the central and southern California coast (figs. 33, 36, 38) was reflected in the diet of nursing females and coincided with an improvement in pup condition and greater growth rates of the 2017 cohort. However, the fattest pups in the time series occurred in the mid-2000s when sardine and anchovy dominated the diet, suggesting that a more diverse diet with inclusion of sardine into sea lion diet results in optimal reproductive efforts of California sea lion females. The rebounding of all three population indices in 2017 and the commensurate shift in the composition of the nursing female diet supports the use of these indices as a measure of forage community shifts in the CCS that affect upper trophic level predators.

DISCUSSION

The biggest takeaway from CCS-wide analyses from mid-2017 to mid-2018 is that many of the indices, from SST and chlorophyll *a* to fish assemblages, were close to average long-term values. However, the CCS is characterized by strong interannual variability, and deviations from the long-term mean are more common than exceptional (Goericke et al. 2004). Indeed, several variables were highly anomalous in 2017–18, and we highlight these in the ensuing paragraphs.

Very low NPGO

Basin scale climate indices (PDO and ONI) were very close to neutral. The NPGO, however, was very low in 2017–18. In fact, through February 2018, three of the lowest monthly NPGO values since January 1950

were recorded (December 2017—3rd lowest; November 2017—8th lowest; and February 2018—9th lowest).

The NPGO is related to the strength of the North Pacific Current (NPC) which flows eastward and meets the west coast of North America at approximately 40°N (Di Lorenzo et al. 2008). At the West Coast, the NPC divides and becomes the northward-flowing Alaska Current and the southward-flowing California Current (CC). Low NPGO values are associated with weaker current flows and warmer, nutrient poor conditions (Di Lorenzo et al. 2008; Di Lorenzo et al. 2009).

The NPGO is based directly on conditions in the CCS, and past studies show that it correlates with ecosystem fluctuations in the CCS (Sydeman and Thompson 2010). For example, Cloern et al. (2010) found that the NPGO index correlated significantly with populations of demersal fishes, crabs, and shrimps in San Francisco Bay, California, and the sign of this correlation varied by species. More recently, Sydeman et al. (2013) provided evidence that oceanographic conditions reflected by the NPGO affect multiple trophic levels in central California. Specifically, there is a positive relationship between *Thysanoessa spinifera* krill abundance and the NPGO (Sydeman et al. 2013). *T. spinifera* is an important prey item for young fishes, and juvenile rockfish abundance is strongly, positively correlated with the abundance of this krill species. Juvenile rockfishes, in turn, are consumed by salmon and seabirds, and there was a very strong ($R^2 = 0.87$), positive relationship between rockfish abundance and that of salmon and seabirds over 8 years in the early 21st century (Sydeman et al. 2013). Our finding that krill and rockfish abundances in 2018 off central California (fig. 33) were low, when winter NPGO values were very low, relative to 2016–17 supports the trophic relationships identified by Sydeman et al. (2013). The low NPGO in winter 2017–18 also indicates that salmon abundances are likely to be low in central California.

Higher Trophic Level Species in the North in 2017

We can now conclusively state that 2017 was a terrible year for many upper trophic level species in the northern California Current. Common murre experienced total reproductive failure in both Yaquina Head, Oregon, and Castle Rock, California, in 2017, and at-sea bird sightings were at the lowest level since records began in 2003 (Wells et al. 2017).

Poor forage conditions for murre likely contributed to their sorry state in the north in 2017. At both Yaquina Head and Castle Rock, there were very few observations of adults carrying fish into the colonies and no observations of adults feeding chicks. Predators also affected murre chick survival as bald eagles and western gulls

were observed consuming numerous eggs and/or chicks at Yaquina Head and Castle Rock, respectively.

The number of salmon returning to spawn in their natal rivers is affected greatly by the abundance of yearlings leaving the river two years prior and the prey field in the ocean encountered by yearlings (Peterson et al. 2014). In 2017 almost all indices related to coho and Chinook salmon return predicted very low returns in 2019. Specifically, the abundance of yearlings, which correlates positively with subsequent returns (Morgan et al. 2018) was very low for both species. In addition, salmon survival tends to be higher when northern, lipid-rich copepods are abundant, and these copepods were very low in 2017. Finally, ichthyoplankton assemblage structure and biomass can affect yearling salmon survival, as higher survival is correlated with overall ichthyoplankton biomass and the presence of species such as sand lance, sculpins, and smelts associated with colder ocean conditions and inshore biogeographic ranges, as opposed to lower survival associated with taxa such as sardine, anchovy, and rockfishes representing warmer ocean conditions and offshore ranges (Daly et al. 2017). In 2017, although the overall ichthyoplankton biomass was relatively high (fig. 29), the assemblage was dominated by taxa with offshore distributions and associated with warm ocean conditions. Hence, by most accounts, we would expect low salmon returns in 2019.

Prospects for salmon returns in 2020 are still equivocal but perhaps less bleak than for 2019. First, the abundance of coho salmon in coastal samples was among the highest on record in 2018. The abundance of yearling Chinook salmon also increased greatly relative to 2017 and was close to average in 2018. Second, the biomass of northern copepods increased greatly in 2018 and was close to average while southern copepods were only slightly above normal. Third, ichthyoplankton biomass was high, although the assemblage was still characterized by warm water taxa that correlate negatively with salmon returns (Daly et al. 2017).

Return to Normal in California ... Except That Anchovy Abundance Was Way Up

Conditions in 2018 in the CC largely appeared to be following the trend from 2016–17, returning to average conditions following the impacts of the North Pacific warming and El Niño of 2014–15. Off Trinidad Head, Monterey Bay, central, southern, and northern Baja California, SST and chlorophyll *a* were close to average from late 2017 to mid-2018.

Salinity in southern California during spring 2018, however, was the one physical feature that stood out from previous years. In fact, the salinity anomaly in the mixed layer in southern California was the 2nd highest since 1994. Typically, high salinity water in spring in

southern California is a signature of cool, upwelled, nutrient rich water near the coast (McClatchie 2014). In 2018, however, upwelling was close to normal in southern California, chlorophyll *a* at 10 m was almost exactly the same as the long-term mean, temperature in the mixed layer was only slightly below normal, and salinity at 10 m was actually higher offshore than inshore. These features are all inconsistent with high upwelling, and examination of sea surface salinity from new satellite imagery showed that saline waters were offshore from the CalCOFI grid and impinged on the sample frame by mid-2018. Movement of saline water from offshore and the south (i.e., North Pacific Central water) into southern California is not uncommon during El Niños (McClatchie 2014), but North Pacific Central water is normally warm as well as saline (Brinton 1962; Moser et al. 1987; McClatchie 2014). Further analysis is necessary to better understand the characteristics of the waters offshore from the CalCOFI grid in 2018 and its impact on physical and biological features of the CCS.

While most physical conditions, with the exception of salinity, trended towards average levels in California, a major biological feature was notable in 2018: anchovy abundances were extremely high in many locations. Indeed, RREAS trawls documented record high anchovy abundance off central California and bongo tows off southern California documented the highest abundance of larval anchovy since the mid-1960s.

The mechanisms that allowed anchovy to increase do not align cleanly with our current understanding of drivers of anchovy populations. The traditional view of sardine and anchovy dynamics is that sardine thrive under warm conditions while anchovy do better when it is cold (Lluch-Belda et al. 1989; Chavez et al. 2003). This concept was largely informed by CalCOFI data showing low sardine and high anchovy abundances from the 1950s to the mid-1970s (cold conditions), an increase in sardine and decrease in anchovy from the 1980s to the early 2000s and then a decrease in sardine (but not an increase in anchovy) between 2000 and 2011 (Zwolinski and Demer 2012). However, McClatchie (2012) pointed out that a time frame of 70 years is too short to understand how fish respond to temperature regimes that last 20–40 years. In addition, paleontological records of anchovy and sardine scale depositions show that over hundreds of years there is no correlation between the PDO and sardine abundance (McClatchie 2012) and that anchovy and sardine populations dynamics seem to be positively correlated (Baumgartner et al. 1992; McClatchie et al. 2017). In light of our current finding that anchovy increased under mostly warm conditions, and that sardine did not, suggests that the paradigm of sardine thriving under warm conditions and anchovy increasing when it is cool is overly simplistic.

An alternative mechanism governing sardine and anchovy dynamics is that, due to differences in size of gill rakers, sardine do well when small-bodied zooplankton prey is plentiful, and anchovy thrive with copious amounts of larger-bodied prey (Rykaczewski and Checkley Jr. 2008). In addition, Rykaczewski and Checkley Jr. (2008) found that larger prey items tend to flourish under high levels of coastal upwelling, while smaller prey are plentiful when wind-stress curl initiates upwelling. Indeed, despite El Niño conditions that typically mute upwelling (McClatchie 2014), upwelling was actually greater than normal in winter 2015–16 in southern California and greater than normal leading into winter 2015–16, and then close to normal within winter 2015–16 in central California. In addition, despite overall warm conditions in 2014–15, upwelling was close to normal in Central California. The mix of normal-high upwelling close to shore with warm water offshore in 2015–16 produced an unusual mix of semitropical species offshore (e.g., pelagic red crabs, *Pleuroncodes planipes*, subtropical mesopelagic fishes) coupled with high abundance of species that favor cooler conditions (e.g., rockfishes) inshore (McClatchie et al. 2016b, Sakuma et al. 2016). It is therefore possible that large-bodied anchovy prey were abundant inshore in California, and that high anchovy abundance in 2018 was the product of a strong recruitment class in winters of 2015 and 2016. Further analysis of prey size and abundance in recent years is needed to evaluate whether the type of prey that is thought to favor anchovy survival was plentiful in recent years.

It is also possible that an unknown mechanism spurred anchovy population growth leading up to 2018. In their recent review of sardine and anchovy dynamics Checkley Jr. et al. (2017) state that our understanding of what controls anchovy and sardine dynamics is based on correlative analyses using data collected mostly from the past ~70 years. They go on to say that our current level of understanding of factors controlling sardine and anchovy “might be sufficient if future climate change were to be similar to past climate variability and if we had a sufficient duration of high quality historical observations to represent all modes of natural variability. Neither is likely true.” Given that unprecedented physical and biological conditions defined much of the last five years, it is conceivable that recent anchovy dynamics were driven by forces novel to researchers.

Regardless of the variables that ultimately govern anchovy dynamics, high anchovy abundances have important economic and ecological implications. Anchovy are important forage for many higher trophic level species (Szoboszlai et al. 2015) and are a potentially valuable resource for commercial fisheries, particularly in recent years as the sardine fishery has been closed since

2015 (McClatchie et al. 2018). Harvest guidelines will necessarily be drawn based from a full anchovy stock assessment (McClatchie et al. 2018), which will consider the historically low levels of anchovy populations in central and southern California through 2015 (MacCall et al. 2016; Davison et al. 2017). However, if the indices reported here are any indication, it is likely that recent assessments will find that anchovy abundances have risen considerably in 2017–18, which could bring relief to commercial fishing in California.

In addition to benefiting fishing, resurgence of anchovy was likely tied to improved sea lion reproduction on San Miguel Island in California. In the early 20th century sea lions were hunted and population reduced to very low levels (Cass 1985). Sea lions became protected under the U.S. Marine Mammals Protection Act in 1972 and surveys since 1975 show that the population has increased approximately 7-fold and is likely near carrying capacity (Laake et al. 2018). Given the high population sizes, sea lion populations are affected when high quality forage is scarce and mothers become malnourished, resulting in low birth rates, lactation, and pup survival (Melin et al. 2010; Melin et al. 2012). The increased production and survival of sea lion pups in 2017 coincided with a spike in anchovy abundance; anchovy remains were observed in nearly all scat samples and fit with the pattern that sea lion pups do well in years when anchovies and/or sardine are abundant (McClatchie et al. 2016a). Anchovy appear to have been abundant in California through 2018, suggesting that sea lion pups will again exhibit high rates of survival in 2018.

Increased anchovy abundance also has the potential to augment bird survival. 2018 surveys from the Southeast Farallon Island indicated that both rhinoceros auklet and common murre chick diets consisted of high proportions of anchovy. Although measurement of rhinoceros auklet productivity was not yet available, common murre productivity at Southeast Farrallon Island increased greatly in 2018 and was the highest since 2013.

... and Semitropical Fish Were Prominent in Southern California

Another novel finding in 2018 was that the southern California larval fish assemblage in spring had high abundances of mesopelagic taxa with southern biogeographic distributions even though the ocean was not warm at this time. These species have been viewed as indicators of warm conditions in southern California that were largely caused by El Niño events (Hsieh et al. 2005, Hsieh et al. 2009). Indeed, analyses of early CalCOFI data demonstrated that this suite of species was associated with the Central North Pacific water mass, and this community was detected in CalCOFI samples when this water mass impinged upon southern California (Moser et al. 1987).

Prior to 1977, it was rare to find these species in the core CalCOFI area outside of summer but following the cool to warm regime shift around 1976 (Hare and Mantua 2000), these species have become increasingly common in CalCOFI samples (Hsieh et al. 2009). Despite the increased overall presence of the southern mesopelagics over the past 40 years, spring 2018 is the first time that these species were so well represented when water temperatures were below average.

A potential explanation for the abundance of the southern mesopelagics is that because of the predominantly warm conditions over the last five years in southern California, fishes in this assemblage are still relatively close to the CalCOFI sampling area even when physical conditions in southern California are cool. Satellite images of SST show that although it was cool in southern California in May 2018, anomalously warm water was just offshore. In addition, highly saline water, which is characteristic of southern mesopelagic fish habitat (McClatchie 2014), was detected in the offshore CalCOFI region in spring 2018, and the mesopelagic fishes may have been transported into the region along with this water. Further analysis will be needed to more definitively determine why the abundance of warm-water associated southern mesopelagics was so high in 2018 even though the water was relatively cool.

... and It Was Historically Warm in Southern California and Northern Baja California in Summer 2018

While surface water temperatures began at seasonally adjusted normal values in 2018, they rapidly rose to extremely high levels off southern California and northern Baja California in July and August 2018. Over the last 70 years elevated water temperatures in southern California were almost always associated with El Niño events. 2018, however, was Niño-neutral, and it appears that the record warmth was generated by mechanisms similar to the 2014 surface warming event. The warm water in 2014 originated in the Gulf of Alaska in response to regional high sea level pressure leading to low winds and lower than normal loss of heat from the upper ocean (Bond et al. 2015). Leading up to August 1, air pressure was anomalously high over the southwestern United States which caused abnormally high air temperatures and anomalously low wind in southern California (<https://www.esrl.noaa.gov/psd/map/clim/>). In addition, high sea level pressure was centered in the Gulf of Alaska rather than over central-northern California from mid-June to August (<https://www.esrl.noaa.gov/psd/map/clim/>), resulting in lower than normal southerly winds and reduced upwelling in southern California in summer 2018. As such, high air temperature, coupled with relatively still conditions

drove sea surface temperatures to record highs in many parts of southern California by August, 2018. Subsequent work will reveal the biological impacts of extreme water temperatures in the southern parts of the CCS.

SUMMARY

Following the large marine heat wave from 2014–16, much of the CCS trended towards more typical conditions in 2018. In the north many invertebrates and fish that are associated with cool conditions were found at the highest level since 2013. However, signatures of the recent warming remained in the north as taxa such as pyrosomes and lipid-poor copepods were still plentiful. In the central region, conditions also were more aligned with long-term averages although anchovy were at all-time highs. In southern California most oceanographic parameters were close to normal through spring 2018. By summer, however, water temperature at the surface hit record high and the spring ichthyoplankton assemblage was characterized by many semitropical taxa along with high abundances of anchovy. Off Baja California, SST was slightly above normal at the beginning of 2018 and chlorophyll *a* and primary production were average. In sum, the CCS appeared to be trending as a whole back to pre-2014 conditions through spring 2018. In summer 2018, however, strong regional warming off southern California and northern Baja California decoupled these regions from the rest of the system. Ongoing research will continue to evaluate the full extent of this latest extreme warming event.

ACKNOWLEDGEMENTS

We wish to thank everyone who contributed to collecting myriad data presented in this report. The manuscript was improved greatly by comments from Noelle Bowlin, Greg Williams, and an anonymous reviewer.

LITERATURE CITED

- Adams, J., C. MacLeod, R. M. Suryan, K. D. Hyrenbach, and J. T. Harvey. 2012. Summer-time use of west coast US National Marine Sanctuaries by migrating sooty shearwaters (*Puffinus griseus*). *Biological Conservation* 156:105–116.
- Alexander, M. A., C. Deser, and M. S. Timlin. 1999. The reemergence of SST anomalies in the North Pacific Ocean. *Journal of Climate* 12.
- Auth, T. D., E. A. Daly, R. D. Brodeur, and J. L. Fisher. 2018. Phenological and distributional shifts in ichthyoplankton associated with recent warming in the northeast Pacific Ocean. *Global Change Biology* 24:259–272.
- Bakun, A. 1973. Coastal upwelling indices, west coast of North America, 1946–71. US Department of Commerce NOAA Technical Report NMFS-SSRF 671:1–103.
- Barcelo, C., L. Ciannelli, and R. D. Brodeur. 2018. Pelagic marine refugia and climatically sensitive areas in an eastern boundary current upwelling system. *Global Change Biology* 24:668–680.
- Baumgartner, T. R., A. Soutar, and V. Ferreira-Bartrina. 1992. Reconstruction of the history of Pacific sardine and northern anchovy populations over the past two millennia from sediments of the Santa Barbara Basin, California. *California Cooperative Oceanic Fisheries Investigations Reports* 33:24–40.
- Black, B. A., I. D. Schroeder, W. J. Sydeman, S. J. Bograd, and P. W. Lawson. 2010. Wintertime ocean conditions synchronize rockfish growth and seabird reproduction in the central California Current ecosystem. *Canadian Journal of Fisheries and Aquatic Sciences* 67:1149–1158.
- Black, B. A., P. van der Sleen, E. Di Lorenzo, D. Griffin, W. J. Sydeman, J. B. Dunham, R. R. Rykaczewski, M. Garcia-Reyes, M. Safeeq, I. Arismendi, and S. J. Bograd. 2018. Rising synchrony controls western North American ecosystems. *Global Change Biology* 24:2305–2314.
- Bograd, S. J., and R. J. Lynn. 2003. Long-term variability in the Southern California Current System. *Deep-Sea Research II* 50:2355–2370.
- Bograd, S. J., I. D. Schroeder, N. Sarkar, X. M. Qiu, W. J. Sydeman, and F. B. Schwing. 2009. Phenology of coastal upwelling in the California Current. *Geophysical Research Letters* 36.
- Bond, N. A., M. F. Cronin, H. Freeland, and N. Mantua. 2015. Causes and impacts of the 2014 warm anomaly in the NE Pacific. *Geophysical Research Letters* 42:3414–3420.
- Brinton, E. 1962. The distribution of Pacific euphausiids. *Bulletin of Scripps Institute of Oceanography* 8:251–270.
- Brodeur, R. D., J. P. Fisher, R. L. Emmett, C. A. Morgan, and E. Casillas. 2005. Species composition and community structure of pelagic nekton off Oregon and Washington under variable oceanographic conditions. *Marine Ecology Progress Series* 298:41–57.
- Brodeur, R. D., I. Perry, J. Boldt, L. Flostrand, M. Galbraith, J. King, J. Murphy, K. M. Sakuma, and A. R. Thompson. 2018. An unusual gelatinous plankton event in the NE Pacific: The Great Pyrosome Bloom of 2017. *PICES Press* 26:22–27.
- Brodeur, R. D., S. Ralston, R. L. Emmett, M. Trudel, T. D. Auth, and A. J. Phillips. 2006. Anomalous pelagic nekton abundance, distribution, and apparent recruitment in the northern California Current in 2004 and 2005. *Geophysical Research Letters* 33:L22S08.
- Carter, H. R., U. W. Wilson, R. W. Lowe, M. S. Rodway, D. A. Manuwal, and J. L. Yee. 2001. Population trends of the Common Murre (*Uria aalge californica*). Pages 33–132 in D. A. Manuwal, H. R. Carter, T. S. Zimmerman, and D. L. Orthmeyer, editors. *Biology and conservation of the common murre in California, Oregon, Washington, and British Columbia, Volume 1: Natural history and population trends United States Geological Survey, Information and Technology Report USGS/BRD/ITR-2000-0012, Fish & Wildlife Service, Northern Prairie Wildlife Research Center, Dixon, CA.*
- Cass, V. 1985. Exploitation of California sea lions, *Zalophus californianus*, prior to 1972. *Marine Fisheries Review* 47:36–38.
- Chavez, F. C., J. Ryan, S. E. Lluch-Cota, and M. C. Niquen. 2003. From anchovies to sardines and back: Multidecadal change in the Pacific Ocean. *Science* 299:217–221.
- Checkley Jr., D. M., R. G. Asch, and R. R. Rykaczewski. 2017. Climate, anchovy, and sardine. *Annual Review of Marine Science* 9:469–493.
- Cloern, J. E., K. A. Hieb, T. Jacobson, B. Sanso, E. Di Lorenzo, M. T. Stacey, J. L. Largier, W. Meiring, W. T. Peterson, T. M. Powell, M. Winder, and A. D. Jassby. 2010. Biological communities in San Francisco Bay track large-scale climate forcing over the North Pacific. *Geophysical Research Letters* 37:L21602.
- Dale, K. E., E. A. Daly, and R. D. Brodeur. 2017. Interannual variability in the feeding and condition of subyearling Chinook salmon off Oregon and Washington in relation to fluctuating ocean conditions. *Fisheries Oceanography* 26:1–26.
- Daly, E. A., R. D. Brodeur, and T. D. Auth. 2017. Anomalous ocean conditions in 2015: impacts on spring Chinook salmon and their prey field. *Marine Ecology Progress Series* 566:169–182.
- Davison, P., W. J. Sydeman, and J. A. Thayer. 2017. Are there temporal or spatial gaps in recent estimates of anchovy off California? *California Cooperative Oceanic Fisheries Investigations Reports* 58:1–13.
- DeLong, R. L., S. R. Melin, J. L. Laake, P. Morris, A. J. Orr, and J. D. Harris. 2017. Age- and sex-specific survival of California sea lions (*Zalophus californianus*) at San Miguel Island, California. *Marine Mammal Science* 33:1097–1125.
- Di Lorenzo, E., J. Fiechter, N. Schneider, A. Bracco, A. J. Miller, P. J. S. Franks, S. J. Bograd, A. M. Moore, A. C. Thomas, W. Crawford, A. Pena, and A. J. Hermann. 2009. Nutrient and salinity decadal variations in the central and eastern North Pacific. *Geophysical Research Letters* 36:L14601.
- Di Lorenzo, E., and N. Mantua. 2016. Multi-year persistence of the 2014/15 North Pacific marine heatwave. *Nature Climate Change* 6:1042–1048.
- Di Lorenzo, E., N. Schneider, K. M. Cobb, P. J. S. Franks, K. Chhak, A. J. Miller, J. C. McWilliams, S. J. Bograd, H. Arango, E. Curchister, T. M. Powell, and P. Riviere. 2008. North Pacific Gyre Oscillation links ocean climate and ecosystem change. *Geophysical Research Letters* 35:L08607.

- Frable, B. W., D. W. Wagman, T. N. Frierson, and B. L. Sidlauskas. 2015. A new species of *Sebastes* (Scorpaeniformes: Sebastidae) from the northeastern Pacific, with a redescription of the blue rockfish, *S. mystinus* (Jordan and Gilbert, 1881). *Fisheries Bulletin* 113:355–377.
- Friskhnecht, M., M. Münnich, and N. Gruber. 2015. Remote versus local influence of ENSO on the California Current System. *Journal Geophysical Research Oceans* 120:1353–1374.
- Friskhnecht, M., M. Münnich, and N. Gruber. 2017. Local atmospheric forcing driving an unexpected California Current System response during the 2015–2016 El Niño. *Geophysical Research Letters* 41:304–311.
- Gladics, A. J., R. M. Suryan, R. D. Brodeur, L. M. Segui, and L. Z. Filliger. 2014. Constancy and change in marine predator diets across a shift in oceanographic conditions in the Northern California Current. *Marine Biology* 161:837–851.
- Gladics, A. J., R. M. Suryan, J. K. Parrish, C. A. Horton, E. A. Daly, and W. T. Peterson. 2015. Environmental drivers and reproductive consequences of variation in the diet of a marine predator. *Journal of Marine Systems* 146:72–81.
- Goericke, R., E. Venrick, J. A. Koslow, W. J. Sydeman, F. B. Schwing, S. J. Bograd, B. Peterson, R. L. Emmett, J. R. L. Lara, G. G. Castro, J. G. Valdez, K. D. Hyrenbach, R. W. Bradley, M. J. Weise, J. T. Harvey, C. Collins, and N. C. H. Lo. 2007. The State of the California Current, 2007–2007: Regional and local processes dominate. *California Cooperative Oceanic Fisheries Investigations Reports* 48:33–66.
- Goericke, R., E. Venrick, A. Mantyla, S. J. Bograd, F. B. Schwing, A. Huyer, R. L. Smith, P. A. Wheeler, R. Hooff, W. T. Peterson, G. Gaxiola-Castro, J. Gomez-Valdez, B. E. Lavanigos, K. D. Hyrenbach, and W. J. Sydeman. 2004. The State of the California Current, 2003–04: A rare “normal” year. *California Cooperative Oceanic Fisheries Investigations Reports* 45:27–59.
- Hare, S. R., and N. Mantua. 2000. Empirical evidence for North Pacific regime shifts in 1977 and 1989. *Progress in Oceanography* 47:103–145.
- Horton, C. A. 2014. Top-down influences of Bald Eagles on Common Murre populations in Oregon. MS thesis. Oregon State University.
- Hsieh, C., C. Reiss, W. Watson, M. J. Allen, J. R. Hunter, R. N. Lea, R. H. Rosenblatt, P. E. Smith, and G. Sugihara. 2005. A comparison of long-term trends and variability in populations of larvae of exploited and unexploited fishes in the Southern California region: A community approach. *Progress in Oceanography* 67:160–185.
- Hsieh, C. H., H. J. Kim, W. Watson, E. Di Lorenzo, and G. Sugihara. 2009. Climate-driven changes in abundance and distribution of larvae of oceanic fishes in the southern California region. *Global Change Biology* 15:2137–2152.
- Hyrenbach, D. K., and R. R. Veit. 2003. Ocean warming and seabird communities of the Southern California Current System (1987–98): response at multiple temporal scales. *Deep Sea Research II* 50:2537–2565.
- Jackson, J. M., G. C. Johnson, H. V. Dossier, and T. Ross. 2018. Warming from recent marine heatwave lingers in deep British Columbia fjord. *Geophysical Research Letters* 45:2018GL078971.
- Jacox, M. G., M. A. Alexander, N. J. Mantua, J. D. Scott, G. Hervieux, R. S. Webb, and F. E. Werner. 2018a. Forcing of multiyear extreme ocean temperatures that impact California Current living marine resources in 2016. *Bulletin of the American Meteorological Society* 99:S27–S33.
- Jacox, M. G., C. A. Edwards, E. L. Hazen, and S. J. Bograd. 2018b. Coastal upwelling revisited: Ekman, Bakun, and improved upwelling indices for the U.S. west coast. *Geophysical Research Letters* in press.
- Jacox, M. G., J. Fiechter, A. M. Moore, and C. A. Edwards. 2015. ENSO and the California Current coastal upwelling response. *Journal Geophysical Research Oceans* 120:1691–1702.
- Jacox, M. G., E. L. Hagen, K. D. Zaba, D. L. Rudnick, C. A. Edwards, A. M. Moore, and S. J. Bograd. 2016. Impacts of the 2015–16 El Niño on the California Current System: Early assessments and comparison to past events. *Geophysical Research Letters* 43:7072–7080.
- Jacox, M. G., A. M. Moore, C. A. Edwards, and J. Fiechter. 2014. Spatially resolved upwelling in the California Current System and its connections to climate variability. *Geophysical Research Letters* 41:3189–3196.
- Jeronimo, G., and J. Gomes-Valdes. 2010. Mixed layer depth variability in the tropical boundary of the California Current, 1997–2007. *Journal Geophysical Research Oceans* 115:C05014.
- Kahru, M., M. G. Jacox, and M. D. Ohman. 2018. CCE1: Decrease in the frequency of oceanic fronts and surface chlorophyll concentration in the California Current System during the 2014–16 northeast Pacific warm anomalies. in press.
- Koslow, J. A., L. Rogers-Bennett, and D. J. Neilson. 2012. A time series of California spiny lobster (*Panulirus interruptus*) phyllosoma from 1951 to 2008 links abundance to warm oceanographic conditions in southern California. *California Cooperative Oceanic Fisheries Investigations Reports* 53:132–139.
- Laake, J. L., M. S. Lowry, R. L. DeLong, S. R. Melin, and J. V. Carretta. 2018. Population growth and status of California sea lions. *The Journal of Wildlife Management* 82:583–595.
- Lavanigos, B., and M. Ohman. 2007. Coherence of long-term fluctuation of zooplankton in tow sectors of the California Current System. *Progress in Oceanography* 75:42–69.
- Leising, A. W., I. D. Schroeder, S. J. Bograd, J. Abell, R. Duranzo, G. Gaxiola-Castro, E. P. Bjorkstedt, J. C. Field, K. M. Sakuma, R. R. Robertson, R. Goericke, W. T. Peterson, R. D. Brodeur, C. Barcelo, T. D. Auth, E. A. Daly, R. M. Suryan, A. J. Gladics, J. M. Porquez, S. McClatchie, E. D. Weber, W. Watson, J. A. Santora, W. J. Sydeman, S. R. Melin, F. C. Chavez, R. T. Golightly, S. R. Schneider, J. Fisher, C. A. Morgan, R. Bradley, and P. Warybok. 2015. State of the California Current 2014–15: Impacts of the warm-water “Blob.” *California Cooperative Oceanic Fisheries Investigations Reports* 56:31–68.
- Luch-Belda, D., R. J. M. Crawford, T. Kawasaki, A. D. Maccall, R. H. Parrish, R. A. Schwartzlose, and P. E. Smith. 1989. Worldwide fluctuations of sardine and anchovy stocks—the regime problem. *South African Journal of Marine Science* 8:195–205.
- MacCall, A. D., W. J. Sydeman, P. Davison, and J. A. Thayer. 2016. Recent collapse of northern anchovy biomass off California. *Fisheries Research* 175:87–94.
- Mantua, N., S. R. Hare, Y. Zhang, J. M. Wallace, and R. C. Francis. 1997. A Pacific decadal climate oscillation with impacts on salmon. *Bulletin of the American Meteorological Society* 78:1069–1079.
- McClatchie, S. 2012. Sardine biomass is poorly correlated with the Pacific Decadal Oscillation off California. *Geophysical Research Letters* 39.
- McClatchie, S. 2014. Regional fisheries oceanography of the California Current System and the CalCOFI program. Springer.
- McClatchie, S., J. C. Field, A. R. Thompson, T. Gerrodette, M. Lowry, P. C. Fiedler, W. Watson, K. M. Nieto, and R. D. Vetter. 2016a. Food limitation of sea lion pups and the decline of forage off central and southern California. *Royal Society Open Science* 3:150628.
- McClatchie, S., R. Goericke, A. Leising, T. D. Auth, E. Bjorkstedt, R. R. Robertson, R. D. Brodeur, X. Du, E. A. Daly, C. A. Morgan, F. P. Chavez, A. J. Debich, J. Hildebrand, J. C. Field, K. M. Sakuma, M. G. Jacox, M. Kahru, R. Kudela, C. Anderson, B. E. Lavanigos, J. Gomes-Valdes, S. P. A. Jimenez-Rosenberg, R. McCabe, S. R. Melin, M. D. Ohman, L. M. Sala, B. Peterson, J. L. Fisher, I. D. Schroeder, S. J. Bograd, E. L. Hazen, S. R. Schneider, R. T. Golightly, R. M. Suryan, A. J. Gladics, S. Loreda, J. M. Porquez, A. R. Thompson, E. D. Weber, W. Watson, V. Trainer, P. Warzybok, R. Bradley, and J. Jahncke. 2016b. State of the California Current 2015–16: Comparisons with the 1997–98 El Niño. *California Cooperative Oceanic Fisheries Investigations Reports* 57:5–61.
- McClatchie, S., I. L. Hendy, A. R. Thompson, and W. Watson. 2017. Collapse and recovery of forage fish populations prior to commercial exploitation. *Geophysical Research Letters* 44:1877–1885.
- McClatchie, S., R. D. Vetter, and I. L. Hendy. 2018. Forage fish, small pelagic fisheries and recovering predators: managing expectations. *Animal Conservation* 1367:9430.
- McClatchie, S., J. Gao, E. J. Drenkard, A. R. Thompson, W. Watson, L. Ciannelli, S. J. Bograd, and J. T. Thorson. 2018. Interannual and secular variability of larvae of mesopelagic and forage fishes in the southern California Current System. *Journal Geophysical Research Oceans* 123:6277–6295.
- Melin, S. R., A. J. Orr, J. D. Harris, J. L. Laake, and R. L. DeLong. 2012. California sea lions: An indicator for integrated ecosystem assessment of the California Current System. *California Cooperative Oceanic Fisheries Investigations Reports* 53:140–152.
- Melin, S. R., A. J. Orr, J. D. Harris, J. L. Laake, R. L. DeLong, F. M. Gulland, and S. Soudt. 2010. Unprecedented mortality of California sea lion pups associated with anomalous oceanographic conditions along the central California coast in 2009. *California Cooperative Oceanic Fisheries Investigations Reports* 51:182–194.
- Morgan, C. A., A. M. Baptista, B. R. Beckman, R. D. Brodeur, B. I. Burke, E. A. Daly, D. D. Huff, K. C. Jacobson, A. J. Miller, E. M. Phillips, D. M. Van Doornik, and J. E. Zamon. 2018. Ocean Survival of Salmonids RME, 1/1/2017–12/31/2017. <https://www.cbfish.org/Document.mvc/Viewer/P159726>.

- Moser, H. G., R. L. Charter, P. E. Smith, D. A. Ambrose, W. Watson, S. R. Charter, and E. M. Sandknop. 2001. Distributional atlas of fish larvae and eggs in the Southern California Bight region: 1951–98. CalCOFI Atlas No. 34.
- Moser, H. G., P. E. Smith, and L. E. Eber. 1987. Larval fish assemblages in the California Current region, 1954–60, a period of dynamic environmental change. California Cooperative Oceanic Fisheries Investigations Reports 28:97–127.
- Newman, M., M. A. Alexander, T. R. Ault, K. M. Cobb, C. Deser, E. Di Lorenzo, N. J. Mantua, A. J. Miller, S. Minobe, H. Nakamura, and N. Schneider. 2016. The Pacific decadal oscillation, revisited. *Journal of Climate* 29:4399–4427.
- Peabody, C. E., A. R. Thompson, D. F. Sax, R. E. Morse, and C. J. Perretti. 2018. Decadal regime shifts in southern California's ichthyoplankton assemblage. *Marine Ecology Progress Series* 607: 71–83
- Peterson, W. T., J. L. Fisher, J. O. Peterson, C. A. Morgan, B. I. Burke, and K. L. Fresh. 2014. Applied fisheries oceanography: ecosystem indicators of ocean conditions inform fisheries management in the California Current ecosystem. *Oceanography* 27:80–89.
- Peterson, W. T., J. L. Fisher, P. T. Strub, X. Du, C. Risien, J. Peterson, and C. T. Shaw. 2017. The pelagic ecosystem in the Northern California Current off Oregon during the 2014–2016 warm anomalies within the context of the past 20 years. *Journal of Geophysical Research: Oceans* 122:7267–7290.
- Phillips, E. M., J. K. Horne, J. Adams, and J. E. Zamon. 2018. Selective occupancy of a persistent yet variable coastal river plume by two seabird species. *Marine Ecology Progress Series* 594:245–261.
- Phillips, E. M., J. K. Horne, and J. E. Zamon. 2017. Predator-prey interactions influenced by a dynamic river plume. *Canadian Journal of Fisheries and Aquatic Sciences* 74:1375–1390.
- Reed, T. E., S. Waneless, M. P. Harris, M. Frederiksen, L. E. B. Kruuk, and E. J. A. Cunningham. 2006. Responding to environmental change: plastic responses vary little in a synchronous breeder. *Proceedings of the Royal Society of London B* 273:2713–2719.
- Rudnick, D. L., K. D. Zaba, R. E. Todd, and R. E. Davis. 2017. A climatology of the California Current System from a network of underwater gliders. *Progress in Oceanography* 154:64–106.
- Rydzewski, R. R., and D. M. Checkley Jr. 2008. Influence of ocean winds on the pelagic ecosystem in upwelling regions. *Proceedings of the National Academy of Science* 105:1965–1970.
- Sakuma, K. M., J. C. Field, B. B. Marinovic, C. N. Carrion, N. J. Mantua, and S. Ralston. 2016. Anomalous epipelagic micronekton assemblage patterns in the neritic waters of the California Current in spring 2015 during a period of extreme ocean conditions. California Cooperative Oceanic Fisheries Investigations Reports 57:163–183.
- Santora, J. A., and W. J. Sydeman. 2015. Persistence of hotspots and variability of seabird species richness and abundance in the southern California Current. *Ecosphere* 6:214.
- Schroeder, I. D., B. A. Black, W. J. Sydeman, S. J. Bograd, E. L. Hazen, J. A. Santora, and B. K. Wells. 2013. The North Pacific High and wintertime pre-conditioning of California Current productivity. *Geophysical Research Letters* 40:541–546.
- Schroeder, I. D., W. J. Sydeman, N. Sarkar, S. A. Thompson, S. J. Bograd, and F. B. Schwing. 2009. Winter pre-conditioning of seabird phenology in the California Current. *Marine Ecology Progress Series* 393:211–233.
- Schwing, F. B., M. O'Farrell, J. M. Steger, and K. Baltz. 1996. Coastal Upwelling indices west coast of North America. NOAA Technical Report NMFS SWFSC NMFS SWFSC 231.
- Sydeman, W. J., J. A. Santora, S. A. Thompson, B. B. Marinovic, and E. Di Lorenzo. 2013. Increasing variance in North Pacific climate relates to unprecedented ecosystem variability off California. *Global Change Biology* 19:1662–1675.
- Sydeman, W. J., and S. A. Thompson. 2010. The California Current Integrated Ecosystem Assessment (IEA), Module II: trends and variability in climate-ecosystem state. Pacific Grove, California.
- Sydeman, W. J., S. A. Thompson, J. A. Santora, J. A. Koslow, R. Goericke, and M. D. Ohman. 2015. Climate-ecosystem change off southern California: Time-dependent seabird predator-prey numerical responses. *Deep Sea Research II* 112:158–170.
- Szoboszlai, A. I., J. A. Thayer, S. A. Wood, W. J. Sydeman, and L. E. Koehn. 2015. Forage species in predator diets: Synthesis of data from the California Current. *Ecological Informatics* 29:45–56.
- Thompson, S. A., W. J. Sydeman, J. A. Santora, K. H. Morgan, W. Crawford, and M. T. Burrows. 2012. Phenology of pelagic seabird abundance relative to marine climate change in the Alaska Gyre. *Marine Ecology Progress Series* 454:159–170.
- Veit, R. R., P. Pyle, and J. A. McGowan. 1996. Ocean warming and long-term change in pelagic bird abundance within the California current system. *Marine Ecology Progress Series* 139:11–18.
- Velarde, E., E. Ezcurra, M. H. Horn, and R. T. Patton. 2015. Warm oceanographic anomalies and fishing pressure drive seabird nesting north. *Science Advances* 1:e1400210.
- Wells, B. K., I. D. Schroeder, S. J. Bograd, E. L. Hazen, M. G. Jacox, A. Leising, N. Mantua, J. A. Santora, J. L. Fisher, W. T. Peterson, E. Bjorkstedt, R. R. Robertson, F. P. Chavez, R. Goericke, R. Kudela, C. Anderson, B. E. Lavaniegos, J. Gomez-Valdes, R. D. Brodeur, E. A. Daly, C. A. Morgan, T. D. Auth, J. C. Field, K. M. Sakuma, S. McClatchie, A. R. Thompson, E. D. Weber, W. Watson, R. M. Suryan, J. K. Parrish, J. Dolliver, S. Loredo, J. M. Porquez, J. E. Zamon, S. R. Schneider, R. T. Golightly, P. Warzybok, R. Bradley, J. Jahncke, W. J. Sydeman, S. R. Melin, J. A. Hildebrand, A. J. Debich, and B. Thayer. 2017. State of the California Current 2016–17: Still anything but “normal” in the north. *CalCOFI Reports* 58:1–55.
- Xie, P., T. Boyer, E. Bayler, Y. Xue, D. Byrne, J. Reagan, R. Locarnini, F. Sun, R. Joyce, and A. Kumar. 2014. An in situ–satellite blended analysis of global sea surface salinity. *Journal Geophysical Research Oceans* 119:6140–6160.
- Zamon, J. E., E. M. Phillips, and T. J. Guy. 2014. Marine bird aggregations associated with the tidally-driven plume and plume fronts of the Columbia River. *Deep-Sea Research Part II-Topical Studies in Oceanography* 107:85–95.
- Zwolinski, J. P., and D. A. Demer. 2012. A cold oceanographic regime with high exploitation rates in the Northeast Pacific forecasts a collapse of the sardine stock. *Proceedings of the National Academy of Science* 109:4175–4180.

EVALUATION OF THE INFLUENCE OF AGE AND LENGTH ON PACIFIC SARDINE (*SARDINOPS SAGAX*) MATURATION AND CHARACTERIZATION OF ITS TEMPORAL VARIABILITY

KEVIN PINER,* JENNY MCDANIEL, HUI-HUA LEE, KEVIN HILL, AND BEVERLY MACEWICZ

Fisheries Resources Division
Southwest Fisheries Science Center
National Marine Fisheries Service
National Oceanic and Atmospheric Administration
8901 La Jolla Shores Dr.
La Jolla, CA 92037
ph: (858) 546-5613
Kevin.Piner@noaa.gov

ABSTRACT

Pacific sardine collected during the spawning season off the coast of California (US) were used to investigate the process of female maturation. Pacific sardine maturation is better described as an age-based rather than a length-based process, and its temporal variation is better described by annual rather than cohort effects. Temporal variation in maturation is large with the age at 50% maturity annually varying by more than 1 year. This results supports that annual variability is substantial and may be driven by environmental rather than density dependent factors. Including time-varying age-based maturation into the assessment model improved model prediction of recruitment. It is recommended that future assessments consider inclusion of this temporal variability of an age-based process.

INTRODUCTION

Understanding the life history of exploited populations plays a critical role in the assessment of their status and the determination of future prospects. Life history commonly takes the forms of the rates of growth and natural mortality, as well as various aspects of the reproductive biology. For assessment purposes, life history is usually quantified as a mathematical relationship or a series of empirical estimates that serves as biological processes governing the population dynamics (Maunder and Piner in press). Although the parameters governing these model processes can be estimated as part of the parameter optimization, reproductive life history such as fecundity relationships (e.g., eggs per gram of spawning female) or female maturation rates are usually specified as fixed values. It is important that life history studies conducted with the goal of informing stock assessments take into consideration how stock assessment models use these biological processes.

The importance of identifying the correct biological units (example: age or length) of a biological process has been shown to have significant effects on the reliability of assessment results (Lee et al., in press). Variability in the population age structure can affect the implications of age-based biological processes very differently

than length-based ones (Lee et al. 2017). Differentiating between the units of age and length is problematic because these attributes are highly correlated (von Bertalanffy 1938) and can operate concurrently (Schnute and Richards 1990). Despite these difficulties, life history studies aimed at informing stock assessments should attempt to characterize their results in the most appropriate units.

The rate at which females mature is one of the most important aspects of reproductive biology. Maturation rate has been characterized as both a length- as well as age-based process. Maturity ogives applied to the population age or length structure determine the segment of the population that contributes to spawning. For highly variable populations, spawning biomass characterized by age-based maturation rates can be substantially different from length-based ones (Piner et al. 2018). In integrated assessments, spawning biomass is linked to estimates of the underlying dynamics through the spawner-recruit process. The spawner-recruit process makes up an important component of the assessment model's production function, which in turn partially determines the population response to fishing (Sippel et al., in press). Accurate depiction of the production function will be crucial to reliably estimating population scale (Lee et al. 2014) and predicting a population's future prospects.

Beyond establishing the biological units for a process like maturity, understanding the most appropriate units of its temporal variability will also be important (Stawitz et al. 2015). Annual (year-specific) changes in life history rates have been linked to environmental forcing (Hagen and Quinn 1991; Black et al. 2008; Stawitz et al. 2015) which affects all age classes present, while cohort-level variability has been linked to density dependent effects (Rijnsdorp and van Leeuwen 1996; Helser and Almeida 1997; Whitten et al. 2013). Characterizing temporal variability (Silva et al. 2006) can be used to help understand the roles of density dependence and environmental influence on population regulation, which in turn has profound impacts on how exploited stocks should be managed (Chavez et al. 2003; Jacobson and MacCall 1995).

Accurate representation of biological processes including their temporal variation is perhaps nowhere more important than for Pacific sardines (*Sardinops sagax*). Pacific sardine are a small pelagic fish that is, at times, a major component of the forage base in California Current ecosystem (Parrish et al. 1989). The northern subpopulation of Pacific sardine is distributed from northern Baja California, Mexico, to British Columbia, Canada, and supports important commercial fisheries (Smith 2005) in addition to providing an important forage base in the ecosystem. Pacific sardine abundance has declined significantly, which has led to serious conservation concerns (Hill et al. 2017) and unwelcomed consequences for both human and nonhuman predators alike (Punt et al. 2016). Due to its relatively short life-span in a fluctuating environment (Chavez et al. 2003), Pacific sardine are thought to have highly plastic life history characteristics (Butler et al. 1996; Silva et al. 2006; Dorval et al. 2015; Brosset et al. 2016) making characterization of temporal variation in maturation potentially important for stock assessment.

The objectives of this study were to evaluate three basic questions on the process of female maturation in the northern subpopulation of Pacific sardine. The first question is whether maturation is better described by an age- or length-based process. It is possible that maturation can be related to both age and length (Schnute and Richards 1990), but for stock assessment purposes do fish mature because they are older or because they are larger? After deciding the biological units of maturation, the second objective is to assess if the temporal variability in maturation is better described by an annual or cohort effect. Finally, this work quantifies the magnitude of the temporal variability and evaluates if this additional process variability should be considered in future stock assessments.

MATERIALS AND METHODS

Study area and sample collection

Adult sardine were collected off of the West Coast of the United States during spring trawl surveys in 1994, 1997, and from 2004–15 (Macewicz et al. 1996; Lo et al. 2005; 2010; Dorval et al. 2015). Females were sampled from trawl gear and standard lengths were measured to the nearest millimeter (mm). Otoliths were removed, cleaned and stored dry. Gonads were removed from females and preserved in 10% neutral buffered formalin. For our analysis, those data were filtered to include only samples collected off of southern and central California between 30°–37°N latitude and 117°–126°W longitude ($n = 3,818$) to ensure only samples from the northern subpopulation were included in the study.

Age and maturation determination

Age determinations were done by counting annual increments on whole sagittae otoliths following the procedures of Yaremko (1996). Ageing error for sardine varies by reader but generally increases above age 4 (Dorval et al. 2013). A piece of the preserved ovary was removed and prepared as a histological slide with hematoxylin and eosin stain. Female maturation was determined through a combination of gross visual and histological examination (Macewicz et al. 1996).

Age- or length-based process

Conditional analysis was used to separate the effects of age- from length-based maturation. The general theory of conditional analysis is an extension from the analytical treatment of paired age-length data developed to estimate growth (Piner et al. 2016) and subsequently to determine age- versus length-based movement (McDaniel et al. 2016). Paired age-length data with maturation information can be analyzed by conditioning the observed distribution of one measurement (age or length) on a discrete unit of the other correlated measurement. Because there is variability in the age-length relationship, each age contains a distribution of lengths, and similarly a distribution of ages for each length. In this example, a solely length-based process of maturation (higher proportion of fish maturing due to increasing length) would lead to identical age distributions of mature and immature fish at length (age conditioned on length). However, if maturation is age-based, the age of mature fish for individual lengths will be older. Conditioning on length rather than age is generally preferred because it is not influenced by size-based sampling, while conditioning length on age is heavily influenced by size selection (Piner et al. 2016).

After determination of the biological units of maturation, the probability of the difference in the observed mean age of mature versus immature fish at length was evaluated using randomization methods. Observations of maturation state were randomized ($n = 1000$) within length to create new mean age of each maturation state. A distribution of possible test statistics (TS) was compared to the observed TS_{obs} . The test statistic is:

$$TS = \sum_l (\mu_{ml} - \mu_{iml})$$

where the test statistic (TS) is mean age at length of mature (μ_m) minus mean age at length immature μ_{im} summed across all lengths (l).

Annual or cohort variability

After determination of the biological units of maturation, evaluation of the temporal variability as either an annual (year-specific) or cohort effect (year-class) was

done using multi-model inference. We fit the maturity data by individual year and by cohort using the logistic function in R with the general linear model procedure with formula of the form:

$$\log\left(\frac{P}{1-P}\right) = \alpha + \beta (X * I) + \varepsilon$$

where P is a probability of mature (being immature as 0 or being mature as 1), X is either length or age depending on the previous evaluation of biological units of maturation, I is year/cohort, α is the inflection, β is the slope of the logistic relationship, and the error term ε follows a binomial distribution with mean zero and variance equal to $P(1-P)$. Akaike information criterion (AIC, Akaike 1974) weights (w_i) were computed for each formula and used to quantify the strength of evidence (Burnham and Anderson 1998) for one hypothesis or the other.

$$AIC = -2\ln L + 2k$$

where L is likelihood function and $-2\ln L$ is known as the deviance and k is number of parameters in the model.

After determination of the units of temporal variability, a separate logistic regression was fit to predict the length or age at 50% maturity (X_{50}) for each year or cohort depending on the previous evaluation of the units of temporal variability. The logistic regression followed the form:

$$\log\left(\frac{P_{X_i}}{1-P_{X_i}}\right) = a + bX_i + e$$

where P_{X_i} is a probability of mature for a given length or age (X_i), a is the inflection, b is the slope of the logistic relationship, and the error term e follows a binomial distribution with mean zero and variance equal to $P_{X_i}(1-P_{X_i})$.

The length or age at which 50% of fish that have reached maturity was calculated by solving the above equation with $P_{X_i} = 0.5$.

$$X_{i,50\%} = -\frac{a}{b}$$

Consistency with population dynamics

To evaluate if the final temporal estimates of maturity are important for our current understanding of the population dynamics, our time-varying maturation estimates (empirical and not model based) replaced the time-invariant (average) maturation estimates in the current stock assessment model (Hill et al. 2017). The estimates of maturity were compiled in the appropriate biological (age or length) and temporal (annual or cohort) units based on the preceding methods. Temporal units with missing maturity information used the long-term average maturity at the appropriate biological unit. This long-term average is the same as in the

current assessment. The current assessment model estimates dynamics from 2005 to 2017 based on a fishing year (July 1–June 30). The 2 parameters of the spawner-recruitment relationship ($\ln R_0$ - unfished recruitment and h -curvature of the relationship) was estimated as part of the integrated assessment model assuming a Beverton and Holt functional form. The assessment model used an empirical weight-at-age approach with catch, observations of the age-structure of the catch, and an acoustic absolute estimates of abundance and its age compositions as likelihood components. The empirical weight-at-age assessment approach bypasses the need for modelling the length-at-age by specifying annual weight-at-age for each fleet and survey. This approach allows considerable flexibility in specifying empirical estimates of the temporal variability in biological processes. For a complete description of the model see Hill et al. (2017).

Model improvement from using the observed temporal variability in the maturity schedule was evaluated using the change in the magnitude of the recruitment residual relative to the model with time-invariant maturity. The recruitment residual is the difference between the estimated recruitment and the expectation based on the spawner-recruit process. Deviations from the spawner-recruit expectation includes not only real fluctuation in recruitment but also process error due to model misspecification. Because the catch-at-age and survey estimates of abundance are the same between models, the absolute recruitment estimates should be the same between models. Therefore any reduction in the recruitment residual would be due to reduction of the process error associated with incorrect specification of the maturity schedule. Thus reduction in the absolute value of the recruitment deviation can be construed as evidence for better consistency between the estimated spawner-recruit process and the data driven estimates of recruitment.

We quantified the change in the recruitment residuals from a model using annual versus time-invariant (table 1) maturity schedules using a measure of relative change (Δp):

$$\Delta p = (abs(p) - abs(\hat{p})) / (abs(p))$$

Where p is the year-specific residual from the assessment model that included time-invariant maturity and \hat{p} is the year-specific residual from the assessment model that included time-varying maturity. Positive Δp is the proportional improvement in consistency of the prediction based on variable maturity and negative Δp would be proportional degradation. If the temporal estimates of the maturity schedule are more consistent with the model structure and the data, we expect mostly positive Δp . Mostly negative or random Δp

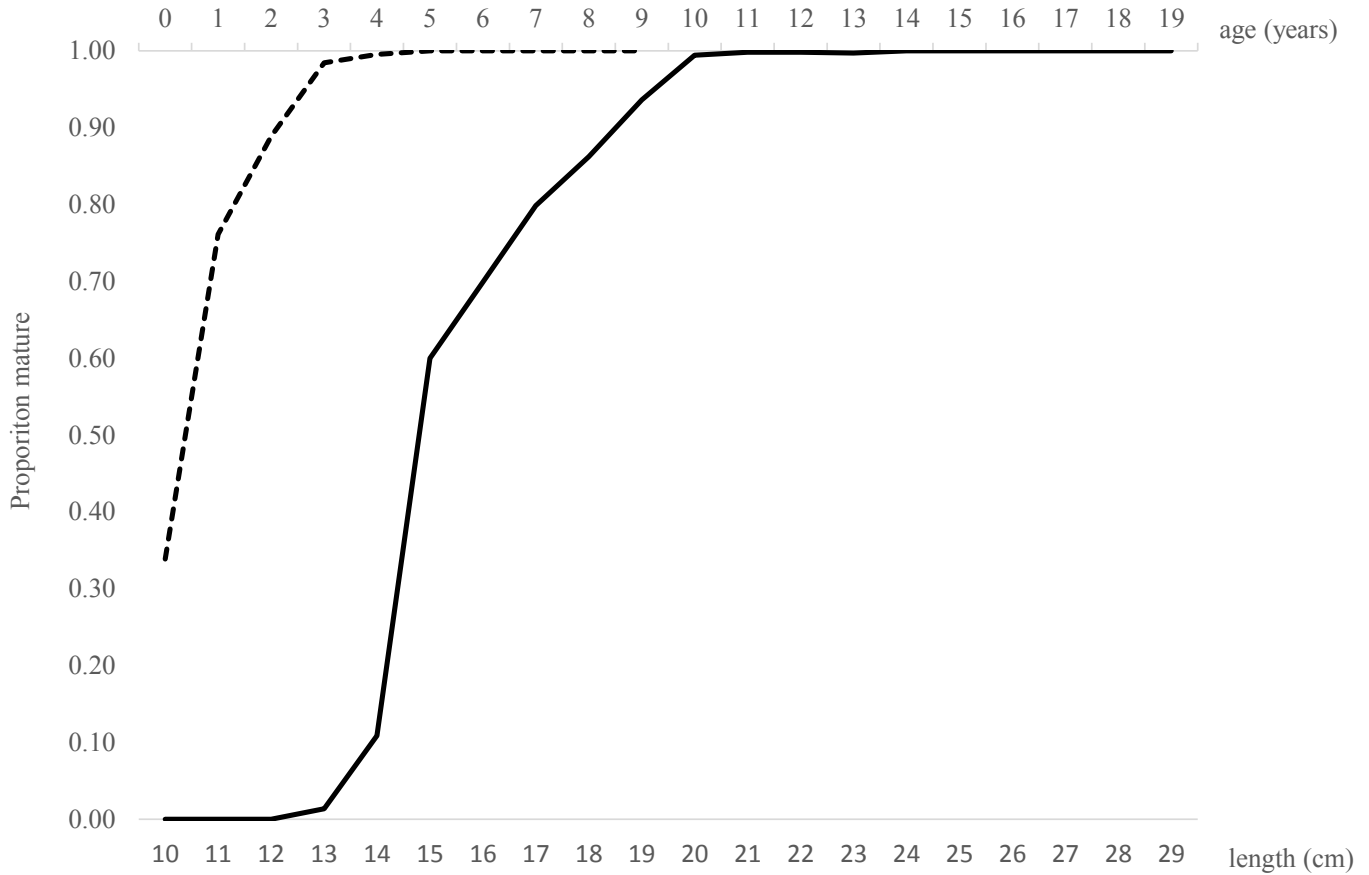


Figure 1. Empirical estimates of the proportion of female Pacific sardine mature by age (dashed line) and length (solid line). Age x-axis is given above the plot and length below. Data were aggregated across all years.

TABLE 1
 Description of the data used in this study to determine female maturity schedules. Sample sizes (*n*) and proportion mature are given by age and length. Samples were aggregated across all years.

age (yr)	<i>n</i>	prop	length (cm)	<i>n</i>	prop
0	251	0.34	10	1	0.00
1	703	0.76	11	2	0.00
2	808	0.89	12	30	0.00
3	840	0.98	13	73	0.01
4	663	1.00	14	92	0.11
5	374	1.00	15	85	0.60
6	135	1.00	16	216	0.70
7	36	1.00	17	362	0.80
8	7	1.00	18	399	0.86
9	1	1.00	19	330	0.94
			20	342	0.99
			21	504	1.00
			22	565	1.00
			23	349	1.00
			24	206	1.00
			25	160	1.00
			26	77	1.00
			27	19	1.00
			28	5	1.00
			29	1	1.00

would indicate those changes in maturation schedules were not consistent with improvement in our understanding of sardine dynamics.

RESULTS

Age- or length-based process

A total of 3,818 fish were used to determine maturation schedules (table 1), which display a pattern of an increasing proportion mature with both increasing age and length (fig. 1). For every length, the proportion mature increases with increasing age (fig. 2). A bimodality exists in the size distribution of age-0 fish that is also related to the state of maturity. The smaller age-0 length mode was primarily immature fish. By age-1 the modal size of immature and mature fish converges but a similar difference between the mean size of immature and mature fish exists for every age. These patterns are consistent with both age- and length-based processes of maturation.

When the mean age of mature and immature fish is conditioned on length, mature fish are roughly 0.25–0.75 years older than immature fish at every length

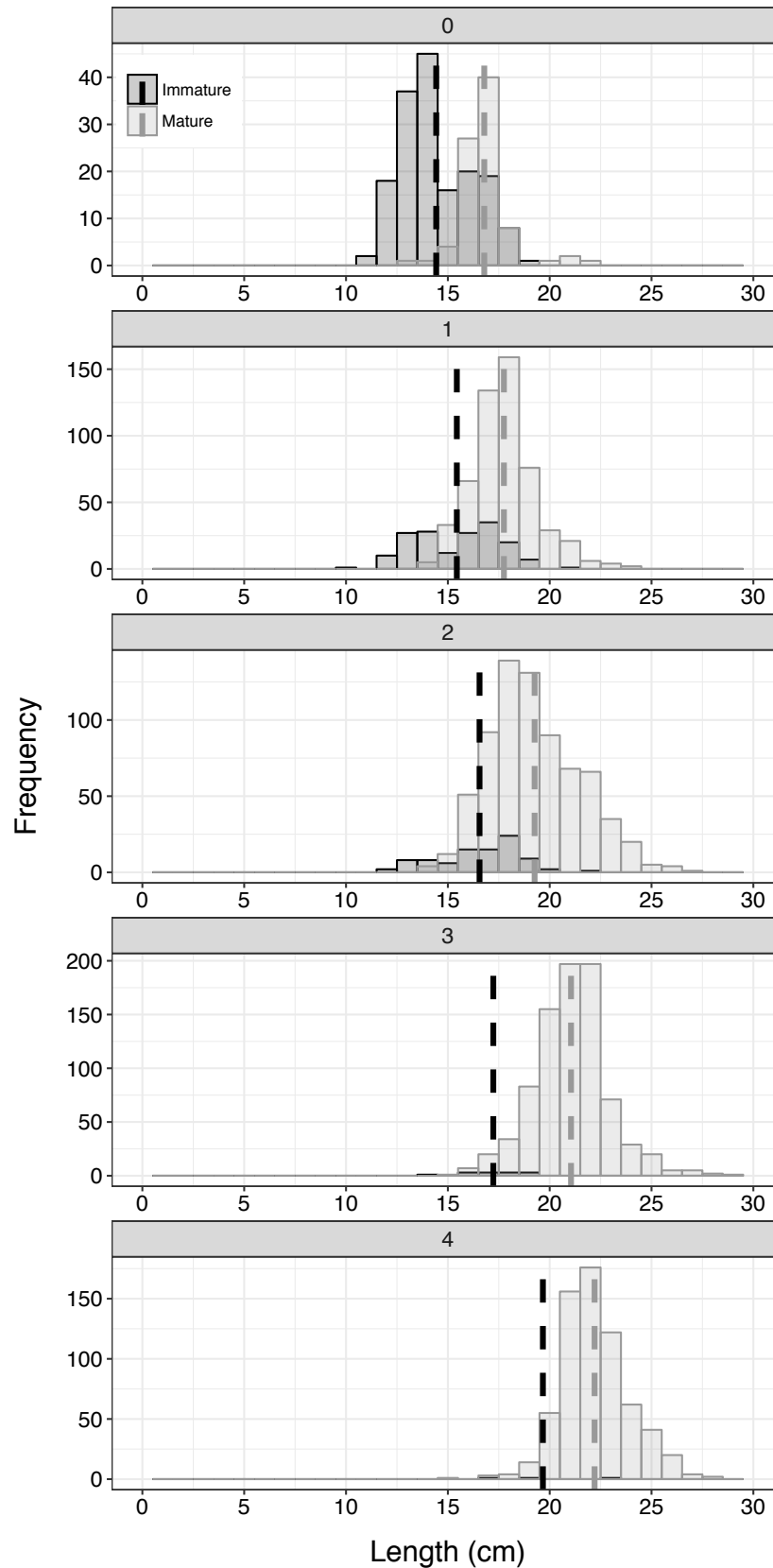


Figure 2. Length frequency of mature (light bars) and immature (dark bars) Pacific sardine by age (age-0 top to age-4 bottom panel). Dark dashed line is mean length of immature and light dashed line is mature fish. Data were aggregated from 1994–2015.

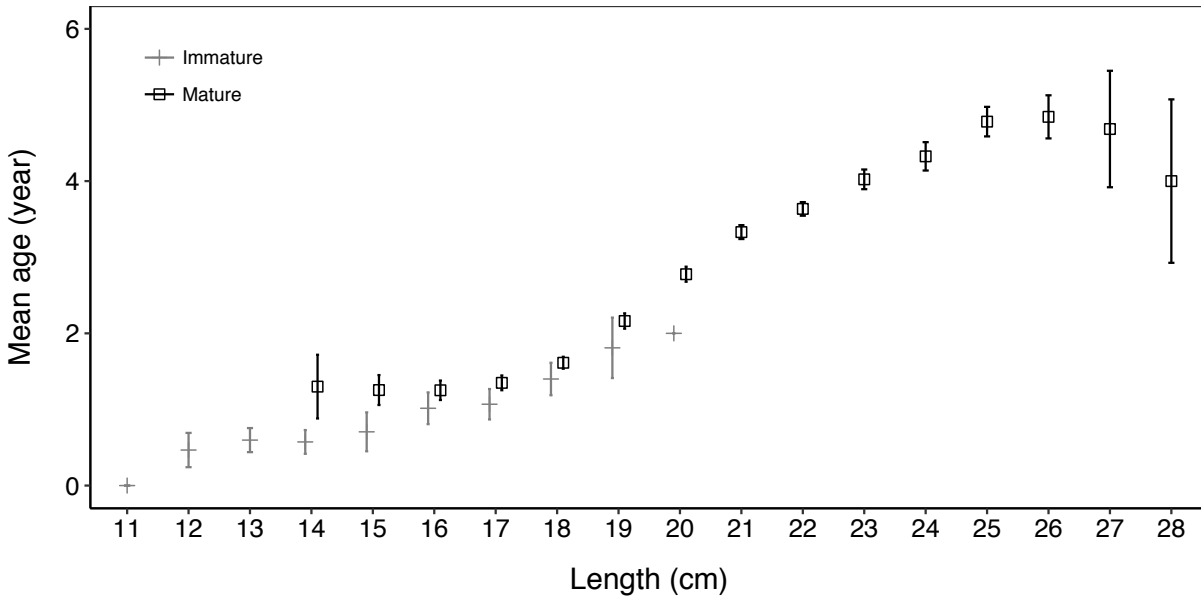


Figure 3. Mean age-at-length of Pacific sardine collected from 1994–2015. Mature fish are depicted by dark squares and immature fish by light crosses. The means of mature fish are plotted offset from lengths by 0.25 cm for presentation. Vertical lines are empirical 95% confidence intervals. Ages are integer ages. All fish greater than 20 cm are mature.

TABLE 2

Number of estimated parameters, model deviances (and degrees of freedom), AIC values and weights (w_i) for two competing age-based logistic models. One model treats temporal variability in female maturity rates as a function of year of collection the other as cohorts. Strength of evidence favoring one model or another can be interpreted from w_i , with values approaching 1 indicating all weight should be given to this model.

Annual model	Estimate (df)
parameters	16
Null deviance	2728.6 (3817)
Residual deviance	1530.8 (3802)
AIC	1562.8
w_i	1.0
Cohort model	
parameters	28
Null deviance	2728.6 (3817)
Residual deviance	1578.0 (3790)
AIC	1634.0
w_i	0.0

(fig. 3). This pattern of older mature fish at every length is unlikely to be random for the given set of data ($p < 0.001$) and is consistent with an age-based process of maturation. However, the randomization procedure does not consider correlations in the data, therefore care should be taken drawing inference to the real population.

Annual or cohort temporal variability

Temporal variability in female maturity schedules was better explained by annual rather than cohort-specific variability. The strength of model evidence heavily

favoring the alternative hypothesis of annual ($w_i = 1.0$) rather than cohort ($w_i = 0.0$) as the temporal units of the variability (table 2). The model used to estimate the age at 50% maturity generally fit the data well, although for some years the absence of younger age groups precluded estimation of that age (fig. 4). Annual variation in the estimated age at 50% maturity ranged by more than 1-year (table 3, fig. 5).

Consistency with population dynamics

Recruitment estimated from the model assuming annual variability in maturity schedules was more consistent with the spawner-recruit process than those estimated assuming a time-invariant (average) maturation schedule. Values of Δp were positive for all years (fig. 6) with some improvement in consistency exceeding 50%. Improvement in estimated recruitment consistency was not due to changes in the population dynamics between models. Recruitment estimates between models was identical with the exception of the poorly informed (limited data informing) last year (fig. 7). Identical catch-at-age was an input into both models (removals) and thus the estimated population numbers at age were the same between models. The changes in spawning biomass (fig. 7) were due solely to the changes in age groups used to calculate spawning biomass from time varying maturation schedules. Changes in the calculation of spawning biomass between models resulted in a small change in the estimated population resilience ($h = 0.36$ time-invariant, $h = 0.35$ time-varying) based on spawner-recruit curvature (fig. 7).

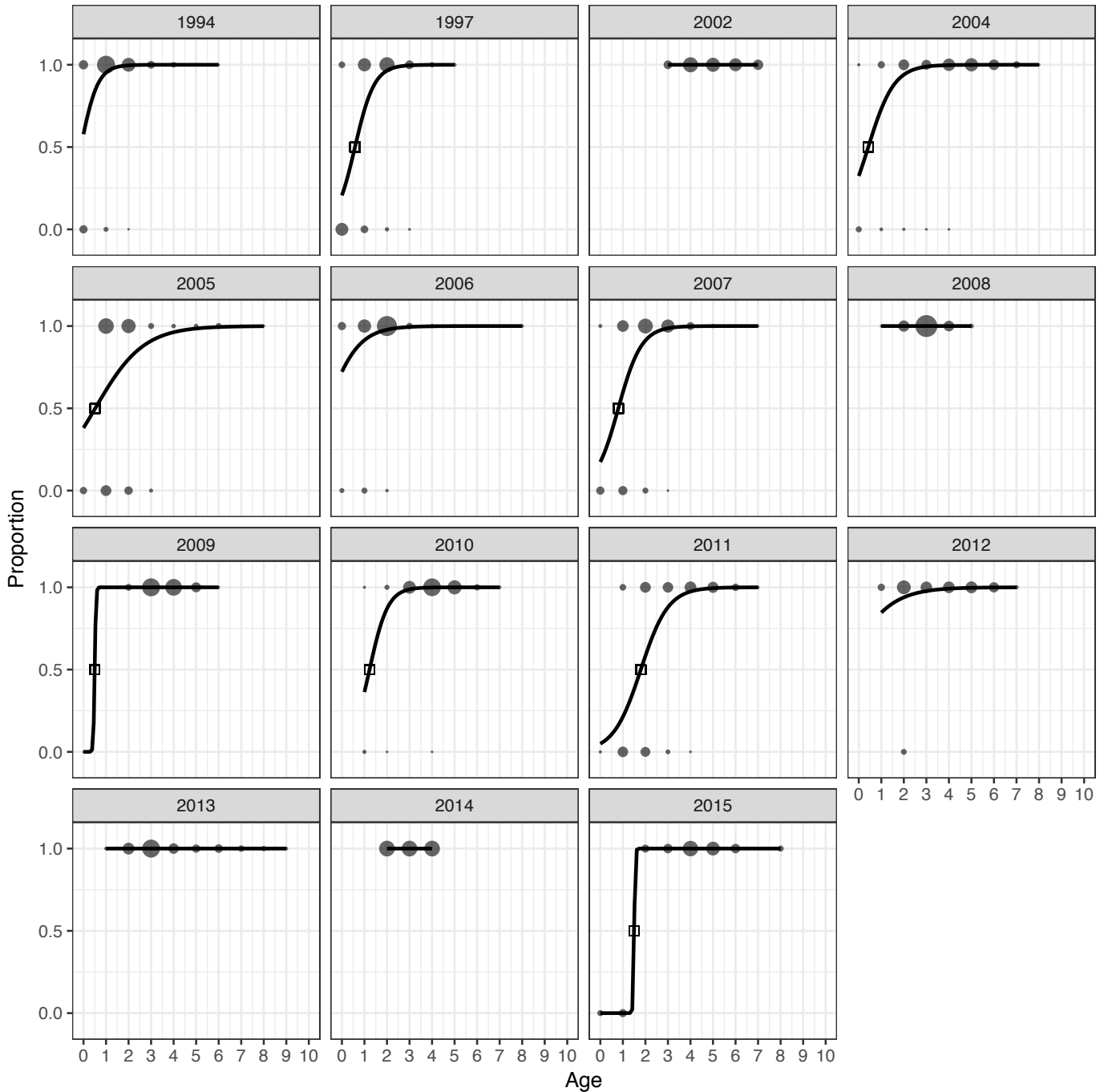


Figure 4. Model predictions of the proportion of Pacific sardine that were mature-at-age by year (solid line). Data are given as shaded circles, with the size of the circle representing the fraction of the total number of fish in that year that were either mature (given on the y-axis 1) or immature (y-axis 0) at a specific age. The open square represents the estimate of the age-at-50% maturity.

DISCUSSION

The process of female maturation in Pacific sardine is better described by an age-based process rather than a length-based one. If maturation was controlled by the size of the body cavity, it would be expected that the ages of mature and immature fish at the same length would have been the same. However, it should not be ruled

out that size-based processes may also operate (Schnute and Richards 1990; Richards et al. 1990). The potential length effects are perhaps most strongly displayed in age-0 fish with its demonstrably smaller mode of immature fish. Three possible explanations for this include: a minimum body size influencing the start of maturation, the larger and mostly mature age-0 fish were born prior

TABLE 3
 Year-specific estimates of parameters of the logistic model fit to annual female maturity-at-age data. Year, sample size (*n*), parameters (standard deviation), and the derived quantity of age at 50% maturity (standard deviation) are given. Standard deviations were generated by bootstrapping. NA denotes that A50 could not be derived from parameter estimates.

year	<i>n</i>	<i>a</i>	<i>b</i>	A50
1994	532	0.32 (0.21)	2.67 (0.37)	-0.12 (0.09)
1997	289	-1.35 (0.27)	2.32 (0.33)	0.58 (0.07)
2002	12	25.57 (0.00)	0.00 (0.00)	NA (NA)
2004	339	-0.73 (0.99)	1.74 (1.03)	0.42 (0.22)
2005	258	-0.49 (0.29)	0.93 (0.21)	0.52 (0.25)
2006	143	0.96 (0.57)	1.41 (1.09)	-0.68 (1.45)
2007	374	-1.56 (0.32)	1.95 (0.25)	0.80 (0.09)
2008	234	26.57 (0.00)	0.00 (0.00)	NA (NA)
2009	562	-18.39 (22.08)	36.93 (17.55)	0.50 (1.34E+11)
2010	398	-3.02 (11.08)	2.46 (8.05)	1.23 (4.81)
2011	358	-2.95 (0.4)	1.65 (0.18)	1.80 (0.1)
2012	156	0.68 (1.77)	1.03 (0.16)	-0.66 (8E+8)
2013	118	26.57 (0.00)	0.00 (0.00)	NA (NA)
2014	6	24.57 (0.00)	0.00 (NA)	NA (NA)
2015	28	-65.99 (22.45)	43.88 (12.01)	1.50 (2E+29)

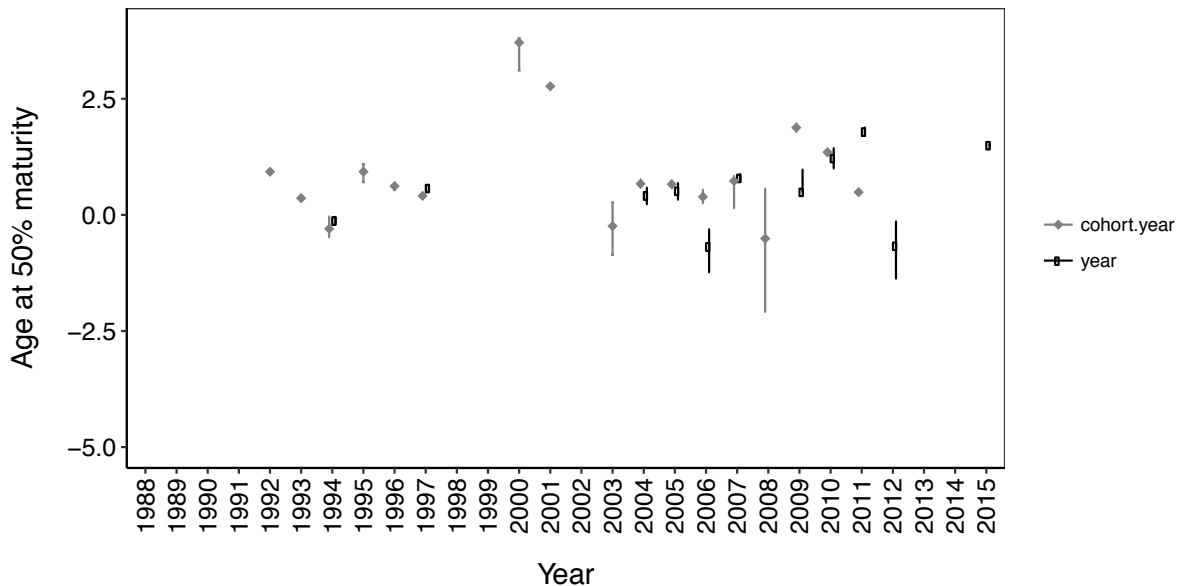


Figure 5. Model estimates of Pacific sardine age at 50% maturity. Model estimates using cohort year are given by lighter symbols and annual by darker symbols. Annual estimates are plotted offset from cohort estimates by 0.25 years for presentation. Ages were integer ages. Predicted values less than zero indicate for that time period age-0 fish were greater than 50% mature. The 80% Confidence Intervals were generated by bootstrapping the data (*n* = 1,000).

to immature fish and therefore potentially age related, or ageing error. Because hatch date may be contributing to the bimodality, future work calculating hatch date for these two groups is warranted. Whatever the cause, it does appear that immature fish at a given age are more likely to be smaller fish, but that for all lengths older fish are more likely to be mature. For assessment purposes where maturity is typically incorporated as either age- or length-based, our results support age as the better unit to describe the maturation process.

Assuming age-based maturation is the best descriptor of the process, our results support that the local environment is perhaps more important than cohort density

on the observed maturation process. Our results provide indirect support for environmental forcing of Pacific sardine population dynamics, which has already been postulated (Jacobson and MacCall 1995; Chavez et al. 2003) and forms a basis for control rules governing its management (Hill et al. 2017). The annual changes in maturation seems to be biologically significant as the age at 50% maturity ranged by more than the average difference in ages between immature and mature fish and by a significant fraction of the total lifespan of Pacific sardine. It may be worth considering that annual effects themselves are closely related to age-based processes, as year is directly related to age.

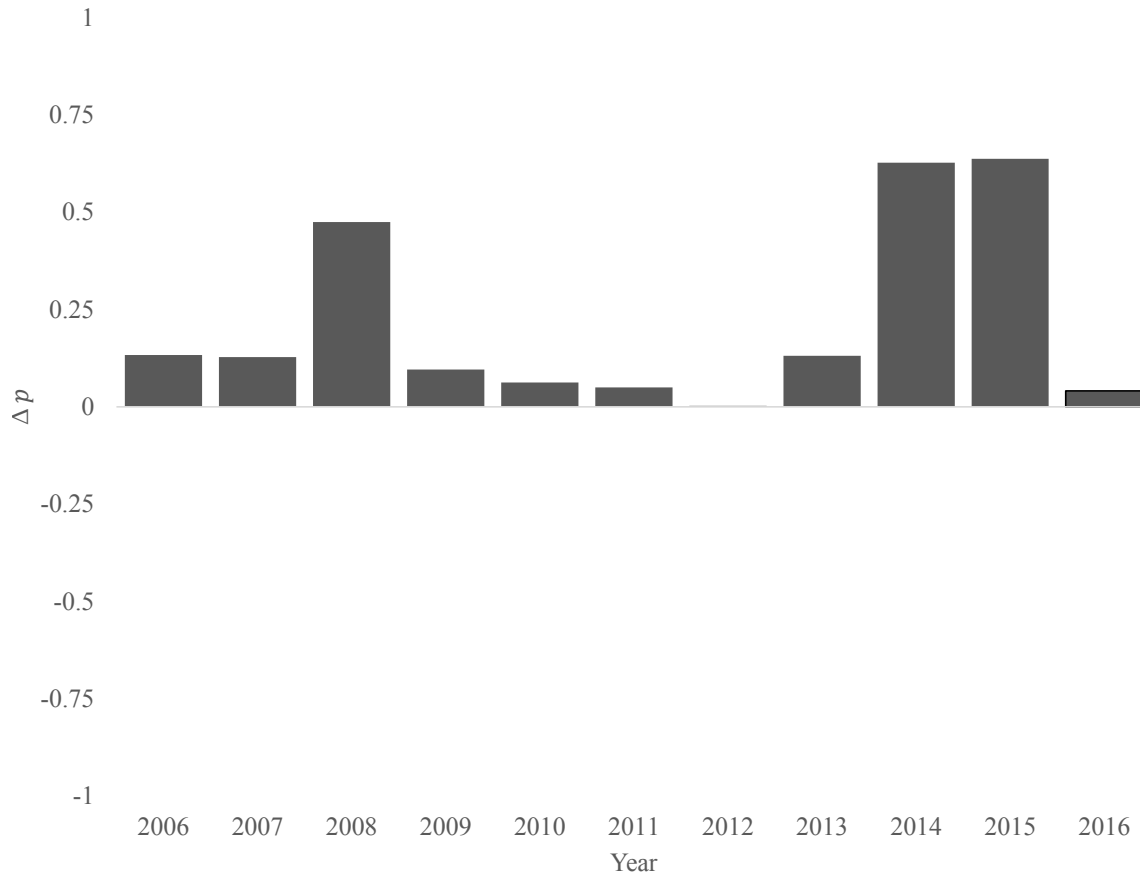


Figure 6. Proportional change in the recruitment residual (Δp) from the expectation of the estimated spawner-recruit relationship. Positive Δp indicated reduced residual when annual variability in maturity schedules is used relative to time-invariant maturity schedule. Negative Δp would indicate a larger residual associated with annual empirical estimates of the maturity schedule. Terminal model year is omitted because estimated recruitment is the expected from the spawner-recruit relationship.

For stock assessments of populations with high natural mortality rates and high variability in recruitment, changes in maturity-at-age can have large effects on the effective spawning stock size. To more completely elucidate the role of maternal stock size, more consideration should be given to other aspects of spawning biology such as variability in the number of egg batches. Unless properly modelled in the stock assessment, temporal variability in reproductive processes could obscure any relationship between maternal stock size and recruitment. It should be noted that the current assessment covers a limited time period of declining recruitment and spawning biomass, and care in interpreting results from a period with a one-way trip in abundance is always warranted.

The comparison of the alternative hypothesis of age- or length-based maturation did not use a model based approach due to differences in data quality between age and length. Sardine mature across 6–8 discrete units of length but only 2–3 units of integer age, and the primary source of measurement error is likely to be ageing error, which affects only age-based models. The different degrees of data coarseness and measurement error pre-

cluded our attempting to use a model-based inference. Instead, we relied on the conditional methods of separating the correlated effects of age from length effects (McDaniel et al. 2016). Our final estimates of maturity schedule were ultimately empirical to avoid the functional form assumptions and to be consistent with how the current stock assessment treats the same data.

Two important criteria must be addressed when developing an analysis to evaluate the alternative hypotheses (Burnham and Anderson 1998). The first question regards if the set of candidate models are objective, reasonable, and defined before beginning the data analyses. This study easily meets the first criteria as the candidate models were relevant for population assessment and determined a priori. Equally important is the appropriateness of the laboratory procedures and sampling designs for the questions examined. The laboratory work followed accepted practices by experienced laboratory scientists. We note that the determination of fish age is the most difficult during the spring spawning season when our samples were taken. This difficulty arises because fish have not yet reached their presumed July

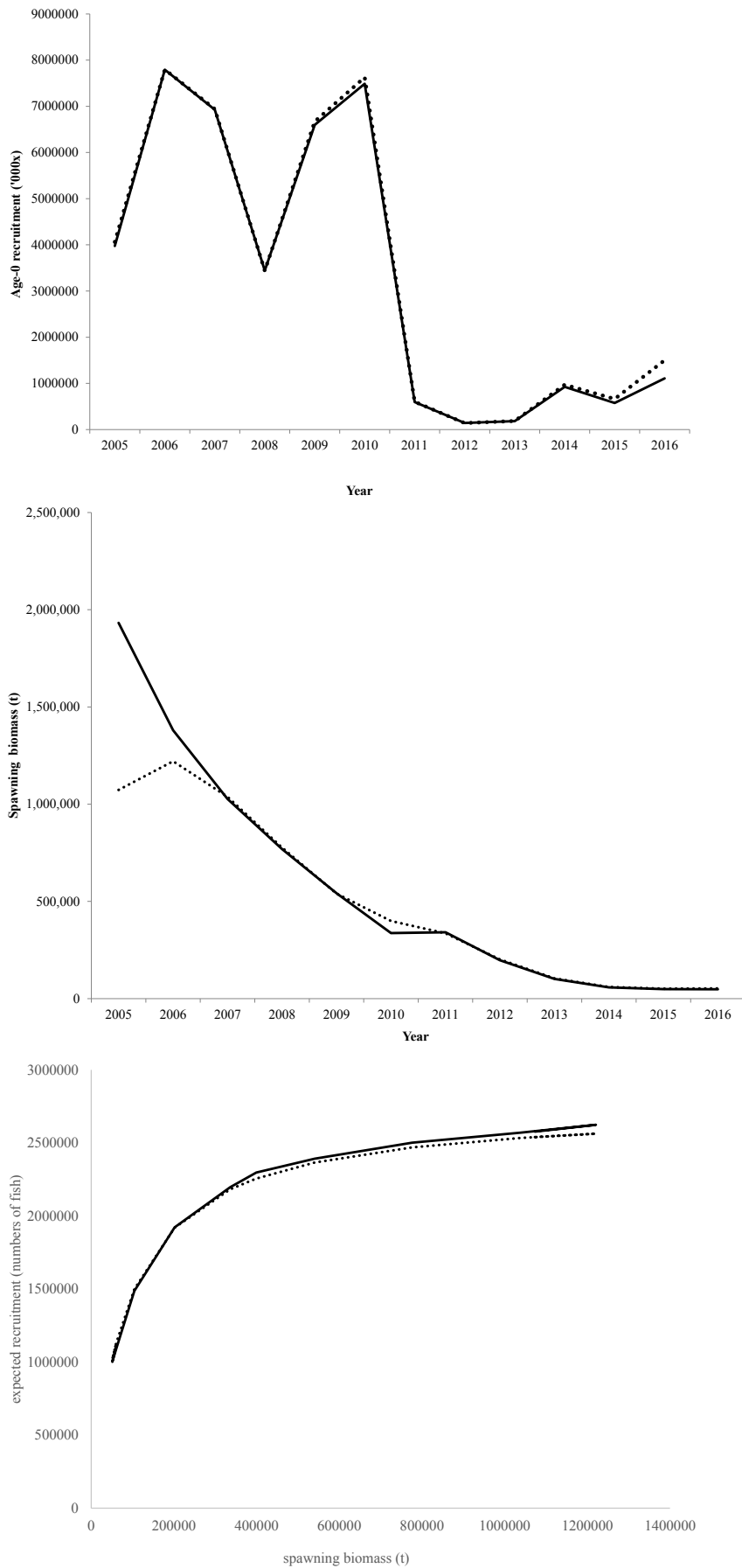


Figure 7. Recruitment (upper panel), spawning biomass (middle panel) and (bottom panel) spawner-recruit estimates from the current assessment (dotted) that uses a time-invariant maturity schedule and a model that includes a time-varying maturity schedule (solid). Terminal model year is omitted because estimated recruitment is the expected from the spawner-recruit relationship.

1st birthday and age assignment can require a subjective determination of the edge classification (annulus formed or is going to form). Ageing errors associated with an incorrect edge classification may be more likely to result in an underestimation of age.

Perhaps our largest caveat relates to the sampling design. Although the samples were taken from a fishery independent survey with established biological sampling protocols, we cannot be certain that sampling issues have not biased our results. Conditioning the maturity information on length removes the size-based sampling issues that are common in fisheries (Piner et al. 2016). Spatial patterns by age (McDaniel et al. 2016) are not as easily dismissed. Preliminary analysis (not shown) of inshore-offshore stratification produced similar conclusions about age-based maturation, but more consideration of the effects of spatial sampling may be needed.

Despite the caveats described above, these are currently the best available data on the process of Pacific sardine maturation and incorporating our results into future stock assessments are relatively straightforward. Maturity should be included as a function of age and not length. Additionally, given the magnitude of the annual variability in maturation some thought in future assessments should be given to including that variability. More specific estimates of spawning biomass could reduce the amount of the recruitment process variability and help clarify the maternal role in recruitment. Given the importance of recruitment strength in predicting safe catch levels for short-lived highly variable species, further work in this area is certainly warranted.

ACKNOWLEDGEMENTS

The authors would like to thank several reviewers both anonymous and known. The scientific results and conclusions, as well as any views or opinions expressed herein, are those of the author(s) and do not necessarily reflect the views of NOAA or the Department of Commerce.

LITERATURE CITED

- Akaike, H. 1974. A new look at the statistical model identification. *IEEE Transactions on Automatic Control* AC 19: 716–723. doi: 10.1109/TAC.1974.1100705.
- Black, B. A., G. W. Boehlert, and M. M. Yoklavich. 2008. Establishing climate-growth relationships for yelloweye rockfish (*Sebastes ruberrimus*) in the northeast Pacific using a dendrochronological approach. *Fish. Oceanogr.* 17(5):368–379. doi:10.1111/j.1365-2419.2008.00484.x.
- von Bertalanffy, L. 1938. A quantitative theory of organic growth (inquiries on growth laws, II). *Hum. Biol.* 10: 181–213.
- Brosset, P., J. Lloret, M. Muñoz, C. Fauvel, E. Van Beveren, V. Marques, J.-M. Fromentin, F. Ménard, and C. Saraux. 2016. Body reserves mediate trade-offs between life-history traits: new insights from small pelagic fish reproduction. *Royal Society Open Science* 3, 160202 DOI: 10.1098/rsos.160202.
- Burnham, K. P., and D. R. Anderson. 1998. Model selection and multimodel inference a practical information-theoretic approach. 2nd edition. Springer Science + Business Media. 488 p.
- Butler, J. L., M. L. Granados, J. T. Barnes, M. Yaremko, and B. J. Macewicz. 1996. Age composition, growth, and maturation of the Pacific sardine (*Sardinops sagax*) during 1994. *Calif. Coop. Oceanic Fish. Invest. Rep.* 37:152–159. doi.
- Chavez, F. P., J. Ryan, S. E. Lluch-Cota, and M. Niquen. 2003. From Anchovies to Sardines and Back: Multidecadal Change in the Pacific Ocean. *Science* 299 (5604), 217–22 DOI: 10.1126/science.1075880.
- Dorval, E., J. D. McDaniel, B. J. Macewicz, and D. L. Porzio. 2015. Changes in growth and maturation parameters of Pacific sardine *Sardinops sagax* collected off California during a period of stock recovery from 1994 to 2010. *J. Fish. Biol.* 87, 286–310. doi: 10.1111/jfb.12718.
- Dorval, E., J. D. McDaniel, D. L., Porzio, R. Felix-Uraga, V. Hodes, and S. Rosenfield. 2013. Computing and selecting ageing errors to include in stock assessment models of Pacific sardine (*Sardinops sagax*). *Cal. Coop. Oceanic Fish. Inv. Rpt.* 54:192–204.
- Hagen, P.T., and T. J. Quinn. 1991. Long-term growth dynamics of young Pacific halibut: evidence of temperature-induced variation. *Fish. Res.* 11(3–4): 283–306. doi:10.1016/0165-7836(91)90006-2.
- Helser, T. E., and F. P. Almeida. 1997. Density-dependent growth and sexual maturity of silver hake in the north-west Atlantic. *J. Fish Biol.* 51(3): 607–623. doi:10.1111/j.1095-8649.1997.tb01516.x.
- Hill, K. T., P. R. Crone, and J. Zwolinski. 2017. Assessment of the Pacific sardine resource in 2017 for U.S. management in 2017–18. NOAA Tech Memo NOAA-TM-NMFS-SWFSC-576. 264 p. <https://swfsc.noaa.gov/publications/TM/SWFSC/NOAA-TM-NMFS-SWFSC-576.pdf>.
- Jacobson, L. D., and A. D. MacCall. 1995. Stock-recruitment models for Pacific sardine (*Sardinops sagax*). *Can. J. Fish. Aquat. Sci.* 52:566–577 doi: 10.1139/f95-057.
- Lee, H. H., K. R. Piner, R. D. Methot Jr., and M. N. Maunder. 2014. Use of likelihood profiling over a global scaling parameter to structure the population dynamics model: an example using blue marlin in the Pacific Ocean. *Fish. Res.* 158:138–146. doi.org/10.1016/j.fishres.2013.12.017.
- Lee, H. H., K. R. Piner, M. N. Maunder, and R. D. Methot Jr. In press. Evaluation of alternative modelling approaches for spatial effects due to age-based movement. *Can. J. Fish. Aquat. Sci.* doi.org/10.1139/cjfas-2016-0294.
- Lee, H. H., L. R. Thomas, K. R. Piner, and M. N. Maunder. 2017. Effects of age-based movement on the estimation of growth assuming random-at-age and random-at-length data. *J. Fish. Bio.* 90: 222–235. doi: 10.1111/jfb.13177.
- Lo, N. C. H., B. J. Macewicz, and D. A. Griffith. 2005. Spawning biomass of Pacific sardine (*Sardinops sagax*), from 1994–2004 off Calif. *Coop. Oceanic Fish. Invest. Rep.* 46: 93–112.
- Lo, N. C. H., B. J. Macewicz, and D. A. Griffith. 2010. Biomass and reproduction of Pacific sardine (*Sardinops sagax*) off the Pacific northwestern United States, 2003–05. *Fish. Bull.* 108: 174–192.
- Macewicz, B. J., J. J. Castro Gonzalez, C. E. Coterio Altamirano, and J. R. Hunter. 1996. Adult reproductive parameters of Pacific sardine (*Sardinops sagax*) during 1994. *California Calif. Coop. Oceanic Fish. Invest. Rep.* 37:140–151.
- Maunder, M., and K. R. Piner. In press. Dealing with data conflicts in statistical inference of population assessment models that integrate information from multiple diverse data sets. *Fish. Res.*
- McDaniel, J., K. Piner, H. H. Lee, K. Hill. 2016. Evidence that the Migration of the Northern Subpopulation of Pacific Sardine (*Sardinops sagax*) off the West Coast of the United States is Age-Based. *PLoS One* 11. doi. org/10.1371/journal.pone.0166780.
- Parrish, R. H., R. Serra, and W. S. Grant. 1989. The monotypic sardines, *Sardinina* and *Sardinops*: their taxonomy, distribution, stock structure, and zoogeography. *Can. J. Fish. Aquat. Sci.* 46:201 9–2836. doi.org/10.1139/f89-251.
- Piner, K., H. H. Lee, and M. N. Maunder. 2016. Evaluation of using conditional age-at-length observations and an equilibrium approximation of the population age structure in fitting the von Bertalanffy growth function. *Fish Res.* 180:128–137. doi: 10.1016/j.fishres.2015.05.024.
- Piner, K., H. H. Lee, and L. R. Thomas. 2018. Bias in estimates of growth when selectivity in models includes effects of gear and availability of fish. *Fish. Bull.* 116:75–80. doi:10.7755/FB.116.1.8.
- Punt, A. E., A. D. MacCall, T. E. Essington, T. B. Francis, F. Hurtado-Ferro, K. F. Johnson, I. C. Kaplan, L. E. Koehn, P. S. Levin, and W. J. Sydeman. 2016. Exploring the implications of the harvest control rule for Pacific sardine, accounting for predator dynamics: a MICE model. *Ecol. Mod.* 337: 79–95 doi.org/10.1016/j.ecolmodel.2016.06.004.

- Richards, L. J., J. T. Schnute, and C. M. Hand. 1990. A multivariate maturity model with a comparative analysis of three lingcod (*Ophiodon elongates*) stocks. *Can. J. Fish. Aquat. Sci.* 47:948–959. doi.org/10.1139/f90-109.
- Rijnsdorp, A. D., and P. I. van Leeuwen. 1996. Changes in growth of North Sea plaice since 1950 in relation to density, eutrophication, beam-trawl effort, and temperature. *ICES J. Mar. Sci.* 53: 1199–1213. doi:10.1006/jmsc.1996.0145.
- Schnute, J. T., and L. J. Richards. 1990. A unified approach to the analysis of fish growth, maturity, and survivorship data. *Can. J. Fish. Aquat. Sci.* 47:24–40. doi.org/10.1139/f90-003.
- Silva, A., M. B. Santos, B. Caneco, G. Pestana, C. Porteiro, P. Carrera, and Y. Stratoudakis. 2006. Temporal and geographic variability of sardine maturity at length in the northeastern Atlantic and the western Mediterranean. *ICES J. Mar. Sci.* 63: 663–676. doi.org/10.1016/j.icesjms.2006.01.005.
- Sippel, T., H. H. Lee, K. R. Piner, and S. Teo. In press. Searching for *M*: is there more information about natural mortality in stock assessments than we realize? *Fish Res.* doi.org/10.1016/j.fishres.2016.12.009.
- Smith, P. E. 2005. A history of proposals for subpopulation structure in the Pacific sardine (*Sardinops sagax*) population off western North America. *California Calif. Coop. Oceanic Fish. Invest. Rep.* 46: 75–82.
- Stawitz, C. C., T. E. Essington, T. A. Branch, M. A. Haltuch, A. B. Hollowed, and P. D. Spencer. 2015. A state-space approach for detecting growth variation and application to North Pacific groundfish. *Can. J. Fish. Aquat. Sci.* 72: 1316–1328 (2015) dx.doi.org/10.1139/cjfas-2014-0558.
- Whitten, A. R., N. L. Klaer, G. N. Tuck, and R. W. Day. 2013. Accounting for cohort-specific variable growth in fisheries stock assessments: a case study from south-eastern Australia. *Fish. Res.* 142: 27–36. doi:10.1016/j.fishres.2012.06.021.
- Yaremko, M. L. 1996. Age determination in Pacific sardine, *Sardinops sagax*. NOAA-TM-NMFS-SWFSC-223 223, 39. <https://swfsc.noaa.gov/publications/TM/SWFSC/NOAA-TM-NMFS-SWFSC-223.PDF>

SPRING SPAWNING DISTRIBUTION OF PACIFIC SARDINE IN US AND MEXICAN WATERS

J. A. VALENCIA-GASTI AND R. DURAZO

Facultad Ciencias Marinas
Universidad Autónoma de Baja California
Ensenada, C.P. 22860
Baja California, México
augusto.valencia@uabc.edu.mx

E. D. WEBER AND S. MCCLATCHIE

NOAA
Southwest Fisheries Science Center
8901 La Jolla Shores Drive
La Jolla, CA 92037-1509

T. BAUMGARTNER

Department of Biological Oceanography
CICESE
Ensenada, C.P. 22860
Baja California, México

C. E. LENNERT-CODY

Inter-American Tropical Tuna Commission
8901 La Jolla Shores Drive
La Jolla, CA 92037-1508

ABSTRACT

The Pacific sardine, *Sardinops sagax*, is a highly migratory coastal pelagic species that occurs from the tip of Baja California to the Gulf of Alaska and in the Gulf of California. We used fishery-independent egg surveys to characterize the relative amounts of sardine spawning habitat in the exclusive economic zones (EEZs) of Mexico and the US during spring 2000–13. Most eggs were captured in the US EEZ from San Francisco to the Mexico–US border in all years sampled. A small fraction ranging from 0% to 10% of all eggs captured occurred in the Mexican EEZ, usually from Punta Eugenia north to the border. The abundance and distribution of eggs found in warmer waters between 15°C to 18°C off northern Baja California appear to be dependent on periods of more intense flow of the California Current, when sardine belonging to the northern subpopulation found in central and southern California extends southward into the nearshore area off Baja California. However, a small fraction of the southern subpopulation may also have spawned in coastal areas of the US–Mexican border during May in some years.

INTRODUCTION

The Pacific sardine, *Sardinops sagax*, is a coastal pelagic forage fish that inhabits the California Current Ecosystem (CCE) in the northeastern Pacific, ranging from the Gulf of Alaska to the southern tip of Baja California peninsula, Mexico, and into the Gulf of California (Clark 1945; Checkley et al. 2009). It is an important component of the CCE because it occupies an intermediate trophic level, serving as a grazer of plankton and an important prey item for pelagic fish, birds, and mammals (Cury et al. 2000; Kaplan et al. 2013). Sardines also support important fisheries when they are available in the exclusive economic zones of Canada, Mexico, and the US (Radovich 1982; Hill et al. 2015). However, sardine abundance fluctuates greatly in response to environmental conditions in the CCE (Marr 1960; Parrish et al. 1981; Lindegren et al. 2013). Sardine were the most

abundant coastal pelagic fish in CCE during the 1930s and 1940s, and from about 1995 to 2005 but the population declined in the last decade to about 1%–2% of its peak abundance in 2007 (Hill et al. 2016). Given these broad population fluctuations, it is important to survey sardine distribution and abundance throughout the entirety of its range for both ecosystem assessment and harvest management.

Two subpopulations or stocks of Pacific sardine, *Sardinops sagax*, exist in CCE and another population occurs mainly in the Gulf of California (Ahlstrom 1960a; Félix-Uraga et al. 2004; Smith 2005). We refer to the two that occur in the CCE as the northern and southern subpopulations. These subpopulations have different morphometric characteristics (Félix-Uraga et al. 2005; García-Rodríguez et al. 2011; Javor et al. 2011), habitat preferences (Félix-Uraga et al. 2004), and spawning aggregations (Marr 1960; Hernandez-Vazquez 1994). However, they cannot be differentiated genetically, suggesting the subpopulations experience some level of interbreeding (Hedgecock 1986; Lecomte et al. 2004; García-Rodríguez et al. 2011). Although the ranges of the northern and southern subpopulations on the Pacific coast overlap, they are spatially segregated during periods of high abundance because the two subpopulations have synchronous north–south annual migration patterns (Félix-Uraga et al. 2004).

The northern subpopulation ranges from Vizcaino Bay (Punta Eugenia, Baja California, Mexico; fig. 1) to the Gulf of Alaska (Clark 1945). The subpopulation inhabits subarctic water mass with salinities in the range of about 32.5 to 33.7 and sea-surface temperatures (SSTs) in the range of about 12° to 17°C (Checkley et al. 2000; Lynn 2003), although off Oregon/Washington, sardine occur in lower salinity water near the Columbia River plume (Emmett et al. 2005). In the 1930–40s, individuals attained total lengths up to 30 cm with life spans greater than 13 years and reaching sexual maturity at 2 years of age (Murphy 1966; Schwartzlose et al. 1999). However, since the early 1990s, the

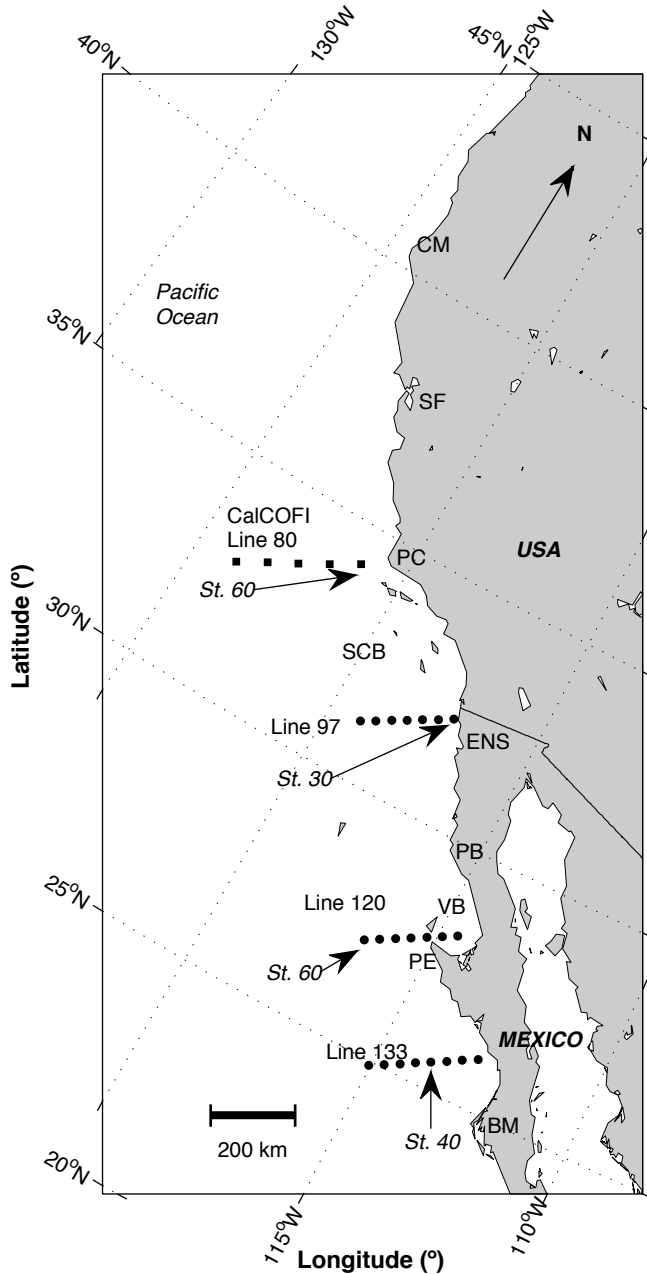


Figure 1. Map of the west coast of North America from Oregon (US) to Baja California (México) showing the location of the sites mentioned in the text; Cape Mendocino (CM), San Francisco (SF), Point Conception (PC), Southern California Bight (SCB), Ensenada (ENS), Punta Baja (PB), Vizcaino Bay (VB), Punta Eugenia (PE), Bahía Magdalena (BM). Some CalCOFI Lines are indicated by square and circles with the numeric ID to the right.

size of sardines caught by the commercial fishery have been less than 27 cm, and reach ages of five or six years with younger age-at-maturity (Lo et al. 2005; McDaniel et al. 2016). These sexually mature sardines aggregate in the southern portion of their range in spring and migrate northward in summer and early fall (Clark and Marr 1955). Spawning occurs in both waters off Baja California, Mexico, and off California in spring,

and sporadically off Oregon (42°–46°N) in early summer (Lo et al. 2010).

The southern subpopulation ranges from the southern tip of Baja California into the southern California Bight. It inhabits Pacific subarctic water mixed with warmer and saltier waters from the south and west. The range of salinity of this water is 33.6 to 34.6 and sea surface temperature vary from 18° to 22°C (Durazo and Baumgartner 2002). Fish from the southern subpopulation tend to be smaller than their northern counterparts and they reach sexual maturity at an earlier age (Butler et al. 1996). This is because the warmer water that they inhabit results in greater metabolic demands (Peck et al. 2013). The southern subpopulation spawns throughout the year along the coast of southern Baja California. Most spawning occurs in summer (July) and the least during the fall (Ahlstrom 1960b; Hernandez-Vazquez 1994). Environmental preferences of the southern subpopulation have usually been evaluated using data from the fishery (Félix-Uraga et al. 2004). Thus, their reported ranges of preferred temperature conditions may be biased by the limited spatial sampling pattern of the commercial fleet. However, preferred spawning habitat conditions have been documented by collection of temperature and salinity data with the continuous underway fish egg sampler (CUFES; Checkley et al. 1997, 2000) used on Mexican fishery-independent surveys (Valencia-Gasti et al. 2015).

The distribution pattern of Pacific sardines has important implications for management because the US stock assessment is assumed to address only the northern subpopulation (Hill et al. 2016). The assessment excludes the monthly catch attributed to the southern subpopulation in the fisheries off northern Baja California and in the Southern California Bight. However, invalid assumptions about the distribution of sardines from each subpopulation and their interannual variability could bias estimates of recruitment and fishing mortality, resulting in inaccurate assessments (Demer and Zwolinski 2014). Recent US sardine stock assessments have relied on acoustic/trawl (Demer et al. 2012) and daily-egg-production (DEPM; Lo et al. 2005) methods combined with an assessment model to estimate sardine biomass of the northern subpopulation. Surveys have been conducted in the spring when the majority of the northern subpopulation is typically aggregated offshore between San Francisco and the Mexico-US border, and in summer when sardine are concentrated farther north in shelf waters along the US West Coast.

Total annual harvest by the Mexican fishery is not regulated by quotas, but there is a minimum legal size limit for sardine to prevent the capture of juveniles (DOF 1993; Sagarpa 2012). Mexico implemented a formal management plan in 2012 and is considering modifica-

TABLE 1.
 CUFES samples conducted in US and Mexican waters: the total number of stations recorded (N) from waters off central California to the southern Baja California peninsula by the research programs: CalCOFI (US) and IMECOCAL (Mexico). The number (n) and percentage (%) of stations at which sardine eggs were found (sardine presence), the mean and standard error (SE) for egg density and their water temperature.

Year	N	Dates	Sardine presence		Temperature (°C)		Egg density	
			n	%	Mean	SE	Mean	SE
U.S.								
2000	801	April 7 to April 29	262	33	13.88	0.05	9.66	0.95
2001	928	April 6 to May 2	425	46	13.13	0.03	5.99	0.57
2002	1622	March 21 to April 14	825	51	13.61	0.02	2.67	0.18
2003	1287	April 4 to April 30	514	40	13.76	0.04	9.78	0.95
2004	780	March 23 to April 22	251	32	13.5	0.04	4.89	0.44
2005	961	March 28 to May 1	297	31	14.25	0.05	3.41	0.41
2006	1385	April 6 to May 8	477	34	13.73	0.07	4.05	0.54
2007	959	March 28 to April 30	606	63	13.74	0.03	2.51	0.18
2008	1628	March 25 to May 1	556	34	13.14	0.03	2.18	0.14
2009	1127	March 8 to May 7	578	51	13.59	0.03	2.57	0.3
2010	1058	April 2 to May 16	242	23	13.64	0.05	2.57	0.42
2011	923	March 25 to April 26	333	36	13.22	0.04	1.38	0.14
2012	962	April 1 to April 28	274	28	12.95	0.03	1.33	0.13
2013	686	April 7 to May 3	179	26	13.27	0.11	2.41	0.34
Mexico								
2000	654	April 4 to April 21	58	9	15.68	0.14	1.36	0.36
2001	426	April 5 to April 14	79	19	14.69	0.12	1.95	0.41
2002	839	April 19 to May 8	82	10	15.85	0.05	0.71	0.09
2003	648	April 4 to April 23	37	6	16.22	0.11	0.44	0.16
2004	735	April 15 to May 7	79	11	16.33	0.12	0.6	0.14
2005	584	April 14 to May 6	3	1	16.63	1.17	0.17	0.12
2006	425	April 20 to May 2	29	7	16.62	0.2	0.69	0.32
2007	334	April 26 to May 7	12	4	15.58	0.21	0.1	0.02
2008	465	April 16 to May 1	15	3	15.23	0.42	0.58	0.43
2009	456	April 9 to April 24	5	1	16.6	0.16	0.11	0.03
2010	512	March 30 to April 17	5	1	16.54	0.6	1.77	1.5
2011	506	April 20 to May 7	42	8	15.48	0.12	0.95	0.32
2012	342	March 8 to March 24	39	11	15.75	0.17	1.06	0.33
2013	377	May 23 to June 7	30	8	16.36	0.32	0.65	0.29

tions to the plan that would include a harvest control rule and monitoring of biomass, similar to the US management plan. These modifications are currently undergoing review by stakeholders and the general public to improve efforts towards sustainable fisheries of small pelagic fish, with the eventual goal of obtaining certification from the Marine Stewardship Council, as was obtained by the sardine fishery in the Gulf of California (SCS 2016).

The goal of this study is to characterize the distribution of spring spawning sardines in the CCE off Mexico and the US. The specific objectives are: 1) Quantify the abundance and distribution of eggs during spring surveys conducted over a 14-year period; and, 2) Qualitatively estimate the fraction of spring-spawning sardines in waters off Mexico relative to the US to provide supporting information for stock assessment.

MATERIALS AND METHODS

Sardine eggs were collected using the CUFES during spring 2000–13 cruises as part of the Investigaciones Mexicanas de la Corriente de California

(IMECOCAL; <http://imecocal.cicese.mx>) program in the Mexican EEZ, the California Cooperative Oceanic Fisheries Investigations program (CalCOFI; reviewed by McClatchie 2013) and sardine acoustic/trawl surveys and DEPM in the US. Sampling extended from central Oregon to southern Baja California. Cruises occurred in March through May but usually were centered on April (table 1).

The CUFES draws samples from 3 m depth with a continuous flow of approximately 640 l/min and filters ichthyoplankton by using an agitator with 200 µm mesh (Checkley et al. 2000). Samples were collected underway at speeds of 7–8 knots off Mexico, and 8–14 knots off the US. Samples generally were collected every 30 min (mean; ±12 SD) but were collected more frequently when the sampling mesh was becoming clogged by debris or large amounts of krill. Longer samples were collected occasionally (fewer than 29% of samples) when no eggs were captured in the mesh for an extended period. Overall, sample times ranged from less than 1 min to 192 min. However, all counts were standard-

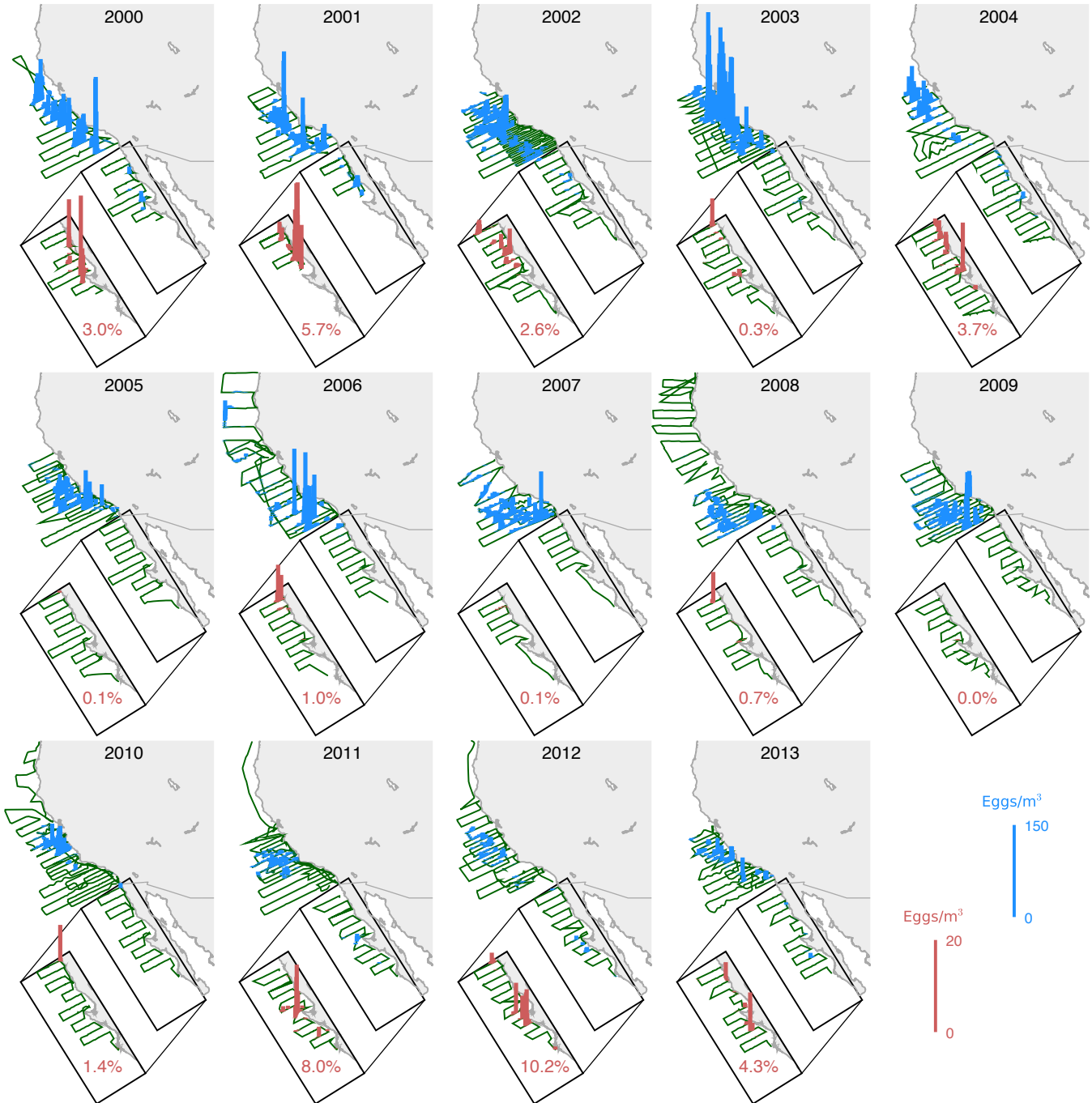


Figure 2. Observed Pacific sardine spatial distribution of eggs in the California Current System during the spring, centered on April from 2000 to 2013. Blue bars indicate sardine eggs per m^{-3} of water filtered for the entire study. Insets depict egg densities in the IMECOAL region at greater magnification to show structure (red bars). The percentage in each panel expresses the fraction of the total number of eggs recorded in the Exclusive Economic Zone of Mexico. The paths of ships where continuous egg sampling by CUFES is performed are shown as green lines. The year of sampling is indicated at the top of each panel.

ized to densities (number of eggs m^{-3} of water sampled). Sardine eggs were identified using the morphometric characteristics described by Moser (1996).

There were 22,410 observations (stations sample) in the data set. Of those, eggs were present in 6,334 (~28%) of the samples (table 1). Sea surface temperature was collected using a thermosalinometer between

each CUFES stations. Mean temperatures and standard error are also summarized in Table 1.

RESULTS

From 2000 to 2013 nearly all spawning in spring occurred between San Francisco ($38^{\circ}N$) and Punta Eugenia, Mexico ($\sim 28^{\circ}N$; fig. 2). The core of the spawn-

ing area was located in waters around Point Conception (34°N) but tended to shift northward and inshore during El Niño events as well as the warm years in the California Current (2003, 2005, and 2010), and southward to offshore of the Southern California Bight during the cooler years from 2006 to 2009. Sampled egg densities were greatest in the early years of the study, 2000–03, when they commonly exceeded 55 eggs/m³ and reached densities as high as 175 eggs/m³ in core spawning areas (fig. 2; table 1). Sampled egg densities generally declined during the study period, falling to densities of 12–29 eggs/m³ in core spawning areas during 2011–13. The mean annual sea-surface temperature in which eggs were captured in US waters ranged 13.0–14.3°C.

Spring spawning in the Mexican EEZ was primarily scattered in coastal areas between Punta Eugenia and the US-Mexican border. In the early 2000s, when egg densities were high, most spring spawning off Baja California occurred between Punta Baja (30°N) and Punta Eugenia (28°N) producing egg densities greater than 4 eggs/m³. Egg densities sampled in Mexican waters were an order of magnitude lower than mean egg densities during the same period off California. During the period 2011–13, when egg densities were low off California, most spawning in the Mexican EEZ occurred around Punta Eugenia with egg maximum densities in the range of 7–10 eggs/m³ (table 1). Some spawning also occurred to the south between Punta Eugenia and Bahía Magdalena (~25°N) during 2011–13. The maximum densities of eggs were higher in 2011–13 (8–10 eggs/m³) than in 2000–03 (4–17 eggs/m³) off Mexico, while the opposite was true off California where maximum egg densities were 12–29 eggs/m³ in 2011–13 and 55–176 eggs/m³ in 2000–03. Most eggs were captured at temperatures between 15° and 17°C.

Only a small portion of the total spring spawning occurred in the Mexican waters off Baja California, ranging from 0.02%–10% of all eggs captured per year, as depicted in Figure 2. The proportion of spring spawning in Mexico was greatest (4%–10%) when overall egg density in the CCE was at its lowest during 2011–13. The proportion of spawning sardine in Mexico was least (0.02%–1%) in 2005–09 when overall egg densities were intermediate.

DISCUSSION

Our study combined high resolution egg survey data from Mexican and US surveys to delimit the spatial distribution of spawning sardines in the spring in greater detail than previous studies using commercial catch data (Félix-Uraga et al. 2004). Our results indicated that most spring spawning, primarily by the northern subpopulation, occurred in US waters. Only 0.0%–10.2% of all eggs captured occurred in Mexican waters during any

year of the study (fig. 2), and less than 5% occurred in Mexican waters in 11 of 14 years. The US sardine management currently assumes that 13% of the northern subpopulation occurs in the Mexican EEZ (Hill et al. 2015). Assuming the distribution of the entire population is proportional to the egg densities observed (i.e., non-spawners are not congregating disproportionately in Mexican waters), our results suggest the true fraction of the northern subpopulation off Mexico rarely exceeds 10% and usually is less than 5%.

Pairing Mexican and US CUFES data provided insight about the spatial structure of the sardine population that could not be gleaned from fishery-dependent data. The sardine spawning habitat stretches latitudinally from waters around Cape Mendocino in the US, to Bahía Magdalena in Mexico, and reaches 500 km offshore in the Southern California bight. In Mexican waters, the spawning area is characterized by a relatively small wedge-shaped distribution in which eggs occur mostly in coastal waters associated with the bifurcation to the south of the California Current (CC) near the coast. During most years, a large gap in egg abundance occurred off northern Baja California, which may have been the intermediate area between the northern and southern subpopulations (fig. 2). If so, the southern subpopulation generally was restricted to Mexican waters with SST greater than about 17°C, as proposed by Félix-Uraga et al. (2004). A limitation of this study is that we cannot differentiate between the northern and southern subpopulations. If CUFES data were available for the peak spawning season of the southern subpopulation in summer off Baja California, it would be possible to model the habitat use and spatial extent both subpopulations throughout the year. The IMECOCAL program does collect such data but has not yet processed a sufficient number of samples to complete such modeling. This future research will be an important step in advancing our understanding of the dynamics of the two subpopulations.

Despite the extension of spawning area southward in 2000–04, there is an offshore gap in sardine spawning distribution across the US-Mexico border in the rest of the time series suggesting that the southern branch of the Southern California eddy may be a physical barrier to the continuity of the habitat some 550 km from the coast. The positive wind stress curl south of Point Conception (34°N) induces a cyclonic circulation in the SCB region that separates the north central region of California from the southern California basin and the Baja California waters (Durazo 2015). The southern border of this large eddy is known as the Ensenada Front (centered at ~31°N) and accounts for the presence of relatively low chlorophyll concentrations in the northern coastal area of the Baja California pen-

insula. The eddy's southern limb advects oligotrophic ocean and CC water to the coast, changing the composition and abundance of phytoplankton (Venrick 2015). Consequently, the phytoplankton community in the SCB coastal zone, dominated by diatoms, is replaced by coccolithophorids transported in warm oligotrophic water from the ocean area by the eddy. As a result, primary production decreases in the southern SCB and the Ensenada Front becomes an ecological and hydrographic boundary for the fauna (Santamaría-del-Ángel et al. 2011). A change in its physical properties at inter-annual and decadal scales has been related to fluctuations in sardine catches (Rykaczewski and Checkley 2008), and has highlighted the importance of this mechanism in restructuring the pelagic ecosystem when changes in environmental conditions occur. High temperatures and salinities at the southern border of the front and also the lower prey quality (see fig. 11 in Lo et al. 2005) may also produce physiological stress in sardine, reducing their fecundity and lead to a lower population density.

It is unknown whether the relatively large proportion of eggs captured in Mexican coastal waters during 2011 and 2012 was due to movement of sardines into Mexican waters or increased production in the coastal area off Bahía Magdalena. Water temperatures in the southern California Bight were relatively cold in 2011, and below average in 2012 (<http://sccoos.org/data/el-nino>). Such conditions have been associated with poor recruitment of sardine (e.g., Marr 1960; Zwolinski and Demer 2014). However, no similar change in egg distributions occurred when conditions were similar in 2008. Densities of sardine eggs collected by the IMECOCAL program in summer, likely belonging the southern subpopulation, have increased in recent years (Valencia-Gasti, unpublished data) as the northern subpopulation has declined to about 1%–2% of its peak abundance in 2007 (Hill et al. 2016). It is possible that the additional spawning in Mexican waters was due to fish from the southern subpopulation spawning outside of their peak season. These results highlight the need to better understand sardine subpopulation dynamics to better manage the fishery.

ACKNOWLEDGMENTS

We especially thank the crew of the R.V. *Fco. de Ulloa* and the numerous scientists and technicians involved in data collection. Financial support of the IMECOCAL program was made available by CONACYT through grants 129140, 99252, 23947, 47044, 42569, G35326T, 017PVD1-1297, G0041T, and 23804. Additional funding was provided by CICESE. In the years 2001–04 IMECOCAL received partial funding from the Inter-American Institute for Global Change Research Collaborative Research Network program: IAI-CRN 062-612301. US CUFES database was provided by SWFSC.

LITERATURE CITED

- Ahlstrom, E. H. 1960a. Synopsis on the biology of the Pacific sardine (*Sardinops caerulea*). In Proceedings of the World Scientific Meeting on the Biology of Sardines and Related Species. H. J. Rosa and G. I. Murphy, ed. Food and Agriculture Organization of the United Nations, Rome, Italy. Pages 415–451.
- Ahlstrom, E. H. 1960b. Fish Spawning in 1957 and 1958. California Cooperative Oceanic Fisheries Investigations Reports 7:173–179.
- Butler, J. L., M. Granados, J. T. Barnes, M. Yakemko, and B. J. Macewicz. 1996. Age composition, growth, and maturation of the Pacific sardine (*Sardinops sagax*) during 1994. California Cooperative Oceanic Fisheries Investigations Report, 37: 152–159.
- Checkley, D., P. Ayon, T. Baumgartner, M. Bernal, J. C. Coetzee, R. L. Emmett, R. Guevara-Carrasco, L. Hutchings, L. Ibaibarriaga, H. Nakata, Y. Oozeki, B. Planque, J. Schweigert, Y. Stratoudakis, and C. D. Van der Lingen. 2009. Habitats. Pages 12–44 in D. Checkley, J. Alheit, Y. Oozeki, and C. Roy, editors. Climate change and small pelagic fish. Cambridge University Press, Cambridge.
- Checkley, D., R. C. Dotson, and D. A. Griffith. 2000. Continuous, underway sampling of eggs of Pacific sardine (*Sardinops sagax*) and northern anchovy (*Engraulis capensis*) in spring 1996 and 1997 off southern and central California. Deep-Sea Research Part II (47):1139–1155.
- Checkley, D., P. B. Ortner, L. R. Settle, and S. R. Cummings. 1997. A continuous, underway fish egg sampler. Fisheries Oceanography 6(2):58–73.
- Clark, F. N. 1945. Results of Tagging Experiments in California Waters on the Sardine (*Sardinops caerulea*). Fish Bulletin 61:1–93.
- Clark, F. N., and J. C. Marr. 1955. Part II: Population dynamics of the Pacific sardine. California Cooperative Oceanic Fisheries Investigations Progress Report 4:11–48.
- Cury, P., A. Bakun, R. Crawford, A. Jarre, R. Quiñones, L. J. Shannon, and H. Verheye. 2000. Small pelagics in upwelling systems: patterns of interaction and structural changes in “wasp-waist” ecosystems. ICES Journal of Marine Science 57(3):603–618.
- Demer, D. A., and J. P. Zwolinski. 2014. Corroboration and refinement of a method for differentiating landings from two stocks of Pacific sardine (*Sardinops sagax*) in the California Current. ICES Journal of Marine Science 71(2):328–335.
- Demer, D. A., J. P. Zwolinski, K. A. Byers, G. R. Cutter, J. S. Renfree, T. S. Sessions, and B. J. Macewicz. 2012. Prediction and confirmation of seasonal migration of Pacific sardine (*Sardinops sagax*) in the California Current Ecosystem. Fishery Bulletin 110(1):52–70.
- DOF (Diario Oficial de la Federación). 1993. Norma Oficial Mexicana 003-PESC-1993, para regular el aprovechamiento de las especies de sardina Monterrey, piña, crinuda, bocona, japonesa y de las especies anchoveta y macarela, con embarcaciones de cerco, en aguas de jurisdicción federal del océano. Diario Oficial de la Federación, Mexico, D.F. 4 pp.
- Durazo, R. 2015. Seasonality of the transitional region of the California Current System off Baja California. Journal of Geophysical Research Oceans 120(2):1173–1196.
- Durazo, R., and T. Baumgartner. 2002. Evolution of oceanographic conditions off Baja California: 1997–1999. Progress in Oceanography 54:7–31.
- Emmett, R. L., T. W. Miller, P. J. Bentley, S. S. Pool, R. D. Brodeur, G. K. Krutzikowsky, and J. McCrae. 2005. Pacific sardine (*Sardinops sagax*) abundance, distribution, and ecological relationships in the Pacific Northwest. California Cooperative Oceanic Fisheries Investigations Reports 46:122–143.
- Félix-Uraga, R., V. M. Gómez-Muñoz, C. Quiñónez-Velázquez, F. N. Melo-Barrera, and W. García-Franco. 2004. On the existence of Pacific sardine groups off the west coast of Baja California and southern California. California Cooperative Oceanic Fisheries Investigations Reports 45:146–151.
- Félix-Uraga, R., V. M. Gómez-Muñoz, C. Quiñónez-Velázquez, F. N. Melo-Barrera, K. Hill, and W. García-Franco. 2005. Pacific sardine (*Sardinops sagax*) stock discrimination off the west coast of Baja California and Southern California using otolith morphometry. California Cooperative Oceanic Fisheries Investigations Reports 46:113–121.
- García-Rodríguez, F. J., S. A. García-Gasca, J. D. La Cruz-Agüero, and V. M. Cota-Gómez. 2011. A study of the population structure of the Pacific sardine *Sardinops sagax* (Jenyns 1842) in Mexico based on morphometric and genetic analyses. Fisheries Research 107(1–3):169–176.
- Hedgecock, D. 1986. Recognizing subpopulations in California's mixed pelagic fish stocks. In Identifying Fish Subpopulations. Proceedings of a

- California Sea Grant Workshop: January 27, 1984. D. Hedgecock, ed. California Sea Grant College Program, institute of marine resources, university of California, La Jolla, CA. Pages 26–31.
- Hernandez-Vazquez, S. 1994. Distribution of eggs and larvae from Sardine and Anchovy off California and Baja California, 1951–89. California Cooperative Oceanic Fisheries Investigations Reports 35:94–107.
- Hill, K., P. R. Crone, E. Dorval, and B. J. Macewicz. 2015. Assessment of the Pacific sardine resource in 2015 for U.S.A. management in 2015–16. Page 1–168. NOAA Technical Memorandum, NMFS-SWFSC-546.
- Hill, K., P. R. Crone, E. Dorval, and B. J. Macewicz. 2016. Assessment of the Pacific sardine resource in 2016 for U.S.A. management in 2016–17. Page 1–169. NOAA Technical Memorandum, NMFS-SWFSC-562.
- Javor, B., N. C. H. Lo, and R. Vetter. 2011. Otolith morphometrics and population structure of Pacific sardine (*Sardinops sagax*) along the west coast of North America. Fishery Bulletin 109(4):402–415.
- Kaplan, I. C., C. J. Brown, E. A. Fulton, I. A. Gray, J. Field, and A. D. M. Smith. 2013. Impacts of depleting forage species in the California Current. Environmental Conservation 40(4):380–393.
- Lecomte, F., W. S. Grant, J. J. Dodson, R. Rodríguez-Sánchez, and B. W. Bowen. 2004. Living with uncertainty: genetic imprints of climate shifts in East Pacific anchovy (*Engraulis mordax*) and sardine (*Sardinops sagax*). Molecular Ecology 13(8):2169–2182.
- Lindegren, M., D. M. Checkley, T. Rouyer, A. D. MacCall, and N. C. Stenseth. 2013. Climate, fishing, and fluctuations of sardine and anchovy in the California Current. Proceedings of the National Academy of Sciences of the United States of America 110(33):13672–7.
- Lo, N. C. H., B. J. Macewicz, and D. A. Griffith. 2005. Spawning biomass of Pacific sardine (*Sardinops sagax*), from 1994–2004 off California. California Cooperative Oceanic Fisheries Investigations Reports 46:93–112.
- Lo, N. C. H., B. J. Macewicz, and D. A. Griffith. 2010. Biomass and reproduction of Pacific sardine (*Sardinops sagax*) off the Pacific northwestern United States, 2003–05. Fishery Bulletin 108:174–192.
- Lynn, R. J. 2003. Variability in the spawning habitat of Pacific sardine (*Sardinops sagax*) off southern and central California. Fisheries Oceanography 12(6):541–553.
- Marr, J. C. 1960. The causes of major variations in the catch of the Pacific sardine, *Sardinops caerulea* (Girard). In Proceedings of the world scientific meeting on the biology of sardines and related species, FAO. J. Rosa and G. Murphy, eds. FAO, Rome. Pages 667–791.
- McClatchie, S. 2013. Regional fisheries oceanography of the California Current System. Springer, La Jolla, CA. 253 pp.
- McDaniel, J., K. Piner, H. Lee, and K. Hill. 2016. Evidence that the migration of the northern subpopulation of Pacific sardine (*Sardinops sagax*) off the west coast of the United States is age-based. PLoS ONE 11(11):e0166780.
- Moser, H. G. 1996. The early stages of fishes in the California current region. California cooperative oceanic fisheries investigations, Atlas No. 33. Allen Press, Lawrence, Kansas. 1505 pp.
- Murphy, G. L. 1966. Population biology of the Pacific sardine (*Sardinops caerulea*). Proceedings of the California Academy of Sciences 34(1):1–84.
- Parrish, R. H., C. S. Nelson, and A. Bakun. 1981. Transport mechanisms and reproductive success of fishes in the California Current. Biological Oceanography 1(2):175–203.
- Peck, M. A., P. Reglero, M. Takahashi, and I. A. Catalán. 2013. Life cycle ecology of small pelagic fish and climate-driven changes in populations. Progress in Oceanography 116:220–245.
- Radovich, J. 1982. The collapse of the California sardine fishery. California Cooperative Oceanic Fisheries Investigations Reports 23:56–77.
- Rykaczewski, R. R., and D. Checkley. 2008. Influence of ocean winds on the pelagic ecosystem in upwelling regions. Proceedings of the National Academy of Sciences of the United States of America 105(6):1965–1970.
- Sagarpa (Secretaría de Agricultura, Ganadería, Desarrollo Rural, Pesca y Alimentación). 2012. Plan de manejo pesquero para la pesquería de pelágicos menores (sardinias, anchovetas, macarelas y afines) del noroeste de México. Secretaría de Agricultura, Ganadería, Desarrollo Rural, Pesca y Alimentación, 54 pp.
- Santamaría-del-Ángel, E., A. González-Silvera, R. Millán-Núñez, M. Callejas-Jiménez, and R. Cajal-Medrano. 2011. Determining dynamic biogeographic regions using remote sensing data. In Handbook of satellite remote sensing image interpretation: Applications for marine living resources conservation and management. J. Morales, V. Stuart, T. Platt, and S. Sathyendranath, eds. EU PRESPO and IOCCG, Dartmouth, Canada. Pages 273–293.
- Scientific Certification Systems (SCS), 2016. Fourth Annual MSC Surveillance Audit Report. Gulf of California Mexican Sardine Fishery. MSC Certification Requirements. 105 pp.
- Schwartzlose, R. A., J. Alheit, A. Bakun, T. Baumgartner, R. Cloete, R. J. M. Crawford, W. J. Fletcher, Y. Green-Ruiz, E. Hagen, T. Kawasaki, D. Lluch-Belda, S. E. Lluch-Cota, A. D. MacCall, Y. Matsuura, M. O. Nevárez-Martínez, R. H. Parrish, C. Roy, R. Serra, K. V. Shust, M. N. Ward, and J. Z. Zuzunaga. 1999. Worldwide large-scale fluctuations of sardine and anchovy populations. South African Journal of Marine Science 21(1):289–347.
- Smith, P. E. 2005. A history of proposals for subpopulation structure in the Pacific sardine (*Sardinops sagax*) population off western North America. California Cooperative Oceanic Fisheries Investigations Reports 46:75–82.
- Valencia-Gasti, J. A., T. Baumgartner, and R. Durazo. 2015. Effects of ocean climate on life cycles and distribution of small pelagic fishes in the California Current System off Baja California. Ciencias Marinas 41:315–348.
- Venrick, E. L. 2015. Phytoplankton species in the California Current System off Southern California: The spatial dimensions. California Cooperative Oceanic Fisheries Investigations Reports 56:1–17.
- Zwolinski, J. P., and D. A. Demer. 2014. Environmental and parental control of Pacific sardine (*Sardinops sagax*) recruitment. ICES Journal of Marine Science 71(8):2198–2207.

POPULATION DYNAMICS OF THE BIGEYE CROAKER *MICROPOGONIAS MEGALOPS* IN THE NORTHERN GULF OF CALIFORNIA

EDGAR ARNOLDO ARZOLA-SOTELO

Centro de Investigaciones Biológicas
del Noroeste, S.C.
Km 2.35 Carretera a Las Tinajas
Colonia Tinajas. CP. 85460
Guaymas, Sonora, México

JUANA LÓPEZ-MARTÍNEZ

Centro de Investigaciones Biológicas
del Noroeste, S.C.
Km 2.35 Carretera a Las Tinajas
Colonia Tinajas. CP. 85460
Guaymas, Sonora, México
ph: +52 (622) 221 2237
fax: +52 (622) 221 2238
jlopez04@cibnor.mx

CARLOS HIRAM RÁBAGO-QUIROZ

Centro Regional de Investigación Pesquera
INAPESCA
Carretera a Pichilingue Km. 1 S/N
Colonia Esterito. CP. 23000
La Paz, B.C.S., México

JESÚS GUADALUPE PADILLA-SERRATO

CONACYT - Facultad de Ecología Marina
Universidad Autónoma de Guerrero
Av. Gran Vía tropical No. 20 fraccionamiento
Las Playas, Acapulco, Guerrero, México

ENRIQUE MORALES-BOJÓRQUEZ

Centro de Investigaciones Biológicas
del Noroeste, S.C.
Av. Instituto Politécnico Nacional 195
Playa Palo de Santa Rita Sur, CP. 23096
La Paz, B.C.S., México

ABSTRACT

Knowledge of biomass and demographic aspects is important in fish stock assessments. These aspects were analyzed on *Micropogonias megalops* in the Gulf of California, Mexico, using biological data from catches in 2010–12. Individual growth was estimated following a multi-model approach. Logistic models were used for first maturity and fishing selectivity, and natural mortality by means of empirical equations and biomass by the Pennington estimation. The results showed that the von Bertalanffy model best described growth for combined data ($w_i = 72.86\%$), females ($w_i = 67.82\%$) and males ($w_i = 69.42\%$), but they showed sexual dimorphism on the species. First maturity was at 357.8 mm, fishing selectivity 323.35 and 366.35 mm for industrial and artisanal fleet, respectively, and average natural mortality of 0.51. Mean biomass was 14 412.9 tons contrasting the officially reported catch that represented only 8.7% of estimated biomass, showing evidence that *M. megalops* is still an underexploited resource.

INTRODUCTION

Globally, overfishing or species fishing at the permissible limit is a constant focus of alert (SOFIA 2016; World Bank 2017). The increasing demand of food by humans causes strong pressure on resources that have not been assessed, which has caused many fisheries to develop despite the lack of basic stock information, such as population dynamics, population renewal rates and available and exploitable biomass of the target species (Cope and Punt 2009; Cope 2013). In third world countries this case is very common (World Bank 2017).

In Latin America, fishing has become an important economic activity, generating employment and income for a large number of families. Likewise, it is an important source for worldwide food security, also making an

important contribution to Latin American economies. Despite the importance of fishing and although management measures have been introduced in the region, problems of overcapacity still persist, and the condition of vulnerability of fishery resources continues to increase (Agüero 2007). It is common to exploit many of the target resources without the slightest knowledge, or concentrate on multispecies fisheries where there are no specific administrative management measures for the most important species of these fisheries. An example is the Bigeye croaker *Micropogonias megalops* (Gilbert 1890) in the Gulf of California, which is an endemic, very abundant and widely distributed species in the region (López-Martínez et al. 2010; Rábago-Quiroz et al. 2011). The Bigeye croaker has been commercially harvested as part of a multispecies fishery (DOF 2010) since the early 1990s, which has been a fishing alternative when shrimp catch rates are low (Román-Rodríguez 2000; Aragón-Noriega et al. 2009). Particularly in the Northern (NGC) and Upper Gulf of California (UGC), the Bigeye croaker is caught by two fishing fleets, artisanal (small vessels) and industrial (large vessels, ships), representing a very important commercial fishery for its high catch volumes and substantial economic value (Aragón-Noriega et al. 2009). The fishing season occurs from March to August when the reproductive period is observed, and its availability to the fishing fleets increases (Castro-González 2004).

Knowledge of basic biological aspects of *M. megalops* is limited, such as average individual growth, natural mortality, reproduction, fishing selectivity and changes in stock biomass. Some studies have been conducted to understand population dynamics, age, growth and reproduction of this species in the Northern and Upper Gulf of California (Román-Rodríguez 2000; Aragón-Noriega et al. 2015). Recently, individual growth was analyzed

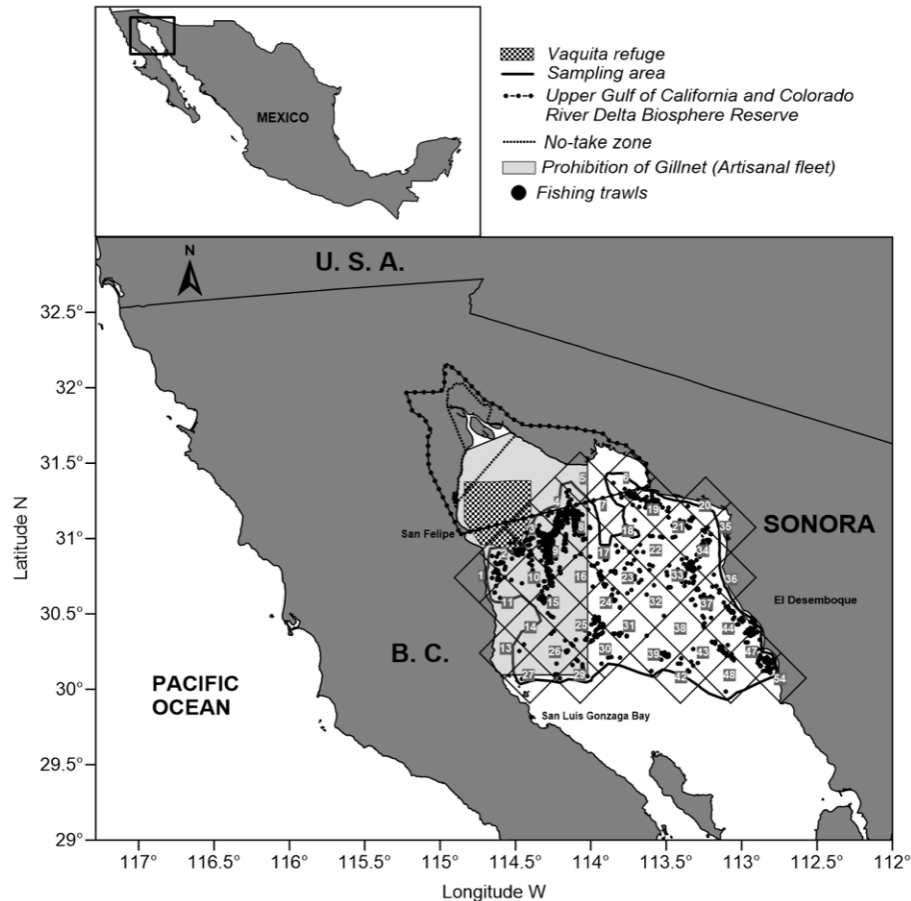


Figure 1. Study area and quadrant location for *Micropogonias megalops* sampling in the Northern Gulf of California (2010–12). Map includes the No-take zone for gillnets fishery (artisanal fleet) which includes the main species fishing areas for this fleet in the Northern Gulf of California, established temporarily in 2015, permanently since 2017, and vaquita refuge zone amplified in 2018 (DOF 2015, 2017, 2018).

based on a multi-model inference approach (Aragón-Noriega et al. 2015), but this analysis was supported on biological data from 1997–98 (Román-Rodríguez 2000). To our knowledge, more information about population dynamics and abundance aspects of the Bigeye croaker in the NGC is not available. For the genus *Micropogonias*, growth estimates have been reported in the Atlantic Ocean (Caribbean and South America) using the von Bertalanffy growth model (VBGM) (Manickchand-Heileman and Kenny 1990; Borthagaray et al. 2011), but more complete studies on population dynamics have not been found. Therefore, the objective of generating reliable, complete and current information on the Bigeye croaker becomes a relevant management matter for the stock in the Northwestern Mexican Pacific Ocean. Consequently, this study assessed important demographic aspects of the resource, such as growth, natural mortality, reproduction (sexual maturity and length at first maturity), fishing selectivity and the mean total biomass in the NGC during the 2010–12 period. The information generated in this study will contribute to the scientific understanding of the current biological and fishing sta-

tus of *M. megalops* population in the NGC. Likewise, this basic information could be used in the near future to adopt alternative fishing strategies for the species due to the recent establishment of a new no-take zone for artisanal fishing gear, such as gillnets (used to catch Bigeye croaker) and longline. This new no-take zone includes now many of the regular fishing areas (fishing grounds) of Bigeye croaker, so the refuge zone was recently amplified as part of the efforts directed to the protection of the vaquita *Phocoena sinus* in the Northern Gulf of California (Erisman et al. 2015; DOF 2015, 2017, 2018).

MATERIALS AND METHODS

Sampling

Bigeye croaker samples were collected from industrial and artisanal fishery catches from the NGC during the period from December 2010 to April 2012 (fig. 1). Additionally, a program of observers was implemented on board the industrial fleet throughout the whole year where fish caught by trawl nets were sampled. The industrial fleet used a net that had two otter boards

with double fishing tackle of 36 m long and mesh size of 90 mm while the artisanal fishery used a gillnet from 100 to 500 m long with 150-mm mesh size. Total length (mm) and total weight (g) of each individual caught were measured with a precision of 0.01 mm and 0.1 g. Sex and gonad maturity were obtained following the Nikolsky's morphochromatic scale (Nikolsky 1963), which is based on color and gonad texture, as well as its space in the abdominal cavity. Bigeye croaker specimens in stages I–II were considered immature (gonads flacid, transparent and less than one half of the space in the abdominal cavity), and those in stages III–V were considered mature (gonads colored and more than one half of the space in the abdominal cavity) (López-Martínez et al. 2011).

Length structure and multinomial analysis

Total length (TL) distributions of Bigeye croaker, for both industrial and artisanal samples in the NGC, were obtained grouping TL frequencies in 5-mm intervals to identify modal groups, length groups or cohorts (year-classes) that refer to groups of individuals of approximately the same age belonging to the same population (Sparre and Venema 1997). Then, a multinomial analysis was performed based on the assumption that length distribution for each cohort showed a normal distribution. To identify the number of cohorts in samples, a visual inspection of the TL frequency distribution was performed, and together with prior knowledge of the species recruitment events, initial values for each modal group were defined as input values in the following multinomial equation:

$$F_i = \sum_{a=1}^n \left[\left(\frac{1}{\sigma_a \sqrt{2\pi}} \right) e^{-\frac{(x_i - \mu_a)^2}{2\sigma_a^2}} \right] * P_a$$

Where F_i was the total frequency of the group length i ; a and n were lower and upper sample limits (TL intervals), respectively; x_i was the medium point of length group i ; μ_a was the medium length of cohort a ; P_a was the weight factor of cohort a ; and σ_a was the standard deviation of the length in cohort a . Parameters in this function were minimised with a nonlinear fit, using the Newton algorithm to determine model parameters with the following negative log likelihood function (Neter et al. 1996):

$$-LL_{\{x|\mu_a, \sigma_a, P_a\}} = \sum_{i=1}^n f_i \ln \left(\frac{F_i}{\sum F_i} \right) - \left[\sum f_i - \sum F_i \right]^2$$

Where $-LL_{\{x|\mu_a, \sigma_a, P_a\}}$ was the negative log likelihood of the data for the parameters μ_a, σ_a, P_a ; f_i was the total of the frequency observed of length group i ; F_i was the total frequency expected for length group i according

to the multinomial model (Haddon 2001; Montgomery et al. 2010; Rodríguez-Domínguez et al. 2012). Finally, Bigeye croaker cohorts were separated according to the separation index (S.I.) using the next equation (Sparre and Venema 1997):

$$S.I. = 2 * \frac{\mu_n - \mu_i}{\sigma_n + \sigma_i}$$

Where μ_n and μ_i were the mean TL of the modal groups n and i , respectively; σ_n and σ_i were the standard deviations of modal groups n and i , respectively. Therefore if $S.I. > 2$, then it would be viable to separate the normal components from the observed frequencies (Sparre and Venema 1997).

Growth

In 2000, Román-Rodríguez (2000) developed an age-length key of Bigeye croaker by means of *M. megalops* otolith readings sampled from 1997 to 1998 in the Upper Gulf of California. In this work, in absence of otolith readings for the Bigeye croaker sampled from 2010–12, we used that age-length key to assign age to the length of each specimen sampled from industrial and artisanal fisheries in the NGC (2010–12). Age assignment to length data of Bigeye croaker, for combined and separated by sex data, was made by means of proportional and percentage conversion of length frequencies to the ages established by this key. The age assignment to length data was made following the methodology proposed by Gulland and Rosenberg (1992) and Sparre and Venema (1997).

Growth models

A multi-model inference approach was followed to estimate growth parameters (Katsanevakis 2006; Katsanevakis and Maravelias 2008). For this purpose, four growth models were used (table 1); von Bertalanffy growth model (1938), Gompertz (1825), Logistic (Ricker 1975), and Schnute (1981). Specifically, for Schnute model, L_∞ and t_0 (defined by Schnute 1981 as τ_0) were calculated using the following equations where a case of solution type 1 was assumed:

$$L_\infty = \left[\frac{e^{aT_2} \gamma_2^b - e^{aT_1} \gamma_1^b}{e^{aT_2} - e^{aT_1}} \right]^{\frac{1}{b}}$$

and

$$\tau_0 = T_1 + T_2 - \frac{1}{a} \ln \left[\frac{e^{aT_2} \gamma_2^b - e^{aT_1} \gamma_1^b}{\gamma_2^b - \gamma_1^b} \right]$$

In this solution case, adjusted values of parameters a and b were different from zero ($a \neq 0, b \neq 0$); projected growth curve shape, theoretical and statistical interpretation bases had equivalence with VBGM.

TABLE 1
 Candidate growth models for *Micropogonias megalops* data in the Northern Gulf of California.

Model	Equation	Parameter description
von Bertalanffy growth model (VBGM)	$L_{(t)} = L_{\infty}(1 - e^{-K(t-t_0)})$	$L_{(t)}$ is length at age t . L_{∞} is asymptotic length.
Gompertz	$L_{(t)} = L_{\infty}e^{-K(t-t_0)}$	K determines the rate of approach to L_{∞} (the curvature parameter). t_0 is the hypothetical age at which the organism showed zero length (initial condition parameter). t is age at size $L_{(t)}$.
Logistic	$L_{(t)} = \frac{L_{\infty}}{(1 + e^{-K(t-t_0)})}$	a is a relative growth rate (time constant). b is an incremental relative growth rate (incremental time constant).
Schnute ($a \neq 0, b \neq 0$)	$L_{(t)} = \left[\gamma_1^b + (\gamma_2^b - \gamma_1^b) \frac{1 - e^{-a(t-T_1)}}{1 - e^{-a(T_2-T_1)}} \right]^{\frac{1}{b}}$	T_1 is the lowest age in the data set. T_2 is the highest age in the data set. γ_1 is the size at age T_1 . γ_2 is the size at age T_2 .

Growth parameters (θ) for all four candidate growth models were fitted using a maximum log likelihood function according to the following equation (Neter et al. 1996).

$$LL_{(\theta|data)} = - \left(\frac{n}{2} \right) (Ln(2\pi) + 2 * Ln(\sigma) + 1)$$

For standard deviation (σ) a multiplicative error structure was assumed where the analytical solution was given by:

$$\sigma = \sqrt{\frac{1}{n} \sum_{t=1}^n [Ln L_{obs(t)} - Ln \hat{L}_{(t)}]}$$

Where n represented the number of ages observed for the Bigeye croaker (Cerdenares-Ladrón de Guevara et al. 2011).

Confidence intervals

Confidence intervals (C.I.) for growth parameters contained in each candidate growth model were calculated using likelihood profiles (Venzon and Moolgavkar 1988; Hilborn and Mangel 1997), which were estimated based on Chi-squared distribution (χ^2) with m degrees of freedom (Zar 1999). Confidence intervals were defined as all values θ that satisfied inequality:

$$2[LL_{(\theta|data)} - LL_{(\theta|best)}] < \chi^2_{1,1-\alpha}$$

Where $LL(\theta|_{best})$ was the log likelihood of the most probable value of θ , and $\chi^2_{1,1-\alpha}$ were the distribution values of χ^2 with one degree freedom at a confidence level of $1-\alpha$; thus, the confidence interval at 95% for θ covered all values of θ that were twice the difference between the log likelihood in the likelihood profile and the best estimate of θ . Those values less than 3.84 were included into confidence intervals (Haddon 2001; Pawitan 2001).

Confidence intervals become wider when considering more than one parameter, which only occurs if there is any correlation between parameters. The von Bertalanffy growth model had the asymptotic length and growth coefficient parameters correlated. In this case the solution was to compute the likelihood based confidence region estimated from contours of constant log-likelihood over the target surface. This procedure was applied to the L_{∞} and K parameters jointly to avoid the problem of parameter correlation. In this case the equation above must satisfy the inequality associated with the χ^2 distribution with two degrees of freedom where the reference value was less than 5.99 for two parameters (Haddon 2001, Pawitan 2001).

Model selection

Growth model selection for the Bigeye croaker was obtained using the Akaike information criterion (AIC) (Burnham and Anderson 2002; Katsanevakis 2006; Katsanevakis and Maravelias 2008) according to the following equation:

$$AIC = (2 \times LL) + (2 \times k)$$

The AIC differences (Δ_i) for each model were given by the following function:

$$\Delta_i = AIC_i - AIC_{min}$$

Where AIC_{min} represented the AIC for the best candidate growth model, and AIC_i was the AIC estimated for the rest of the growth models. For each growth model i , plausibility was estimated with the Akaike weight (w_i) given by (Burnham and Anderson 2002):

$$w_i = \frac{\exp\left(-\frac{1}{2} \Delta_i\right)}{\sum_{k=1}^4 \exp\left(-\frac{1}{2} \Delta_k\right)}$$

Following the multi-model inference approach, an “averaged” model was calculated for L_∞ taking into account values of L_∞ and w_i of all four models by the following equation (Burnham and Anderson 2002):

$$\bar{L}_\infty = \sum_{i=1}^4 w_i \hat{L}_{\infty,i}$$

Confidence intervals (95%) of asymptotic length values were estimated by means of t Student test using the following equation:

$$\hat{L}_\infty \pm t_{d.f.,0.95} S.E.(\hat{L}_\infty)$$

Where

$$SE_g(\bar{L}_\infty) = \sum_{i=1}^4 w_i * \left(\text{var}(\hat{L}_{\infty,i} | g_i) + (\hat{L}_{\infty,i} - \bar{L}_\infty)^2 \right)^{\frac{1}{2}}$$

Both growth theoretical curve (best candidate model) and observed age-length data were graphed out to show shape and trajectory of growth, for all data and separated by sex in Bigeye croaker.

Natural mortality, reproduction and selectivity

Natural mortality (M), which is one of the most cryptic parameters in population dynamics, was estimated for all data (combined) and separated by sex (females and males) of Bigeye croaker. It was based on metapopulation and empirical functions proposed by Pauly (1980), Jensen (1996), Richter and Efanov (1977), Hewitt and Hoenig (2005), and Then et al. (2015). The parameter values used to estimate M were those identified by the best candidate growth model (VBGM) for the species according to the multi-model analysis; age of first maturity based on size L_{50} was obtained through the Logistic model; longevity was obtained by the Taylor equation (1962) that involved L_∞ and K parameter values of VBGM; finally annual average water temperature ($^{\circ}\text{C}$) in the NGC (23°C) was used (Siegfried and Sansó 2009).

For reproduction and selectivity analysis a Logistic model was used. When the reproduction analysis was carried out, only mature female data were considered from both industrial and artisanal fisheries. Mature females were considered as those individuals in stages from III to V. For calculating length-at-first sexual maturity (FSM), the probability of mature females accumulated in each length interval was used; parameter values were obtained with the Logistic model proposed by King (2007):

$$P_i = \frac{1}{(1 + e^{-r(TL - L_{50})})}$$

Where P_i is mature females proportion; r is the slope of the logistic curve; TL is the observed length interval; and L_{50} is the average total length at which the individuals are found sexually mature. Parameter values in Logistic equation were fitted using Newton’s method and as objective function the sum of squares criterion (Neter et al. 1996).

For the selectivity analysis both male and female organisms in all sizes were considered and analyzed separately for industrial and artisanal fishery data because both fisheries have differences in fishing gear characteristics (mesh size, length) and fishing ways or maneuvers (industrial trawling; artisanal gillnetting). In this case, the selectivity curve calculating P_i in the Logistic model is the proportion of Bigeye croaker organisms; r is the slope of the logistic curve; TL is the observed length interval; and L_{50} is the average length at which the species is caught by the fishing gear (industrial or artisanal). Parameter values in the Logistic equation were fitted also using Newton’s method and as objective function the sum of squares criterion (Neter et al. 1996).

Biomass estimation

To estimate the total stock biomass during the fishing season, the swept area method was applied. Fishing operation data (geographic position, trawling speed and duration) obtained by onboard observers (industrial fleet) were used, as well as onboard registered catch and catch data reported by commercial fleet in NGC were considered. Swept area is the effective trawling area of one tow in a determinate time, and covered area is the effective area covered during each fishing trip. It was estimated by: $\alpha = \omega * \nu * d$, where ω was the effective trawl net width; ν was towing velocity; and d was tow duration. Once the swept area was estimated, total biomass (B) in the fishing ground was given by: $B = Cw/\nu * (A/a)$, where Cw was catch rate; ν was vulnerability of fish to the net; A was total area, and a was the swept area. Vulnerability of fish to trawling was difficult to estimate (King 1997), but values ranging from 0.5 (in current work) to 1 were normally assumed (Francis et al. 2003). To obtain a greater precision (a smaller variance) in the abundance estimates, a stratification of the total area was carried out, obtaining abundance estimates for a determinate sampled area (quadrant) and improving estimation efficiency; then, the sample was extrapolated to the total area of influence of the industrial fleet in the NGC ($A = 12\,683\text{ km}^2$).

The abundance estimates by the swept area method were used in this study based on the following assumptions: (a) the distribution area “total area” of the population was constant and, therefore, the average population density was at all times directly proportional to the total size of the “total area”; (b) the population was homogeneously distributed in the “total area”, so if we sampled

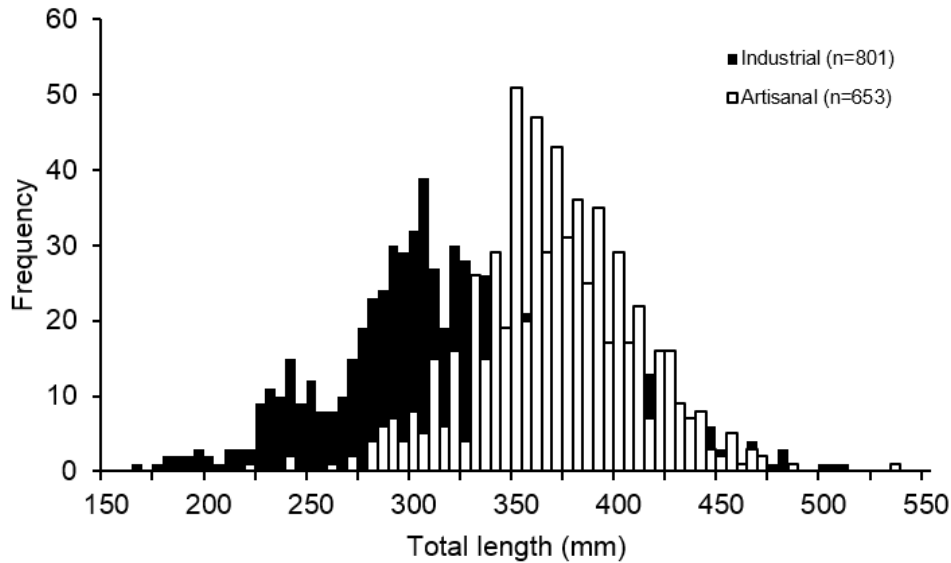


Figure 2. Length frequency distribution of *Micropogonias megalops* in the Northern Gulf of California (2010–12). Catches of industrial fishery (full bars) and artisanal fishery (empty bars).

a fraction, its density represented a quantity of individuals per area that was equal to the average density of the total population; (c) all individuals had the same catch probability; and (d) the swept area was standardized to one hour.

Due to the large number of zeros in the fishing hauls and to reduce the variance caused by the spatial distribution of the species, the abundance estimates were supported in the calculation of the mean and the variance of a delta distribution. The Pennington estimator (which uses delta distribution) was used to obtain average abundance estimates per quadrant and for the total area of the sampled quadrants. For this analysis, the NAN-SIS program developed by Jeppe Kolding (Version Sept 2000) was used (Pennington 1985, 1996; Pierce et al. 1998; Folmer and Pennington 2000; Morales-Bojórquez 2002).

RESULTS

A total of 1454 Bigeye croaker specimens were analyzed from industrial and artisanal fishery in the NGC, of which total length (TL) ranged from 165 to 535 mm. The organisms from industrial fisheries showed a total length interval from 165 to 508 mm while those caught from artisanal fishery varied from 220 to 535 mm (fig. 2). The industrial fishery caught smaller individuals than those observed in the total length structure of the artisanal fishery; the average total length of Bigeye croaker in the industrial fishery was $325.6 \text{ mm} \pm 59.9 \text{ mm}$, and for artisanal fishery the average was $367.85 \text{ mm} \pm 39.47 \text{ mm}$. The industrial fishery showed four modal values in total length structure, which were based on the observed maximal peaks in the total length frequencies (195 mm, 240 mm, 305 mm, 370 mm and 415 mm); in

contrast, the artisanal fishery showed only three modal values of 300 mm, 350 mm and 425 mm. The qualitative data description showed evidence of a difference in the age groups that were harvested by each fleet.

Multinomial analysis

Separation of Bigeye croaker cohorts was performed for the nine sampling periods available where seven belonged to the industrial fleet (December 2010–March 2012) and two to the artisanal fleet (March–April 2012) (fig. 3). The industrial fishery caught three to four cohorts, of which the lowest and highest mean length were $191.21 \text{ mm} \pm 9.73$ and $507.50 \text{ mm} \pm 1.87$, respectively (table 2). The artisanal fishery also caught three to four cohorts, of which the smallest and highest mean length were $297.17 \text{ mm} \pm 20.08$ and $549.1 \text{ mm} \pm 17.06$ respectively (table 3).

The length analysis combining both information sources showed the presence of a total of five modal groups, whose average length are shown in the order from the smallest to the largest: (1) $191.2 \pm 13.0 \text{ mm TL}$ (12.3%); (2) $237.7 \pm 12.7 \text{ mm TL}$ (15.3%); (3) $292.2 \pm 16.5 \text{ mm TL}$ (18.8%); (4) 363.2 ± 42.0 (23.4%); and (5) $465.6 \pm 35.5 \text{ mm TL}$ (30.0%).

Growth

Age was assigned to the sampled organisms, whose ages were from 1–17 years. The best-represented ages were two- and five-year old individuals. The smallest individual had a length of 171.0 mm TL and an age of two years while the largest one had a length of 490.50 mm TL with an assigned age of 12 years. Bigeye croaker age-length data were adjusted to the four candidate

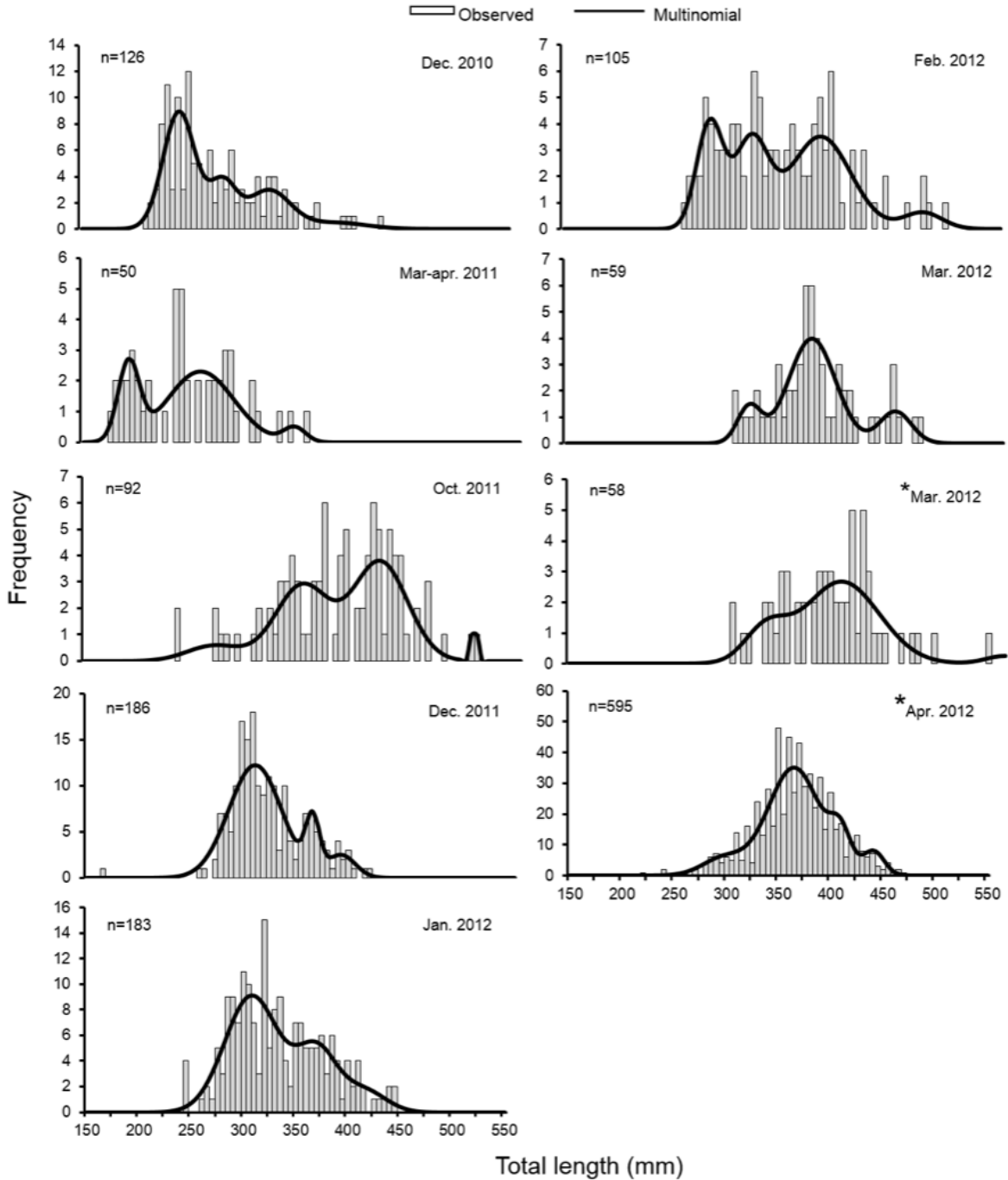


Figure 3. Multinomial analysis of *Micropogonias megalops* in the Northern Gulf of California. *Artisanal Fishery.

growth models for all combined and separated by sex data; parameter values, confidence intervals and Chi-square values are shown in Table 4. The VBGM and Schnute growth models showed the highest asymptotic lengths and lowest growth coefficient values among all candidate models. In the same case, when sex separated data were analyzed, higher values in asymptotic length and lower in growth coefficient were recorded by females compared to males. Best growth model

selection considering AIC and w_i values and confidence intervals (95%) for the Bigeye croaker are shown in Table 5. VBGM was the model that best adjusted to Bigeye croaker age-length data according to AIC and w_i for combined and sex separated data. Figure 4 shows curve trajectories projected by the VBGM, as well as the likelihood contour joint confidence intervals of these parameters L_∞ and K , where covariance in values is evidenced for the species. Likelihood profiles for

TABLE 2
Cohorts of Bigeye croaker *Micropogonias megalops*
caught in the Northern Gulf of California by
industrial fishery (2010–12). TL is total length in mm,
S.D. is standard deviation and S.I. is separation index.

Date	Cohort	TL (mm)	S.D.	S.I.	Age (years)
Industrial fishery					
Dec. 2010	1	240.89	15	n.a	3
n: 126	2	281.44	12.6	2.93	3
	3	324.65	20.24	2.62	4
	4	387.19	28.61	2.55	5
Mar–Apr. 2011	1	191.21	9.73	n.a	2
n: 50	2	257.11	30.48	3.27	2
	3	343.25	10.17	4.23	4
Oct. 2011	1	269.14	24.92	n.a	3
n: 92	2	349.63	24.57	3.25	4
	3	421.21	24.99	2.88	5
	4	507.5	1.87	6.42	*
Dec. 2011	1	307.09	24.65	n.a	3
n: 186	2	360.71	6.54	3.43	4
	3	387.79	13.23	2.73	5
Jan. 2012	1	307.52	25.74	n.a	3
n: 183	2	369.67	19.57	2.74	4
	3	415.62	20.75	2.27	5
Feb. 2012	1	283.37	12.11	n.a	3
n: 105	2	321.59	15.59	2.75	4
	3	385.13	27.69	2.93	5
	4	478.82	17.48	4.14	11
Mar. 2012	1	317.67	10.9	n.a	4
n: 59	2	375.05	21.43	3.54	4
	3	451.47	14.47	4.25	12

TABLE 3
Cohorts of Bigeye croaker *Micropogonias megalops*
caught in the Northern Gulf of California by
artisanal fishery (2012). TL is total length in mm,
S.D. is standard deviation and S.I. is separation index.

Date	Cohort	TL (mm)	S.D.	S.I.	Age (years)
Artisanal fishery					
Mar. 2012					
n: 58	1	330.45	19.31	n.a	3
	2	399.82	34.65	2.57	4
	3	549.10	17.06	5.77	*
Apr. 2012					
n: 595	1	297.17	20.08	n.a	3
	2	364.57	24.98	2.99	4
	3	409.15	10.03	2.54	4
	4	440.79	10.04	3.15	9

*Not assigned by the age-length key

TABLE 4
Parameter values, confidence intervals (95%) and Chi-squared probability (χ^2) obtained with likelihood profiles for each candidate model for *Micropogonias megalops* combined data and separated by sex data in the Northern Gulf of California. L_∞ is asymptotic total length; K determines the rate of approach to L_∞ ; t_0 is the hypothetical age at which the organism showed zero length; a is relative growth rate; b is incremental relative growth rate; Y_1 is length at age T_1 ; and Y_2 is length at age T_2 .

Model	Combined (C.I. 95%)	χ^2	Female (C.I. 95%)	χ^2	Male (C.I. 95%)	χ^2
VBGM						
L_∞ (mm)	439.8 (437.65–442.15)	0.072	458.83 (455.28–462.64)	0.051	423.25 (418.8–427.6)	0.018
K (annual)	0.264 (0.261–0.267)	0.023	0.235 (0.231–0.238)	0.107	0.302 (0.295–0.310)	0.047
t_0 (years ⁻¹)	-1.97 (-1.91–-2.03)	0.018	-2.24 (-2.34–-2.16)	0.082	-1.65 (-1.75–-1.56)	0.068
Gompertz						
L_∞ (mm)	429.6 (428–432)	0.206	447.07 (443.50–450.50)	0.031	412.93 (408.55–417.10)	0.041
K (annual)	0.346 (0.342–0.352)	0.134	0.312 (0.305–0.321)	0.091	0.399 (0.387–0.412)	0.027
t_0 (years ⁻¹)	-0.55 (-0.62–-0.50)	0.056	-0.64 (-0.725–-0.565)	0.023	-0.41 (-0.50–0.30)	0.015
Logistic						
L_∞ (mm)	422.6 (420.5–424.5)	0.094	439.09 (435.50–442.50)	0.041	405.94 (401.75–410.25)	0.019
K (annual)	0.432 (0.424–0.442)	0.001	0.393 (0.380–0.407)	0.110	0.50 (0.480–0.522)	0.043
t_0 (years ⁻¹)	0.34 (0.29–0.40)	0.020	0.36 (0.27–0.45)	0.048	0.39 (0.285–0.485)	0.037
Schnute						
a	0.264 (0.256–0.272)	0.033	0.235 (0.225–0.247)	0.044	0.302 (0.285–0.320)	0.010
b	1.010 (1.009–1.011)	0.122	1.016 (1.015–1.017)	0.140	1.004 (1.003–1.006)	0.170
Y_1 (mm)	225.40 (222.5–228.5)	0.046	224.49 (220.34–228.85)	0.006	227.59 (222.00–233.40)	0.027
Y_2 (mm)	411.2 (408.0–414.5)	0.099	414.83 (409.75–420.0)	0.025	410.77 (404.35–417.30)	0.030
L_∞ (mm)	444.83	—	467.73	—	425.04	—
t_0 (years ⁻¹)	-1.94	—	-2.20	—	-1.64	—

TABLE 5

Growth model selection for *Micropogonias megalops* combined and sex separated data in the Northern Gulf of California, where k is the number of parameters for each model; AIC is the Akaike's information criterion; Δ_i is Akaike's differences; w_i is Akaike's weight for each model; TL is total length in mm, and S.E. is the standard deviation.

Data	Models	k	AIC	Δ_i	w_i (%)	Asymptotic TL	S.E.
Combined	VBGM	3	2334.48	0.00	72.86	439.86	1.25
	Gompertz	3	2345.26	10.78	0.33	429.68	0.04
	Logistic	3	2353.46	18.98	0.01	422.64	0.00
	Schnute	4	2336.48	2.00	26.80	444.84	1.03
	Multi-model averaged					441.16	2.32
Female	VBGM	3	1040.41	0.00	67.82	458.83	1.16
	Gompertz	3	1045.22	4.81	6.13	447.08	0.80
	Logistic	3	1048.66	8.25	1.10	439.10	0.23
	Schnute	4	1042.41	2.00	24.95	467.73	1.92
	Multi-model averaged					460.12	4.11
Male	VBGM	3	672.84	0.00	69.44	423.25	0.79
	Gompertz	3	678.28	5.44	4.57	412.93	0.47
	Logistic	3	682.97	10.13	0.44	405.94	0.08
	Schnute	4	674.84	2.00	25.55	425.04	0.56
	Multi-model averaged					423.17	1.89

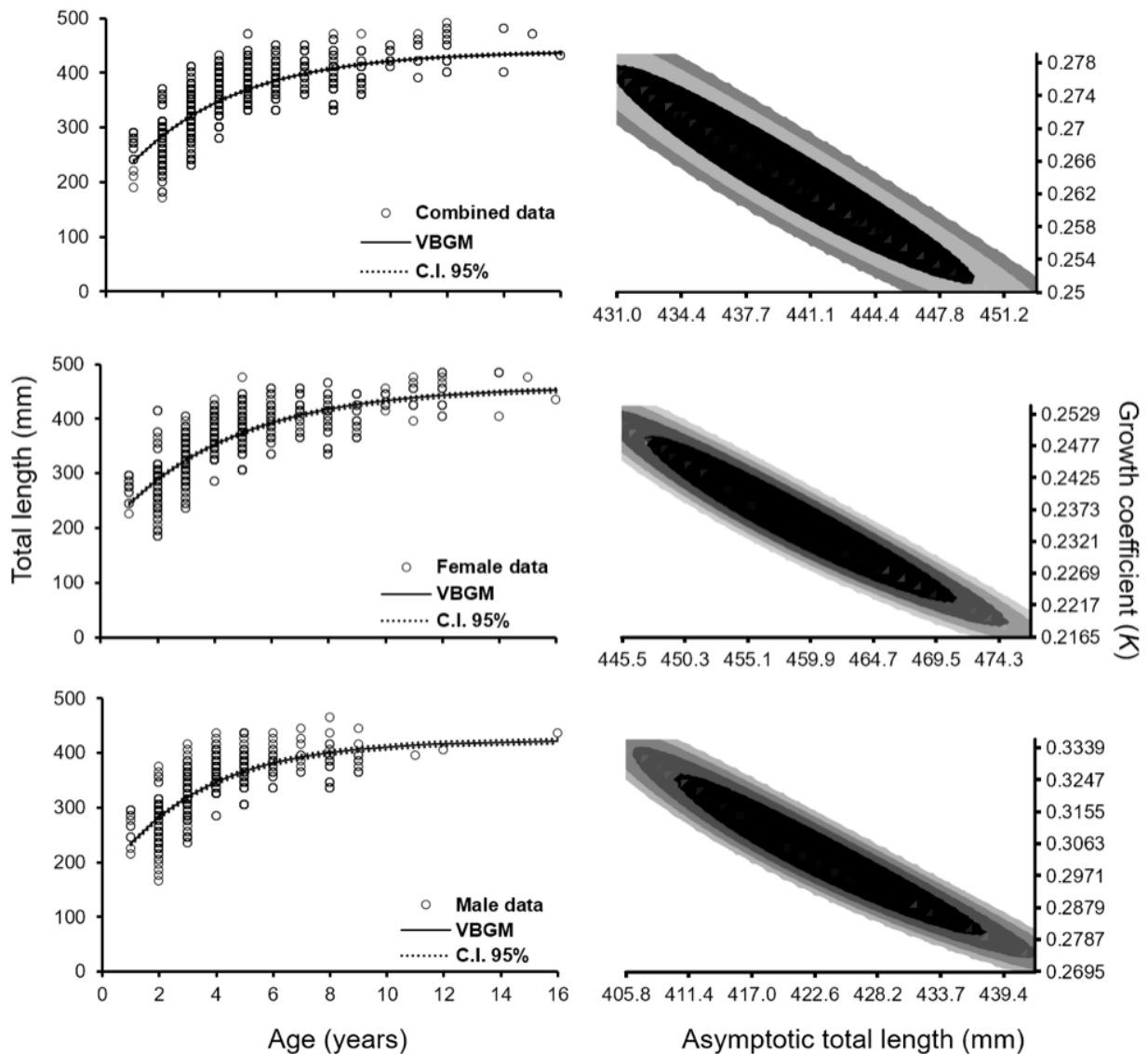


Figure 4. Growth curves and likelihood contours for parameters L_{∞} and K estimated by the von Bertalanffy growth model for Bigeye croaker *Micropogonias megalops* combined and sex separated data in the Northern Gulf of California. The area in black denotes joint confidence intervals (χ^2 test, $p < 0.05$).

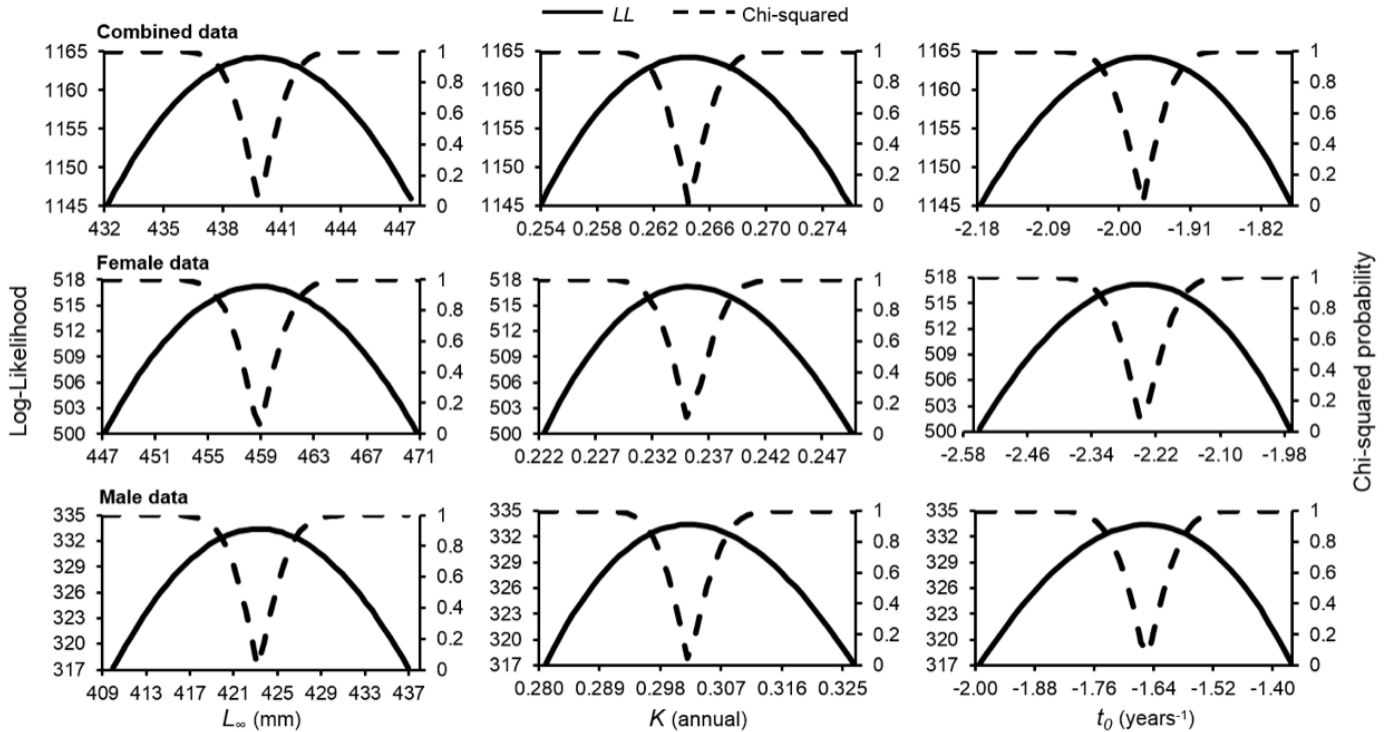


Figure 5. Likelihood profiles for parameters L_{∞} , K and t_0 estimated by the von Bertalanffy growth model for Bigeye croaker *Micropogonias megalops* combined and sex separated data.

TABLE 6

Comparison of the growth parameter values obtained by means of the von Bertalanffy model for Bigeye croaker in previous and current work in the Northern Gulf of California. Growth parameter values obtained are shown using combined and separated by sex data.

Source	L_{∞} (mm)	K (annual)
Román-Rodríguez 2000 (combined)	815.90	0.51
Females	826.90	0.53
Males	814.40	0.48
Aragón-Noriega et al. 2015 (combined)	448.00	0.37
Females	461.00	0.37
Males	429.00	0.41
Current work (combined)	439.86	0.26
Females	458.83	0.23
Males	423.25	0.30

each growth parameter of the best growth model are shown in Figure 5. Table 6 shows comparison between the growth parameter values obtained by the VBGM in current work and those obtained by the same growth model in previous works for the species in the Northern Gulf of California.

Natural mortality, reproduction and selectivity

Natural Mortality (M) of the Bigeye croaker was obtained taking into account the adjusted growth parameter values from the VBGM. Table 7 shows annual M values for the species according to six different equations:

TABLE 7

Natural mortality obtained through six different empirical equations that involve growth parameter values, age of massive maturity and longevity of the Bigeye croaker, and mean sea surface temperature in the Northern Gulf of California. M values are shown for combined data and separated by sex, also average global values of Natural mortality and standard deviations are shown.

Equation	M (combined)	M (Females)	M (Males)
Pauly (1980)	0.60	0.55	0.67
Jensen (1996)	0.39	0.35	0.45
Richter and Efanov (1977)	0.52	0.52	0.52
Hewitt and Hoenig (2005)	0.45	0.40	0.51
Then et al. (2015) T_{max}	0.63	0.57	0.71
Then et al. (2015) K and L_{∞}	0.44	0.40	0.50
Average	0.51	0.46	0.56
Standard deviation	0.09	0.09	0.10
Lim inf. 95 %	0.41	0.37	0.46
Lim sup. 95 %	0.60	0.56	0.66

Pauly (1980), Jensen (1996), Richter and Efanov (1977), Hewitt and Hoenig (2005) and Then et al. (2015) when considering longevity values in years (T_{max} combined = 9.39; females = 10.5; males = 8.27) and when considering growth parameter values. The results indicated that Bigeye croaker showed that M values in males were higher than those recorded by females for all six equations.

Monthly percentages of Bigeye croaker mature females for an annual cycle in the NGC are shown in

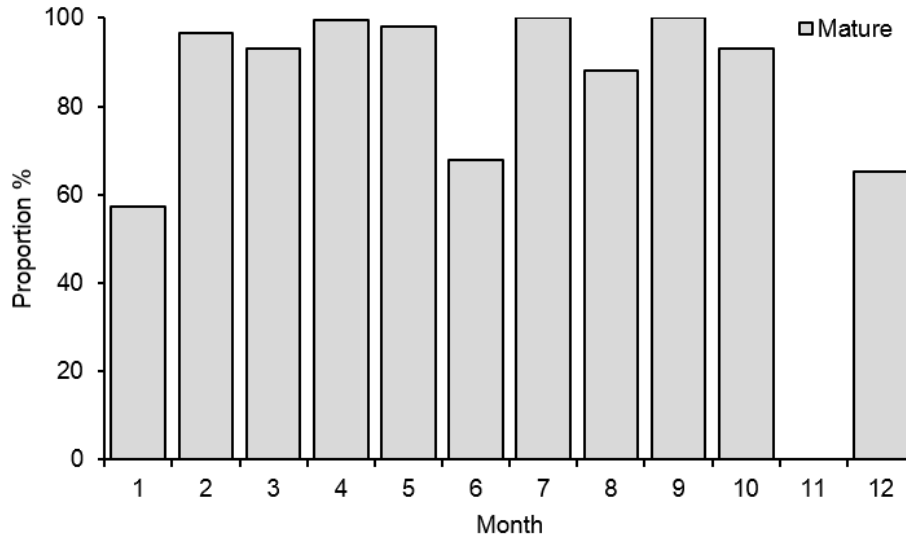


Figure 6. Monthly percentage of mature females of *Micropogonias megalops* in the Northern Gulf of California during an annual cycle.

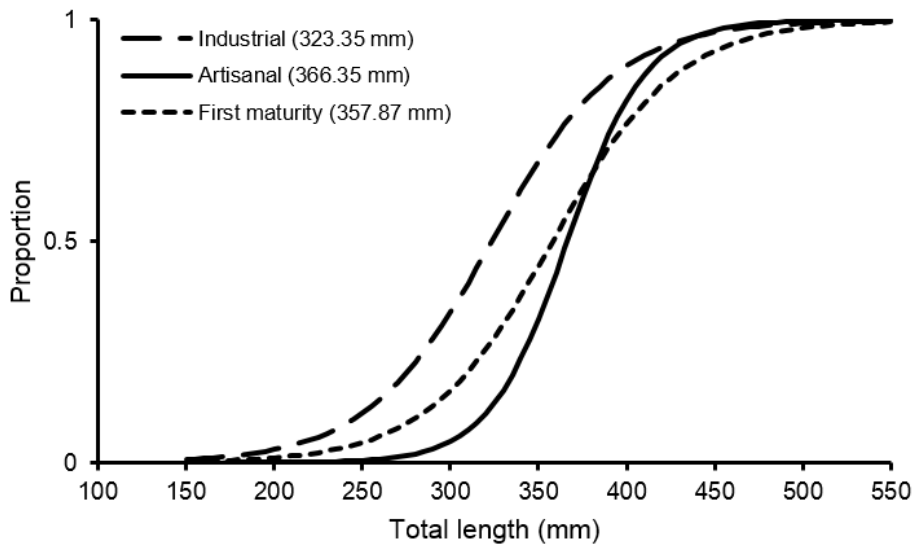


Figure 7. Length at first sexual maturity curve and fishing selectivity curves for *Micropogonias megalops* during the period from 2010 to 2012 in the Northern Gulf of California.

Figure 6. The L_{50} value obtained by the Logistic model for the species FSM was 357.87 mm TL ($a = 10.08$; $b = 0.028$; $r = 0.028$) with an adjusted value of $R^2 = 0.983$, according to the sum of squared residuals. Likewise, for selectivity curve calculation the following values were obtained; for industrial gear selectivity L_{50} value was 323.35 mm TL ($a = 9.13$; $b = 0.03$; $r = 0.03$) and an adjusted value of $R^2 = 0.986$ while for artisanal selectivity L_{50} value was 366.35 mm TL ($a = 16.44$; $b = 0.04$; $r = 0.04$) and an adjusted value of $R^2 = 0.998$. Figure 7 shows comparing projected curves obtained by the Logistic model for reproduction and both industrial and artisanal gear selectivity on Bigeye croaker.

Biomass estimation

Fishing hauls ($N = 254$) were used to estimate total biomass in a total area of 54 quadrants. Only 184 hauls (20 quadrants) were performed for Bigeye croaker caught in the NGC from June 2010 to July 2011. Table 8 shows the mean biomass estimates by quadrant. Five quadrants had 88% of the estimated total biomass (30, 33, 37, 44 and 47). The mean biomass estimate in the total area was 14 412 t. The official Bigeye croaker total catch for NGC in study period was 1 248 t. This catch represented only 8.7% of the estimated biomass of the resource in current work.

TABLE 8
Quadrant relative biomass estimation and mean relative biomass for *Micropogonias megalops* in the Northern Gulf of California during the 2010–11 period.

Quadrant	Quadrant area (Km ²)	Mean Biomass (Tons)	Lower and upper limits
2	320	105.2	(4.3–206.1)
3	273	91.1	(11.8–170.3)
4	307	76.2	(24.4–129.1)
6	239	145.5	(8.5–282.5)
7	195	4	
8	570	149.3	(97.6–201.0)
9	592	190.4	(108.0–272.7)
10	592	321.4	(45.7–597.0)
15	588	61.9	(11.8–111.9)
16	592	75.2	(7.8–142.6)
17	510	8	
19	449	2	
24	592	2	
30	532	2143	
33	592	3006	(1513.8–4498.2)
34	532	76.3	(21.5–131.2)
37	592	2482.7	(250.8–4714.6)
44	592	2645	(25.1–5264.3)
47	487	2413.7	(697.5–4129.9)
54	40.18	414	(40.2–787.8)
Mean total biomass		14412.9	
Quadrant mean biomass		720.645	

DISCUSSION

Many world fishery resources lack the necessary information to carry out robust stock assessments in a timely manner before being exploited by humans. Fish stock assessments consider several sources of biological information, such as average individual growth, maturation, natural mortality rates, changes in length or age composition, and stock abundance estimates (Hilborn and Walters 1992; Quinn and Deriso 1999; Cooper 2006). Thus, the importance of research, such as the study presented here, that generates information dependent and independent of the fisheries, allows management decisions in situations of limited information of the target species of the fishery (Ricard et al. 2011).

Bigeye croaker stock is an example of that situation where a lack of updated biological and fishery information for a stock exists and urgently needs to be generated, since the species has commercial importance in the NGC (Aragón-Noriega et al. 2009). Román-Rodríguez (2000) has the most complete research up to now for the species in the UGC, in which population dynamics and fishery data are presented. It is known that from the 1997–98 period until years close to current work (2010–12), fishing effort (artisanal fleet) increased by 38.7% (Aragón-Noriega et al. 2009), which by itself is a sufficient reason to carry out precise analyses of the resource situation today. Recently, individual growth of Bigeye croaker has been analyzed (Aragón-Noriega et al. 2015) even though this analysis was carried out using

population age and size data obtained in 1997–98 period (Román-Rodríguez 2000). It is known that environmental and anthropogenic (fishing) forcing could have effects on fish population structure and biology (Hsieh et al. 2010; Perry et al. 2010; Hidalgo et al. 2011), hence the importance to evaluate more recent Bigeye croaker fishery data (Páez-Osuna et al. 2016; García-Morales et al. 2017). However, it is up to this study in which basic aspects of this species population were considered, incorporating two recent data sources that were the industrial and artisanal fishery catches in the NGC (2010–12).

Bigeye croaker lengths found in both industrial and artisanal fishery catches in NGC were variable between months and years where cohort displacements were shown throughout time; this phenomenon is associated with biological and ecological aspects, such as reproduction, food or the environment (Román-Rodríguez 2000). In the global analysis of total length, the largest individuals were recorded in samples obtained by artisanal fishery (220–535 mm TL) and not by those obtained by industrial fishery (165–508 mm TL). It could be explained by selectivity of the fishing gear used by each fishery since they showed differences in mesh size that could have influenced the length range caught (Catalano and Allen 2010). Another possible factor is the fishing area where fleets (industrial and artisanal) operate. Based on the geographical coordinate data obtained by the industrial fleet, it has been shown that this fleet operates mainly from the southern part of the Reserve line of the UGC and covers a great part of the NGC. According to Rodríguez-Quiroz (2008) and Erisman et al. (2015), the artisanal fleet in UGC and NGC caught Bigeye croaker from the southern part of the nuclear area in the Upper Gulf, including part of the northwestern area of the vaquita (*Phocoena sinus*) refuge zone and along the northern coast of the state of Sonora. This fleet was performing its activities mainly within the reserve, exploiting approximately 75% of the area (Rodríguez-Quiroz 2008). Since 2015, 2017 and 2018 a new permanent no-take zone has been established for artisanal fishing gears like gill nets and longline (fig. 1). This measure is part of the efforts aimed at the protection of the vaquita *Phocoena sinus* in the Northern Gulf of California. Erisman et al. (2015) mentioned that according to the Bigeye croaker traditional fishing areas, this new no-take zone included the complete and most important fishing areas for the artisanal fleet (DOF 2015, 2017, 2018). Taking this measure has affected artisanal fisheries and fishermen in the area negatively due now to lesser fishing grounds and number of target species that they can fish, which could bring serious socioeconomic problems in the near future in NGC.

The multinomial analysis of the population denoted mean lengths from three to four cohorts per sampling

period. General length structure (2010–12) showed a total of five well-defined cohorts, showing that commercial fishing (industrial and artisanal) in the area does not act on isolated cohorts of Bigeye croaker but upon several age groups simultaneously (Cadima 2003). Individual growth assessment of Bigeye croaker was performed from a multi-model approach (Burnham and Anderson 2002), which is relatively new in fisheries (Cruz-Vázquez et al. 2012). It was used for the first time on new age-length data of this species (2010–12) in the NGC. Theoretical growth curves shown for each model according to the observed data described very similar trajectories with an accelerated growth at the beginning of curves to stabilize as they got to greater lengths and older ages.

For this growth analysis in Bigeye croaker when combined and female and male age-length data were modeled, the VBGGM showed the highest Akaike weight followed by Schnute model. Based on the fact that w_i values were <90% for all four models, an averaged model was calculated using L_∞ parameter values from all models (Burnham and Anderson 2002; Katsanevakis 2006; Katsanevakis and Maravelias 2008). This averaged model showed a value of $L_\infty = 441.16$ mm TL for combined data, 460.12 mm LT for females and 423.17 mm LT for males. Because it did not show any biological assumption or a specific curve type, its information was limited to one parameter (L_∞), which can be translated to a poor understanding of the species individual growth from physiological and ontogenical viewpoints. Recently, Mendivil-Mendoza et al. (2017) showed that obtaining a true average model was possible in this kind of analysis. It was achieved for a species from the same Family (Scaenidae) as Bigeye croaker, the gulf curvina (*Cynoscion othonopterus*), species distributed in the same study area of current work. For that analysis, they used the special solution cases of the Schnute model, where they obtained curve trajectories and growth parameter values (K and L_∞) with equal biological bases and statistical interpretation of those models that have been used traditionally for individual growth analysis in fishery sciences (VBGGM, Logistic and Gompertz). These are particular properties of the Schnute growth model because it is a nested and versatile model that has the ability to project both asymptotic and non-asymptotic growth curves in a particular age-length data set (Schnute 1981). The Schnute growth model and its special solution cases are recommended for even finer studies that describe growth in the species. In our study, the growth parameters obtained by the VBGGM were considered as the most reliable for this analysis to describe growth of the Bigeye croaker, based on AIC and Akaike weight values. Our results coincide with those obtained by Aragón-Noriega et al. (2015) where they also showed that the VBGGM was the best model for this species.

Confidence intervals obtained for both L_∞ and K growth parameters jointly, estimated by VBGGM, showed a probability surface contour where the asymptotic length and growth coefficient values showed a strongly inverse correlation; when one of the parameters increased its value, the other one decreased and vice versa. This covariance of growth parameters in the species occurs in the same way for data of the entire population, as well as data separated by sex.

Maximum observed length data in Bigeye croaker from 2010–12 in the NGC was 535 mm TL while that reported in 2000 was 490 mm TL (Román-Rodríguez 2000; Aragón-Noriega et al. 2015). Theoretical values obtained by VBGGM for this work showed a much lower value of L_∞ than those reported in Román-Rodríguez (2000) for the species by using the same model. On the other hand, Aragón-Noriega et al. (2015), when analyzing age-length data reported by Román-Rodríguez (2000) but from a multi-model approach, also concluded that VBGGM best described the Bigeye croaker growth ($w_i = 91.87\%$) with L_∞ values close but little higher to those obtained in this work (combined and separated by sex). Fischer et al. (1995) mentioned that *M. megalops* reaches to an approximate length of 40 cm (400 mm). At an international level, individual growth of *M. furnieri* in a coastal lagoon of Uruguay obtained $L_\infty = 302$ mm TL (Borthagaray et al. 2011) estimated with VBGGM, which was less than the value estimated for the Bigeye croaker of the NGC. Growth of *M. furnieri* individuals that live in Rocha Lagoon, Uruguay was more accelerated ($K = 0.19$) than that of those that live in the continental shelf (Borthagaray et al. 2011). Its growth was analyzed in waters of Trinidad where the parameter values for VBGGM were separated by sex, in males $L_\infty = 653$ mm TL and $K = 0.16$ and in females $L_\infty = 829$ mm TL and $K = 0.13$ (Manickchand-Heileman and Kenny 1990). Data confirmed that this species showed a greater asymptotic length and a slower growth, according to K in waters of Trinidad than in Rocha Lagoon in Uruguay. The Bigeye croaker *M. megalops* in the NGC showed a similar growth pattern with parameter values of $L_\infty = 439.8$ mm TL and $K = 0.26$ for all data but showed differences in between sexes, being females the ones that reached larger sizes with a less accelerated growth compared to male data. The growth coefficient value was lower than those reported by Román-Rodríguez (2000) and by Aragón-Noriega et al. (2015). Differences in L_∞ and K values are currently notable, less than those described for the species before (table 6). These differences could be due to mainly two reasons: (1) a bad estimate of growth parameters in 2000 (improved by Aragón-Noriega et al. 2015), which could be a probable explanation since the value of L_∞ shown for the Bigeye croaker in Román-Rodríguez (2000) did not come close to that reported for the spe-

cies in specialized fish databases as in Fischer et al. (1995), Nelson (2006), Froese and Pauly (2016) and Robertson and Allen (2015); (2) the possible explanation is that the values of the estimated parameters for 2000 decreased due to environmental changes through time or a continuous and intense fisheries of the population in the NGC and UGC (Hsieh et al. 2010; Perry et al. 2010; Hidalgo et al. 2011; Páez-Osuna et al. 2016; García-Morales et al. 2017). It could be explained by the fact that biological needs of *M. megalops* changed throughout approximately 15 years (from 1997–98 to 2010–12), investing the greatest part of the energy obtained by feeding in reproduction and not in growth (Quinn and Deriso 1999). Thus, the species tends to reach its sexual maturity at a younger age and smaller length as a type of survival strategy or mechanism. The length at first sexual maturity (FSM) obtained by the Logistic model in this study was $L_{50} = 357.87$ mm TL, theoretically reached at three years of age. Román-Rodríguez (2000) reported a value of $L_{50} = 394.84$ mm TL, which was 10% greater (36.98 mm) than that obtained in this study. Although the difference is little, there is evidence of a decrease in average length at which the Bigeye croaker reaches its reproductive maturity. If FSM (357.86 mm TL) and L_{∞} (439.86 mm TL) were obtained for the 2010–12 data in the NGC, a difference of 82 mm could be noted between the occurrence of one phenomenon and the other one. Likewise, the information analyzed sustained the Bigeye croaker FSM reached 81% of asymptotic length, which is why it is very likely that during the species growth, the arrival of FSM represents the most important point of inflexion of the ontogenic cycle of the species. In such a way that species growth is accelerated during the first years and slows down after the arrival of the FSM. According to that shown by the lengths during all the analysis period, the population showed a fraction of mature individuals at all times, which is why although the species reproduction takes place as maximum from March to August (Castro-González 2004), in favorable conditions it showed a continuous recruitment.

As to Natural mortality (M) of Bigeye croaker six values were calculated by means of six different equations for all combined, female and male data. These M values varied between sexes and also by the methods used (table 7). Several authors have mentioned that the instantaneous coefficient of M is the most cryptic parameter in population dynamics (Gallucci et al. 1996; Quinn and Deriso 1999) and the majority of estimates are made by means of empirical equations, taking as a reference other key processes of population life, such as size of first maturity, longevity, among others (Then et al. 2015). Pauly (1980) and Pauly et al. (1984) highlighted their equation of mortality that included, in addition to the speed of growth, the environmental conditions imperative in

the environment as forcing the metabolism, which is the average temperature of the environment. This ultimate equation derives from the analysis of several fish species belonging to several families, which already contain natural mortality estimates. The Bigeye croaker showed natural mortality values ($M_{\text{average}} = 0.51, 0.46$ and 0.56 for combined, female and male data respectively) similar to those observed by families where the species are more long-lived than what occurred in the Gulf of California as the Scianids (same Family as the *M. megalops*) where the M values were $0.20\text{--}0.80$ and to the members of the Family Merlucciidae with values of $M = 0.37\text{--}0.69$. Nevertheless, there are evident differences in M values between sexes where males have a little superior value compared to females. Román-Rodríguez (2000) estimated by Pauly's (1984) equation a value of $M = 0.36$, which is a little lower but closer to those estimated in the NGC for the 2010–12 data. The low M value is a phenomenon that is regularly present in fish populations, as the Bigeye croaker, with slow growth (low K) and high longevity (17 years according to Román-Rodríguez 2000). Moreover, the M calculus must be certain since this phenomenon is related with the growth parameters L_{∞} and K of VBGM (Pauly 1980; Jensen 1996; Then et al. 2015), which besides being sustained with physiological basis, it turned out to be statistically the best model within the candidate models in the description of the Bigeye croaker growth. These natural mortality results, together with the low FSM, could be the evidence that Bigeye croaker still has high capacity of population doubling, which translates into a highly available biomass of the resource in the study area. The biomass estimated for this resource showed evidence of that previously mentioned since higher values were recorded in relation to what has been caught of Bigeye croaker in the NGC during the last years. Annual landing values in metric tons in the area were around 3000 in 2009, 2600 in 2010 and 3500 in 2011 (Aragón-Noriega et al. 2015). The official catches reported during the study period represented a small fraction (8.7%) of the mean biomass estimated in the NGC, showing evidence that *M. megalops* was an underexploited resource, but this information should be checked and contrasted with other methods depending on the fishery.

In terms of current management, the Bigeye croaker is part of a multispecies fishery that takes place in the northern part of the Gulf of California (DOF 2010), where as mentioned, there are two types of fleet, artisanal (small vessels) and industrial (ships). However, considering the volumes caught, the economic yield generated from them and the importance of job creation (Aragón Noriega et al. 2009), the Bigeye croaker should be managed as an independent fishery; the information in this study could contribute to this change in management.

According to the National Fisheries Charter (Carta Nacional Pesquera CNP) (a normative instrument that specifies management schemes for Mexican fishery resources), continuing with the current management scheme (multispecific fishery) would make it difficult to specify the maximum fishing effort of the different populations that compose this complex resource; the same CNP mentioned that it was necessary to increase the information available to develop prediction models.

One of the most important challenges to address if this change is made for a specific fishery of the Bigeye croaker is the establishment of specific fishing grounds and fishing gears for resource captures, in order to not adversely affect endangered species, such as the vaquita (*Phocoena sinus*) or the totoaba (*Totoaba macdonaldi*) in the UGC Reserve zone. Likewise, spatial and temporal runs (route of migration and movements) of the resource should be better known to establish new areas with catchability in places far away from critical areas (breeding or co-habitat of endangered species) in the UGC and NGC.

If the Bigeye croaker is separated as an independent fishery, it will be possible to implement specific administrative measures that consider, among others: fishing period, fishing gear allowed, size of first catch by regulation of selective fishing gear and effort limitations considering that it is a resource shared by two fleets. Likewise, actions should be carried out once the resource is separated as an independent fishery, as preparing the Fishery Management Plan that would ultimately contribute to a sustainable management of the resource in accordance with the guidelines of international standards. On the other hand, the correct management will benefit the region economically and ecologically, considering that good management is critical for an area of interest for biodiversity as the NGC where a protected natural area exists bordering the area dealt with in this study.

ACKNOWLEDGMENTS

This research was financed with Centro de Investigaciones Biológicas Del Noroeste, S.C. (CIBNOR) EP projects and Produce Sonora 895-1. The authors would like to thank the staff of the Fisheries Laboratory at CIBNOR Guaymas, specifically to Eloisa Herrera Valdivia and Rufino Morales Azpeitia; Diana Fischer for editorial services in English.

LITERATURE CITED

Agüero, M. 2007. Alternativas de medición y gestión de la capacidad y esfuerzo pesquero en América Latina y el Caribe. 37–58 pp. In: Agüero, M. (ed.). Capacidad de pesca y manejo pesquero en América Latina y el Caribe. FAO Documento Técnico de Pesca. No. 461. Roma, FAO. 403p.

Aragón-Noriega, E. A., W. Valenzuela-Quiónes, H. Esparza-Leal, A. Ortega-Rubio, and G. Rodríguez-Quiroz. 2009. Analysis of management options for artisanal fishing of the bigeye croaker *Micropogonias megalops* (Gilbert, 1890) in the upper Gulf of California. *Int J Biodivers Sci Ecosyst Serv Manage.* 5: 208–214.

Aragón-Noriega, E. A., E. Alcántara-Razo, W. Valenzuela-Quiónes, and G. Rodríguez-Quiroz. 2015. Multi-model inference for growth parameter estimation of the Bigeye Croaker *Micropogonias megalops* in the Upper Gulf of California. *Rev Biol Mar Ocean.* 50(1), 25–38.

Bertalanffy, L. von. 1938. A quantitative theory of organic growth (Inquiries on growth laws. II). *Hum Biol.* 10: 181–213.

Borthagaray, A. I., J. Verocai, and W. Norbis. 2011. Age validation and growth of *Micropogonias furnieri* (Pisces-Sciaenidae) in a temporally open coastal lagoon (Southwestern Atlantic-Rocha-Uruguay) based on otolith analysis. *J Appl Ichthyol.* 27: 1212–1217.

Burnham, K. P., and D. R. Anderson. 2002. Model selection and multimodel inference: A practical information-theoretic approach. Springer. 2nd Ed. New York, N.Y. 488p.

Cadima, E. L. 2003. Manual de evaluación de recursos pesqueros. Documento Técnico de Pesca. No. 393. Roma, FAO. 162p.

Castro-González, J. J. 2004. Estudio base y estrategias de manejo del chano *Micropogonias megalops*, caso Alto Golfo de California. Tesis de maestría, Ensenada, B.C: Universidad Autónoma de Baja California.

Catalano, M. J., and M. S. Allen. 2010. A size- and age-structured model to estimate fish recruitment, growth, mortality, and gear selectivity. *Fish Res.* 105: 38–45.

Cerdenares-Ladrón-De-Guevara, G., E. Morales-Bojórquez, and R. Rodríguez-Sánchez. 2011. Age and growth of the sailfish *Istiophorus platypterus* (Istiophoridae) in the Gulf of Tehuantepec, Mexico. *Marine Biology Research.* 7(5): 488–499.

Cope J. M. 2013. Implementing a statistical catch-at-age model (Stock Synthesis) as a tool for deriving overfishing limits in data-limited situations. *Fish. Res.* 142:3–14.

Cope J. M. and A.E. Punt 2009. Length-Based Reference Points for Data-Limited Situations: Applications and Restrictions. *Marine and Coastal Fisheries: Dynamics, Management, and Ecosystem Science* 1:169–186.

Cruz-Vásquez, R., G. Rodríguez-Domínguez, E. Alcántara-Razo, and E. A. Aragón-Noriega. 2012. Estimation of individual growth parameters of the Cortes geoduck *Panopea globosa* from the central Gulf of California using a multimodel approach. *J Shellfish Res.* 31(3): 725–732.

Diario Oficial de la Federación. 2010. Acuerdo mediante el cual se da a conocer la actualización de la Carta Nacional Pesquera. Jueves 2 de diciembre de 2010. México, DF. CNP 2010.

Diario Oficial de la Federación. 2015. Acuerdo por el que se suspende temporalmente la pesca comercial mediante el uso de redes de enmalle, cimbras y/o palangres operadas con embarcaciones menores, en el Norte del Golfo de California. Diario Oficial de la Federación. 10/04/2015. México. (Cons. 13/02/2018).

Diario Oficial de la Federación. 2017. Acuerdo por el que se prohíben artes, sistemas, métodos, técnicas y horarios para la realización de actividades de pesca con embarcaciones menores en aguas marinas de jurisdicción federal de los Estados Unidos Mexicanos en el Norte del Golfo de California, y se establecen sitios de desembarque, así como el uso de sistemas de monitoreo para dichas embarcaciones. Diario Oficial de la Federación. 30/06/2017. México. (Cons. 13/02/2018).

Diario Oficial de la Federación. 2018. Acuerdo por el que se modifican diversas disposiciones del diverso por el que se establece el área de refugio para la protección de la vaquita (*Phocoena sinus*). Diario Oficial de la Federación. 20/04/2018. México. (Cons. 20/04/2018).

Fischer, W., F. Krupp, W. Schneider, C. Sommer, K. E. Carpenter, and V. H. Niem. 1995. Pacífico centro oriental; Guía FAO para la identificación de especies para los fines de la pesca. FAO; Roma. II–III: 648–1652p.

Folmer, O., and M. Pennington. 2000. A statistical evaluation of the design and precision of the shrimp trawl survey off West Greenland. *Fish Res.* 49(2), 165–178.

Francis, C. R., R. J. Hurst and J. A. Renwick. 2003. Quantifying annual variation in catchability for commercial and research fishing. *Fish. Bull.*, 101(2), 293–304.

Froese, R., and D. Pauly. 2016. FishBase. www.fishbase.org, version (10/2016).

Gallucci, V. F., S. B. Saila, D. J. Gustafson, and B. J. Rothschild. 1996. Stock Assessment: Quantitative methods and applications for small scale fisheries. (Vol. 1). CRC Press, Boca Raton, Florida.

García-Morales, R., J. López-Martínez, J. E. Valdez-Holguin, H. Herrera-Cervantes, and L. D. Espinosa-Chaurand. 2017. Environmental Variability and Oceanographic Dynamics of the Central and Southern Coastal Zone of Sonora in the Gulf of California. *Remote Sensing.* 9(9), 925.

- Gilbert, C. H. 1890. A preliminary report on the fishes collected by the steamer 'Albatross' on the Pacific coast of North America during the year 1889, with descriptions of twelve new genera and ninety-two new species. Proc US Nat Mus. 13: 49–126.
- Gompertz, B. 1825. On the nature of the function expressive of the law of human mortality, and on a new mode of determining the value of life contingencies. Philos Trans R Soc Lond B Biol Sci. 115: 513–583.
- Gulland, J. A., and A. A. Rosenberg. 1992. Examen de los métodos que se basan en la talla para evaluar las poblaciones de peces. FAO Documento Técnico de Pesca No. 323. Roma, FAO. 112p.
- Haddon, M. 2001. Modelling and quantitative methods in fisheries. Boca Raton, FL: Chapman and Hall/CRC. 406p.
- Hidalgo, M., T. Rouyer, J. C. Molinero, E. Massutí, J. Moranta, B. Guijarro, and N. Stenseth. 2011. Synergistic effects of fishing-induced demographic changes and climate variation on fish population dynamics. Marine Ecology Progress Series, 426, 1–12.
- Hilborn, R., and M. Mangel. 1997. The ecological detective. Confronting models with data. Monographs in Population Biology. Princeton, NJ: Princeton Academic Press. 315p.
- Hilborn, R., and C. J. Walters. 1992. Quantitative Fisheries Stock Assessment: Choice, Dynamics and Uncertainty. Kluwer Academic Publishers, New York.
- Hsieh, C. H., A. Yamauchi, T. Nakazawa, and W. F. Wang. 2010. Fishing effects on age and spatial structures undermine population stability of fishes. Aquatic Sciences, 72(2), 165–178.
- Jensen, A. L. 1996. Beverton and Holt life history invariants result from optimal tradeoff of reproduction and survival. Can J Fish Aquat Sci. 54: 987–989.
- Katsanevakis, S. 2006. Modelling fish growth: model selection, multi-model inference and model selection uncertainty. Fish Res. 81: 229–235.
- Katsanevakis, S., and D. Maravelias. 2008. Modelling fish growth: multi-model inference as a better alternative to a priori using von Bertalanffy equation. Fish Fish. 9: 178–187.
- King, M. G. 1997. Fisheries biology, assesment and management. Fishing news books. Osney Mead, Oxford, England. 341p
- King, M. G. 2007. Fisheries Biology, Assessment and Management. 2nd edition, Blackwell Scientific Publications, Oxford: pp. 211–219.
- López-Martínez, J., J. Rodríguez-Romero, N. Y. Hernández-Saavedra and E. Herrera-Valdivia. 2011. Population parameters of the Pacific flagfin mojarra *Eucinostomus currani* (Perciformes: Gerreidae) captured by shrimp trawling fishery in the Gulf of California. Revista de Biología Tropical, 59(2), 887–897.
- López-Martínez J., E. Herrera-Valdivia, J. Rodríguez-Romero, and S. Hernández-Vázquez. 2010. Composición taxonómica de peces integrantes de la fauna de acompañamiento de la pesca industrial de camarón del Golfo de California, México. Rev Biol Trop. 58: 925–942.
- Manickchand-Heileman, S. C., and J. S. Kenny. 1990. Reproduction, age, and growth of the whitemouth croaker *Micropogonias furnieri* (Desmarest 1823) in Trinidad waters. Fish Bull. U.S. 88: 523–529.
- Mendivil-Mendoza, J. E., Rodríguez-Domínguez, G., Castillo-Vargasmachuca, S. G., Ortega-Lizárraga, G. G., and Aragón-Noriega, E. A. 2017. Estimación de los parámetros de crecimiento de la curvina golfinia *Cynoscion othonopterus* (pisces: Sciaenidae) por medio de los casos del modelo de Schnute. Interciencia, 42(9).
- Montgomery, S. S., C. T. Walsh, M. Haddon, C. L. Kesby, and D. D. Johnson. 2010. Using length data in the Schnute Model to describe growth in a metapenaeid from waters off Australia. Mar Freshwater Res. 61: 1435–1445.
- Morales-Bojórquez, E. 2002. Bayes theorem applied to the yield estimate of the Pacific sardine (*Sardinops sagax caeruleus* Girard) from Bahía Magdalena, Baja California Sur, Mexico. Cienc Mar. 28(2), 167–179.
- Nelson, J. S. 2006. Fishes of the World. 4th ed. Hoboken. New Jersey, USA: John Wiley and Sons. XIX: 601p.
- Neter, J., M. H. Kutner, C. J. Nachtsheim, and W. Wasserman. 1996. Applied linear statistical models. New York, NY: McGraw-Hill. 1408p.
- Nikolsky, G. V. 1963. The Ecology of Fishes. Academic Press. London, UK. 352 pp.
- Páez-Osuna, F., J. A. Sánchez-Cabeza, A. C. Ruíz-Fernández, R. Alonso-Rodríguez, A. Piñón-Gimate, J. G. Cardoso-Mohedano, F. J. Flores-Verdugo, J. L. Carballo, M. A. Cisneros-Mata, and S. Álvarez-Borrego. 2016. Environmental status of the Gulf of California: A review of responses to climate change and climate variability. Earth-Science Reviews, 162, 253–268.
- Pauly, D. 1980. On the interrelationships between natural mortality, growth parameters, and mean environmental temperature in 175 fish stocks. J Conseil. 39(2), 175–192.
- Pauly, D., J. Ingles, and R. Neal. 1984. Application to shrimp stocks of objective methods for the estimation of growth, mortality and recruitment-related parameters from length-frequency data (ELEFAN I and II).
- Pawitan, Y. 2001. In All Likelihood: statistical modeling and inference using likelihood. Oxford: Oxford University Press. 528p.
- Pennington, M. 1983. Efficient estimators of abundance, for fish and plankton surveys. Biometrics, 281–286.
- Pennington, M. 1985. Some statistical techniques for estimating abundance indices from trawl surveys. Fish Bull. U.S. 84: 519–526.
- Pennington, M. 1996. Estimating the mean and variance from highly skewed marine data. Fish Bull. 94(3), 498–505.
- Perry, R. I., P. Cury, K. Brander, S. Jennings, C. Möllmann, and B. Planque. 2010. Sensitivity of marine systems to climate and fishing: concepts, issues and management responses. Journal of Marine Systems, 79(3–4), 427–435.
- Pierce, G. J., N. Bailey, Y. Stratoudakis, and A. Newton. 1998. Distribution and abundance of the fished population of *Loligo forbesi* in Scottish waters: analysis of research cruise data. ICES J Mar Sci: J. Conseil. 55(1), 14–33.
- Quinn, J. T., and R. B. Deriso. 1999. Quantitative fish dynamics. Oxford University Press. New York. 452p.
- Rábago-Quiroz, C. H., J. López-Martínez, J. E. Valdez-Holguín, and M. Nevárez-Martínez. 2011. Distribución latitudinal y batimétrica de las especies más abundantes y frecuentes en la fauna acompañante del camarón del Golfo de California, México. Rev Biol Trop. 59: 255–267.
- Ricard, D., C. Minto, O. P. Jensen, and J. K. Baum. 2012. Examining the knowledge base and status of commercially exploited marine species with the RAM Legacy Stock Assessment Database. Fish Fish. 13(4): 380–398.
- Ricker, W. E. 1975. Computation and interpretation of biological statistics of fish populations. J Fish Res Board Can. 191: 383p.
- Robertson, D. R., and G. R. Allen. 2015. Peces Costeros del Pacífico Oriental Tropical: un sistema de información. Instituto Smithsonian de Investigaciones Tropicales, Balboa, República de Panamá.
- Rodríguez-Domínguez, G., S. G. Castillo-Vargasmachuca, R. Pérez-González, and E. A. Aragón-Noriega. 2012. Estimation of the individual growth parameters of the brown crab *Callinectes bellicosus* (Brachyura, Portunidae) using a multi-model approach. Crustaceana. 85(1): 55–69.
- Rodríguez-Quiroz, G. 2008. Sociedad, pesca y conservación en la Reserva de la Biosfera del Alto Golfo de California y Delta del Río Colorado. CIBNOR. Tesis de doctorado. 134p.
- Román-Rodríguez, M. J. 2000. Estudio poblacional del chano norteño, *Micropogonias megalops* y la curvina Golfinia *Cynoscion othonopterus* (Gilbert) (Pisces: Sciaenidae), especies endémicas del Alto Golfo de California, México. Instituto del Medio Ambiente y Desarrollo Sustentable del Estado de Sonora. Informe final SNIB-CONABIO proyecto No. L298. México, DF.
- Schnute, J. 1981. A versatile growth model with statistically stable parameters. Can J Fish Aquat Sci. 38: 1128–1140.
- Siegfried, K., and B. Sansó. 2009. A review for estimating natural mortality in fish populations. Tech. rep., SEDAR 19 Research Document 29.
- SOFIA 2016, El estado mundial de la pesca y la acuicultura 2016. Contribución a la seguridad alimentaria y la nutrición para todos. FAO Roma. 224 pp
- Sparre, P., and S. C. Venema. 1997. Introducción a la evaluación de recursos pesqueros Tropicales. Parte 1. Manual. FAO Documento Técnico de Pesca. Valparaíso, Chile. 306 (1): 420p.
- Taylor, C. C. 1962. Growth equations with metabolic parameters. J. Conseil. 27 (3): 270–286.
- Then, A. Y., J. M. Hoenig, N. G. Hall and D. A. Hewitt. 2015. Evaluating the predictive performance of empirical estimators of natural mortality rate using information on over 200 fish species. ICES J Mar Sci, 72(1), 82–92.
- Venzon, D. J., and S. H. Moolgavkar. 1988. A method for computing profile-likelihood-based confidence intervals. Appl Stat. 37: 87–94.
- World Bank. 2017. The Sunken Billions Revisited: Progress and Challenges in Global Marine Fisheries. Washington, DC: World Bank. Environment and Sustainable Development series. Doi: 10.1596/978-1-4648-0919-4. License: Creative Commons Attribution CC BY 3.0 IGO.
- Zar, J. H. 1999. Biostatistical Analysis. Englewood Cliffs, NJ: Prentice-Hall. 633p.

REPRODUCTIVE TACTICS OF CALIFORNIA HALIBUT (*PARALICHTHYS CALIFORNICUS*): COMBINING SPAWNING SEASON, INTERSPAUNING INTERVAL, AND BATCH FECUNDITY TO ESTIMATE ANNUAL REPRODUCTIVE OUTPUT FOR A MULTIPLE-BATCH SPAWNING FISH

CHERYL L. BARNES

Moss Landing Marine Laboratories
8272 Moss Landing Road
Moss Landing, CA 95039
ph: (831) 334-3484
cheryl.barnes@alaska.edu

RICHARD M. STARR

Moss Landing Marine Laboratories
8272 Moss Landing Road
Moss Landing, CA 95039
starr@mlml.calstate.edu

ABSTRACT

Baseline reproductive information is crucial to identifying species responses to spatiotemporal variation and changing environmental conditions. We collected 205 central California halibut (2012 and 2013) to better understand the reproductive tactics of a batch spawner with indeterminate fecundity. We used histology to identify subphases of actively spawning fish, approximated spawning duration based on weekly proportions of reproductive females, calculated daily spawning fractions to estimate interspawning intervals, and quantified batch fecundity using the hydrated oocyte method. The spawning season lasted approximately 10 weeks. Interspawning intervals were 1.3 to 2.7 d, depending upon the spawning marker (i.e., hydrated oocytes or POFs) used. Mean batch fecundity for fish in the late hydration subphase of spawning was $597,445 \pm 318,419$ eggs, resulting in annual fecundities that ranged from 5.2×10^6 to 8.1×10^7 eggs per fish. These findings provide a preliminary assessment of reproductive output for California halibut and foundation data for future spatiotemporal analyses.

INTRODUCTION

The need to assess variation in reproductive characteristics across size and age classes (e.g., Fitzhugh et al. 2012), at several spatial and temporal scales (e.g., Ganas et al. 2004; Lowerre-Barbieri et al. 2011), and under different environmental conditions (e.g., Pecquerie et al. 2009) has been thoroughly conveyed in the scientific literature. However, we still lack basic information about the reproductive biology of many species, thus preventing more extensive investigations into the mechanistic relationships among specific reproductive tactics and demographic, spatiotemporal, or environmental factors. A poor understanding about how one generation is connected to the next is especially problematic for species targeted in commercial and recreational fisheries because changes in reproductive output are amplified by size-selective fishing (Trippel et al. 1997; Wright and Trippel 2009).

California halibut (*Paralichthys californicus*) has long been valued in commercial and recreational fisheries

along the west coast of North America (Frey 1971). Although a number of researchers have assessed variation in life history traits of California halibut (e.g., multiple studies in Haugen 1990; MacNair et al. 2001; Barnes et al. 2015), relatively few have reported information about the reproductive characteristics of wild-caught fish. Macroscopic assessments of California halibut ovaries have indicated that 50% of females reach sexual maturity by 47 cm (4.0 yr) off southern California (Love and Brooks 1990), whereas 50% of females reach sexual maturity by 62.8 cm (4.9 yr) off central California (Lesyna and Barnes 2016). Pelagic eggs are found year-round off the coasts of southern California and Mexico, with peak spawning taking place nearshore in spring and early summer (Haaker 1975; Lavenberg et al. 1986; Allen 1988; Barnes et al. 2015). Changes in mean gonadosomatic index suggest peak spawning in midsummer north of Point Conception (Barnes et al. 2015).

California halibut are batch spawners that exhibit indeterminate fecundity and undergo asynchronous ovarian development (Caddell et al. 1990; Murua and Saborido-Rey 2003; Lesyna and Barnes 2016). A study of captive females held under environmental conditions typical for southern California indicated interspawning intervals (i.e., the time elapsed between individual spawning events) between 7 and 14 d. Spawning frequencies from that study were 12 to 13 times per year and batch fecundity (i.e., the number of eggs produced per female per spawning event) ranged from 455,000 to 589,000 eggs (Caddell et al. 1990). This equated to a mean annual fecundity of 5.5×10^6 to 7.7×10^6 eggs per female.

The primary objective of our study was to estimate annual fecundity for California halibut found north of Point Conception. To do so, we quantified the duration of the spawning season, daily spawning fraction (S), interspawning interval (ISI), spawning frequency (F), and batch fecundity of wild-caught fish. We also identified subphases of actively spawning females to more accurately estimate batch fecundity using an opportunistic sampling design. Our goal was to provide a preliminary assessment of the reproductive output of California halibut, establish baseline data for future demographic or

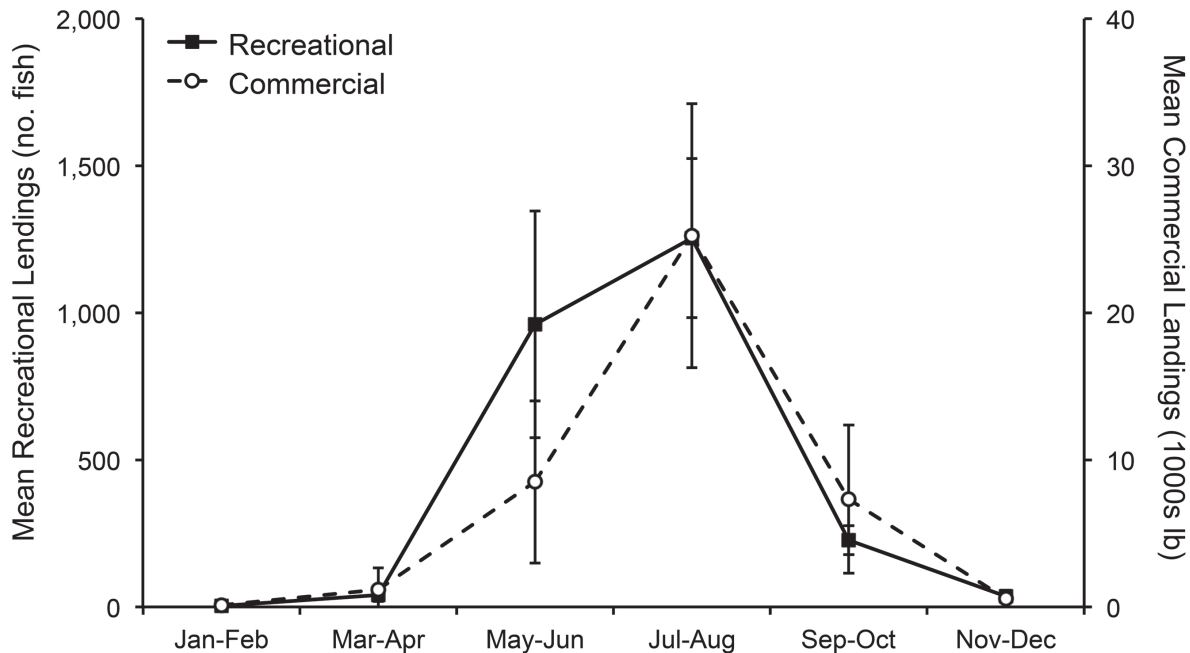


Figure 1. Bimonthly mean landings of California halibut for Santa Cruz, Monterey, and San Luis Obispo counties (2004 to 2013). The solid line and filled squares represent recreational landings (numbers of fish). The dashed line and open circles represent commercial landings (1000s lb). Errors bars denote one standard error. Recreational landings data were obtained from the Recreational Fisheries Information Network (RecFIN, <https://www.recfin.org/>), which is managed by the Pacific States Marine Fisheries Commission. Summarized commercial landings data were provided by the California Department of Fish and Wildlife (CDFW, unpublished data).

spatiotemporal comparisons, and enhance our understanding about the reproductive biology of an economically important multiple-batch spawner with indeterminate fecundity.

METHODS

We collected adult California halibut females as filleted carcasses from commercial and recreational hook-and-line fishers, seafood processors, and spearfishers between late May and mid-September (2012 and 2013), when California halibut are known to reproduce near-shore (Love and Brooks 1990; Barnes et al. 2015). We also collected a few individuals in October and November of 2013. We were unable to sample during the winter months because landings from central California fisheries are consistently low from November to April (CDFW unpublished data, fig. 1). Sampled fish were caught in shallow (<40 m) coastal waters near five primary locations: Santa Cruz, Moss Landing, Monterey, Morro Bay, and Port San Luis (fig. 2). One additional female was caught near Half Moon Bay, approximately 50 miles north of Santa Cruz. In 2012, we sampled wharfs and harbors in and around Santa Cruz four to five times per week. All other locations were sampled two to three times per month. We also processed carcasses donated from port samplers and private anglers as they became available. In 2013, we sampled all sites two times per week from mid-May to September. All fish were placed

on ice immediately after filleting and kept cold until fully processed in the laboratory (typically within 12 hr; maximum 24 hr period).

We recorded capture date, location, pre-fillet fork length (FL, mm), and body weight (W, g). When samples were received as filleted carcasses, we recorded post-fillet fork lengths (mm) and converted to pre-fillet fork lengths (mm) using the linear relationship described by Barnes et al. (2015). We extracted and thin-sectioned sagittal otoliths to age fish following methods described by the Committee of Age-Reading Experts (CARE 2006). We preserved ovaries in 10% buffered formalin and removed prepared transverse sections for histological processing, which involved dehydrating the tissue, embedding it in paraffin wax, thin-sectioning and mounting it to a microscope slide, and staining it with hematoxylin and eosin (Luna 1968; Hunter and Macewicz 1980; Hunter and Macewicz 1985). We identified stages of ovarian development as developing, spawning capable, actively spawning, regressing (i.e., spent), or regenerating (i.e., resting) according to histological characteristics described by Lesyna and Barnes (2016). We further classified actively spawning fish into subphases based on the two most advanced stages of oocyte development (MAS₁ and MAS₂) and the incidence and relative ages of postovulatory follicles (POFs), which are spawning markers that denote the recent release of an egg. Oocyte developmental stages used to categorize actively spawning

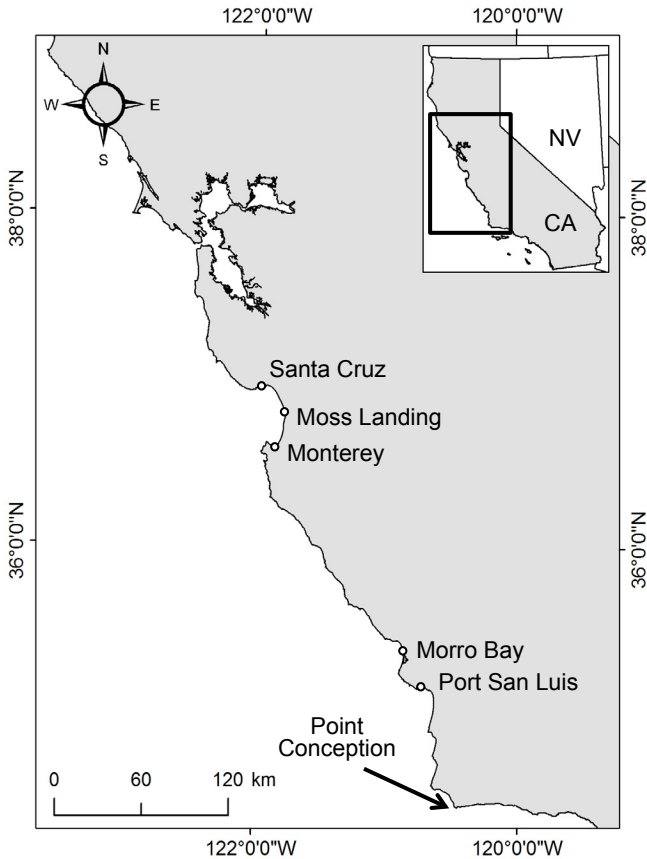


Figure 2. Primary locations used to sample adult California halibut females from commercial and recreational fisheries (2012 and 2013).

subphases (in order from least to most developed) were cortical alveoli (CA), yolk granule (YG; all vitellogenic substages), final maturation (FM; also described as germinal vesicle migration, yolk coalescence, and germinal vesicle breakdown), and hydrated (HD) (fig. 3). Because exact ages of POFs remain unknown for California halibut, we assigned relative POF ages based on descriptions for northern anchovy (*Engraulis mordax*), another batch spawning species that releases pelagic eggs and occupies similar latitudes (Hunter and Goldberg 1980; Hunter and Macewicz 1985; fig. 3). We categorized POFs as “new” and assumed that they indicated spawning activity within 24 hours of capture if they were relatively large, irregularly shaped, and showed little or no signs of degradation (e.g., expansive lumen, clearly recognizable and intact granulosa epithelial layer). We identified POFs as “old”, representing a spawning event that had taken place more than 24 hours prior to capture, if they appeared shrunken with a narrowed lumen and degraded granulosa.

Spawning Season and Daily Spawning Fraction

We defined the duration of the spawning season as the number of consecutive weeks in which two-thirds of our samples were identified as spawning capable (i.e.,

fish possessing tertiary vitellogenic oocytes) or actively spawning (i.e., those possessing hydrated oocytes and/or POFs of any age). We calculated daily spawning fraction (S) based on the proportion of females containing 1) hydrated oocytes and 2) new POFs. Calculating two S estimates allowed us to assess the extent to which this reproductive metric may vary based on the specific spawning marker used. For populations with low spawning synchronicity and/or broad spawning seasons, it is common to apply a correction to daily spawning fractions using the equation: $S = 24 * S/D$, where D is the duration (hr) of the spawning marker (Hunter and Macewicz 1985; Murua et al. 2003; Kurita et al. 2011; Lowerre-Barbieri et al. 2011). Additionally, spawning marker durations are known to vary with temperature (e.g., Ganas et al. 2007a; Kurita et al. 2011). Without information about the duration of spawning markers for California halibut, we assumed temperature-dependent relationships developed for Japanese flounder, *Paralichthys olivaceus* (Kurita et al. 2011). Like California halibut, Japanese flounder are multiple-batch spawners that exhibit indeterminate fecundity. They also experience temperatures similar to central California halibut and display comparable spawning seasons. Thus, we used the following relationships to estimate temperature-dependent durations of spawning markers for California halibut: $D = 59.4 * e^{-0.122T}$ for hydrated oocytes and $D = 62.9 * e^{-0.118T}$ for new POFs (Kurita et al. 2011), where T was mean daily sea surface temperature ($^{\circ}\text{C}$) for each capture date. Sea surface temperatures were obtained from the National Oceanic and Atmospheric Administration’s National Data Buoy Center (Station 46114; <https://www.ndbc.noaa.gov/>). Bottom temperature data were not available for the dates and locations of our samples. Using temperature-dependent durations for each spawning marker, we calculated corrected S for all days in which we collected three or more fish. We estimated interspawning interval (ISI), which represents the number of days between spawning events, by taking the reciprocal of \bar{S} (Wootton et al. 1978; Murua et al. 2003; Lowerre-Barbieri et al. 2011). Finally, we calculated spawning frequency (F), defined as the number of spawning events per female per season, by dividing the duration of the spawning season by ISI . Due to sample size limitations in 2012, spawning season, S , ISI , and F were estimated for 2013 only.

Batch Fecundity

For species with indeterminate fecundity, the number of eggs produced is not fixed prior to the onset of spawning (Hunter et al. 1985, Hunter et al. 1992, and Ganas 2013). Instead, primary growth oocytes continue to be recruited to the supply of secondary growth oocytes throughout the spawning season. Therefore, the



Figure 3. Oocyte developmental stages for an actively spawning California halibut female (PN: perinucleolar; CA: cortical alveoli; YG: yolk granule (includes all substages of vitellogenesis); FM: final maturation (including germinal vesicle migration, yolk coalescence, and germinal vesicle breakdown substages); HD: hydrated). Postovulatory follicles (POFs, new and old) are also indicated.

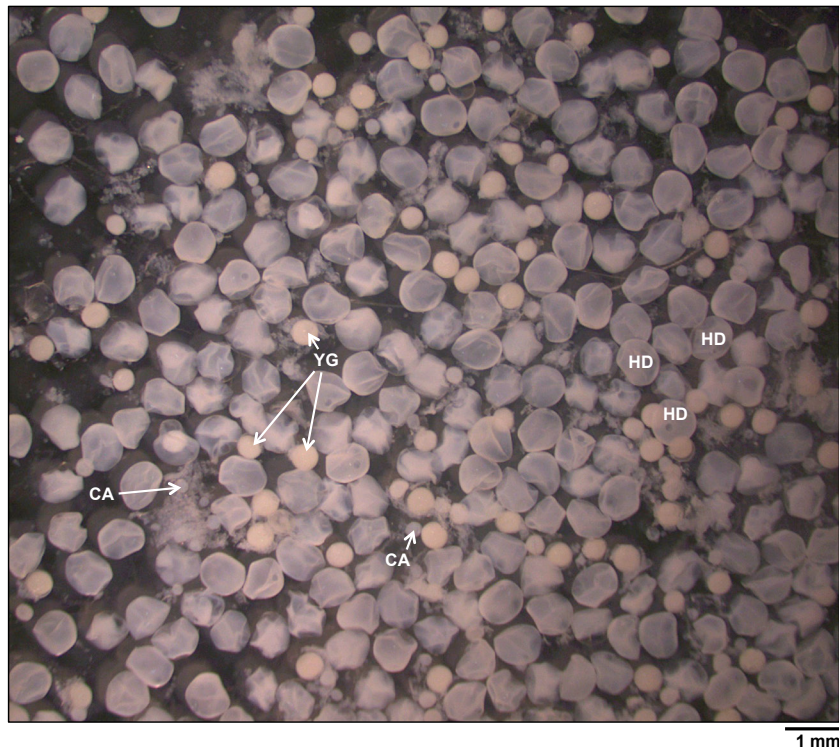


Figure 4. Whole mount image of preserved ovarian tissue from a California halibut female in the late hydration subphase of spawning. Oocyte developmental stages (CA: cortical alveoli; YG: yolk granule (includes all substages of vitellogenesis); HD: hydrated) were identified based on characteristics (e.g., relative size, coloration) observed during histological analyses. There is no final maturation (FM) stage for the late hydration subphase.

TABLE 1
Criteria used to identify subphases of actively spawning California halibut females. The most advanced stage (MAS₁) and second most stage (MAS₂) of oocyte development are listed, along with the incidence and relative age of postovulatory follicles (POFs; NP = not present) and sample sizes (n). Oocyte developmental stages, in order from least to most advanced, are cortical alveoli (CA), yolk granule (YG), final maturation (FM), and hydrated (HD).

Actively Spawning Subphase	MAS ₁	MAS ₂	POF	n
Early Hydration	HD	FM	NP	6
Late Hydration	HD	YG	NP	17
Spawning in Progress	HD	FM or YG	New	16
Recently Spawning	FM or YG	YG or CA	New or Old	1

potential annual fecundity for an individual is a product of the spawning frequency and number of eggs released per spawning event (i.e., batch fecundity). When viewing whole mounts, it can be difficult to differentiate types of secondary growth oocytes that make up distinct batches, especially when there are no clear differences in mean oocyte diameter (Lesyna and Barnes 2016). Thus, we counted only hydrated oocytes from whole mount samples because they were easily distinguishable from earlier stages of oocyte development based upon their large size, translucent color, irregular shape, and obvious presence of an oil globule (fig. 4).

We estimated batch fecundity for actively spawning California halibut using gravimetric and hydrated oocyte methods (Bagenal 1978; Hunter and Goldberg 1980; Hunter et al. 1985). We blotted and weighed ovaries. We then separated ovarian tissue from the ovarian wall, weighed the ovarian wall (0.1 g), and subtracted its mass from that of the preserved ovary. Doing so yielded a more accurate measure of total ovarian tissue (g), from which we removed five subsamples (0.3 to 0.5 g). We counted the number of hydrated oocytes in each subsample and multiplied mean egg density (number of eggs per gram) by the total ovarian tissue mass to estimate absolute batch fecundity (Hunter and Goldberg 1980; Macewicz and Hunter 1993). We then divided absolute batch fecundity by somatic body weight (i.e., total body weight minus ovary mass) to estimate relative batch fecundity. This procedure for estimating batch fecundity was suitable for the ovaries (n = 14) that contained a thorough mixture of all oocyte developmental stages. However, some females (n = 26) exhibited an accumulation of hydrated eggs in the oviduct and/or ovarian lumen. This resulted in at least one section of the ovary that was made up exclusively of hydrated eggs and another that consisted of an assortment of all developmental stages. To appropriately subsample these fish, we separated “hydrated-only” sections from the remaining ovarian tissue. We then subsampled “hydrated-only” and

mixed oocyte sections as previously described. Mean egg densities for each section were multiplied by their respective total masses and then added together to estimate batch fecundity for these fish, which were captured after spawning had already been initiated. Finally, we quantified the log-linear relationship between batch fecundity and fork length and used an analysis of variance (ANOVA) to test for differences in mean batch fecundity by age and year (v3.4.2, R Core Team 2017). We did not have sufficient data to test the relationship between body weight and batch fecundity.

Annual Fecundity

We calculated both absolute and relative annual fecundity for central California halibut. Each estimate involved multiplying batch fecundity by F, which varied based on the spawning marker used to calculate S and ISI (Murua et al. 2003).

RESULTS

We collected a total of 205 California halibut females between 2012 and 2013. Sampling efforts resulted in the collection of 40 fish on 31 different days in 2012 and 165 fish on 57 different days in 2013. Fork lengths measured from 532 to 1110 mm (848 ± 105 SD), ages ranged from 3 to 19 yr (8.2 ± 2.2 SD), and capture depths were all less than 40 m (16 ± 6 SD). Actively spawning females (all subphases) were collected at depths of 18.1 ± 5.6 (SD) m. We conducted histological analyses on all samples, but four fish could not be aged due to missing or unreadable otoliths. We identified four subphases of actively spawning fish: “early hydration”, “late hydration”, “spawning in progress”, and “recently spawned” (table 1). Ovaries with both hydrated eggs and oocytes in the final maturation stage of development (FM or germinal vesicle migration [GVM]) were identified as being in the early hydration subphase at the time of capture. We classified fish as being in the late hydration subphase once all FM oocytes had begun to hydrate, resulting in yolk granule as the second most advanced stage of oocyte development. Ovaries in early and late hydration subphases did not possess POFs. New POFs were only observed in spawning in progress and recently spawned fish. Those with both hydrated oocytes and new POFs were termed spawning in progress. As soon as hydrated oocytes were no longer detected, but new and/or old POFs remained, fish were categorized as having recently spawned.

Spawning Season and Daily Spawning Fraction

We collected three or more adult females on only one sampling day in 2012; therefore, we were unable to calculate reproductive metrics for that year. In 2013, We collected three or more fish on 26 different days. More

TABLE 2
 Numbers of adult California halibut females sampled, by reproductive phase and week (2013 only).
 Sample sizes (n) and weekly portions of spawning fish (i.e., spawning capable and actively spawning phases) are also listed.
 The area in gray represents the supposed duration of the summer spawning season.

Week	Developing	Spawning Capable	Actively Spawning	Regressing	Regenerating	n	Proportion Spawning
23		1				1	
24	1	1			1	3	0.33
25	1		4			5	0.80
26		2	3			5	1.00
27	1	5	3	1		10	0.80
28		11	2			13	1.00
29	1	11	5			17	0.94
30	1	8	5			14	0.93
31	2	13	9			24	0.92
32	2	9	8			19	0.89
33		12	5			17	1.00
34	1	3	2		1	7	0.71
35	1	7	9	2		19	0.84
36	1	3				4	0.75
37							
39							
40							
41	2	1		2		5	0.20
42							
43					1	1	
44							
45							
46							
47			1			1	

than two-thirds of fish sampled every week between June 22 and September 2 were identified as spawning capable or actively spawning (table 2). Thus, we supposed that the spawning season lasted approximately 10 weeks in 2013. However, considerably low catches in both commercial and recreational fisheries restricted our ability to sample prior to mid-June (n = 4) and after the first week of September (n = 7) (fig. 1). Mean *S* based on proportions of fish with hydrated oocytes was 0.78 ± 0.63 , whereas *S* based on proportions of fish with new POFs equaled 0.38 ± 0.37 (n = 25) (Supplementary tables 1 and 2). Thus, *ISI* estimates ($1/S$) were 1.28 d and 2.65 d using hydrated oocytes and new POFs as spawning markers, respectively. When dividing the duration of the spawning season by *ISI*, we estimated mean *F* to be between 26.4 (hydrated oocytes) and 54.9 (new POFs) batches per female per season.

We assessed biweekly proportions of each reproductive phase in 2013 (n = 14 [165 fish]) and found that proportions of actively spawning females were relatively constant (0.36 ± 0.07 SD) throughout the summer (fig 5). Spawning capable (0.53 ± 0.33 SD) and developing (0.11 ± 0.13 SD) fish were present throughout the sampling period, but proportions of these fish displayed greater variation through time. We encountered few regenerating females (i.e., resting) throughout the study period. Females in the regenerating phase were found in mid-June, at the end of August, and in mid-October.

Two-thirds of these occurrences were outside of what we considered to be the summer spawning season. We also observed a relatively large proportion of regressing (i.e., spent) females in early fall (0.40 at the end of September). Although sample sizes were limited, decreased landings of California halibut in nearshore waters, combined with increased proportions of regressing individuals, suggests a cessation of spawning activity in September and October. Small proportions of regressing and regenerating individuals were found within the spawning season identified (mid to late June and mid-August), suggesting some degree of asynchronicity in spawning activity among individual California halibut.

Batch Fecundity

We initially estimated batch fecundity for 40 actively spawning California halibut females (8 from 2012 and 32 from 2013) measuring 680 to 924 mm fork length (table 3). Of all four actively spawning subphases, we found that the late hydration subphase accounted for the greatest minimum (198,608), mean ($597,445 \pm 318,419$ SD; n = 17) and maximum (1,474,584) estimates of batch fecundity. We considered this particular spawning subphase to be the ideal target for assessing reproductive output of California halibut because ovaries in the late hydration subphase would possess a complete batch of eggs that had fully hydrated, but had not yet been released. This was evidenced by the presence of hydrated

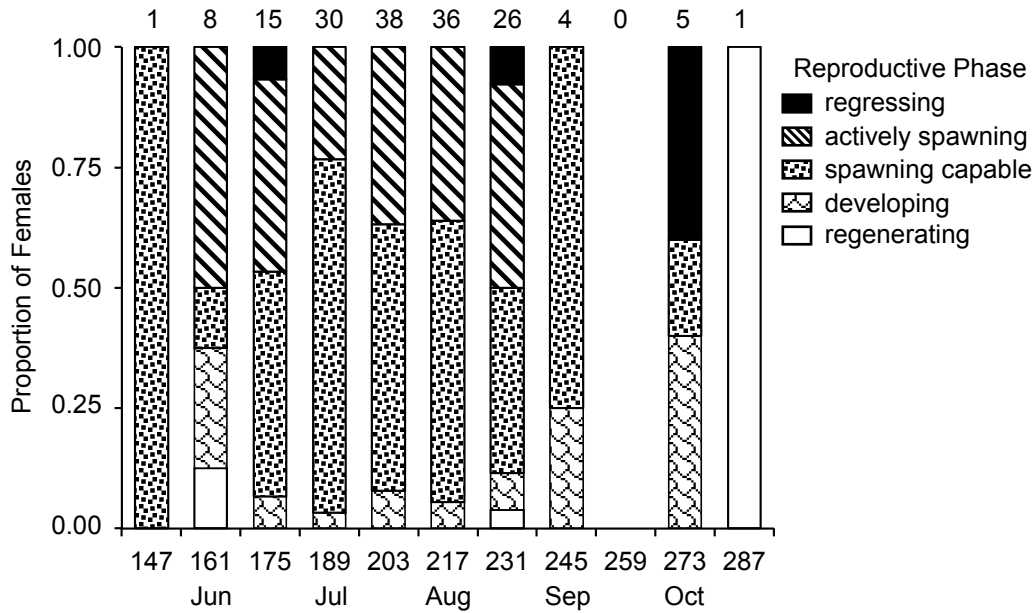


Figure 5. Biweekly proportions of California halibut, by reproductive phase and Julian day (2013 only). Sample sizes are indicated above each bar and the approximate starts of each month are also shown. One additional mature fish was sampled in late November (not shown).

oocytes, absence of the next most advanced stage of oocyte development (i.e., FM), and lack of POFs. Batch fecundity for females in the early hydration subphase would be underestimated because only a portion of the complete spawning batch of eggs would have been hydrated at the time of capture (i.e., FM oocytes would eventually hydrate and be released along with co-occurring HD oocytes). Batch fecundity would also be underestimated for females found to be spawning-in-progress given the prevalence of spawning markers (i.e., new and old POFs), which signify the partial release of HD oocytes—either through spawning or handling. Recently spawned fish would possess POFs, but no hydrated eggs with which to estimate batch fecundity.

We found a log-linear relationship between fork length and batch fecundity ($\log BF = 5.91(\log FL) - 26.63$; $R_{adj} = 0.429$, $F_{0.1(2), 1,15} = 13.03$, $p < 0.01$) for females captured in the late hydration subphase of spawning (fig. 6A). An ANOVA indicated that there were no signifi-

cant differences in batch fecundity by age ($F_{0.1(6), 1,14} = 0.86$, $p = 0.37$). This was due to substantial variability in batch fecundity and because all females in the late hydration subphase were between 6 and 9 yr of age (fig. 6B). There was no difference in batch fecundity between 2012 and 2013 ($F_{0.1(2), 14} = 0.92$, $p = 0.36$). Thus, we pooled year-specific batch fecundity data for California halibut. Relative batch fecundity for fish in the late hydration subphase was 84 ± 46 (SD) eggs per gram ($n = 8$).

Annual Fecundity

We estimated absolute annual fecundity for central California halibut to be between 5.2×10^6 and 3.8×10^7 eggs per female per season (mean = $32,798,772 \pm 18,085,548$ SD) using new POFs as the spawning marker to calculate *S*, *ISI*, and *F*. Using hydrated oocytes as the designated spawning marker, the range for absolute annual fecundity was 1.1×10^7 to 8.1×10^7 eggs per female per season (mean = $15,504,874 \pm 8,549,532$ SD). Mean relative annual fecundity ranged from 867 to 4,226 eggs per gram ($2,036 \pm 1,125$ SD) using the new POF spawning marker and 1,835 to 8,940 eggs per gram ($4,307 \pm 2,380$ SD) using the hydrated oocyte spawning marker.

DISCUSSION

This study represents an initial investigation into various reproductive tactics of California halibut. Previous studies involved estimating length- and age-at-maturity (Love and Brooks 1990; Lesyna and Barnes 2016), dis-

TABLE 3
 Estimates of batch fecundity (number of eggs)
 for California halibut, by actively spawning subphase.
 Sample sizes (n) are also shown.

Actively Spawning Subphase	Min	Mean (\pm SD)	Max	n
Early Hydration	93,394	505,058 \pm 222,273	722,791	6
Late Hydration	198,608	597,445 \pm 318,419	1,474,584	17
Spawning in Progress	39,681	400,533 \pm 231,748	908,587	17
Recently Spawned	N/A	N/A	N/A	0
All Subphases	39,681	499,899 \pm 280,035	1,474,584	40

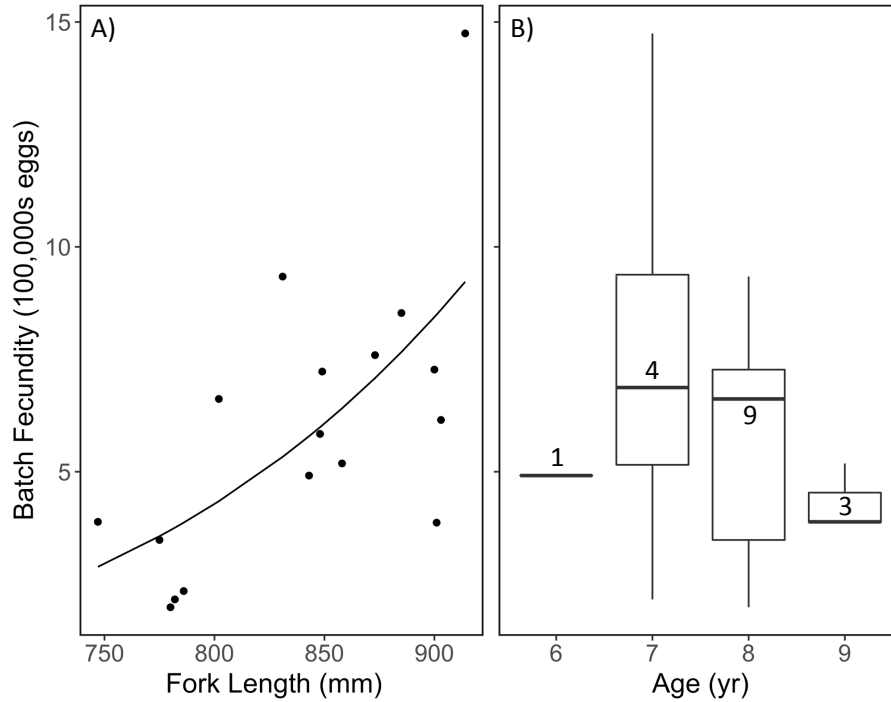


Figure 6. Estimates of batch fecundity (100,000s hydrated eggs) for California halibut captured in the late hydration subphase of spawning, by A) fork length (mm) and B) age (yr). The predicted log-linear relationship between fork length and batch fecundity is shown. Numbers indicate sample sizes for each age (yr).

cussions of spawning seasonality (Barnes et al. 2016), and measures of reproductive output from fish held in captivity. We combined estimates of spawning duration, S , ISI , F , and batch fecundity to assess annual reproductive output for this multiple-batch spawning species. Here, we have proposed an approximate spawning season of 10 weeks (June to September) for central California halibut. Mean S ranged from 0.38 to 0.78, depending upon the specific spawning marker (i.e., hydrated oocytes or new POFs). This resulted in variable estimates of ISI and F , which ranged from 1.3 to 2.7 d and 26 to 55 spawning batches per female per season, respectively. Even though we assessed a narrow range of sizes, we found that batch fecundity for California halibut in the late hydration subphase of spawning significantly increased with fork length. Mean batch fecundity was $597,445 \pm 318,419$ eggs per female (relative batch fecundity = 84 ± 46 eggs per gram). When we scaled batch fecundity by F , we found that annual fecundity for central California halibut ranged from 5.2×10^6 to 8.1×10^7 eggs per female per season. Each of these reproductive metrics are similar to those reported for other batch spawning species with indeterminate fecundity (e.g., spawning duration, Minami and Tanaka 1992; ISI , Lefebvre et al. 2016; relative batch fecundity, Almatar et al. 2004).

We postulated that the spawning season for central California halibut was relatively short and restricted to the summer months. We observed spawning capable and

actively spawning females from the end of June to the beginning of September. A study of captive fish from southern California showed spawning activity between February and mid-May and mid-May through September, depending upon water temperatures and photoperiod (Caddell et al. 1990). Love and Brooks (1990) also observed spring and summer spawning from analyzing fish catches in southern California, though the incidence of California halibut larvae during CalCOFI ichthyoplankton surveys suggests that spawning activity may occur year-round south of Point Conception (Barnes et al. 2015). We were unable to assess spawning activity for central California halibut in winter or spring because of considerably reduced or non-existent landings during this time. The apparent regional differences in spawning seasons may be due to the limited timeframe of our sampling. However, given that spawning seasons for other paralicthyid flatfishes become more protracted as latitude decreases (e.g., Minami and Tanaka 1992; Ganas et al. 2015), we believe it is plausible that central California halibut undergo shorter spawning durations relative to southern California conspecifics.

In addition to a potentially brief spawning season, we found fairly short $ISIs$. We estimated that, on average, wild-caught fish from central California spawned once every 1.3 to 2.7 d. Captive fish held under “natural conditions” in southern California were reported to spawn once every 7.0 to 14.0 d (Caddell et al. 1990; excluding

data from 1986 to 1987, when severe bacterial infections were found). We acknowledge that using proxies such as stage descriptions for POFs of northern anchovy (Hunter et al. 1985) and temperature-dependent spawning marker durations obtained from Japanese flounder (Kurita et al. 2011) may be inappropriate for California halibut due to different life history strategies, metabolic rates, and other unidentified factors that may lead to variable degradation rates. For instance, incorrectly assuming that oocyte hydration was completed within 24 hr or that “new” POFs were generated less than one day prior to capture would lead to artificially high estimates of S , deceptively short ISI , and overestimated F . We also do not yet understand which spawning marker is most appropriate for use in calculations of various reproductive metrics for California halibut. Finally, the use of sea surface temperature may impact our estimates of spawning marker duration for California halibut, which is generally considered a bottom-associated species. S , ISI , and F values reported here could be improved upon by detailed stage descriptions and temperature-dependent spawning marker durations that are specific to California halibut.

Although our ISI estimates were assumed to be constant throughout the proposed spawning season, this is unrealistic given the temporal changes in spawning activity reported for California halibut held in captivity. Caddell et al. (1990) found sporadic spawning at the start of each season, increased frequencies (i.e., to daily or once every other day) with increasing temperature and photoperiod, and noticeable decreases toward the end of the season (Caddell et al. 1990). In addition to assuming constant ISI through time, we necessarily made the assumption that spawning duration was equal among all fish. Yet individual spawning periods are often much shorter than the timeframe over which spawning activity is observed at the population level (Rijnsdorp et al. 2015). Given the temporal overlap among developing, spawning capable, and regressing females, we assert that there is some degree of asynchronicity in spawning duration for California halibut. While some fish may spawn from beginning to end, it is probable that a number of fish do not spawn until well into the season. A portion of the population may also enter the regressing phase before a particular season comes to a close (Kjesbu et al. 1996; Wright and Trippel 2009). Variations in spawning frequency and duration can be due to size, age, or local environmental conditions (Lambert 1990; Hutchings and Myers 1993; Trippel et al. 1997). For example, smaller (younger) individuals tend to exhibit shorter, more delayed spawning periods and less frequent spawning than larger (older) conspecifics (Ganias et al. 2007b; Klibansky and Scharf 2013; Lefebvre et al. 2016). These demographic effects on various reproductive metrics can substantially alter estimates of reproductive output

for individual fish, especially if population means (e.g., spawning duration, S , ISI , F) are extrapolated outside the range of sizes or ages sampled.

Another important consideration when assessing S , ISI , and F for central California halibut is the possibility that this population feeds and spawns nearshore during the summer and moves offshore or southward for the remainder of the year. We believe that these seasonal migrations are plausible based on limited commercial and recreational catches north of Point Conception in late fall, winter, and early spring. If central California halibut remain nearshore only to feed and spawn in summer, samples may have been obtained from spawning aggregations rather than mixed populations of spawning and non-spawning fish, which would inflate estimates of spawning activity. A year-round movement study would allow for an evaluation of our hypothesis that central California halibut undergo seasonal migrations. If paired with reproductive analyses, movement data could elucidate whether or not there is spatial separation between spawning and non-spawning fish and support or refute our assertion that spawning is restricted to the summer months off central California. Despite these caveats, however, our estimates of ISI fall well within the range of those reported for other flatfish species (typically 1 to 4 days; Rijnsdorp et al. 2015). Many paralichthyids, including Japanese flounder (*Paralichthys olivaceus*; Kurita et al. 2011), Pacific sanddab (*Citharichthys sordidus*; Lefebvre et al. 2016), and longfin sanddab (*Citharichthys xanthostigma*; Goldberg 1982) spawn on daily time steps in temperate regions. If California halibut spawn as we have described, the combination of brief spawning seasons and short $ISIs$ would suggest a unique reproductive tactic north of Point Conception. This would involve decreasing the time between spawning events when favorable conditions (e.g., warmer temperatures, longer photoperiods, and increased food availability) are constrained to a few months, as opposed to southern California and Mexico, when conditions for spawning are favorable nearly year-round (Caddell et al. 1990; Barnes et al. 2015).

As with many of the more detailed aspects of their reproductive biology, diel patterns in spawning behavior (e.g., the exact time of day that eggs are released) remain unknown for California halibut. When this is the case for other multiple-batch spawners that exhibit indeterminate fecundity, we recommend the use of histological analyses to identify subphases of actively spawning females. Doing so will enable the selection of the late hydration subphase, which is most appropriate for estimating batch fecundity using the hydrated oocyte method (Hunter et al. 1985). Any other subphase to estimate batch fecundity based on hydrated oocytes would result in underestimations due to incomplete hydration

or partial spawning. However, focusing on a small subset of adult fish, such as those in the late hydration sub-phase, leads to a considerable reduction in sample sizes.

Because of small sample sizes from a narrow range of fork lengths (747 to 914 mm), we consider our fecundity estimates to be preliminary. Although these estimates pertain to the sizes of California halibut most commonly caught in commercial and recreational fisheries north of Point Conception, they do not embody the full extent of fish that are considered sexually mature (i.e., ≥ 466 mm; Lesyna and Barnes 2016). Because spawning duration, S , ISI , F , and batch fecundity are known to vary among size classes of individuals within the same species (e.g., *Citharichthys sordidus*, Lefebvre et al. 2016), our estimates would benefit from additional sampling of both smaller and larger adults.

Batch fecundities were similar between our study ($597,445 \pm 318,419$; $n = 17$) and the only other estimate for the species (approximately 522,000; $n = 7$, Caddell et al. 1990). However, differences in F led to a substantial disparity in annual fecundity. We found that spawning occurred 26 to 55 times per female per season, north of Point Conception. Estimates of F for captive fish from Southern California were reported to be between 5 and 13 (Caddell et al. 1990). Contrasting F values resulted in annual fecundities that were substantially greater for central California halibut (5.2×10^6 to 8.1×10^7 eggs per female per season) when compared to captive females from Southern California (6.6×10^6 eggs per female per season). Notably, reproductive estimates obtained from fish held in captivity may be conservative due to physiological limitations within an artificial environment. However, the fish we sampled were also larger (863 ± 67 mm) than those from the captive study (means ranged from 505 to 589 mm). Because we observed a significant log-linear relationship between fork length and batch fecundity even within a narrow range of sizes, additional fecundity estimates from smaller central California halibut would aid in regional comparisons of fecundity.

We have provided baseline information that improves our understanding about the reproduction tactics of California halibut: a prolific, multiple-batch spawner with indeterminate fecundity. However, there is still much to learn about the spawning activities of this commercially and recreationally important species. Because our analyses were restricted to the narrow range of sizes and ages commonly caught in recreational and commercial fisheries, we were unable to effectively quantify relationships among spawning season, S , ISI , F , or batch fecundity and length, weight, or age. This would be a worthwhile area of study in the future. Continued data collection on the spawning activities of California halibut with similar demographic characteristics would also be valu-

able because of the small sample sizes that were available during this study and because each of the reproductive metrics we have presented may change under different environmental or ecological conditions (Armstrong and Witthames 2012). Finally, a thorough investigation into the relationships between reproductive output and environmental variation would aid in our understanding about drivers of California halibut recruitment, thereby improving data inputs for stock assessment models pertaining to this species.

ACKNOWLEDGMENTS

Financial and logistical support for this project was provided by Moss Landing Marine Laboratories (MLML), San Jose State University, and California Sea Grant. We would like to thank Scott L. Hamilton (MLML), James T. Harvey (MLML), and Paul N. Reilly (California Department of Fish and Wildlife) for providing substantial guidance throughout the development, implementation, and synthesis of this research. Our sincere gratitude goes to the California Recreational Fisheries Survey (California Fish and Wildlife), Capitola Boat and Bait, H&H Fresh Fish, and many individual commercial and recreational fishers for their help with sample collections. We received additional field- and lab-based assistance from Alexandra Aines, Daniel Anaya, Kaitlyn Beck, Adam Chorazyczewski, Caitrin Doles, Hallie Heath, Kristine Lesyna, Rhiannon McCollough, Matt Michie, Ken Oda, David Osorio, Elizabeth Schurig, Nikki Siababa, Aaron Sloan, Kenji Soto, and Travis Tanaka.

LITERATURE CITED

- Allen, M. J. 1988. The biological environment of the California halibut, *Paralichthys californicus*. Pages 7–30. In C. W. Haugen, editor. The California halibut, *Paralichthys californicus*, resource and fisheries. California Department of Fish and Game. Fish Bull. 174.
- Almatar, S. M., K. P. Lone, T. S. Abu-Rezq, and A. A. Yousef. 2004. Spawning frequency, fecundity, egg weight and spawning type of silver pomfret, *Pampus argenteus*, (Euphrasen) (Stromateidae), in Kuwait waters. J. Appl. Ichthyol. 20: 176–188.
- Armstrong, M. J., and P. R. Witthames. 2012. Developments in understanding of fecundity of fish stocks in relation to egg production methods for estimating spawning stock biomass. Fish. Res. 117–118:35–47.
- Bagenal, T. B. 1978. Aspects of fish fecundity. Pages 75–101. In S. D. Gerking, editor. Ecology of freshwater fish production. Blackwell. London, England.
- Barnes, C. L., R. M. Starr, and P. N. Reilly. 2015. Growth, mortality, and reproductive seasonality of California halibut (*Paralichthys californicus*): a biogeographic approach. Calif. Coop. Oceanic Fish. Invest. Rep. 56:110–118.
- Caddell, S. M., D. M. Gadomski, and L. R. Abbott. 1990. Induced spawning of the California halibut, *Paralichthys californicus*, (Pisces: Paralichthyidae) under artificial and natural conditions. Pages 175–198. In C. W. Haugen, editor. The California halibut, *Paralichthys californicus*, resource and fisheries. California Department of Fish and Game. Fish Bull. 174.
- Committee of Age-Reading Experts (CARE). 2006. Manual on generalized age determination: procedures for groundfish. Pacific States Marine Fisheries Commission. 57 pp.
- Fitzhugh, G. R., K. W. Shertzer, G. T. Kellison, and D. M. Wyanski. 2012. Review of size- and age-dependence in batch spawning: implications for stock assessment of fish species exhibiting indeterminate fecundity. Fish. Bull. 110:413–425.

- Frey, H. W. 1971. California's living marine resources and their utilization. Calif. Dept. Fish Game. Sacramento, California. 148 pp.
- Ganias, K., S. Somarakis, A. Machias, and A. Theodorou. 2004. Pattern of oocyte development and batch fecundity in the Mediterranean sardine. *Fish. Res.* 67:13–23.
- Ganias, K., C. Nunes, and Y. Stratoudakis. 2007a. Degeneration of postovulatory follicles in the Iberian sardine *Sardina pilchardus*: structural changes and factors affecting resorption. *Fish. Bull.* 105:131–139.
- Ganias, K., S. Somarakis, C. Koutsikopoulos, and A. Machias. 2007b. Factors affecting the spawning period of sardine in two highly oligotrophic seas. *Mar. Biol.* 151:1559–1569.
- Ganias, K. 2013. Determining the indeterminate: evolving concepts and methods on the assessment of the fecundity pattern of fishes. *Fish. Res.* 138:23–30.
- Ganias, K., S. K. Lowerre-Barbieri, and W. Cooper. 2015. Understanding the determinate–indeterminate fecundity dichotomy in fish populations using a temperature dependent oocyte growth model. *J. Sea Res.* 95:1–10.
- Goldberg, S. R. 1982. Seasonal spawning cycle of the longfin sanddab, *Citharichthys xanhostigma* (Bothidae). *Fish. Bull.* 80:906–907.
- Haaker, P. L. 1975. The biology of the California halibut, *Paralichthys californicus* (Ayres) in Anaheim Bay. Pages 137–151. *In* E. D. Lane and C. W. Hill, editors. *The Marine Resources of Anaheim Bay*. California Department of Fish and Game. Fish Bull. 165.
- Haugen, C. W. 1990. The California halibut, *Paralichthys californicus*. Fish Bull. 174. 475 pp.
- Hunter, J. R., and S. R. Goldberg. 1980. Spawning incidence and batch fecundity in northern anchovy, *Engraulis mordax*. United States Department of Commerce. Fishery Bull. 77:641–652.
- Hunter, J. R., and B. J. Macewicz. 1980. Sexual maturity, batch fecundity, spawning frequency and temporal pattern in the northern anchovy, *Engraulis mordax*, during the 1979 spawning season. *Calif. Coop. Oceanic Fish. Invest. Rep.* 21:139–149.
- Hunter, J. R., and B. J. Macewicz. 1985. Rates of atresia of the ovary of captive and wild northern anchovy, *Engraulis mordax*. United States Department of Commerce. Fishery Bull. 83:119–136.
- Hunter, J. R., N. C. H. Lo, and R. J. H. Leong. 1985. Batch fecundity in multiple spawning fishes. *Nat. Mar. Fish. Techn. Rep.* 8547:67–77.
- Hunter, J. R., B. J. Macewicz, N. C. H. Lo, and C. A. Kimbrell. 1992. Fecundity, spawning, and maturity of female Dover Sole, *Microstomus pacificus*, with and evaluation of assumptions and precision. United States Department of Commerce. Fishery Bull. 90:101–128.
- Hutchings, J. A., and R. A. Myers. 1993. Effect of age on the seasonality of maturation and spawning of Atlantic Cod, *Gadus morhua*, in the Northwest Atlantic. *Can. J. Fish. Aquat. Sci.* 50:2468–2474.
- Kjesbu, O. S., H. Kyrvi, and B. Norberg. 1996. Oocyte size and structure in relation to blood plasma steroid hormones in individually monitored, spawning Atlantic cod. *J. Fish Biol.* 49:1197–1215.
- Klibansky, N., and F. S. Scharf. 2013. Size-dependent and temporal variability in batch number and fecundity of Red Porgy, a protogynous, indeterminate spawner, in the U.S. South Atlantic. *Mar. Coast. Fish. Dyn., Mgmt., and Ecosys. Sci.* 5:39–52.
- Kurita, Y., Y. Fujinami, and M. Amano. 2011. The effect of temperature on the duration of spawning marker—migratory-nucleus and hydrated oocytes and postovulatory follicles—in the multiple-batch spawner Japanese flounder (*Paralichthys olivaceus*). United States Department of Commerce. Fishery Bull. 109:79–89.
- Lambert, T. C. 1990. The effect of population structure on recruitment in herring. *J. Cons. Intern. L'Explor. Mer.* 47: 249–255.
- Lavenberg, R. J., G. E. McGowen, A. E. Jahn, J. H. Petersen, and T. C. Sciarrotta. 1986. Abundance of southern California nearshore ichthyoplankton: 1978–1984. *Calif. Coop. Oceanic Fish. Invest. Rep.* 27:53–64.
- Lefebvre, L. S., A. M. Payne, and J. C. Field. 2016. Reproductive dynamics of Pacific Sanddab, *Citharichthys sordidus*, off the central coast of California. *J. Sea Res.* 107:100–111.
- Lesyna, K. M., and C. L. Barnes. 2016. Assessment of length- and age-at-maturity for California halibut (*Paralichthys californicus*), including a histologically-based maturity staging system. *Calif. Dept. Fish Game.* 102(3):79–100.
- Lowerre-Barbieri, S. K., K. Ganias, F. Saborido-Rey, and H. Murua. 2011. Reproductive timing in marine fishes: variability, temporal scales, and methods. *Mar. Coast. Fish.: Dyn., Mgmt., Ecosy. Sci.* 3:71–91.
- Love, M. S., and A. Brooks. 1990. Size and age at first maturity of the California halibut, *Paralichthys californicus*, in the Southern California Bight. Pages 167–174. *In* C. W. Haugen, editor. *The California halibut, Paralichthys californicus*, resource and fisheries. California Department of Fish and Game. Fish Bull. 174.
- Luna, L. G. 1968. Manual of histologic staining methods of the armed forces institute of pathology, third edition. McGraw-Hill. New York, NY. 258 pp.
- Macewicz, H. J., and J. R. Hunter. 1993. Spawning frequency and batch fecundity of jack mackerel, *Tachurus symmetricus*, off California during 1991. *Calif. Coop. Oceanic Fish. Invest. Rep.* 34:112–121.
- MacNair, L. S., M. L. Domeier, and C. S. Y. Chun. 2001. Age, growth, and mortality of California halibut, *Paralichthys californicus*, along southern and central California. *Fish. Bull.* 99(4):588–600.
- Minami, T., and M. Tanaka. 1992. Life history cycles in flatfish from the northwestern Pacific, with particular reference to their early life histories. *Netherlands J. Sea Res.* 29:35–48.
- Murua, H., and F. Saborido-Rey. 2003. Female reproductive strategies of marine fish species of the North Atlantic. *J. Northw. Atl. Fish. Sci.* 33:23–31.
- Murua, H., G. Kraus, F. Saborido-Rey, P. R. Witthames, A. Thorsen, and S. Junquera. 2003. Procedures to estimate fecundity of marine fish species in relation to their reproductive strategy. *J. Northw. Atl. Fish. Sci.* 33:33–54.
- Pecquerie, L., P. Petitgas, and S.A.L.M. Kooijman. 2009. Modeling fish growth and reproduction in the context of the dynamic energy budget theory to predict environmental impact on anchovy spawning duration. *J. Sea Res.* 62:93–105.
- R Core Team. R: A language and environment for statistical computing. R Foundation for Statistical Computing. Vienna, Austria. 2017. <http://www.R-project.org/>.
- Rijnsdorp, A. D., C. J. G. van Damme, and P. R. Witthames. 2015. Ecology of reproduction. Pages 101–131. *In* R. N. Gibson, R. D. M. Nash, A. J. Gefen, and H. W. van der Veer, editors. *Flatfishes: Biology and Exploitation* (Second Edition). Fisheries and Aquatic Research Series 16. John Wiley and Sons Ltd. Chichester, United Kingdom.
- Trippel, E. A., O. S. Kjesbu, and P. Solemdal. 1997. Effects of adult age and size structure on reproductive output in marine fishes. *In* Early life history and recruitment in fish populations. R. C. Chambers and E. A. Trippel (eds). Chapman and Hall. London. 31–62.
- Wright, P. J., and E. A. Trippel. 2009. Fishery-induced demographic changes in the timing of spawning: consequences for reproductive success. *Fish. Fish.* 10(3):283–304.
- Wootton, R. J., G. W. Evans, and L. A. Mills. 1978. Annual cycle in female three-spined sticklebacks (*Gasterosteus aculeatus* L.) from an upland and lowland population. *J. Fish Biol.* 12:331–343.

SUPPLEMENTARY TABLE 1

Numbers of California halibut females sampled (n), proportions of individuals with hydrated oocytes, mean daily sea surface temperatures (T, °C), temperature-dependent durations of hydrated oocytes, and corrected spawning fractions (S) by sampling date (2013 only). Temperature data were obtained from the National Oceanic and Atmospheric Administration's National Data Buoy Center (Stn 46114). Temperature-dependent durations (D, hr) of hydrated oocytes were calculated using the equation $D = 59.4 * e^{-0.122T}$ (*Paralichthys olivaceus*, Kurita et al. 2011).

Date	n	Proportion with Hydrated Oocytes	T (°C)	Estimated Duration of Hydrated Oocytes (hr)	Corrected S
6/22/13	3	0.33	13.15	11.9	0.67
6/23/13	2		13.33	11.7	
6/25/13	3	0.33	13.63	11.3	0.71
6/26/13	1		14.13	10.6	
6/28/13	1		13.07	12.1	
7/1/13	2		13.45	11.5	
7/2/13	2		13.90	10.9	
7/5/13	1		14.01	10.8	
7/6/13	4	0.50	13.15	11.9	1.00
7/7/13	1		13.99	10.8	
7/10/13	1		13.72	11.1	
7/12/13	3	0.67	13.52	11.4	1.40
7/13/13	8	0.00	13.52	11.4	0.00
7/14/13	1		13.41	11.6	
7/15/13	3	0.33	13.45	11.5	0.69
7/16/13	5	0.40	14.26	10.4	0.92
7/17/13	1		14.59	10.0	
7/19/13	6	0.17	13.24	11.8	0.34
7/20/13	1		13.30	11.7	
7/21/13	1		13.47	11.5	
7/23/13	1		14.21	10.5	
7/24/13	1		14.38	10.3	
7/25/13	5	0.20	14.39	10.3	0.47
7/27/13	2		14.31	10.4	
7/28/13	5	0.40	14.49	10.1	0.95
7/29/13	1		14.60	10.0	
7/30/13	1		14.89	9.7	
7/31/13	1		14.76	9.8	
8/1/13	4	0.25	14.22	10.5	0.57
8/2/13	2		13.55	11.4	
8/3/13	7	0.14	13.58	11.3	0.30
8/4/13	8	0.25	13.09	12.0	0.50
8/6/13	1		13.64	11.2	
8/7/13	5	0.00	14.46	10.2	0.00
8/8/13	3	1.00	14.99	9.5	2.52
8/9/13	7	0.43	14.97	9.6	1.08
8/11/13	3	0.33	14.11	10.6	0.75
8/13/13	5	0.60	13.97	10.8	1.33
8/14/13	1		14.07	10.7	
8/15/13	2		13.45	11.5	
8/17/13	2		14.05	10.7	
8/18/13	7	0.14	12.81	12.4	0.28
8/20/13	1		15.25	9.2	
8/24/13	3	0.33	14.55	10.1	0.79
8/25/13	3	0.33	14.75	9.8	0.81
8/26/13	6	0.83	15.34	9.1	2.19
8/28/13	5	0.00	14.72	9.9	0.00
8/30/13	5	0.60	13.91	10.9	1.32
9/1/13	2			10.7	
9/2/13	4	0.00	14.33	10.0	0.00
2013	147	0.34	14.01	10.8	0.78

SUPPLEMENTARY TABLE 2

Numbers of California halibut females sampled (n), proportions of individuals with new postovulatory follicles (POFs), mean daily sea surface temperatures (T, °C), temperature-dependent durations of new POFs, and corrected spawning fractions (S) by sampling date (2013 only). Temperature data were obtained from the National Oceanic and Atmospheric Administration's National Data Buoy Center (Stn 46114). Temperature-dependent durations (D, hr) of new POFs were calculated using the equation $D = 62.9 * e^{-0.118T}$ (*Paralichthys olivaceus*, Kurita et al. 2011).

Date	n	Proportion with New POFs	T (°C)	Estimated Duration of New POFs (hr)	Corrected S
6/22/13	3	0.33	13.15	13.3	0.60
6/23/13	2		13.33	13.0	
6/25/13	3	0.00	13.63	12.6	0.00
6/26/13	1		14.13	11.9	
6/28/13	1		13.07	13.5	
7/1/13	2		13.45	12.9	
7/2/13	2		13.90	12.2	
7/5/13	1		14.01	12.0	
7/6/13	4	0.00	13.15	13.3	0.00
7/7/13	1		13.99	12.1	
7/10/13	1		13.72	12.5	
7/12/13	3	0.33	13.52	12.8	0.63
7/13/13	8	0.00	13.52	12.8	0.00
7/14/13	1		13.41	12.9	
7/15/13	3	0.00	13.45	12.9	0.00
7/16/13	5	0.20	14.26	11.7	0.41
7/17/13	1		14.59	11.2	
7/19/13	6	0.00	13.24	13.2	0.00
7/20/13	1		13.30	13.1	
7/21/13	1		13.47	12.8	
7/23/13	1		14.21	11.8	
7/24/13	1		14.38	11.5	
7/25/13	5	0.20	14.39	11.5	0.42
7/27/13	2		14.31	11.6	
7/28/13	5	0.20	14.49	11.4	0.42
7/29/13	1		14.60	11.2	
7/30/13	1		14.89	10.9	
7/31/13	1		14.76	11.0	
8/1/13	4	0.50	14.22	11.7	1.02
8/2/13	2		13.55	12.7	
8/3/13	7	0.14	13.58	12.7	0.27
8/4/13	8	0.25	13.09	13.4	0.45
8/6/13	1		13.64	12.6	
8/7/13	5	0.00	14.46	11.4	0.00
8/8/13	3	0.33	14.99	10.7	0.75
8/9/13	7	0.00	14.97	10.8	0.00
8/11/13	3	0.33	14.11	11.9	0.67
8/13/13	5	0.20	13.97	12.1	0.40
8/14/13	1		14.07	12.0	
8/15/13	2		13.45	12.9	
8/17/13	2		14.05	12.0	
8/18/13	7	0.00	12.81	13.9	0.00
8/20/13	1		15.25	10.4	
8/24/13	3	0.33	14.55	11.3	0.71
8/25/13	3	0.33	14.75	11.0	0.73
8/26/13	6	0.33	15.34	10.3	0.78
8/28/13	5	0.00	14.72	11.1	0.00
8/30/13	5	0.60	13.91	12.2	1.18
9/1/13	2			10.7	
9/2/13	4	0.00	14.33	10.0	0.00
2013	147	0.18	14.01	12.1	0.38

INSTRUCTIONS TO AUTHORS

CalCOFI Reports is a peer-reviewed journal. Papers submitted for publication in the “Scientific Contributions” section are read by two or more referees and by arbiters when necessary; “Symposium” papers are invited by the convener of the annual symposium and are reviewed and edited at the convener’s discretion. The “Reports, Review, and Publications” section contains newsworthy information on the status of stocks and environmental conditions; the papers in this section are not peer reviewed; the CalCOFI Editorial Board will not consider unsolicited review papers.

The CalCOFI Editorial Board will consider for publication in the “Scientific Contributions” section manuscripts not previously published elsewhere that address the following in relation to the North Pacific, the California Current, and the Gulf of California: marine organisms; marine chemistry, fertility, and food chains; marine fishery modeling, prediction, policy, and management; marine climatology, paleoclimatology, ecology, and paleoecology; marine pollution; physical, chemical, and biological oceanography; and new marine instrumentation and methods.

Submission Guidelines

Submissions are open year-round. Please submit manuscripts as MS word documents in electronic format via email to: calcofi_coordinator@coast.ucsd.edu. (use Word; see “Manuscript Guidelines” below for more details on preparing tables and figures). Include one complete file with all tables and figures for reviewers.

The manuscript should contain the following parts:

1. A title page containing the manuscript’s title, your name, your institutional affiliation and contact information (address, telephone and fax numbers, e-mail address), and a word count
2. An abstract of no more than 150 words that succinctly expresses only the manuscript’s most central points, using the active voice
3. Body of the text, including any footnotes
4. Literature cited, in alphabetical order
5. Acknowledgments, if any
6. Tables
7. Figures and captions

Manuscript Guidelines

Length. Unless previously approved by the Scientific Editor, manuscripts should not exceed 6,000 words, including title page, abstract, text body, footnotes, acknowledgments, and literature cited but excluding figures and tables.

Text. Double-space all elements of the text, allow margins of at least 1 inch on all sides, and use a standard font (such as Times or Times New Roman) no smaller than 12 points. Number the pages consecutively. Eliminate all nonessential formatting. Indi-

cate subordination of heads consistently; for example, use all caps for the main heads, boldface for the next level, and italics for the third level. To indent paragraphs, use the tab key, not the space bar or a “style” feature of any sort. Never use letters for numbers or vice versa; in other words, do not type the lowercase “el” for the number “one” or the capital letter “oh” for zero. Use your word-processor’s automatic footnoting feature to insert footnotes. Acknowledgments, if included, should be placed at the end of the text and may include funding sources. Place the entire text (title page, abstract, text body, footnotes, acknowledgments, and literature cited) in one document file, and label it with your name—for example, “Smith text.doc.”

Tables. Use your word-processor’s *Table* feature, rather than spaces or tabs, to create the columns and rows. Use *minimal* formatting, and do not insert vertical or horizontal rules. Double-space the tables and use a standard font, such as Times or Times New Roman. Number the tables consecutively, and provide a brief title for each. Place explanatory material and sources in a note beneath the table. Be sure each table is specifically referred to in the text.

Figures. Figures should be in black and white or color. Submit figures—whether drawings, graphs, or photographs—as separate, high-resolution electronic files (preferably 300 ppi for better printing purposes). Label the files, for example, “Smith fig 1” and “Smith fig 2.” If you are submitting as a PDF, please embed all fonts. If your figures are embedded in your Word docs, please create separate high-resolution PDF files of each figure from the original art file. Please review your files after saving them as PDFs, to make sure all your figures translated correctly. Contributors are advised to make a trial reduction of complex figures to ensure that patterns, shading, and letters will remain distinct when reduced. Include a north arrow and latitude and longitude lines on maps. Use consistent labels and abbreviations and the same style of lettering for all figures if possible. Number figures consecutively, and specifically refer to each in the text. Provide a caption for each figure. Gather the captions together, and place them at the end of the electronic text file, following the “Literature Cited” section.

Editorial Style

For matters of editorial style, contributors should consult recent editions of *CalCOFI Reports*. Contributors may also refer to *The Chicago Manual of Style*, 15th ed. Whenever possible, write in the first person, and use active verbs. Use the full name of a person, organization, program, or agency when mentioning it for the first time in your manuscript. Double-check the spelling of non-English words, and include special characters such as accents and umlauts. Use correct SI symbols for *units of measure* in figures, tables, and text (other units may be given in parentheses). Prepare *equations* in accordance with similar expressions in the printed literature.

Cite *sources* in the text as Smith (1999) or Smith and Jones (2000) or (Gabriel et al. 1998; Smith and Jones 2000) (the latter when there are three or more authors). There should be no comma between author and date. References should be cited in chronological order from the oldest to the most recent.

In the "Literature Cited" section, show sources alphabetically by the first author's surname, and secondarily in chronological order with earliest dates first. Provide surnames and first initials of all authors; do not use "et al." for multi-authored works. No source should appear in the "Literature Cited" section unless it is specifically cited in the text, tables, or figure captions. *Personal communications* and *unpublished documents* should not be included in the "Literature Cited" section but may be cited in the text in parentheses; use footnotes only when parentheses will not suffice. Abbreviate journal titles to match BIOSYS usage. Each source must be complete according to the following guidelines. Please note that initials follow the primary author's surname, but for secondary authors initials come before the surnames:

ARTICLE IN A JOURNAL:

Barnes, J. T., L. D. Jacobson, A. D. MacCall, and P. Wolf. 1992. Recent population trends and abundance estimates for the Pacific sardine (*Sardinops sagax*). Calif. Coop. Oceanic Fish. Invest. Rep. 33:60–75.

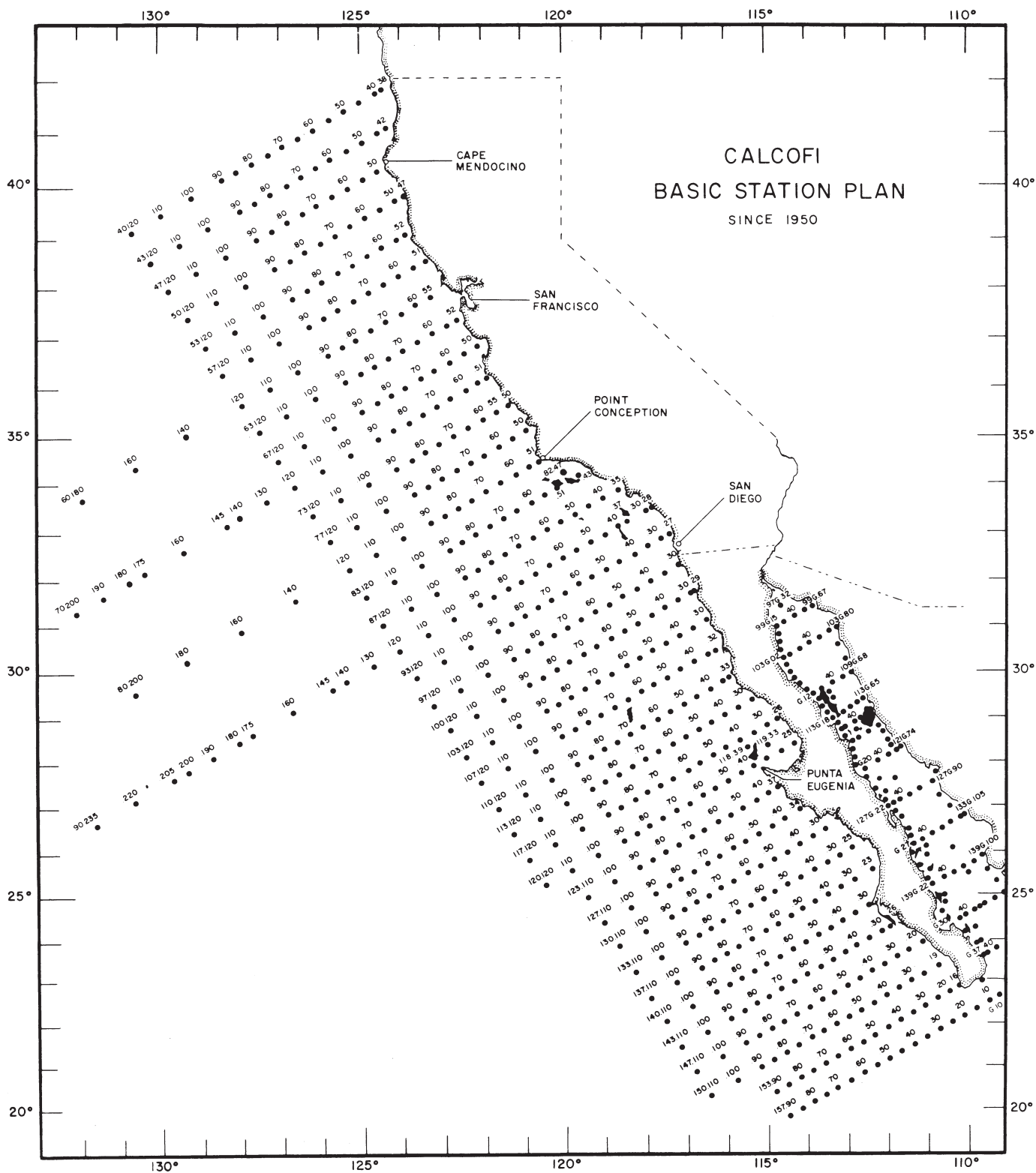
BOOK:

Odum, E. P. 1959. Fundamentals of ecology. 2nd ed. Philadelphia: Saunders. 546 pp.

CHAPTER IN A BOOK:

Wooster, W. S., and J. L. Reid Jr. 1963. Eastern boundary currents. In *The sea*, M. N. Hill, ed. New York: Interscience Pub., pp. 253–280.

If your manuscript is accepted for publication, we will provide further guidance regarding preparing it for editing.



CALCOFI

BASIC STATION PLAN
SINCE 1950